

Exploring the Role of GABA in Stomatal CO₂ Responses and Carbon Metabolism

Adriane Piechatzek

A thesis submitted in fulfilment of the requirements
for the degree of Doctor of Philosophy

School of Agriculture, Food and Wine
The University of Adelaide



July 2022

Abstract

Rapid acclimation to alterations in environmental conditions is vital for the survival of plants in an everchanging world. This includes the adjustment of stomatal apertures in accordance with environmental stimuli as well as metabolic changes, particularly, those related to cellular respiration and photosynthesis. A signal that is synthesised rapidly and in large concentrations to a great number of different environmental factors is γ -aminobutyric acid (GABA). Recently, GABA was found to fine-tune stomatal opening by negatively regulating the anion channel Aluminium-activated malate transporter 9 (ALMT9) in response to stomatal opening stimuli. However, the GABA signalling pathway is largely unexplored.

In this thesis, a potential link between GABA and high/low CO₂ signalling in guard cells was investigated using mutant lines altered in their GABA metabolism. These lines were mutated in one or several genes encoding members of a family of GABA synthesis enzymes, known as Glutamate decarboxylases (GADs). Gas exchange measurements in corresponding *GAD* knockout plants revealed a wild-type stomatal response to low/high atmospheric CO₂, except for one mutant line (*gad2-1*). Whole genome sequencing unveiled a second-site mutation in *gad2-1* in a gene encoding a crucial regulator of high CO₂ signalling, known as Mitogen-activated protein kinase 12 (MPK12), as well as in its neighbour gene *BYPASS2* (*BPS2*). This deletion mutation is associated with more open stomata and reduced CO₂ sensitivity. Re-expressing *MPK12* in the guard cells of *gad2-1* restored CO₂ sensitivity and proved that the aberrant CO₂ phenotype of this mutant line was linked to the absence of *MPK12* rather than the mutated *GAD2*. In this way, the study demonstrated that GABA signalling and the high/low CO₂-induced signal transduction pathway do not overlap. Moreover, it was also shown that stomatal opening responses to low atmospheric CO₂ occur independently of the opening channel ALMT9.

Since GABA production is associated with the release of CO₂ as a by-product into the cytosol, the impact of disrupted GABA synthesis on photosynthetic CO₂ assimilation and biomass accumulation under ambient and high CO₂ conditions was investigated in a different experimental series. The study provided data-driven evidence that GABA deficiency has no effect on the photosynthetic capacity of plants as well as on plant

growth, neither under standard conditions nor upon high CO₂ exposure. Instead, an RNA-seq analysis uncovered the upregulation of genes that are associated with carbohydrate and cell-wall metabolic processes. This was accompanied by largely elevated concentrations of the cell-wall monosaccharide xylose in the GABA-depleted mutant lines.

Together, the presented findings here reject the hypothesis that GABA is involved in CO₂ signalling in guard cells, as well as the speculation that GABA production affects CO₂ uptake for photosynthetic carbon assimilation. Furthermore, this work provides detailed information about an unrelated mutation to the gene of interest in a commonly used *gad* knockout line to prevent misinterpretations of its stomatal phenotype in future studies. In addition, some novel, GABA-unrelated insights into guard cell function, which involve, *inter alia*, stomatal opening anion channels and their role in low CO₂ responses, as well as some new aspects regarding GABA functioning in carbohydrate metabolism are discussed, thereby providing a platform for more in-depth research.

Thesis declaration

I certify that this work contains no material which has been accepted for the award of any other degree or diploma in my name, in any university or other tertiary institution and, to the best of my knowledge and belief, contains no material previously published or written by another person, except where due reference has been made in the text. In addition, I certify that no part of this work will, in the future, be used in a submission in my name, for any other degree or diploma in any university or other tertiary institution without the prior approval of the University of Adelaide and where applicable, any partner institution responsible for the joint-award of this degree.

I acknowledge that copyright of published works contained within this thesis resides with the copyright holder(s) of those works.

I also give permission for the digital version of my thesis to be made available on the web, via the University's digital research repository, the Library Search and also through web search engines, unless permission has been granted by the University to restrict access for a period of time.

I acknowledge the support I have received for my research through the provision of an Australian Government Research Training Program Scholarship.

Adriane Piechatzek

Signature: _

Date: 15/07/2022

Acknowledgements

Firstly, I would like to express my special thanks to my supervisors Professor Matthew Gilliham and Dr Bo (Weasley) Xu. I am very fortunate to have been supervised by you. Many thanks to you, Matt, for having given me the opportunity to conduct research on such an intriguing research topic and for providing the resources for this undertaking. I would also like to express my gratitude for the excellent supervision by always having a sympathetic ear and by giving me great advice and numerous valuable ideas regarding experimental designs and data analysis, which helped me a lot and guided me along my path. Also, thank you for the financial support towards the end of my PhD. I am also immensely grateful to you, Weasley, for the enormous help inside and outside the lab, when I required support with data analysis/interpretation or tips and great ideas while planning or conducting experiments. Thank you for always being so patient, reliable, and approachable.

I also thank the University of Adelaide and GOstralia! for granting me the UoA/Gostralia! Scholarship, which covered my living expenses and tuition fees.

In addition, I would like to thank my colleagues Xueying and Charlotte who have become great friends of mine. Thank you both for the many exciting discussions around stomata and GABA. In particular, I am grateful for the brilliant support from you, Xueying, as you have helped me a great deal with my research and always had a friendly ear for me. I also thank you, Charlotte, for your assistance with transcriptomic analysis as well as with stomatal aperture measurements by developing and providing the very useful stomata auto-measuring system StomaAI.

Moreover, I have to thank my other lovely colleagues since without them my research project would not have been possible. Foremost, I would like to thank Dr Rebecca Vandeleur. You were like a good fairy who made everything possible. I thank you for that and wish you all the best. Also, many thanks to you, Wendy for all the technical support and assistance. Thank you so much for providing me with tons of CO₂ cartridges for my LiCOR experiments. Probably, at the Mitre 10 shop where you got them, the cashiers already got suspicious of you. I would also like to extend my thanks to all the helpers at the lab who I am not mentioning here.

In general, thanks to all people at the Plant Research Centre for being profoundly helpful, friendly, and for making me experience a good work climate. Because of you, I always had a lot of fun and many reasons to laugh and to be cheerful. Some of my fellow students have also become dear friends, like Andrés, Hoai, Lilly, Juju, and Mel. At this this point, I would like to acknowledge the tremendous help I have received from you, Andrés. Thank you heaps for always being on the spot and supporting me in every distress situation. Also, many thanks for providing me with such delicious food, which has helped a lot, especially, towards the end of my PhD. Thanks also to the rest of the 'lunch crew', including Hoai, Juju, Mel, Lilly, and Charlotte. Thank you for making the PRC more like home for me. At the same time, I would also like to acknowledge the help I have received so many times from you, Hoai, particularly in terms of moving houses. These weren't easy times and having a dear friend helping me in these situations meant a lot to me.

Additional thank you notes also to my other friends in Australia (and Indonesia): I thank you from the bottom of my heart for the marvellous time I had outside the lab. You helped me to keep a good work-life balance and considerably contributed to my happiness. Thanks a million to you, Putri. You have supported me in a most difficult period, and I will remain always grateful to you. Thank you also for being a fantastic tour guide on our trip to Indonesia. It was an immense delight to get to know your many family members and friends there. Hopefully, we will meet again and go on another big adventure together. I would like to extent my thanks to you, Dian. Many thanks for all the incredibly tasty meals you shared with me and for the lovely chats, either at your own place or at a coffee shop over a cup of yummy coffee/hot chocolate. Another dear friend who I have to thank is you, Valerie. You have been one of my first friends here in Adelaide and your friendship means a lot to me. I really enjoy your laid-back nature and hope we will explore many more French restaurants together. Also, thanks to you, Esther, for your joyful and uplifting nature; your presence brightens up the room and has cheered me up, particularly, during hard times.

Finally, I would like to express gratitude to my friends in Germany for their lovely support at any time, even though they are thousands of kilometres away. Without you guys, I would not have found the strength to continue in extremely tough time periods. Thank you so much for your love and support from afar. Thank you heaps, dear Asin, for periodically checking up on me to see if I am still alive and for the joyful chats via

WhatsApp. Your lovely gifts have cheered up my heart. Same goes for you, Lea and Jana. You know how to make me laugh, you sent me amazing gifts, and get in touch with me on a regular basis. Thank you so much for this, guys! Thank you, Kuni, for all the post cards, presents, and updating via WhatsApp. Also, thanks to you, Daniel, Vio, and Anna! Although we had less contact in the last years, we did not lose track of each other. Many thanks for your friendship, it means a lot to me.

Zum Schluss möchte ich vom ganzen Herzen meiner Familie danken – zum einen, meinen Eltern. Danke, dass ihr immer für mich da seid - zu jeder Zeit, auch wenn es 3 Uhr in der Nacht ist. Es ist schwierig in Worte zu fassen, was ich für euch empfinde. Maren, ich bin unglaublich dankbar, dich als Schwester zu haben. Danke, dass du mir immer zuhörst und mich unterstützt. Liebe Oma Magda, ich bin auch sehr froh, dich in meinem Leben zu haben und hoffe, du hältst dich noch lange gesund und glücklich! Ihr seid einfach nur toll!

Table of Contents

| | |
|--|------------|
| Abstract | i |
| Thesis declaration | iii |
| Acknowledgements | iv |
| List of Abbreviations | i |
| Chapter 1: General introduction and Literature review | 1 |
| 1.1 Research context..... | 1 |
| 1.2 GABA in plants | 5 |
| 1.2.1 Various environmental stimuli induce GABA synthesis in plants | 5 |
| 1.2.2 Aluminium-activated malate transporters (ALMTs) are plant ‘GABA receptors’ | 8 |
| 1.3 Signal transduction in guard cells..... | 10 |
| 1.3.1 Stomatal movement occurs in response to different environmental stimuli..... | 10 |
| 1.3.2 Changes in external CO ₂ concentrations lead to a variation in stomatal responses. | 12 |
| 1.3.3 GABA functions as a signal in guard cells..... | 18 |
| 1.3.4 Are there functional links between GABA and CO ₂ signalling in stomatal regulation? | 21 |
| 1.4 The role of GABA in plant carbon metabolism | 22 |
| 1.4.1 CO ₂ is a product of GABA synthesis and a substrate of photosynthesis..... | 22 |
| 1.4.2 GABA deficiency is linked to alterations in respiratory carbon metabolism | 24 |
| 1.4.3 Which role does GABA play in carbon metabolism? | 25 |
| 1.5 Research gaps | 26 |
| 1.6 Project objectives | 27 |
| Chapter 2: GABA deficiency does not result in reduced CO₂ sensitivity in Arabidopsis | 28 |
| Abstract | 32 |
| Introduction | 33 |
| Materials and Methods | 35 |
| Plant materials and growth conditions..... | 35 |
| GABA measurement | 36 |
| Gas exchange measurements | 37 |

| | |
|--|-----------|
| Stomatal aperture and density measurements..... | 37 |
| Real time quantitative PCR (RT-qPCR)..... | 38 |
| Reverse transcriptional PCR..... | 39 |
| Microarray analysis | 40 |
| RNA sequencing..... | 40 |
| Whole genome resequencing..... | 41 |
| Plasmid construction and plant transformation | 42 |
| Genotyping PCR..... | 43 |
| Statistical analysis | 44 |
| Results | 44 |
| CO ₂ sensitivity is abolished in <i>gad2-1</i> | 44 |
| Higher order <i>GAD</i> mutants are CO ₂ -sensitive..... | 46 |
| Allelic mutant lines <i>gad2-1</i> and <i>gad2-2</i> reveal opposing CO ₂ responses..... | 50 |
| Genomic and transcriptomic analyses reveal additional genetic differences in ‘GABA mutants’ | 52 |
| CO ₂ sensitivity in <i>gad2-1</i> is restored by guard cell-specific <i>MPK12</i> complementation .. | 60 |
| Discussion | 62 |
| Supplementary Tables and Figures | 71 |
| Acknowledgements | 86 |
| Chapter 3: GABA deficiency does not alter photosynthetic CO₂ assimilation in Arabidopsis | 88 |
| Abstract | 92 |
| Introduction | 93 |
| Material and Methods..... | 96 |
| Plant materials and growth conditions..... | 96 |
| GABA measurements..... | 97 |
| Gas exchange measurements | 98 |
| A _N /C _i curve analysis | 99 |
| Respiration measurements..... | 100 |
| Biomass and stomatal density analysis in high CO ₂ -treated plants..... | 100 |

| | |
|--|------------|
| RNA sequencing..... | 101 |
| Microarray analysis | 102 |
| Statistical analysis | 102 |
| Results | 104 |
| Knocking out GABA synthesis does not result in higher CO ₂ uptake | 104 |
| GABA deficiency does not lead to a decrease in plant biomass | 107 |
| GABA deficiency is associated with increased monosaccharide concentrations..... | 110 |
| Discussion | 114 |
| Supplementary Tables and Figures | 120 |
| Acknowledgements | 130 |
| Chapter 4: General discussion and future outlook..... | 132 |
| 4.0 Key findings | 132 |
| 4.1 Which anion channels other than GABA-regulated ALMT9 are implicated in low CO ₂ responses of guard cells? | 134 |
| 4.2 Which mutation(s) restored the wild-type phenotype in <i>gad1/2/4/5</i> ? | 138 |
| 4.3 Which other signalling pathways does GABA signalling interact with? | 145 |
| 4.4 Under which circumstances does GABA influence photosynthetic carbon assimilation in plants?..... | 148 |
| 4.5 Is cell wall-derived sugar salvage promoted in the GABA-deficient lines?..... | 149 |
| 4.6 Concluding remarks..... | 153 |
| Appendix I: Preliminary results revealing accelerated guard cell responses to CO₂ in <i>gad2-2</i>..... | 154 |
| Material and Methods..... | 154 |
| Results and Discussion..... | 155 |
| Appendix II: Preliminary results showing increased photosynthetic rates in <i>gad1/2/4/5</i> | 160 |
| Material and Methods..... | 160 |
| Results and Discussion..... | 162 |
| Bibliography..... | 169 |

List of Abbreviations

| | |
|------------------|---|
| ABRC | Arabidopsis Biological Resource Center |
| AIR | Alcohol insoluble residue |
| ALMT | Aluminium-activated malate transporter |
| Al ³⁺ | Aluminium trivalent cation |
| A _N | Net assimilation |
| APX | Ascorbate peroxidase |
| AsA | Ascorbic acid |
| ATP | Adenosine triphosphate |
| βCA1 | β-Carbonic anhydrase 1 |
| βCA4 | β-Carbonic anhydrase 4 |
| BNS | Basal nutrient solution |
| BPS2 | Bypass 2 |
| BXL | β-D-xylosidase |
| CaM | Calmodulin |
| CaMD | Calmodulin binding domain |
| CBC1/2 | Convergence of blue light and CO ₂ 1/2 |
| Chr | Chromosome |
| C _i | Leaf internal CO ₂ concentration |
| Cl ⁻ | Chloride ion |
| Col-0 | Columbia-0 |
| CO ₂ | Carbon dioxide |
| Cvi | Cape Verde Islands |
| d | Days |

| | |
|-------------------------------|---|
| DEGs | Differentially expressed genes |
| DEPs | Differentially expressed proteins |
| DM | Dry mass |
| ET | Ethylene |
| EtOH | Ethanol |
| FACE | Free air CO ₂ enrichment |
| FAD | Flavin adenine dinucleotide |
| Fc | Fold change |
| FDR | False discovery rates |
| FL | Full length |
| FM | Fresh mass |
| g | Grams |
| GABA | Gamma aminobutyric acid |
| GABA-T | GABA transaminase |
| GC | Guard cell |
| GCA2 | Growth controlled by abscisic acid 2 |
| GC-MS | Gas chromatography-mass spectrometry |
| Glu | Glutamate |
| GLR | Glutamate receptor |
| GO | Gene ontology |
| GS | Germination solution |
| h | Hour |
| HCO ₃ ⁻ | Bicarbonate |
| HPAEC-PAD | High-performance anion exchange chromatography-with pulsed amperometric detection |

| | |
|-------------------|---|
| HT1 | High leaf temperature 1 |
| JAR1 | Jasmonate resistant 1 |
| J_{\max} | Maximum rate of photosynthetic electron transport |
| KEGG | Kyoto encyclopedia of genes and genomes |
| LED | Light emitting diode |
| Mal^{2-} | Malate anion |
| MAPP | Micro array polymer profiling |
| MATE | Multi-antimicrobial extrusion protein |
| MES | 2-(N-morpholino) ethanesulfonic acid |
| min | Minutes |
| MPK4 | Mitogen-activated protein kinase 4 |
| MPK12 | Mitogen-activated protein kinase 12 |
| MS | Murashige and Skoog |
| NADP | Nicotinamide adenine dinucleotide phosphate |
| NO | Nitric oxide |
| N_2 | Nitrogen |
| OST1 | Open stomata 1 |
| QUAC1 | Quickly activating anion channel 1 |
| P adj. | P-value adjusted |
| PCA | Principal component analysis |
| PDC | Pyruvate dehydrogenase complex |
| 3-PGA | 3-phosphoglycerate |
| Phot1/2 | Phototropin 1/2 |
| PIP2;1 | Plasma membrane intrinsic protein 2-1 |

| | |
|-------------------|---|
| PLP-dependent | Pyridoxal phosphate-dependent |
| ppm | Parts per million |
| PX | Peroxidase |
| R_{dark} | Rate respiration/ O_2 consumption in the dark |
| RHC1 | Resistance to high CO_2 1 |
| RNA-seq | RNA sequencing |
| ROS | Reactive oxygen species |
| R-type | Rapid type |
| Rubisco | Ribulose-1,5-bisphosphate carboxylase-oxygenase |
| RuBP | Ribulose-1,5-bisphosphate |
| SAIL | Syngenta Arabidopsis insertion library |
| SEM | Standard error of the mean |
| SLAC1 | Slow anion channel 1 |
| SSA | Succinic semialdehyde |
| S-type | Slow type |
| TAIR | The Arabidopsis Information Resource |
| TCA cycle | Tricarboxylic acid cycle |
| TPM | Transcripts per million |
| TPX2 | Thioredoxin-dependent peroxidase 2 |
| UDP | Uridine diphosphate |
| UGT | UDP-glycosyltransferase |
| UPLC | Ultrahigh pressure liquid chromatography |
| V_{cmax} | Maximum velocity of Rubisco carboxylation |
| VPD | Vapour-pressure deficit |

WUE

Water use efficiency

XTH

Xyloglucan endotransglycosylase/hydrolase

Chapter 1: General introduction and Literature review

1.1 Research context

Climate change is a serious issue that affects all living beings on this planet whether human, animal, or plant. Climate change is linked to rapidly increasing atmospheric carbon dioxide (CO₂) concentrations, which seem to be attributable, *inter alia*, to human activities (Falkowski *et al.*, 2000; Ziska *et al.*, 2009). While atmospheric CO₂ concentrations amounted to 369.55 ppm in November 2000, they had increased to 409.8 ppm by 2019 as recorded by the National Oceanic and Atmospheric Administration (NOAA)/ Earth System Research Laboratory (ESRL; global average CO₂ concentration; Figure 1). While global CO₂ levels increased by 0.6 ± 0.1 ppm per year in the 1960s, CO₂ concentrations already rose by 2.5 ± 0.1 ppm per year in 2018 (Lindsey, 2020; NOAA). It is estimated that global CO₂ concentrations will have risen up to levels between 500 to 1000 ppm by the year 2100 (Taub, 2010).

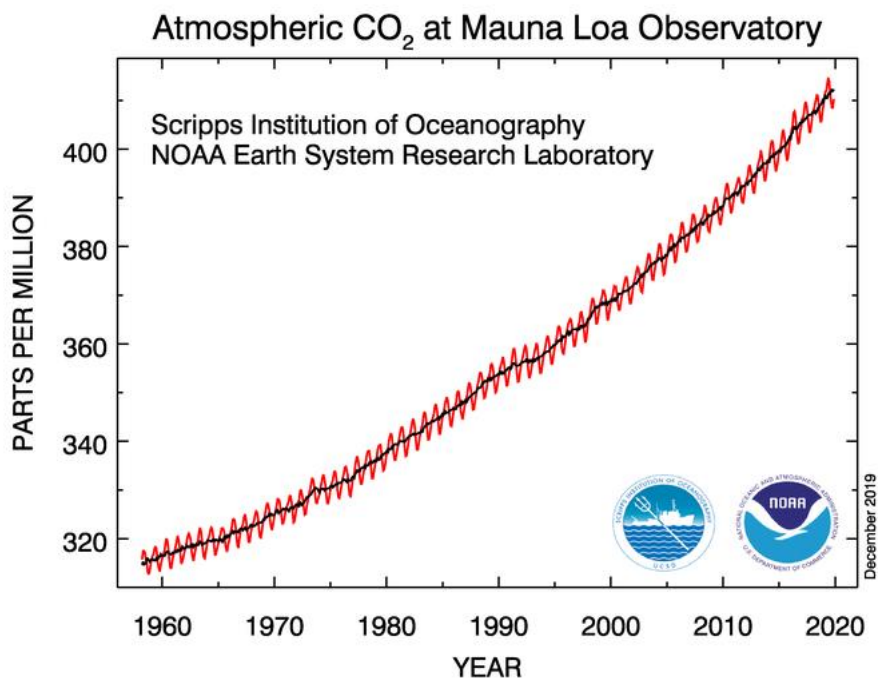


Figure 1: Global CO₂ concentration increases steadily.

Measurements were conducted at Mauna Loa Observatory, Hawaii. Measured as mole fractions in dry air; the red line indicates the monthly measured values; the black line denotes the averages [Tans (2019); The Earth System Research Laboratory (ESRL)/National Oceanic and Atmospheric Administration (NOAA)].

Climate change is usually associated with increasing the frequency of extreme weather events and imposing environmental stresses like heat and drought on plants. These are factors that negatively affect plant performance and thereby can have a severe impact on the global economy, especially, in terms of crop production and food security (Gunasekera *et al.*, 2007; Wang and Frei, 2011). Furthermore, the steady rise in atmospheric CO₂ concentrations greatly influences plant physiology and development itself, and is proposed to significantly influence crop production in the future (Taub *et al.*, 2008; Taub and Wang, 2008; Norby and Zak, 2011). Studies have shown that alterations in CO₂ concentrations influence both plant growth and stomatal apertures (Norby and Zak, 2011; Kollist *et al.*, 2014). To clarify, stomata are pores on leaf surfaces and are major regulators of the rate of plant gas exchange. This is a fundamental process in plants that absorbs CO₂, and emits water (H₂O) and oxygen (O₂). The CO₂ that plants take in is essential for photosynthesis. Up to a specific point, atmospheric CO₂ enrichment results in an increase in photosynthetic rates and plant growth (Norby and Zak, 2011). On the one hand, a high CO₂-promoted increase in biomass is desirable for the production of heat, biogas, and electricity (Lima *et al.*, 2017). In addition, a clear increase in yield was detected in a large range of different crops, which is linked to the global rise in CO₂ concentrations (Kimball *et al.*, 1993). However, as research in soybean revealed, an elevation in atmospheric CO₂ does not always result in higher crop yields, but might cause an enlargement of leaf canopy instead (Ainsworth *et al.*, 2002). Furthermore, it should be noted that CO₂ does not differentiate between desirable and non-desirable plant species (Ziska *et al.*, 2009). Accordingly, high CO₂ is likely to enhance the biomass production not only of crop plants but also of weeds (Ziska *et al.*, 2009). In addition, a recent research synthesizing over 100 elevated CO₂ experiments found a trade-off between increased plant biomass and soil organic carbon storage, correlated to nutrient availability: when plant growth is more nutrient constrained, more carbon is accumulated belowground (Terrer *et al.*, 2021). Elevated CO₂ has also been found to lower protein and mineral nutrient storage within rice grains and may negatively impact human health (Terrer *et al.*, 2021). Moreover, higher CO₂ concentrations do not necessarily enhance photosynthetic carbon assimilation, due to depleted nutrient availability as well as exhausted photosynthetic capacity (Sharkey *et al.*, 2007; Ehleringer and Sandquist, 2015).

Significantly, plants have been found to modulate stomatal apertures in accordance with the surrounding CO₂ concentration. To be specific, plants promote stomatal opening in response to low CO₂ concentrations, while they respond to high CO₂ levels by decreasing stomatal aperture width (Morison, 1987; Bunce, 2004; Kollist *et al.*, 2014). Apart from this, it is also known that stomatal closure can cause a significant increase in leaf temperature, due to a reduced rate of transpiration (Hashimoto *et al.* 2006). Generally, when there is sufficient water available, plants induce stomatal opening to cool their leaves and thereby counteract rising leaf temperatures (Mittler, 2006). When plants encounter high temperatures in combination with elevated atmospheric CO₂, they tend to reduce stomatal conductance (Zvereva and Kozlov, 2006). As a consequence, plants could possibly suffer extreme heat stress in the future as it is predicted that the global temperature is continuing to rise (Ohama *et al.*, 2017).

Overall, it is known that stomatal movement plays vital roles in plant productivity, water sustainability and stress acclimation. Therefore, understanding the underlying mechanism of stomatal movement in response to various plant stresses and other environmental inputs is an important pathway to enhancing the stress resilience of plants.

A metabolite that is involved in plant responses to a large range of different stresses is gamma aminobutyric acid (GABA) (Ramesh *et al.*, 2015). What is more, GABA has been found to regulate stomatal movement by inhibiting the activity of specific anion channels in guard cells, known as Aluminium-activated Malate Transporters (ALMTs) (Xu *et al.*, 2021a). By controlling stomatal apertures, GABA activity significantly increases the drought tolerance of plants, which makes it an important guard cell-signalling component to study (Mekonnen *et al.*, 2016; Xu *et al.*, 2021a). However, GABA signalling is largely unexplored, and it is not known which signalling pathways GABA uses to regulate ALMT activity and consequently stomatal movement (Ramesh *et al.*, 2017; Xu *et al.*, 2021a).

The regulation of stomatal movement is complex and involves a sophisticated signalling network of phytohormones, secondary messengers, and other signalling molecules which perform crosstalk with each other (Kim *et al.*, 2010; Raghavendra and Murata, 2017). Consequently, an alteration in the activity of one factor could possibly affect other components of the network. For this reason, it is not only important to

identify the key players of signalling pathways but also to determine the cross points of interaction between signalling compounds from different signal transduction pathways. However, the existing literature provides only sparse information about possible connections between GABA and other guard cell regulators and yet there are clues that pinpoint to the merger of pathways of GABA and other signals, which will be examined in the next subchapters.

Both stomatal movements and high CO₂ influence plant growth. Moreover, GABA acts not only as a guard cell signal but also functions as an important plant carbon metabolite. A major GABA biosynthesis pathway is the GABA shunt which by-passes the major respiratory pathway known as the Krebs cycle (also known as tricarboxylic acid [TCA] cycle), and leads to the formation of CO₂ as a side-product (Bown and Shelp, 2016). A previous study has reported that GABA deficiency is linked to major alterations in the concentrations of Krebs cycle intermediates, sugar content, and amino acid composition (Mekonnen *et al.*, 2016).

Furthermore, not only the respiratory pathway but also the photosynthetic carbon reactions might be affected by GABA depletion, due to the generation of CO₂ during GABA synthesis. If GABA plays a role in photosynthesis and biomass accumulation, this knowledge could be highly relevant for growing plants under rising atmospheric CO₂ conditions. However, information about the involvement of GABA in the broader plant carbon metabolism is scarce, and yet there are clues that are indicative of a possible connection and will be reviewed in detail in the next subchapters.

The following literature review describes the signalling functions of GABA and will introduce GABA's putative role in CO₂ responses of guard cells. Furthermore, it will discuss the connection between GABA and plant carbon metabolism with regards to CO₂ assimilation and plant biomass accumulation. In doing so, it will outline the research gaps and questions in more detail that provided the inspiration for this study.

1.2 GABA in plants

1.2.1 Various environmental stimuli induce GABA synthesis in plants

Environmental stress can impact plant health. Plants must react rapidly in response to environmental situations as their survival depends on it. ‘Flight’ is not an option for plants as sessile living beings and the alternative for them is ‘fight’, or in other words, adaptation to the respective environmental challenge. For this purpose, plants have evolved environmental sensors which perceive a specific environmental input and activate the respective downstream stress response cascades (Taiz *et al.*, 2015). Different kinds of molecules are used by the plant as signals such as abscisic acid (ABA) to heat and drought (Hauser *et al.*, 2017), ethylene-gibberellin acid to submergence (Kuroha *et al.*, 2018), and jasmonic acid to wounding (Li *et al.*, 2001). Furthermore, the role of primary metabolites like glutamate and derivatives of these, like GABA, are emerging as crucial components of a number of stress signalling cascades (Fromm, 2020).

The four-carbon non-proteinogenic amino acid GABA is a well-known neurotransmitter in mammal brains. For many years, it was only known for its signalling functions in animals. In plants, GABA was ‘merely’ considered as a carbon-nitrogen metabolite (Ramesh *et al.*, 2017). The main functions that were attributed to GABA are roles in maintaining the plant C:N balance, in nitrogen supply, in cellular redox and pH regulation processes as well as in energy metabolism [Bouché and Fromm (2004) and references therein; Fait *et al.* (2007)]. In recent years, however, it became evident that GABA acts as a signalling molecule in both animals and plants. Several findings have confirmed this hypothesis.

According to Taiz *et al.* (2015), the concentration of a signalling molecule must be tightly regulated. Specifically, the concentration of signalling molecules is usually low at the signal’s action sites under normal conditions, but rises significantly in response to certain stimuli and drops back to the original state, achieved either by compartmentation, catabolism, or modification of the signal (Ramesh *et al.*, 2017; Fromm, 2020). Moreover, signalling molecules induce the activation or deactivation of so-called effectors by binding and changing the conformation of these proteins (Ramesh *et al.*, 2017; Fromm, 2020).

GABA fulfils these criteria. On the one hand, GABA can increase rapidly to high concentrations upon specific environmental stimuli. For instance, it was reported that GABA concentrations can rise up to 1,000-fold and vary between 0.03 and 6 $\mu\text{mol g}^{-1}$ FM in response to various stress factors (Ramesh *et al.*, 2017; Bown and Shelp, 2020). These stresses include anoxia and hypoxia, cold, heat, drought, flooding, pathogens, salinity, herbivory, acidosis, and mechanical stress [Ramesh *et al.* (2017), Shelp and Bown (2020) and references therein]. GABA production can occur via several different anabolic pathways, which include peroxisomal polyamine degradation (putrescine and spermidine), plastid polyamine anabolism, a non-enzymatic reaction from proline (Signorelli *et al.*, 2015), and glutamate decarboxylation by Glutamate decarboxylases (GADs) [Bown and Shelp (2020) and references therein]. GABA synthesis via glutamate decarboxylation takes place in the cytosol during a pathway defined as the ‘GABA shunt’ (Bown and Shelp, 2020; Figure 2). This reaction bypasses the Krebs cycle and is also associated with the metabolism of several other amino acids (Fait *et al.*, 2008; Li *et al.*, 2017). If a plant is exposed to a specific stress factor like drought, for instance, an oxidative burst in the form of reactive oxygen species (ROS) accumulation arises inside its cells (Zhang *et al.*, 2001; Song *et al.*, 2014). This burst triggers the inhibition of the Krebs cycle enzyme 2-oxoglutarate dehydrogenase (2-OGDH), followed by the transport of 2-oxoglutarate from the mitochondrion into the cytosol where GABA synthesis takes place (Gilliham and Tyerman, 2016; Bown and Shelp, 2020). According to Bown and Shelp (2020), 2-oxoglutarate is presumably redirected to the cytosol not due to an alteration in the catalytic capacity of 2-OGDH but rather as a result of reduced cytosolic 2-oxoglutarate concentration. In the cytosol, 2-oxoglutarate is turned into glutamate by the activity of glutamate dehydrogenase (GDH; Bouché and Fromm, 2004). Subsequently, glutamate is converted to GABA in a reaction that is catalysed by GAD, which is a key enzyme of GABA synthesis (Bouché and Fromm, 2004; Ramesh *et al.*, 2017). It is encoded by five copies, but only *GAD1* and *GAD2* are abundantly expressed in Arabidopsis and the knockout of both genes results in drastic GABA depletion (Mekonnen *et al.*, 2016). While *GAD1* is predominantly localised to roots, *GAD2* is detectable in nearly all tissues and was found to be the main GABA biosynthesis enzyme in leaves (Scholz *et al.*, 2015). *GAD3* and *GAD4*, however, are only minimally expressed in leaves and roots under non-stress conditions (Mekonnen *et al.*, 2016). Conversely, the expression of *GAD4* is significantly increased in response to various stresses like cold, drought, hypoxia, and

salt stress (Renault *et al.*, 2010). *GAD5*, on the other hand, seems to be predominantly located to male gametes and is not detectable in leaves or roots (Scholz *et al.*, 2015). GAD activity appears to follow a diurnal pattern, as it is significantly elevated three hours after a dark-to-light transition (Pelvan *et al.*, 2021). Significantly, CO₂ is generated as a by-product of GAD activity which can be stimulated by a low cytosolic pH (Bouché and Fromm, 2004; Michaeli and Fromm, 2015) and by the Calcium (Ca²⁺)-binding protein calmodulin (Snedden *et al.*, 1995). It is suggested that most plant GAD enzymes, including GAD2 in Arabidopsis, possess an auto-inhibitory CaM binding domain (CaMD) which binds free cytosolic Ca²⁺ ions upon stress events (Baum *et al.*, 1996; Zik *et al.*, 1998; Du *et al.*, 2011). Baum *et al.* (1996) showed that transgenic tobacco plants expressing a truncated version of petunia GAD and lacking the specific CaMD generated significantly higher GABA levels compared to wild-type plants.

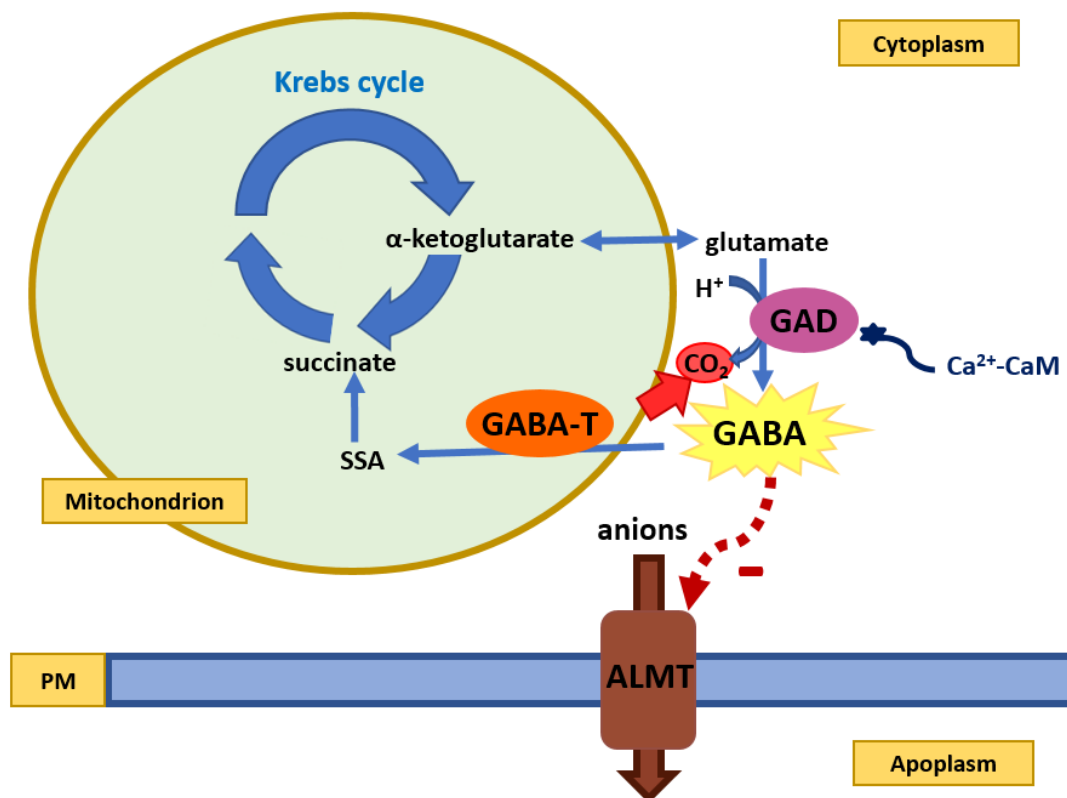


Figure 2: Regulation sites of GABA accumulation.

In response to various stress stimuli, GABA accumulates rapidly and in large concentrations in plants. Its synthesis takes place during the GABA shunt pathway, which bypasses the Krebs cycle (also known as TCA cycle). Thereby, the GABA synthesis enzyme GAD is activated by Ca²⁺/calmodulin as well as by a decrease in cytosolic pH and thereupon catalyses the conversion of glutamate to GABA; a reaction that consumes protons and leads to the release of CO₂ as a side-product. The glutamate that functions as a substrate for GAD is produced from

2-oxoglutarate (or α -ketoglutarate) in the cytosol. GABA in turn negatively regulates anion flux across the plasma membrane and tonoplast by inhibiting specific anion channels that are known as ALMTs. After cessation of the stress signal, GABA is degraded to succinic semialdehyde (SSA) by the activity of the enzyme GABA transaminase (GABA-T) and then further to succinate, and thereby fed back into the Krebs cycle. Own work; after Gilliam and Tyerman (2016).

The inhibition of succinic semialdehyde (SSA) dehydrogenase by a stress-related rise in redox potential also seems to contribute to the immense increase in GABA concentration (Bown and Shelp, 2020). When the stress is subsiding, GABA is transported back into the mitochondrion via GABA permease (GABP) and turned into SSA by GABA transaminase (GABA-T) (Meyer *et al.*, 2006). SSA is then converted into succinate by SSA dehydrogenase (Bouché and Fromm, 2004). Knocking out *GABA-T* leads to hyperaccumulation of GABA as observed in the loss-of-function mutant *pop2 (gaba-t)* (Bouche and Fromm, 2004; Renault *et al.*, 2010).

Further evidence for the hypothesis that GABA functions as a signal in plants is provided by the recent discovery of ALMTs negatively regulated by GABA (Ramesh *et al.*, 2015). The functions of these specific anion transporters will be discussed in more detail in Subsection 1.2.2.

1.2.2 Aluminium-activated malate transporters (ALMTs) are plant ‘GABA receptors’

In mammals, GABA was found to exert major signalling functions as an inhibitory neurotransmitter in the cerebellum and the cerebrum (Singer *et al.*, 2014). There, GABA activates GABA_A and GABA_B receptors and thereby induces ion flux through neuron membranes, leading to neuron hyperpolarization and consequently inhibition of neuron excitation (Ramesh *et al.*, 2017).

Although GABA is also present in plants, plant orthologs of GABA_A and GABA_B receptors have not been found (Ramesh *et al.*, 2017). Instead, it was reported that members of the so-called ALMT family do not only possess a 12 amino acid stretch that is homologous to a GABA binding motif in GABA_A receptors, but their activity is also regulated by GABA (Ramesh *et al.*, 2015; Ramesh *et al.*, 2017). With this

discovery, it became obvious that ALMTs function as ‘GABA receptors’ in plants (Žárský, 2015).

What is more, several members of the ALMT family are implicated in guard cell movement. In *Arabidopsis*, this family comprises 14 members, out of which seven have been demonstrated or proposed to be expressed in guard cells (*ALMT4-6, 9* and *12-14*) (Meyer *et al.*, 2011; Eisenach *et al.*, 2017). Out of these, four ALMT family-members (*ALMT4-6* and *9*) span across the tonoplast, while the other three (*ALMT12-14*) are localised to the plasma membrane (Meyer *et al.*, 2010; Meyer *et al.*, 2011; De Angeli *et al.*, 2013; Eisenach *et al.*, 2017). The designation ‘ALMT’ can be misleading, as most members of the ALMT family are not capable of mediating Aluminium (Al^{3+})-induced malate transport. In fact, only *ALMT1* has been found to be activated by Al^{3+} . *ALMT1* transports malate (Mal^{2-}) anions out of roots and thereby counteracts Al^{3+} toxicity through facilitating chelation between Al^{3+} and Mal^{2-} ions (Ramesh *et al.*, 2015). In general, ALMTs are known to be activated by Mal^{2-} and are permeable to anions like chloride (Cl^-), nitrate (NO_3^-), and/or Mal^{2-} (Sasaki *et al.*, 2010; Bown and Shelp, 2016), and GABA (Ramesh *et al.*, 2018). Apparently, GABA functions as an antagonist of malate as it was found to inhibit the electrogenic anion transport activity by ALMTs (Gilliam and Tyerman, 2016). Based on their differential subcellular localisation and transport properties, different ALMT isoforms are either involved in the regulation of stomatal opening or closure (Eisenach *et al.*, 2017). To be specific, *ALMT4* and *ALMT12* appear to function in stomatal closure, whilst *ALMT9* has been found to function in stomatal opening (De Angeli *et al.*, 2013; Eisenach *et al.*, 2017; Meyer *et al.*, 2010). The exact roles of *ALMT13* and *ALMT14* still need to be elucidated and *ALMT6* has proven to be redundant in guard cells (Meyer *et al.*, 2010; Meyer *et al.*, 2011). *ALMT12* has been proposed to be the molecular identity of a protein underlying the majority of the rapid (R)-type anion currents detected in guard cell plasma membranes, while *ALMT13* and *ALMT14* probably make up the rest (Meyer *et al.*, 2010). The designation ‘R-type’ is based on the rapid activation of these channels. Due to this property, this *ALMT12* has also been named ‘Quick-activating anion channel’ (QUAC1) (Linder and Raschke, 1992; Roelfsema *et al.*, 2012). Notably, it has been shown that GABA is implicated in stomatal movement by negatively regulating ALMTs, which will be further discussed in Subchapter 1.3.

1.3 Signal transduction in guard cells

1.3.1 Stomatal movement occurs in response to different environmental stimuli

Water is critical to sustain all forms of life on earth. Since plants are sessile living organisms, they have to make do with the water available at their location. However, they have developed several strategies for controlling and regulating their water balance. Among others, plants have evolved ‘little guards’ which control free air passages into leaves. To be specific, leaves and stems possess little pores, designated as stomata, on their surfaces. Pairs of guard cells delineate these stomatal pores and regulate the rate of gas exchange by controlling the pore aperture (open or closed). Thereby, these cells are highly sensitive to environmental changes and adjust pore apertures accordingly.

Principally, in dicotyledons (e.g. Arabidopsis), stomatal movement depends on the control of guard cell turgor pressure (Waggoner and Zelitch, 1965); in grass species (e.g. barley and wheat), guard cells and subsidiary cells (adjacent to guard cells) coordinate this process in concert (Raschke and Fellows, 1971). Stomatal opening occurs when guard cells perceive certain environmental opening stimuli like blue light impulses or drastic reductions in intercellular CO₂ concentrations (Zeiger, 2015). Subsequently, guard cells increase the concentration of cytosolic and vacuolar osmolytes. This results in the build-up of turgor pressure due to water absorption, causing guard cell swelling and consequently stomatal opening (Figure 3). In contrast, a decrease in cytoplasmic and vacuolar osmolytes reduces turgor pressure, leading to guard cell shrinking and stomatal closure. The mobilisation of these osmolytes is mediated by specific anion channels that are localised to the tonoplast and plasma membrane of the guard cells.

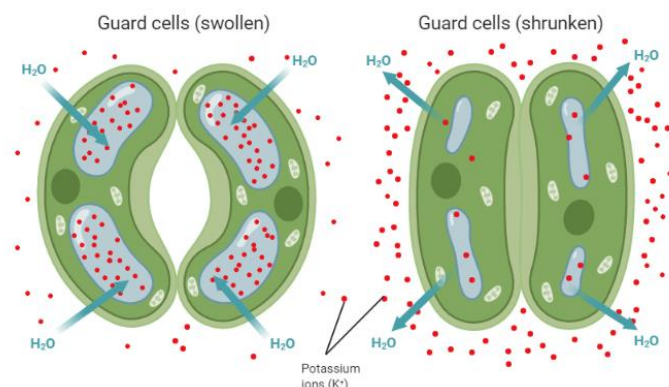


Figure 3: Opening vs. closing of guard cells.

Upon stomatal opening, osmolytes are transported from the apoplast into the guard cells, where they are predominantly stored inside vacuoles. The elevated solute concentration inside the cells in comparison to their surroundings causes a negative water potential. As a result, water enters the guard cells, which leads to an increase in turgor pressure, guard cell swelling and, consequently, stomatal opening. On the other hand, when plasma membrane and tonoplast transporters drive osmolytes out of guard cells, followed by water efflux, the turgor pressure inside the cells is reduced, which is associated with guard cell shrinkage and stomatal closure. Own work on the basis of Reece and Wassermann (2013). Image was created in BioRender.

It has been observed that the anion channels that confer anion efflux from guard cells show the lowest activity at a neutral pH or a membrane potential of less than -150 mV (Roelfsema *et al.*, 2012). This negative membrane potential is sustained by the activity of plasma membrane- and tonoplast-localised H⁺-ATPases (Blumwald and Mittler, 2015). Conversely, due to the stimulation of anion efflux during stomatal closure, the membrane potential depolarises as these H⁺-ATPases are inhibited by cytosolic Ca²⁺ (Kinoshita *et al.*, 1995). The change in membrane potential due to anion efflux activates voltage-gated Guard cell outwardly-rectifying K⁺ (GORK) channels in the plasma membrane and Vacuolar K⁺ (VK)-channels in the tonoplast, resulting in a release of K⁺ ions into the apoplast [Hosy *et al.* (2003) in Daszkowska-Golec and Szarejko (2013)]. Thereupon, water follows the escaping ions, which is associated with a reduction in turgor pressure, guard cell shrinkage and consequently a decrease in stomatal aperture. At the same time, extracellular K⁺ ions are hindered from entering the cell by Ca²⁺-mediated inhibition of K⁺ inwardly-rectifying channels (Hosy *et al.*, 2003; Taiz *et al.*, 2015). There are many known proteins underlying many of these steps and a complex signalling network controlling the fluxes, which have been reviewed extensively elsewhere (Cotelle and Leonhardt, 2019; Saito and Uozumi, 2019; Dubeaux *et al.*, 2021; Hsu *et al.*, 2021).

This opening and closure mechanism of guard cell stomata is pivotal for plant survival due to two central functions. Firstly, stomatal opening allows plant transpiration to occur as the waxy cuticle layer on leaf surfaces makes it nearly impossible for water vapour to pass through (Domínguez *et al.*, 2017). To clarify, transpiration is a process in which water is transported from the soil into roots to leaf and stem surfaces. From there, the water leaves the plant through open stomata in the form of water vapour

(Holbrook, 2015). In addition, open stomata allow for the gas exchange required for CO₂ assimilation via the process of photosynthesis. However, due to the threat of desiccation, plants cannot afford to have their stomata constantly open. In fact, the concentration gradient for CO₂ absorption is 50 times lower than the concentration gradient that allows water evaporation (Ehleringer and Sandquist, 2015). Consequently, plants are permanently forced to juggle between stomata opening for CO₂ uptake and stomatal closure for water conservation. Strictly speaking, the ability of a plant to differentiate between the necessity to keep stomata open and the opportunity to induce stomatal closure without compromising CO₂ assimilation increases a plant's water use efficiency (WUE). WUE defines the ratio of CO₂ uptake for photosynthesis to water use (Hatfield & Dold 2019) and has been intensively studied in the past years for the enhancement of crop productivity (Stanhill, 1986; Lawson *et al.*, 2014; Lavergne *et al.*, 2019; Leakey *et al.*, 2019).

To be able to adequately react to environmental changes, guard cells have evolved to be highly sensitive to environmental signals such as increases or decreases in humidity, light to dark transitions or *vice versa*, changes in air temperature, or alterations in atmospheric CO₂ levels (Kollist *et al.*, 2014; Engineer *et al.*, 2016; DiMario *et al.*, 2017; Driesen *et al.*, 2020). Once environmental stimuli have been perceived by specific stress sensors, respective downstream signal transduction pathways are activated. For instance, abscisic acid (ABA) is a very well-explored phytohormone that protects plants from drought stress by activating a signalling cascade leading to stomatal closure (Munemasa *et al.*, 2015). CO₂ also functions as a guard cell signal and triggers the activation of specific CO₂ signalling cascades, which will be outlined in the next subsection (1.3.2).

1.3.2 Changes in external CO₂ concentrations lead to a variation in stomatal responses

Plants require CO₂ as building material for carbohydrate biosynthesis. In general, CO₂ is a diffusible molecule that can easily penetrate cell membranes. The cuticle, however, constitutes not only an insurmountable barrier for H₂O but also for CO₂ (Zeiger, 2015); free access is only granted via stomatal pores. What is more, CO₂ itself regulates the opening and closure of these pores. Plants modify stomatal apertures in response to

alterations in atmospheric CO₂ levels (ambient \cong ~417 ppm; NOAA/ESRL, 2021). Specifically, plants reduce stomatal apertures in response to high atmospheric CO₂ (such as 800 ppm CO₂,) while they increase stomatal apertures and consequently stomatal conductance when they encounter low CO₂ levels (such as 100 ppm CO₂; Figure 4). Furthermore, research has shown that atmospheric CO₂ levels do not only have an impact on stomatal apertures but also affect stomatal density. To be specific, it has been observed that long-term exposure of plants to elevated CO₂ significantly reduces their stomatal density (Woodward and Kelly, 1995; Li *et al.*, 2020). The ability to distinguish between low and elevated CO₂ and respond accordingly increases a plant's water use efficiency (Li *et al.*, 2020). Treating plants with increased or decreased [CO₂], as done in many gas exchange experiments, is a way of mimicking high or low internal leaf CO₂ concentrations, which either induce stomatal closure or opening respectively. A drop in CO₂ concentration in the intercellular spaces of the leaf (C_i), is a signal for guard cells to open, while an elevation in C_i signals guard cells to promote stomatal closure (Hosotani *et al.*, 2021). The rise and fall of C_i is closely connected to the photosynthetic activity of plants. To be more exact, photosynthesis is a process that involves CO₂ fixation and in doing so, it decreases C_i (Tominaga *et al.*, 2018). Consequently, the plant's demand for CO₂ increases and stomata respond accordingly by enhancing stomatal opening (Matthews *et al.*, 2017). On the other hand, when C_i is high, the plant can afford to close its stomata and, thereby, it minimises water loss through evaporation.

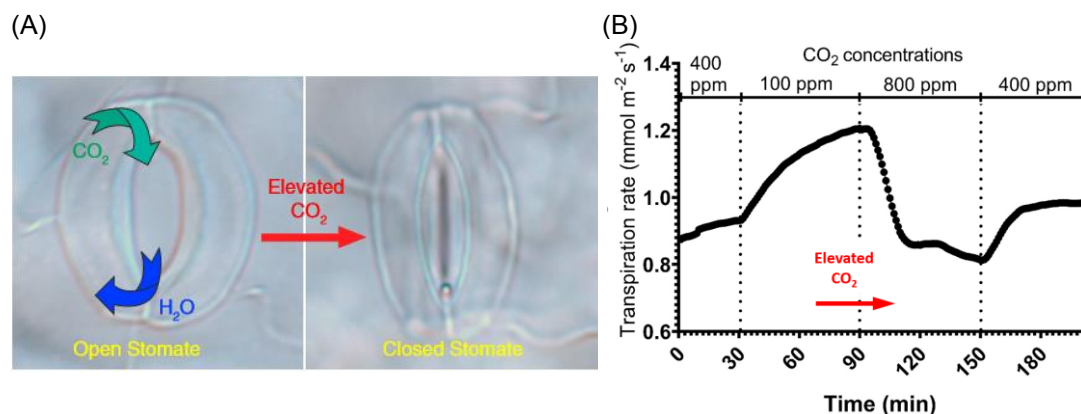


Figure 4: Changes in atmospheric CO₂ levels lead to a variation in stomatal responses.

Plants adjust stomatal apertures for gas exchange in accordance to surrounding CO₂ concentrations. High CO₂ levels (like 800 ppm) lead to a decrease in stomatal conductance.

Conversely, when CO₂ concentrations are low (like 100 ppm) plants increase stomatal conductance. A: Zhang *et al.*, 2018; B: Own work.

Taken together, stomatal pore movement and carbon gain have to be fine-tuned and, for this purpose, plants have evolved a CO₂ sensing mechanism and signalling pathway which are activated by changes in atmospheric CO₂ and result in adequate stomatal adjustment. Carbonic anhydrases (CAs) function as upstream regulators of high CO₂-induced stomatal movement by accelerating the conversion of CO₂ and H₂O into H⁺ and HCO₃⁻ (Hu *et al.*, 2010; Kim *et al.*, 2010; Engineer *et al.*, 2016). Studies have shown that the genes that encode the β -carbonic anhydrases β CA1, β CA2, and β CA4 are the most highly expressed CA genes in the mesophyll, while transcript abundance of β CA1, β CA4, and β CA6 is highest in guard cells (Hu *et al.*, 2010; DiMario *et al.*, 2017). In guard cells, activation of β CA1 and β CA4 by high CO₂ initiates a CO₂ signal transduction pathway that leads to stomatal closure. Another proposed key component in this pathway is the aquaporin Plasma membrane Intrinsic Protein 2-1 (PIP2;1) which was found to interact with plasma-membrane located β CA4 to allow CO₂ to pass through the cell wall into the cell (Wang *et al.*, 2016). Furthermore, CA activity triggers the activation of the synergistically functioning Mitogen-activated protein kinases (MPK) 4 and 12 via a yet unidentified mechanism (Töldsepp *et al.*, 2018; Zhang *et al.*, 2018). To be specific, a previous study has demonstrated that the single mutant *mpk12* shows a clear decrease in CO₂ sensitivity, albeit a slight CO₂ response (Töldsepp *et al.*, 2018). In contrast, CO₂ sensitivity appears to be completely abolished in transgenic lines lacking both MPK4 and MPK12 in guard cells (Figure 5) (Hörak *et al.*, 2016; Töldsepp *et al.*, 2018). Presumably, MPK4 and MPK12 function upstream or in parallel to ABA signalling as ABA-mediated stomatal closure was found to be unaffected in the aforementioned mutant lines (Hörak *et al.*, 2016; Jakobson *et al.*, 2016; Töldsepp *et al.*, 2018).

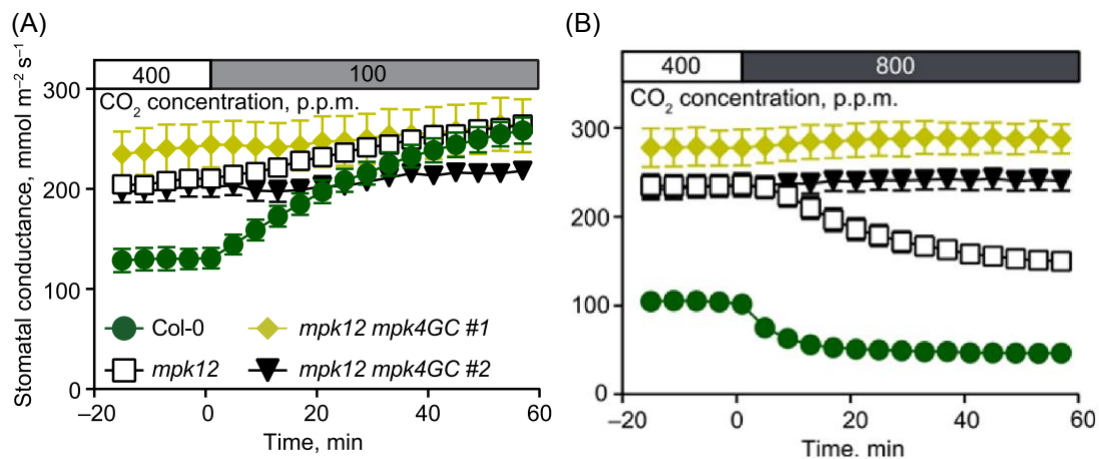


Figure 5: MPK12 and MPK4 regulate CO₂-induced stomatal closure in concert.

The transgenic mutant line *mpk12* reveals a ‘more open stomata’ phenotype and reduced sensitivity to a drop in CO₂ concentration (A; 100 ppm). While *mpk12* is still responding to high CO₂ (B; 800 ppm), the double mutant *mpk12 mpk14GC* is fully CO₂-insensitive under high as well as low CO₂ conditions. Data represents means of n=6-7, ±SEM. Taken from Töldsepp *et al.* (2018).

The Multi-antimicrobial extrusion protein (MATE)-type transporter Resistance to high CO₂ (RHC1) was identified as a putative guard cell HCO₃⁻ sensor (Tian *et al.*, 2015). However, according to Töldsepp *et al.* (2018), this protein might only play a minor role in CO₂ signalling. Moreover, it is believed that RHC1 is not part of the unidentified signalling cascade leading up to MPK12 and MPK4 phosphorylation. Instead, data suggests that both MPK12/4 and RHC1 inhibit a negative regulator of the high CO₂ signalling pathway, known as High leaf temperature 1 (HT1) (Hashimoto *et al.*, 2006; Tian *et al.*, 2015; Hõrak *et al.*, 2016). Upon inactivation of HT1 activity, CO₂ signal transduction is no longer suppressed. Initially, it was believed that HT1 in its active form would target Open stomata 1 (OST1), which is a kinase that phosphorylates NADPH oxidases and thereby mediates the generation of reactive oxygen species (ROS) during ABA-induced closure responses (Pei *et al.*, 2000; Song *et al.*, 2014; Matrosova *et al.*, 2015; Tian *et al.*, 2015). This assumption was based on studies that had shown a physical interaction between OST1 and HT1 via bimolecular fluorescence complementation (Matrosova *et al.*, 2015; Tian *et al.*, 2015). However, kinase assays as well as *in vitro* FRET analyses did not confirm the previously observed effect of high CO₂ (or HT1) on OST1 activity and rather suggest an OST1-independent pathway for CO₂ signalling (Hõrak *et al.*, 2016; Hsu *et al.*, 2018; Zhang *et al.*, 2020a). On the other

hand, OST1 has proven to be a main component of the abscisic acid (ABA) signalling pathway (Mustilli *et al.*, 2002). It is established the ABA and CO₂ signalling pathways in guard cells are in part taking place independently from each other but merge at some point, from where they seem to share the same signalling components (Ma and Bai, 2021). Studies have also shown that CO₂-induced stomatal responses depend on basal ABA signal transduction (Raschke, 1975; Hsu *et al.*, 2018; Zhang *et al.*, 2020a). Conversely, ABA signalling appears to occur independently of CO₂ signalling (Hsu *et al.*, 2018).

Growth controlled by abscisic acid 2 (GCA2) has also been proposed as a converging point between CO₂ and ABA signal transduction pathways (Young *et al.*, 2006; Kim *et al.*, 2010). Young *et al.* (2006) postulated that GCA2 is involved in a process defined as ‘Ca²⁺ sensitivity priming’, which appears to be part of both CO₂ and ABA signalling pathways (Hubbard *et al.*, 2012; Engineer *et al.*, 2016). It seems that both stimuli, CO₂ and ABA, enhance (‘prime’) the sensitivity of stomatal closing mechanisms to cytosolic Ca²⁺ (Israelsson *et al.*, 2006; Hubbard *et al.*, 2012). Transgenic plants that lack functional *GCA2* do not show the specific Ca²⁺ pattern that usually occurs during CO₂/ABA-mediated stomatal closure (Young *et al.*, 2006). ROS might constitute another node between CO₂ and ABA signalling pathways. They are generated in the cytosol in response to increased ABA/CO₂ concentrations and contribute to a rise in free cytosolic Ca²⁺ by activating plasma membrane- and tonoplast-located Ca²⁺ channels (Ma and Bai, 2021). The drastic increase in cytosolic Ca²⁺ leads to the activation of the S-type anion channel Slow anion channel 1 (SLAC1), while ALMT12/QUAC1 seems to be regulated in a Ca²⁺-independent way (Geiger *et al.*, 2010; Imes *et al.*, 2013). Furthermore, it was suggested that SLAC1 activation occurs through the leucine-rich repeat receptor-like protein kinase Guard cell hydrogen peroxide-resistant 1 (GHR1) and seems to be inhibited by the kinase HT1 (Hörak *et al.*, 2016).

Stomatal responses to high CO₂ are apparently not only impaired in the absence of SLAC1 but also upon absent ALMT12/QUAC1 (Negi *et al.*, 2008; Meyer *et al.*, 2010). Clearly, *atalmt12* failed to induce as rapid stomatal closure in response to high CO₂ as wild-type plants, while stomatal opening was not affected (Figure 6). ALMT12/QUAC1 plays a major role in driving osmolytes like Mal²⁻, Cl⁻, and NO₃⁻ out

of guard cells for turgor reduction and guard cell shrinkage during stomatal closure, but does not seem to be involved in the stomatal opening processes (Meyer *et al.*, 2010).

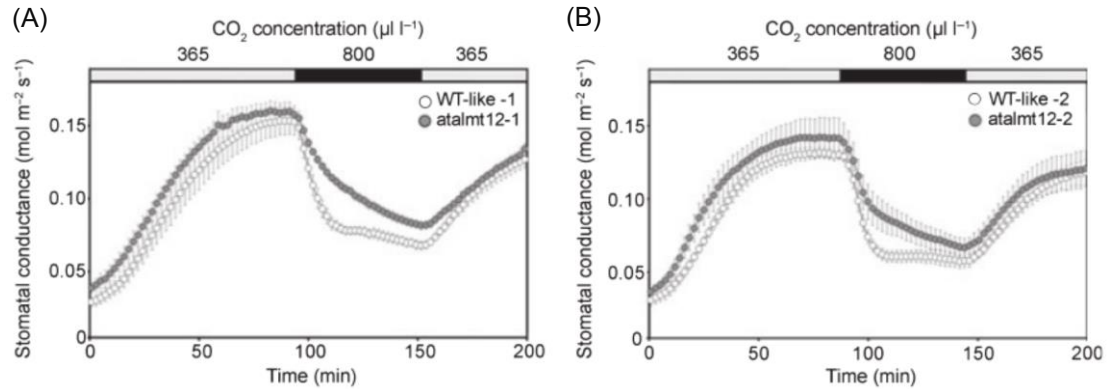


Figure 6: *ALMT12* is required for full high CO₂-induced stomatal responses of guard cells.

Transgenic lines *atalmt12-1* (A) and *atalmt12-2* (B), which carry a loss-of-function mutation in *ALMT12*, are impaired in their full stomatal closure responses to high CO₂ (800 ppm) as revealed by attenuated stomatal conductance rates in comparison to WT-like 1/ WT-like 2. Stomatal opening on the other hand is not affected (n=6 for WT-like-1, n=5 for *atalmt12-1*, and n=4 for *atalmt12-2* and WT-like-2; error bars represent ± SEM). Taken from Meyer *et al.* (2010).

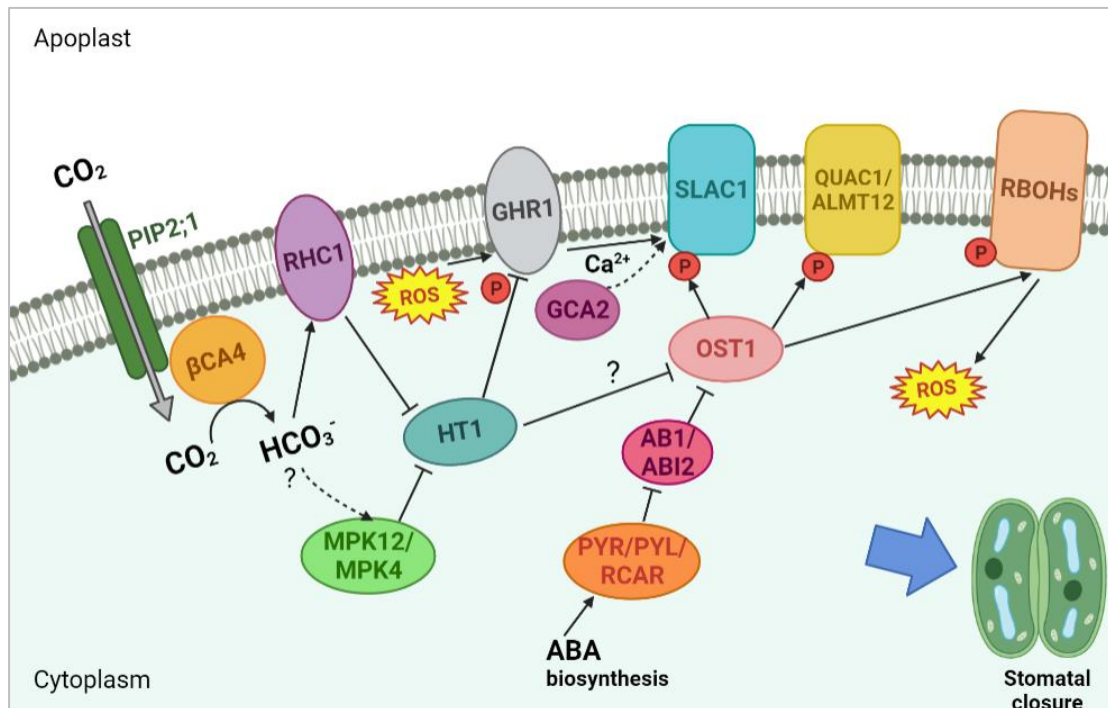


Figure 7: A schematic illustration of the high CO₂ signalling pathway leading to stomatal closure.

Elevated CO₂ concentrations activate carbonic anhydrases, such as βCA1 and βCA4, which catalyse the conversion of CO₂ and H₂O to HCO₃⁻ and H⁺. This reaction leads to the activation of RHC1 and MPK12/4 via an unidentified mechanism, resulting in the suppression of HT1, which is known to be a negative regulator of high CO₂-induced stomatal closure. Initially, HT1 was believed to be a suppressor of OST1 but this assumption is contradictory to recent findings, which clearly exclude a role for OST1 in CO₂ signalling. Up to this point, it was assumed that OST1 would constitute a node between ABA and CO₂ signalling pathways. However, in their active forms, the kinases OST1 and GCA2 generally activate the S-type anion channel SLAC1. OST1 additionally triggers the activation of the R-type channel ALMT12 (also known as QUAC1). Regardless of OST1 being part of CO₂ signal transduction, the activation of SLAC1 and QUAC1/ALMT12 during CO₂ signalling leads to anion efflux and consequently stomatal closure. SLAC1 activity was also found to be suppressed by HT1 (not shown in image). Own work on the basis of Ma and Bai (2021), including information from Hörak *et al.* (2016), Jakobson *et al.* (2016), Zhang *et al.* (2018), and Dubeaux *et al.* (2021). Image was created in BioRender.

GABA, which is a non-proteinogenic amino acid, has recently been identified as another signalling molecule in guard cells (Xu *et al.*, 2021a). Its role in stomatal regulation through inhibition of ALMTs and putative links to CO₂ responses of guard cells will be reviewed in more detail in the next two subsections (1.3.3 and 1.3.4).

1.3.3 GABA functions as a signal in guard cells

For a long time, GABA has been merely known for its metabolic functions in plants. Over the last decade, however, evidence has emerged that GABA plays a vital role in stomatal movements. Eventually, a recent study was able to present clear evidence for GABA's signalling function in guard cells (Xu *et al.*, 2021a).

As mentioned above, ALMT anion channels are a central part of the stomatal opening/closing mechanism of guard cells. At this point, GABA comes into play as it negatively regulates ALMTs that are involved in stomatal opening or closure. Epidermal strip assays as well as leaf feeding assays in a variety of plant species revealed that GABA considerably interferes with stomatal responses to dark-to-light or light-to-dark transitions (Xu *et al.*, 2021a). To be specific, it antagonises stomatal opening during dark-to-light transitions and stomatal closure in response to light-to-dark shifts. Thereby, GABA seemingly does not induce a specific stomatal response

itself. It rather acts like a buffer that dampens the respective response, regardless of it being opening or closure. In terms of stomatal opening, it was demonstrated that GABA negatively modulates tonoplast-localised ALMT9 channels, which drive anions into the vacuole (De Angeli *et al.*, 2013; Xu *et al.*, 2021a). Relative water content quantification proved that ALMT9-dependent GABA inhibition of stomatal opening is crucial for water conservation under drought conditions (Xu *et al.*, 2021a). For stomatal closure responses, a different anion channel from the ALMT gene family seems to be involved, namely plasma membrane-located ALMT12/QUAC1. While ALMT9 activity was ascertained in both epidermal strip assays and leaf feeding assays, ALMT12/QUAC1 involvement could only be detected in epidermal strip assays (Xu *et al.*, 2021a). One explanation for this observation could be the absence of mesophyll in epidermal strips, whereas leaf feeding assays are performed in intact leaves, which comprise both mesophyll and guard cells (Xu *et al.*, 2021a). Hypothetically, signals from the mesophyll might prevent GABA inhibition of ALMT12/QUAC1. Guard cell-mesophyll interaction is another research area with considerable knowledge gaps (Lawson *et al.*, 2014). Interestingly, guard cell-specific GABA synthesis seems to be sufficient for inhibiting stomatal opening. This was demonstrated through comparison between the highly drought susceptible GABA-deficient mutant lines *gad2-1* with the guard cell-specific complementation lines *gad2-1/GC1::GAD2Δ* and *gad2-1/GC1::GAD2-FL*. Stomatal opening was significantly promoted in *gad2-1* and *gad2-2* under drought as well as well-watered conditions; an observation that is in line with another study which found a ‘more open stomata’ phenotype in the double mutant *gad1/2* (Mekonnen *et al.*, 2016). According to Xu *et al.* (2021a), knockout of *GAD2*, which is considered as the main GABA synthesis enzyme in leaves (Bouché and Fromm, 2004), results in GABA depletion in leaves and consequently in the absence of ALMT9 inhibition by GABA. As a result, ALMT9 constitutively drives anions into guard cell vacuoles and thereby counteracts stomatal closure under both normal and drought conditions (Figure 8). On the other hand, the guard cell complementation lines *gad2-1/GC1::GAD2Δ* and *gad2-1/GC1::GAD2-FL* exhibited a wild type-like stomatal closure response upon drought treatment. The transgenic line *gad2-1/GC1::GAD2-FL* carries the full-length *GAD2* sequence in guard cells, whereas *gad2-1/GC1::GAD2Δ* harbours a truncated version of *GAD2* which lacks the auto-inhibitory CaM binding domain and therefore generates GABA constantly. However, under standard conditions, *gad2-1/GC1::GAD2-FL* was not capable of reducing stomatal conductance

to wild-type level, in contrast to *gad2-1/GC1::GAD2Δ* and another transgenic line with constitutive expression of *GAD2-FL* (due to the activity of a 35S-CaMV promoter; Xu *et al.*, 2021a). This might imply that GAD2 operates at full capacity only under stress conditions, while it functions merely at basal levels under normal conditions.

Clearly, Xu *et al.* (2021a) have unveiled GABA's signalling function in guard cells. However, the GABA signalling pathway as a whole is largely unexplored. Moreover, signalling pathways do not occur in isolation but are connected to other signalling cascades, thereby forming a sophisticated signalling network (Taiz *et al.*, 2015). Thus, it is highly likely that the GABA signal transduction pathway converges with other signalling pathways as well, like the high CO₂ signalling cascade for instance. Interestingly, there are several indications of an interplay between GABA and CO₂ signalling pathways, which are discussed in the subsection 1.3.4.

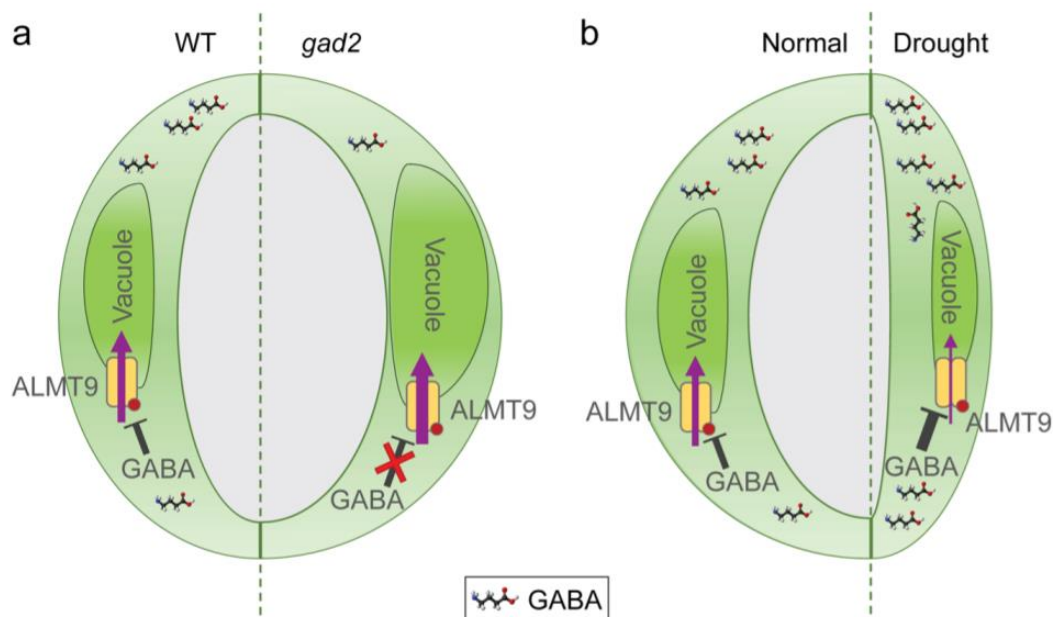


Figure 8: GABA regulates stomatal opening by inhibiting ALMT9 in guard cells.

GABA slows down stomatal opening by inhibiting the tonoplast-localised anion transporter ALMT9. (b) Under well-watered conditions, ALMT9 mediates anion flux into the vacuole and thereby contributes to a rising turgor pressure, which is associated with stomatal opening. In contrast, under drought conditions, ALMT9 is suppressed by GABA and the plasma membrane-localised channel ALMT12 (not shown in the figure) facilitates apoplast-directed anion efflux, leading to a reduction in turgor pressure and stomatal closure. (a) In the GABA-deficient mutant *gad2*, however, GABA is absent and ALMT9 constitutively active, leading to massive anion flux

into the vacuole, which prevents stomatal closure under both normal and drought conditions. Taken from Xu *et al.* (2021a).

1.3.4 Are there functional links between GABA and CO₂ signalling in stomatal regulation?

Importantly, high CO₂ signalling in guard cells triggers an increase in free cytosolic Ca²⁺. Other factors are the release of protons during CA-mediated CO₂ turnover to HCO₃⁻ and the generation of ROS. These are factors that play a role during GABA synthesis. It is established that GAD-mediated GABA synthesis is a process that consumes protons and is stimulated by Ca²⁺ binding. At the same time, ROS accumulation has been reported to hamper the activity of SSA dehydrogenase and 2-oxoglutarate dehydrogenase, which are both linked to enhanced GABA production (Bown and Shelp, 2020). This raises the question if these chemical changes that come along with CO₂ signalling effectively modulate the anabolism and activity of GABA during stomatal movement.

What is more, as mentioned above, ALMT12/QUAC1 is an important downstream component of the high CO₂-induced signalling pathway. It has been observed that stomatal responses to high CO₂ are impaired in the absence of ALMT12/QUAC1 (Meyer *et al.*, 2010). At the same time, this anion channel has been proposed to be negatively regulated by GABA. Thus, the question occurs if GABA and high CO₂ signalling pathways are cross-linked, either via downstream targets like ALMTs or more indirectly through upstream signalling components. Furthermore, it is known that GABA synthesis by GAD enzymes results in the release of CO₂ as a side-product into the cytosol. As alterations in CO₂ concentrations have been found to modulate stomatal activity, the question arises if GABA synthesis-dependent cytosolic CO₂ accumulation influences CO₂ signalling in guard cells.

1.4 The role of GABA in plant carbon metabolism

1.4.1 CO₂ is a product of GABA synthesis and a substrate of photosynthesis

Long-term studies like the so-called Free-air carbon dioxide enrichment (FACE) experiment have demonstrated that plants significantly increase their net biomass production in response to CO₂-enriched air (Norby and Zak, 2011). A variety of different plant species has been examined within the scope of this experiment and overall, a 40% increase in photosynthetic rates has been observed in plants that were subjected to CO₂ concentrations between 475 – 600 ppm (concentrations above ambient CO₂; $\cong \sim\sim 417$ ppm; NOAA/ESRL, 2021). CO₂ is absorbed by plants from the atmosphere as building material of which they are composed of, i.e. carbon skeletons (Taub, 2010). These carbon skeletons are synthesised during the carbon (or dark) reactions of photosynthesis. One explanation for the stimulating effect of high CO₂ levels on photosynthetic rates and consequently plant growth is that, at ambient CO₂ levels, most plants are lacking the amount of CO₂ that they would require to operate at their highest photosynthetic capacity (Ziska *et al.*, 2009). Before CO₂ is chemically reduced during the carbon reactions of photosynthesis, it is fixed by a key enzyme of photosynthesis, known as Ribulose 1,5-bisphosphate carboxylase/oxygenase or short Rubisco (Figure 9) (Jensen, 2004; Taub, 2010). In response to increased CO₂ concentrations, the carboxylase activity of Rubisco is significantly promoted at the expense of Rubisco's oxygenase activity (Jensen, 2004). Importantly, Rubisco's oxygenation reaction (also referred to as photorespiration) is much less energy efficient than its carboxylation activity, as it leads to the accumulation of 2-Phosphoglycolate, whose removal requires numerous catabolic steps (Wingler *et al.*, 2000). The increased carboxylation to oxygenation ratio at high CO₂ is another explanation for the observed elevation in photosynthetic capacity and biomass of plants. Considerably, an increase in photosynthetic rates occurs only when growth conditions are favourable. In other words, only if water, nutrient, and light availability are sufficient, elevated CO₂ levels will stimulate plant growth. Furthermore, after an initial exponential growth in photosynthetic rates, a steady state is reached. This occurs due to a limited rate of ribulose-1,5-bisphosphate (RuBP) regeneration (Sharkey *et al.*, 2007).

Photosynthetic rates under low CO₂ (below 200 ppm) are limited by the availability of substrate required to achieve maximum rates of Rubisco carboxylase activity (V_{cmax})

(Sharkey *et al.*, 2007). V_{cmax} as well as the maximum rate of electron transport to CO_2 (J_{max}) are both factors that can be used for determining biochemical limitations on photosynthetic rates and are calculated by fitting a mathematical model to the response of photosynthesis to varying CO_2 concentrations (Farquhar *et al.*, 1980; Stinziano *et al.*, 2019). Plotting assimilation (A) rates against intercellular CO_2 concentrations (C_i) is a way to evaluate the photosynthetic acclimation of plants to alterations in their environment (Stinziano *et al.*, 2019). It also helps to understand how future environmental conditions might shape carbon assimilation in plants.

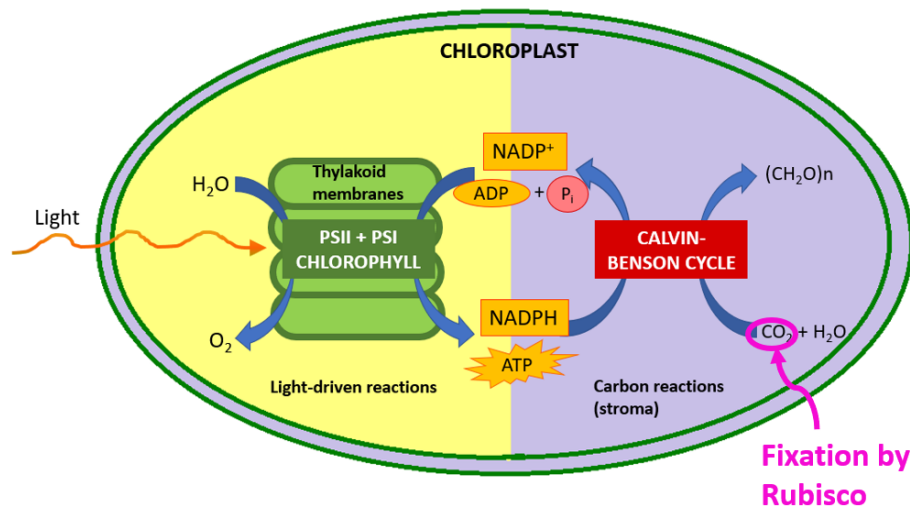


Figure 9: Overview of simplified photosynthetic reactions in plants.

Photosynthesis comprises two main types of reactions, the light-driven reactions at the thylakoid membrane in chloroplasts and the dark or carbon reactions in the chloroplast stroma. The light-driven reactions generate the energy storage compound ATP as well as the reducing agent NADPH for the subsequent carbon reactions. As part of the carbon reactions, Rubisco fixes CO_2 , which constitutes the substrate for the carbon skeletons that are generated during the Calvin-Benson cycle and thereby reduces the intercellular CO_2 concentration. Own work on the basis of Buchanan and Wolosiuk (2015).

Photosynthesis is a process that generates the sugars that serve as fuel molecules for another major metabolic process in which GABA synthesis might play an important role, namely cellular (or aerobic) respiration.

1.4.2 GABA deficiency is linked to alterations in respiratory carbon metabolism

Principally, cellular respiration is the process that releases the energy that is stored in the form of sugars (predominantly starch and sucrose) (Møller *et al.*, 2015; O'Leary and Plaxton, 2016). It comprises three main pathways; namely glycolysis, which occurs as a gradual degradation of sugars into pyruvate, the Krebs cycle, during which pyruvate is fully oxidised to CO₂, and ultimately, the synthesis of the energy storage form ATP via the electron transport chain (Møller *et al.*, 2015). Notably, plant aerobic respiration is extremely flexible as plants are sedentary organisms and are consequently required to be highly adaptive to their surroundings (O'Leary and Plaxton, 2016). The term 'metabolic flexibility' refers to the ability of plants to perform one metabolic step in multiple different ways (Plaxton, 2010). The GABA shunt pathway, which bypasses the Krebs cycle, is a fitting example for this 'metabolic flexibility' as it is activated in response to a number of different environmental stress factors. Significantly, two molecules of CO₂ are released into the mitochondrion during the Krebs cycle, while one CO₂ molecule is generated inside the mitochondrion in a preceding reaction that is catalysed by the pyruvate dehydrogenase complex (PDC; Figure 10). Conversely, O₂ is consumed during the mitochondrial electron transport chain reaction (not shown), resulting in the formation of H₂O. The point where the amount of CO₂ absorbed during photosynthetic carbon assimilation is equal to the quantity of CO₂ released by cellular respiration is defined as compensation point and gives information about the equilibrium between photosynthetic, respiratory, and photorespiration rates (Smith *et al.*, 1976; Sandquist, 2015).

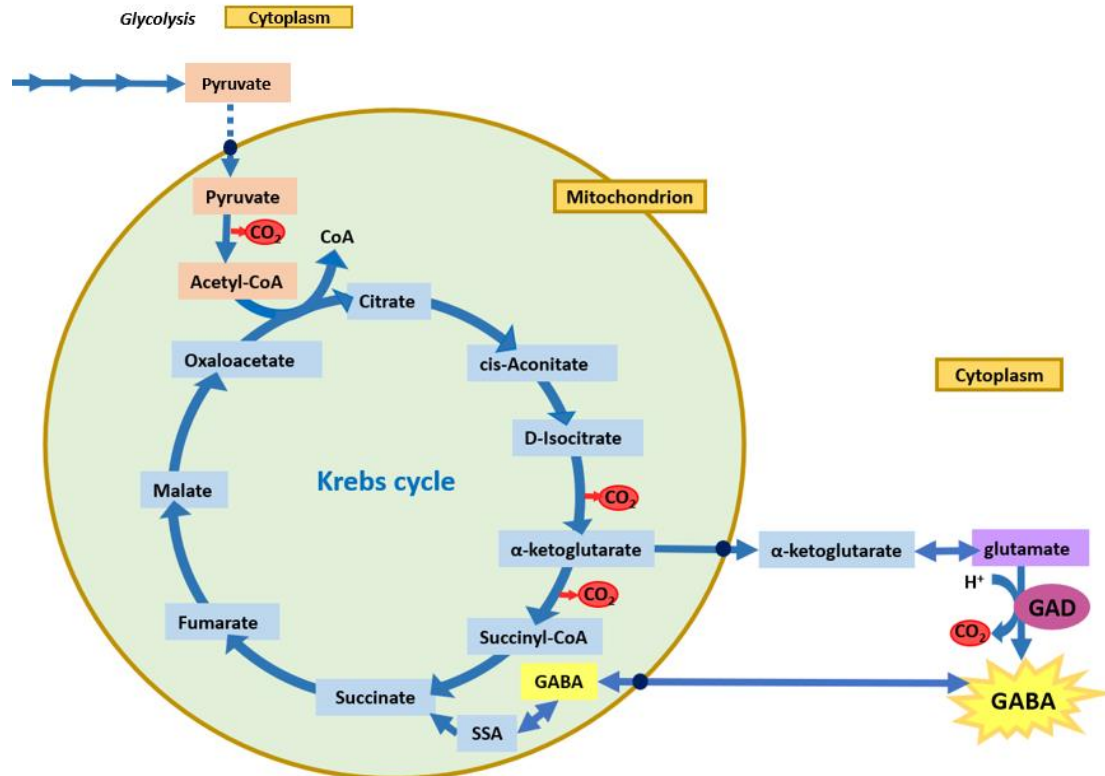


Figure 10: Simplified scheme of the Krebs cycle and GABA shunt in plants.

The Krebs cycle (also known as TCA cycle) and pyruvate decarboxylation are part of cellular respiration and generate three molecules of CO₂ inside the mitochondrion, while the GABA shunt pathway is associated with the release of one CO₂ molecule into the cytoplasm. For simplification, enzymes have been omitted. Own work on the basis of Gilliam and Tyerman (2016) and O'Leary and Plaxton (2016).

1.4.3 Which role does GABA play in carbon metabolism?

Under normal conditions, GAD activity has been found to fluctuate throughout the day, having its maximum three hours after the beginning of the new day cycle (Pelvan *et al.*, 2021). Not only GABA, but also CO₂, is released into the cytosol as a side-product of this activity. Since CO₂ is the main substrate for photosynthetic carbohydrate synthesis, its concentration in the leaf alternates in coordination with the diurnal rhythm of photosynthesis (Geiger and Servaites, 1994; Matthews *et al.*, 2017). Hence, there is a question of whether CO₂ generated during the GABA shunt pathway has an effect on the photosynthetic activity of plants. So far, not much research has been conducted in that regard. Solely, Zeng *et al.* (2021) has found an effect of GABA on net photosynthetic rates in creeping bentgrass. Upon GABA treatment for several days and

in the absence of a stress factor, no difference in net photosynthetic rates was detected (Zeng *et al.*, 2021). Contrary to this, GABA application induced a significant increase in net photosynthetic rates in combination with heat stress (Zeng *et al.*, 2021). However, exogenous GABA has been applied to these plants, which does not give any indication of the effect of GABA synthesis on the photosynthetic capacity of plants.

Moreover, GABA is an important plant metabolite, and its synthesis interacts with the Krebs cycle. Specifically, GABA synthesis takes place via the GABA shunt pathway, which bypasses the Krebs cycle. When GAD enzymes are absent and GABA synthesis is halted, plants have been found to accumulate large amounts of glutamate. To be precise, a previous study by Mekonnen *et al.* (2016) detected highly increased glutamate concentrations in root and shoot tissue of the loss-of-function mutant *gad1/2*. However, this study does not provide any information about the sink for the significantly increased amounts of glutamate. What happens if several GAD genes are knocked out and GABA synthesis via the GABA shunt is eliminated? Furthermore, how does the disruption of the GABA shunt affect carbon metabolism in roots? These are all interesting questions that demand clarification.

1.5 Research gaps

Based on the review above, research gaps pertaining to GABA are summarised and remain to be addressed:

- Information on GABA function in guard cells is in general widely unexplored. To date, most of the GABA signalling components have not been identified.
- It is not known how GABA crosstalk occurs with other signals.
- There is a possibility that the CO₂ signal transduction pathway is linked to GABA signalling; however, this putative link has not yet been researched.
- Despite a few indications of a putative link, GABA synthesis in connection with photosynthetic rates has not been rigorously investigated.
- Previous research has shed some light on the effect of blocked GABA synthesis on the respiratory carbon metabolism in plants. However, many pieces of the puzzle are still missing.

1.6 Project objectives

Overall, this research sought to unravel parts of the GABA signalling network in guard cells and to explore the role of GABA in the photosynthetic and respiratory carbon metabolism of plants. In doing so, this work aimed at gaining beneficial knowledge for developing water use-efficient plants with regard to the continuous increase in global CO₂ levels.

Initially, this study investigated a putative connection between GABA and CO₂ signalling in guard cells via genetic manipulation of GABA metabolism. For this purpose, this project used mutants with impaired GABA synthesis to investigate the effect of GABA deficiency on high CO₂-induced stomatal responses through a series of physiological and genetic studies. Later, the same transgenic lines were used for determining the effect of GABA deficiency on carbon metabolism and photosynthetic CO₂ uptake as well as on biomass accumulation under high CO₂ conditions.

Taken together, two main objectives were set for this study:

- Objective 1 (Chapter 2): Ascertain whether GABA metabolism contributes to the regulation of stomatal CO₂ responses.
- Objective 2 (Chapter 3): Elucidate whether impaired GABA metabolism alters carbon metabolism and plant growth.

Two appendices are included which discuss preliminary results that were very intriguing but could not be replicated in subsequent experiments.

- Appendix I: Preliminary results revealing accelerated guard cell responses to CO₂ in *gad2-2*.
- Appendix II: Preliminary results showing increased photosynthetic rates in *gad1/2/4/5*.

As this thesis is written in the form of a combination of Conventional thesis and Thesis by publication (Chapter 2 and 3 are written in the form of paper manuscripts), content-related repetitions could not be avoided.

Chapter 2: GABA deficiency does not result in reduced CO₂ sensitivity in Arabidopsis

Adriane Piechatek^{1,2}, Xueying Feng^{1,2}, Na Sai^{1,2}, Changyu Yi³, Bhavna Hurgobin³, Mathew Lewsey³, Johannes Herrmann⁴, Peter Ache⁴, Tobias Müller⁵, Rainer Hedrich⁴, Bo Xu^{1,2,*} & Matthew Gilliam^{1,2,*}

¹ Plant Transport and Signalling Lab, ARC Centre of Excellence in Plant Energy Biology, Waite Research Institute, Glen Osmond, SA 5064, Australia

² School of Agriculture, Food and Wine, Waite Research Precinct, University of Adelaide, Glen Osmond, SA 5064, Australia

³ Animal, Plant and Soil Science, La Trobe University, Melbourne, VIC 3086, Australia

⁴ Institute for Molecular Plant Physiology and Biophysics, University of Würzburg, Würzburg 97078, Germany

⁵ Department of Bioinformatics, University of Würzburg, Würzburg 97078, Germany

* Correspondence should be addressed to:

Dr Bo Xu
Email: b.xu@adelaide.edu;

Professor Matthew Gilliam
Email: matthew.gilliam@adelaide.edu.au
Phone: +61 8 8313 8145

Key words: ALMTs, CO₂ signalling, GABA, genomics, MPK12, stomatal movement.

Statement of Authorship

| | |
|---------------------|---|
| Title of Paper | GABA deficiency does not result in reduced CO ₂ sensitivity in Arabidopsis |
| Publication Status | <input type="checkbox"/> Published <input type="checkbox"/> Accepted for Publication <input type="checkbox"/> Submitted for Publication <input checked="" type="checkbox"/> Unpublished and Unsubmitted work written in manuscript style |
| Publication Details | Piechatzek, A., Xu, B., Feng, X., Sai, N., Yi, C., Hurgobin, B., Lewsey, M., Hermann, J., Ache, P., Müller, T., Hedrich, R., Gilliam, M. (2022). GABA deficiency does not result in reduced CO ₂ sensitivity in Arabidopsis. |

Principal Author

| | | | | |
|--------------------------------------|--|------------|------|------------|
| Name of Principal Author (Candidate) | Adriane Piechatzek | | | |
| Contribution to the Paper | Designed and conducted the experiments, analysed most of the data, interpreted it, and wrote the manuscript. | | | |
| Overall percentage (%) | 75 | | | |
| Certification: | This paper reports on original research I conducted during the period of my Higher Degree by Research candidature and is not subject to any obligations or contractual agreements with a third party that would constrain its inclusion in this thesis. I am the primary author of this paper. | | | |
| Signature | <table border="1" style="width: 100%;"> <tr> <td style="width: 80%;"></td> <td style="width: 20%;">Date</td> <td>13/01/2022</td> </tr> </table> | | Date | 13/01/2022 |
| | Date | 13/01/2022 | | |

Co-Author Contributions

By signing the Statement of Authorship, each author certifies that:

- i. the candidate's stated contribution to the publication is accurate (as detailed above);
- ii. permission is granted for the candidate to include the publication in the thesis; and
- iii. the sum of all co-author contributions is equal to 100% less the candidate's stated contribution.

| | | | | |
|---------------------------|---|------------|------|------------|
| Name of Co-Author | Bo Xu | | | |
| Contribution to the Paper | Supervised and designed experiments, was involved in building the <i>GC1::MPK12</i> vector construct for <i>gad2-1</i> complementation, performed the <i>Agrobacterium</i> transformation, floral dipping and screening of the complementation lines, measured GABA content in <i>gad2-2</i> leaves, interpreted data, and edited the manuscript. | | | |
| Signature | <table border="1" style="width: 100%;"> <tr> <td style="width: 80%;"></td> <td style="width: 20%;">Date</td> <td>14/01/2022</td> </tr> </table> | | Date | 14/01/2022 |
| | Date | 14/01/2022 | | |

| | | | | |
|---------------------------|---|------------|------|------------|
| Name of Co-Author | Xueying Feng | | | |
| Contribution to the Paper | Involved in sample preparation for the microarray analysis and measured GABA content in <i>gad1/2/4/5</i> leaves. | | | |
| Signature | <table border="1" style="width: 100%;"> <tr> <td style="width: 80%;"></td> <td style="width: 20%;">Date</td> <td>20/01/2022</td> </tr> </table> | | Date | 20/01/2022 |
| | Date | 20/01/2022 | | |

| | | | |
|---------------------------|---|------|------------|
| Name of Co-Author | Na Sai | | |
| Contribution to the Paper | Assisted in stomatal aperture measurements. | | |
| Signature | | Date | 14/01/2022 |

| | | | |
|---------------------------|---|------|------------|
| Name of Co-Author | Changyu Yi | | |
| Contribution to the Paper | Conducted the analysis of the RNA-seq data. | | |
| Signature | | Date | 19/01/2022 |

| | | | |
|---------------------------|--|------|------------|
| Name of Co-Author | Bhavna Hurgobin | | |
| Contribution to the Paper | Analysed the whole genome sequencing data. | | |
| Signature | | Date | 19/01/2022 |

| | | | |
|---------------------------|--|------|---------|
| Name of Co-Author | Mathew Lewsey | | |
| Contribution to the Paper | Supervised the RNA-seq and whole genome sequencing analyses. | | |
| Signature | | Date | 19/1/22 |

| | | | |
|---------------------------|--|------|------------|
| Name of Co-Author | Johannes Herrmann | | |
| Contribution to the Paper | Conducted preliminary CO ₂ response curves. | | |
| Signature | | Date | 18.01.2022 |

| | | | |
|---------------------------|-------------------------------------|------|------------|
| Name of Co-Author | Peter Ache | | |
| Contribution to the Paper | Supervised the microarray analysis. | | |
| Signature | | Date | 19.01.2022 |

| | | | |
|---------------------------|------------------------------|------|---------|
| Name of Co-Author | Tobias Müller | | |
| Contribution to the Paper | Analysis of microarray data. | | |
| Signature | | Date | 18.1.22 |

| | | | |
|---------------------------|------------------------------------|------|------------|
| Name of Co-Author | Rainer Hedrich | | |
| Contribution to the Paper | Contributed to the project design. | | |
| Signature | | Date | 19.01.2022 |

| | | | |
|---------------------------|---|------|------------|
| Name of Co-Author | Matthew Gilliam | | |
| Contribution to the Paper | Supervised and designed the project, interpreted data, and edited the manuscript. | | |
| Signature | | Date | 20/01/2022 |

Abstract

Optimal stomatal regulation is highly important for plant adaptation to changing environmental conditions, and for maintaining crop yield. GABA has recently been identified as a regulator of stomatal aperture. However, the GABA signalling network in guard cells is largely unexplored. Here, we investigated a putative connection between GABA signalling and the more clearly defined CO₂ signalling pathway in guard cells to investigate whether this could contribute beneficial knowledge for plant improvement in the context of an increasing global atmospheric CO₂ concentration. The *Glutamate decarboxylase* (*GAD*) knockout lines *gad2-1*, *gad2-2*, and *gad1/2/4/5*, which have dramatically reduced GABA concentrations, were examined for their sensitivity to various CO₂ concentrations by monitoring transpiration rates and stomatal apertures. Our findings show a phenotypical discrepancy between the allelic mutant lines *gad2-1* and *gad2-2*, which is reflected in opposing CO₂ responses – a weakened response in *gad2-1* (GABI_474_E05) in contrast to a wild-type response of *gad2-2* (SALK_028819). Through transcriptomic and genomic investigations, we could trace the response of *gad2-1* to an additional deletion of full-length *Mitogen-activated protein kinase 12* (*MPK12*) in the GABI-KAT line. Guard cell-specific expression of *MPK12* under the guard cell promoter *GCI* complemented the *gad2-1* CO₂ phenotype, which confirms previous studies outlining the importance of *MPK12* to CO₂ sensitivity. Additionally, we found the GABA-modulated anion channel *ALMT9*, which contributes to opening, to be functionally redundant in low CO₂-triggered stomatal opening responses. Our results confirm that GABA has a role in modulating the rate of stomatal opening and closing – but not in response to CO₂ *per se*. Furthermore, these findings demonstrate the necessity of performing genetic analyses in parallel to phenotypical studies, and the use of examining several mutant alleles, to reduce the risk of misleading phenotypical interpretations.

Introduction

Pairs of guard cells delineate a stomatal pore to regulate the rate of gas exchange, a process that emits oxygen (O₂) and water (H₂O) vapour, and absorbs carbon dioxide (CO₂). This process defines a plant's carbon gain and water use efficiency (the ratio of carbon gain per water loss), which are factors essential for underpinning crop yield and drought tolerance (Leakey *et al.*, 2019).

The non-proteinogenic amino acid γ -aminobutyric acid (GABA) was recently shown to be a signal that regulates plant gas exchange and stress tolerance by modulating the opening and closure of stomata (Xu *et al.*, 2021a). GABA is predominantly produced via the GABA shunt pathway, which bypasses reactions that are ordinarily confined to the mitochondrial-based Krebs cycle, converting the C5 amino acid glutamate into the C4 amino acid GABA through succinate (C4), thereby generating carbon dioxide (CO₂) as a side-product within the cytoplasm. The GABA synthesis enzyme Glutamate Decarboxylase 2 (GAD2) is detectable in nearly all plant tissues and was found to be the main GABA synthesis enzyme in leaves (Mekonnen *et al.*, 2016; Xu *et al.*, 2021a). Consequently, its absence results in a drastic reduction in GABA in leaf tissue, which makes *GAD2* knockout lines (*gad2*) perfect models for investigating the signalling role of GABA in guard cells. In total, five *GAD* isoforms exist in *Arabidopsis thaliana*. *GAD1* is predominantly abundant in root tissue and *GAD5* is mainly expressed in male gametes, while *GAD3* and *GAD4* are lowly expressed under non-stressed conditions in leaves and roots (Scholz *et al.*, 2015). Conversely, in response to various stresses like cold, drought, hypoxia, and salt stress, the expression of *GAD4* has been found to be significantly increased (Renault *et al.*, 2010); *GAD3* is stimulated by heat or high light stress (Balfagón *et al.*, 2021).

To date, it is known that GABA modulates stomatal movement by negatively regulating so-called Aluminium-activated malate transporters (ALMTs). In guard cells, ALMTs are not activated by aluminium (rather by anions and voltage), and mediate anion flux across guard cell membranes to attenuate stomatal responses, be it closure or opening. Xu *et al.* (2021a) demonstrated that plants lacking GABA synthesis in leaves display enhanced stomatal opening due to de-regulated ALMT9 activity in guard cells. ALMT9 has been identified as a tonoplast-localised anion channel that is crucial for stomatal opening (De Angeli *et al.*, 2013). Plasma-membrane located ALMT12/Quick-

activating anion channel 1 (QUAC1) could potentially be involved in GABA regulation of the stomatal closure processes but needs further verification (Xu *et al.*, 2021a). However, it is unknown whether additional signalling events lead up to the inhibition of ALMTs by GABA, further, is it not clear if other well-known signalling elements are involved in this process. In plants, signalling pathways are known to have elements of crosstalk, and due to the complex nature of cellular processes never function in isolation. Rather they are integrated in a dense signalling web (Taiz *et al.*, 2015). In this context, Xu *et al.* (2021a) discovered that GABA application significantly affects stomatal responses to the stomatal signals abscisic acid (ABA), hydrogen peroxide (H₂O₂), and coronatine, so GABA may well interact with multiple abiotic and biotic stress signalling pathways. In addition, as GABA impacts were also detected under standard light/dark cycles, GABA is likely to modulate standard responses to the environment (Xu *et al.*, 2021a).

Another stomatal regulator is CO₂, which is consumed by plants as a fuel molecule for photosynthetic carbon assimilation. In high concentrations, CO₂ is known to stimulate stomatal closure by indirectly activating specific anion channels, including ALMT12/QUAC1 (Meyer *et al.*, 2010). Stomatal closure in response to elevated CO₂, is a way of plants to increase their water use efficiency. This is because under high CO₂ conditions, plants are sufficiently supplied with CO₂ for photosynthesis and can therefore afford to promote stomatal closure in order to minimise water loss through transpiration (Lawson *et al.*, 2014). On the other hand, low CO₂ concentrations promote stomatal opening (Roelfsema and Hedrich, 2005; Hiyama *et al.*, 2017).

Besides ALMT12/QUAC1, the β -Carbonic anhydrases β -CA1 and β -CA4, as well as the Mitogen-activated protein kinase 12 (MPK12) are also crucial signalling components of the CO₂ signal transduction pathway. The CO₂-binding proteins β -CA1 and β -CA4 were found to initiate the high CO₂ signalling pathway by catalysing the conversion of CO₂ to bicarbonate (Hu *et al.*, 2010). Plants lacking these carbonic anhydrases have impaired sensitivity to high CO₂ as revealed by studies in the double mutant *ca1/ca4* (Hu *et al.*, 2010). MPK12 functions as an inhibitor of a major negative regulator of high CO₂-induced stomatal closure, known as High leaf temperature 1 (HT1) (Hashimoto *et al.*, 2006; Hörak *et al.*, 2016; Jakobson *et al.*, 2016).

Hence, if MPK12 is absent, as it is the case in the T-DNA insertion line *mpk12-3*, stomatal closure is constantly repressed by HT1 (Jakobson *et al.*, 2016).

Here, we sought to reveal the effect of GABA depletion on stomatal CO₂ sensitivity. We present the results of gas exchange measurements in low (100 ppm) and high (800 ppm) CO₂-treated GABA-deficient mutant lines in combination with sequencing-based approaches. Based on evidence from this study, we could link a genomic deletion of *MPK12* to reduced CO₂ responsiveness in one of our GABA-deficient lines. In doing so, we eliminated the possibility of GABA deficiency being associated with a decrease in CO₂ sensitivity. At the same time, we show that the GABA-regulated anion channel ALMT9 as well as ALMT6 are not part of low CO₂-induced stomatal opening and present data that imply links between mutations in *MPK12/GAD2* and the deregulation of essential stomata-related genes.

Materials and Methods

Plant materials and growth conditions

In all experiments, the following *Arabidopsis thaliana* lines were used: Wild-type ecotype Columbia (Col-0) and mutant lines generated in the Col-0 background. The two allelic mutant lines *gad2-1* (GABI_474E05) and *gad2-2* (SALK_028819), as well as additional transgenic lines, such as *pop2-8* (SALK_007661), *mpk12-3* (SAIL_543_F07), *ca1/ca4* (*SALK_106570* and *WiscDsLox508D11*), *almt6-1* (GABI_259D05), and *almt6-2* (FLAG_425D02) were obtained from the Arabidopsis Biological Resource Centre (ABRC). The transgenic line *almt9-1* (SALK_055490) was described in a previous study (De Angeli *et al.*, 2013). The transgenic mutant line *gad1/2/4/5* was generated by crossing *gad1-1* (SALK_017810), *gad4* (SALK_106240), *gad5* (SALK_203883), and *gad2-1* (GABI_474E05), and was obtained from Shuqun Zhang (Deng *et al.*, 2020). Further mutant lines used in this study were *gad2-1/GC1::GAD2Δ* and *gad2-1/GC1::GAD2-FL* (full length), which express either a truncated version of *GAD2* or full-length *GAD2* fused to a guard cell-specific promoter (GC1) in *gad2-1* and are described elsewhere (Xu *et al.*, 2021a). The mutant line *gad2-1/GC1::MPK12* was generated through transformation of *gad2-1* with the guard cell-specific promoter GC1 (Yang *et al.*, 2008) fused to full-length *MPK12*. All primers

used for the genotyping PCR and cloning reactions are listed in the [Supplementary Table 1](#). Unless noted, all plants were raised in hydroponics for five to six weeks following Conn *et al.* (2013): all seeds were stratified for two days at 4°C in the dark and then transferred to short-day growth conditions [10 hrs light (~100 $\mu\text{mol photons m}^{-2} \text{ s}^{-1}$)/14 hrs dark, average temperature of 22°C, and 56% relative humidity]. In the first three to four weeks, plants grew within the lids of customised black microcentrifuge tubes, with a hole, that had been filled with 0.7% agar and fitted on a 24 well floating microtube rack. The small hydroponic container that contained the rack was filled with a modified Hoagland solution, named Germination Solution (GS), which was replaced every week (nutrient composition is listed in the [Supplementary Table 2](#)). The small hydroponic container was covered with cling wrap, which was perforated after two weeks of growth and completely removed three days before the plant transfer to hydroponic tanks. For a smooth transition from GS to higher concentrated Basal Nutrient Solution (BNS; nutrient composition is listed in the [Supplementary Table 3](#)), after two weeks of growth, GS was exchanged by 1/3 with BNS on three subsequent days. After three and a half weeks of growth, seedlings with the same estimated leaf area were transplanted to individual 50 mL falcon tubes (with bottoms removed) inside aerated hydroponic tanks filled with BNS. For all experiments, different genotypes grew side by side in a randomised design under the same growth conditions and were analysed within a time period of 10 days.

GABA measurement

Leaf GABA concentrations were determined using Ultra performance liquid chromatography (UPLC). Briefly, rosette leaves were snap-frozen and homogenised in liquid nitrogen using mortar and pestle. For UPLC analysis, about 50 mg of ground tissue were used. The UPLC analysis was conducted at the Australian Centre for Plant Functional Genomics (University of Adelaide) in accordance with a method described by Xu *et al.* (2021a).

Gas exchange measurements

Stomatal conductance in single leaves of five-to-six-week-old *Arabidopsis* plants was determined using an AP4 Porometer (Delta-T Devices). Leaf recordings (n=3) of three leaves per plant (n=6) were averaged.

For time-resolved infrared gas analysis in whole rosettes, four-and-a-half- to five-and-a-half-week-old plants were transferred to 50 mL falcon centrifuge tubes filled with BNS solution (Conn *et al.*, 2013). The falcon tubes were placed in a LI-6400XT Portable photosynthesis system (LI-COR Biosciences) fitted with a 6400-17 Whole Plant *Arabidopsis* Chamber. Prior to the gas exchange measurements, to maximise gas exchange rates, plants were acclimated to an irradiance of 350 $\mu\text{mol photons m}^{-2} \text{s}^{-1}$ for one hour (30W LED Panel, Arlec). Transpiration rates of the plants inside the chamber were recorded in response to a variety of CO₂ concentrations (100 ppm, 800 ppm, and 400 ppm CO₂) under the following chamber conditions: 350 $\mu\text{mol photons m}^{-2} \text{s}^{-1}$ light intensity with a portion of 10% blue light, 50-60% relative humidity, an average temperature of $\sim 22^{\circ}\text{C}$, and an airflow rate of 350 $\mu\text{mol s}^{-1}$. Measurements were logged every minute and IRGAs were matched at the start of the measurements and then every five minutes. The duration of measurements at each CO₂ step was one hour. For data visualisation, the first 30 minutes of recording (at 400 ppm CO₂) were omitted. During the last hour of the experiment, gas exchange was recorded in the dark. Following the gas exchange measurements, leaf rosette surfaces of each analysed plant were captured using a Nikon D5100 camera and were measured using the 'Threshold Color' tool in ImageJ. All recorded transpiration rates were normalised to leaf rosette areas. Changes in transpiration rates per minute were calculated using the formula $d\text{Transpiration}/dt$ (min).

Stomatal aperture and density measurements

For stomatal aperture determination, five-to-six-week-old plants of four different genotypes (Col-0, *gad2-1*, *gad2-2*, and *gad1/2/4/5*) were adapted to a light intensity of $\sim 350 \mu\text{mol s}^{-1} \text{m}^{-2}$ (30W LED Panel, Arlec) at growth room conditions ($\sim 22^{\circ}\text{C}$ and 56% relative humidity) for one hour before being transferred to a LI-6400XT Portable photosynthesis system (LI-COR Biosciences) fitted with a 6400-17 Whole Plant *Arabidopsis* Chamber for another hour at CO₂ concentrations of either 400 or 800 ppm.

At the same time, the light intensity was set to $350 \mu\text{mol s}^{-1} \text{m}^{-2}$. The chamber temperature (22°C) and the humidity (50-60 %) were adjusted to growth room conditions. For the production of epidermal peels, single leaves were cut off from the 'CO₂-treated' plants and glued with their adaxial side to the adhesive surface of a piece of masking tape. Sticky tape was attached to the abaxial side of the leaf and the abaxial epidermal layer was peeled off along with the sticky tape. Instantly, the epidermal peel was transferred to a specific opening buffer which contained 5 mM malic acid, 10 mM 2-(N-morpholino) ethanesulfonic acid (MES), and 10 mM potassium chloride (KCl), adjusted to a pH of 6.0 using 1 M Tris (Xu *et al.*, 2021a). Images of stomata were captured using an Axiophot Pol Photomicroscope (Carl Zeiss) with a 20x objective lens and were measured using either the image processing program ImageJ or a newly developed stomata auto-measuring system, known as StomaAI (Sai *et al.*, 2022).

For stomatal density determination, stomata were captured using a 10x objective lens on an Axiophot Pol Photomicroscope (Carl Zeiss) and were counted using the multi-point tool in ImageJ. For each experiment, three to four biological plant replicates and three leaves per replicate were used.

Real time quantitative PCR (RT-qPCR)

Total RNA was extracted from whole rosette leaves of five-week-old plants using three to four biological replicates per genotype. The rosette leaves were snap-frozen and ground to fine powder in liquid N₂. Next, the ground material was transferred to 1 mL TRIzol reagent (TRIzol RNA Isolation Reagents, Invitrogen) inside a 2-mL microcentrifuge tube. After having added 200 μL acidic chloroform, the mixture was centrifuged at maximum speed for 15 min at 4°C . The supernatant was transferred to tubes that contained 500 μL 100% Isopropanol and the mixture was incubated for 10 min at 4°C . After centrifugation at 11 400 rpm at 4°C , the isolated RNA was washed in 1 mL 75% EtOH and air-dried. Subsequently, the dried RNA pellet was resuspended in 20 μL nuclease-free H₂O. For removal of gDNA contamination, the RNA eluate was treated with DNase using a TURBO DNA-free kit (Ambion) in accordance with the manufacturer's instructions.

The RNA integrity was evaluated using gel electrophoresis as well as spectrophotometry (ND-1000; NanoDrop Technologies), whilst the RNA quantity was determined fluorometrically (Invitrogen Qubit[®] fluorometer).

For cDNA synthesis, 1 µg of total RNA from each sample was used in combination with SuperScript III Reverse Transcriptase (Invitrogen) and oligo(dT) primers (Promega) in accordance with the manufacturer's instructions.

For subsequent RT-quantitative PCR analysis, RT-qPCR primers specific to *GAD2* and the housekeeping genes *Elongation-factor-1-α* (AT1G07940) and *Actin2* (AT3G18780; Supplementary Table 1) were used in combination with a KAPA SYBR[®] FAST qPCR Kit (Roche) in a QuantStudio 12 Flex Real-Time PCR System (Thermo Fisher Scientific). Relative *GAD2* expression was normalised to manually calculated normalisation factors based on the geometric mean of the two housekeeping genes that had been amplified in parallel with *GAD2*. Copy numbers of the *GAD2* transcript were estimated using a standard curve that had been created on the basis of a dilution series of exactly defined cDNA amounts. For each biological sample, three technical replicates were used. The qPCR run was conducted as follows: 40 cycles of a 2-step protocol: 1 sec at 95°C, 20 sec at 56°C. The melt curve was generated through heating from 56°C to 95°C by 0.05°C per second.

Reverse transcriptional PCR

For reverse transcriptional PCR, the cDNA (synthesis as described in the previous subsection, RT-qPCR) was amplified using Phire[®] Green Hot Start II PCR Master Mix enzyme (Thermo Fisher) and primer pairs specific to *MPK12*, *GAD2*, and the housekeeping gene *Actin2* (Supplementary Table 1), following the manufacturer's instructions. The PCR run was conducted as follows: initial denaturation phase for 1 min at 98°C, followed by 25 cycles (*GAD2* and *Actin2*) or 28 cycles (*MPK12*) of 10 sec at 98°C, 10 sec at 57°C, and 20 sec of 72°C, and a final extension for 1 min at 72°C. In a last step, the PCR products were verified via gel electrophoresis.

Microarray analysis

RNA isolation from rosette leaves was performed as described in an earlier subsection (RT-qPCR). RNA integrity and concentration were determined using an RNA 6000 Labchip on an Agilent 2100 BioAnalyzer (Version C.01.069) at ACRF Cancer Genomics Facility (SA Pathology and University of South Australia). Only samples with an RNA Integrity Number (RIN) ≥ 8 were selected for the microarray analysis.

Microarray hybridisation and data processing were conducted by collaborators at Julius-von-Sachs-Institute for Biosciences (Department of Molecular Plant Physiology and Biophysics - Botany I, University of Wuerzburg, Germany), following a method described by Dittrich *et al.* (2019).

RNA sequencing

Total RNA was extracted from whole rosettes of five-week-old plants using TRIzol reagent (Invitrogen) and four biological replicates per genotype (Col-0, *gad2-1*, and *gad2-2*). The extraction as well as the RNA integrity and RNA concentration determination were conducted as previously described (RT-qPCR and Microarray subsections).

RNA sequencing was performed at Animal Plant and Soil Sciences (La Trobe University, Australia). In brief, RNA-seq libraries were constructed using the TruSeq Stranded mRNA Library Prep Kit in accordance with the manufacturer's instructions (Illumina) and sequenced on a NextSeq500 system (Illumina) as 75 bp single-end reads with at least 30 million reads per sample. Reads quality were examined using FastQC (<http://www.bioinformatics.babraham.ac.uk/projects/fastqc>) and low-quality reads and adapters were trimmed using Trim Galore (<https://github.com/FelixKrueger/TrimGalore>). To obtain transcript abundances as transcripts per million (TPM) and estimated counts, trimmed reads were mapped to the Arabidopsis reference transcriptome (Araport 11) using Salmon (Cheng *et al.*, 2017; Patro *et al.*, 2017). Gene-level TPM and count estimates were obtained using tximport (Soneson *et al.*, 2016). Genes with total counts more than 10 in all samples were retained for differential gene expression analysis using DESeq2 and genes with a false discovery rate < 0.05 were considered as differentially expressed genes (Love *et al.*,

2014). Gene ontology enrichment analysis was performed using clusterProfiler (Yu *et al.*, 2012). A Principal component analysis (PCA) was calculated using the DESeq2 R package and the 500 highest variable genes and plotted using the ggplot2 package in R.

Whole genome resequencing

Genomic DNA was extracted from five-week-old plants of five different genotypes (Col-0, *gad2-1*, *gad2-2*, *gad1/2/4/5*, and *pop2-8*).

For tissue disruption, whole rosette leaves were snap-frozen and ground to fine powder in liquid N₂ using mortar and pestle. Afterwards, 750 µL DNA extraction buffer and 750 µL phenol/chloroform/iso-amyl alcohol (25:24:1) were added to 150 mg of the disrupted leaf tissue on ice. After the solution was mixed by vortexing, it was centrifuged at maximum speed for 15 min. For removal of residual RNA, the upper fraction, which contained the gDNA, was treated with 10 µL autoclaved RNase (50 mg/ml) at 4°C for three days. To investigate the presence of RNA contamination, the solution was loaded onto a 1% agarose gel for gel electrophoresis at 70 V for 1 ½ hours. When the sample had been assessed as RNA free, the rest of the gDNA solution was used for a second phenol/chloroform/isoamyl alcohol extraction to remove the remaining RNase. For this purpose, 720 µL phenol/chloroform/iso-amyl alcohol (25:24:1) was added to the RNase-treated aqueous supernatant and the mixture was placed on ice. Prior to a 10 min centrifugation step at room temperature, all samples were mixed thoroughly by vortexing. Afterwards, the upper aqueous phase was isolated and mixed with 504 µL 3 M Na-acetate (pH 4.8)/Isopropanol (1:10). The gDNA was allowed to participate overnight at -20°C and then pelleted by centrifugation at maximum speed for 20 min. Ice-cold 75% Ethanol was added twice to wash the gDNA pellet. For each wash step, the samples were mixed thoroughly by vortexing and centrifuged at maximum speed for 1 min. In a last step, the DNA pellet was dissolved in 50 µL nuclease-free H₂O.

Traditionally, RNase digestion is performed on the purified DNA eluate and requires a repetition of the phenol/chloroform/isoamyl alcohol extraction, washing steps and DNA elution. Here, to prevent additional DNA loss through a second round of DNA purification, RNase treatment was conducted in between two

phenol/chloroform/isoamyl alcohol extractions in order to save additional washing and DNA elution steps (Healey *et al.*, 2014).

Validation of the insertion lines was performed as described by Narsai *et al.* (2017) by our collaborators at Animal Plant and Soil Sciences (La Trobe University). Whole genome resequencing was performed to confirm that only single insertions were present in the T-DNA insertion lines, and that the insertions occurred at the target loci/genes. Genomic libraries were constructed with the Nextera DNA Library Preparation kit (Illumina) according to the manufacturer's instructions. Libraries were enriched for large inserts by size selection with a 0.5X SPRI beads clean up. Sequencing in paired-end mode (75 bp) on an Illumina NextSeq 500 yielded 27-45 M reads per library. The quality of the raw data was assessed using FASTQC (Andrews, 2010) v.0.11.8 and multiQC (Ewels *et al.*, 2016) v.1.8. Reads were trimmed with Trim Galore! (<https://github.com/FelixKrueger/TrimGalore>) v.0.6.3 and mapped with bowtie2 (Langmead and Salzberg, 2012) v. 2.4.1 against a modified version of the TAIR10 (Col-0 ecotype) genome comprising TAIR10, the pROK2 and pAC161 T-DNA vector sequences as supplementary chromosomes (Ülker *et al.*, 2008). In order to identify T-DNA insertion sites, read pairs with one read mapping to the TAIR10 genome and its mate mapping to the T-DNA vector were extracted from the mappings with the following awk commands: '\$3 == "pROK2_T-DNA_only" && \$7! = "="' (for T-DNA insertion lines in pROK2 vector) and '\$3 == "pAC161_T-DNA" && \$7! = "="' (for T-DNA insertion lines in pAC161 vector). Read mappings were visualised using JBrowse (Buels *et al.*, 2016) v.1.16.9.

Plasmid construction and plant transformation

For guard cell-specific complementation, *gad2-1* from the GABI_Kat collection was complemented with *MPK12* driven by the guard cell-promoter *GCI*. The coding sequences of *MPK12* (At5G05440) and *pGCI* [At1g22690; Yang *et al.* (2008)] were separately amplified from *Arabidopsis thaliana* using Phire[®] Green Hot Start II PCR Master Mix enzyme (Thermo Fisher) with primer sets that are listed in the [Supplementary Table 1](#). Both PCR fragments were combined with each other through an overlap PCR. The PCR product was then inserted into a pCR[®]8/GW/TOPO[®] vector (Invitrogen) at EcoR1 restriction sites. In a next step, the pCR8-*pGCI-MPK12*

construct was cloned into the T-DNA destination vector pMDC107 via LR reaction using an LR Clonase™ II Enzyme mix (Invitrogen). Subsequently, the recombinant plasmid was driven into competent *Escherichia coli* (self-prepared) cells via heat-shock transformation. After the cloning construct had been verified by Sanger sequencing, the plasmids were transformed into *Agrobacterium tumefaciens* strain *AGL1* using the Freeze-Thaw Method (Glazebrook and Weigel, 2002). For plant transformation, flowering *gad2-1* mutant lines were floral-dipped into a suspension that contained successfully transformed *Agrobacterium* cells in accordance to a method described by Zhang *et al.* (2006). For gas exchange measurements, T2 plants were used that had been selected on ½ MS medium containing hygromycin (25 µg/mL) and that were later transferred to hydroponics. The presence of *MPK12* in these plants was confirmed via Reverse transcriptional PCR as described above, using the primers listed in the [Supplementary Table 1](#).

Genotyping PCR

For extracting gDNA from leaf tissue, two small young leaf discs were excised and transferred to 1.5 mL reaction tubes. Subsequently, the leaf material was homogenised in 200 µL Edward's buffer that contained 200 mM Tris/HCl (pH 7.5), 200 mM NaCl, 25 mM EDTA, and 0.5% SDS using a disposable pestle (Edwards *et al.*, 1991). Samples were mixed for five seconds by vortexing and centrifuged (13 400 rpm) at room temperature for nine minutes. The DNA was precipitated by mixing the supernatant with Isopropanol (Chem Supply) at a ratio of 1:1 (v/v) before the samples were centrifuged for six minutes at 13 400 rpm. In a next step, the DNA pellet was washed with 300 µL 70% EtOH (Chem Supply), centrifuged at the same speed as before, dried, and resuspended in 100 µL nuclease-free H₂O. The DNA quantity was determined using a ND-1000 Spectrophotometer (NanoDrop Technologies).

The extracted gDNA (100-120 ng/µL) was subsequently amplified using Phire® Green Hot Start II PCR Master Mix enzyme (Thermo Fisher) and the primer sets listed in the [Supplementary Table 1](#), following the manufacturer's instructions. The PCR run was conducted as follows: initial denaturation phase for 3 min at 94°C, followed by 30 cycles of 30 sec at 94°C, 30 sec at 56°C, and 30 sec of 72°C, and a final extension for 10 min at 72°C. In a last step, the PCR products were verified via gel electrophoresis.

Statistical analysis

Unless noted, GraphPad Prism (Version 9.0.0 for Windows) was used for statistical analysis of the data presented in this study. In a first step, it was determined whether the data followed a Gaussian distribution using a D'Agostino & Pearson test.

Depending on the data type, one-way or two-way ANOVA, unpaired or multiple unpaired t-tests were performed. Under the assumption of a Gaussian distribution, one-way Tukey's multiple comparisons test or unpaired t-tests were applied on the data for mean comparisons between different genotypes. If the data was not normally distributed, a one-way ANOVA Dunnett's multiple comparison test was performed. For the statistical analysis of the 'change in transpiration rate' data, two-way ANOVA Tukey's multiple comparison test was used. Changes in stomatal transpiration rates per minute were statistically analysed using multiple one-way Mann-Whitney test (multiple t-tests). All data are presented as mean \pm SEM.

Results

CO₂ sensitivity is abolished in *gad2-1*

To explore the effect of GABA manipulation on CO₂-induced stomatal movement, gas exchange measurements were conducted in intact wild-type (Col-0) plants and the loss-of-function mutant line *gad2-1*. The transgenic line *gad2-1* has recently been studied in detail by Xu *et al.* (2021a) and also as a parental mutant for the double mutant *gad1/gad2* (Mekonnen *et al.*, 2016), and in both studies guard cells were shown to have an aberrant behaviour. First, an attempt was made to replicate the *gad2-1* phenotype that had been observed in Xu *et al.* (2021a). In agreement with previous observations, reduced *GAD2* expression and GABA production and a 'more open stomata' phenotype were detected in *gad2-1* (Supplementary Figures 1 and 2).

In the next step, *gad2-1* and wild-type transpiration rates were monitored in a time-lapse experiment in response to varying CO₂ concentrations (Figure 1 A). In wild-type plants, infrared gas analysis revealed a significant increase in leaf transpiration rates (0.272 ± 0.022 mmol m⁻² s⁻¹ in total) in response to low (100 ppm) and a significant

drop in transpiration rates upon treatment with high (800 ppm) CO₂ (0.384 ± 0.055 mmol m⁻² s⁻¹ in total). A subsequent reduction to ambient CO₂ (400 ppm), brought transpiration rates back to their initial level. In contrast, transpiration rates in *gad2-1* increased by only 0.092 ± 0.017 mmol m⁻² s⁻¹ and decreased by 0.098 ± 0.016 mmol m⁻² s⁻¹ upon low/high CO₂ conditions, revealing a reduced CO₂ sensitivity. Again, the ‘more open stomata’ phenotype was reflected in a higher transpiration rate baseline in *gad2-1* (transpiration rates were higher at the start of the experiment and remained above those of the wild type).

Additionally, we recorded time-resolved CO₂ responses of mutant lines that are impaired in the CO₂ signalling pathway for comparison with the *gad2-1* phenotype. The stomatal phenotype of *mpk12-3* resembled the weakened CO₂ response of *gad2-1*, while the *cal/ca4* transpiration rates were even higher and slightly more alternating (Figure 1 B).

In another experiment, we investigated the CO₂ responsiveness of the guard cell complementation lines *gad2-1/GC1::GAD2Δ* and *gad2-1/GC1::GAD2-FL* (Figure 1 C). These mutants had been complemented either with full-length (FL) *GAD2* or a constitutively active form of *GAD2* specifically in their guard cells. In both cases, transpiration rates varied only slightly in accordance with the alterations in CO₂ concentrations, revealing that CO₂ responsiveness could not be recovered by guard cell specific *GAD2* complementation. Gas exchange measurements in the GABA overproducing T-DNA insertion mutant *pop2-8* (Supplementary Figure 4 A) did not show any differences in transpiration rates in comparison to the wild type.

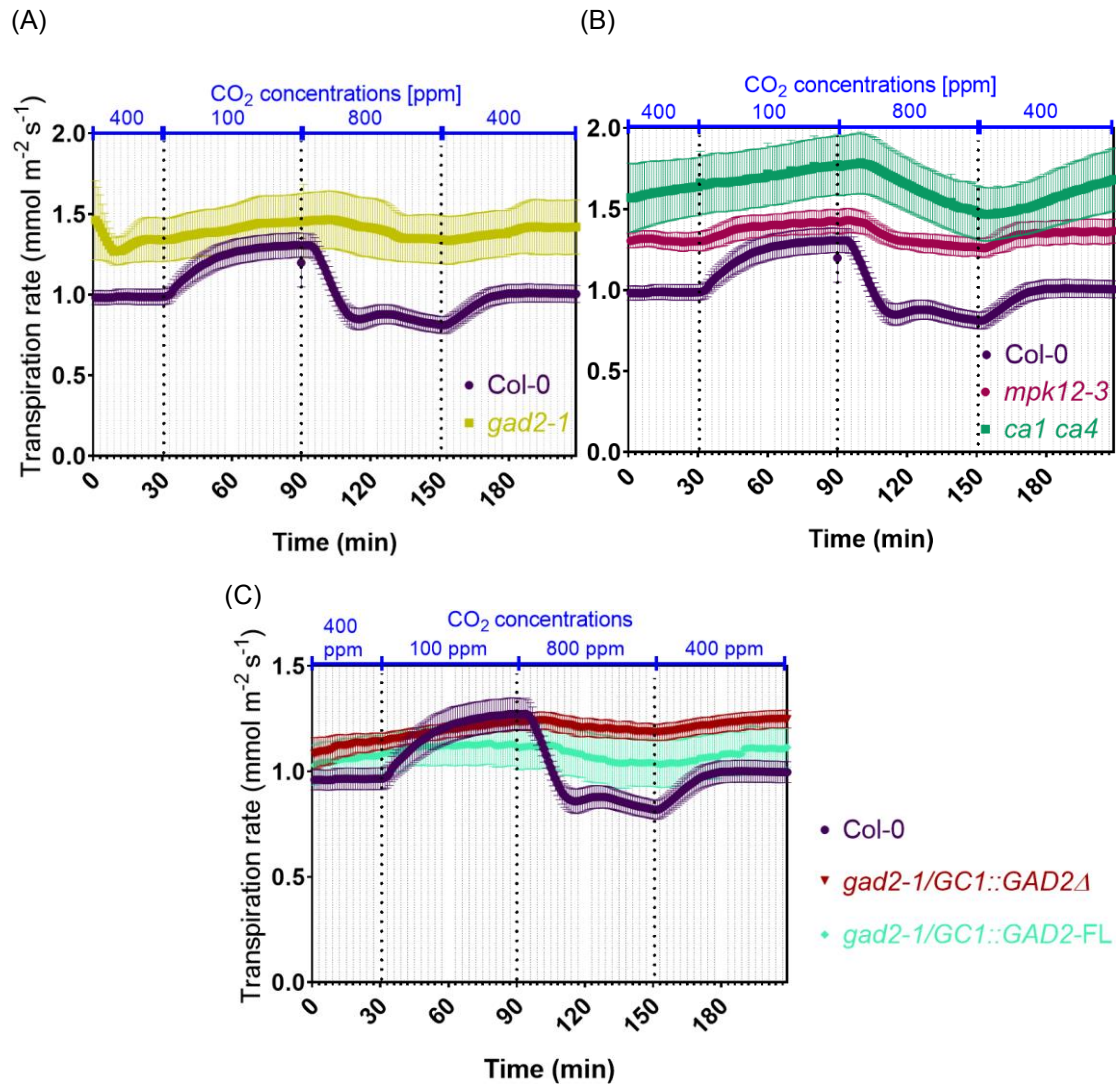


Figure 1: Impaired CO₂ phenotypes in *gad2* and CO₂ signalling mutants.

Time courses of transpiration rates in response to ambient (400 ppm), low (100 ppm), and elevated (800 ppm) CO₂ concentrations in intact *A. thaliana* (A) wild-type (Col-0; n=10), and GABA-deficient *gad2-1* (n=8) plants, (B) CO₂ signalling mutant lines *mpk12-13* (n=3) and *ca1/ca4* (n=5), and (C) guard cell-specific *GAD2* complementation lines *gad2-1/GC1::GAD2Δ* (n=4) and *gad2-1/GC1::GAD2-FL* (Full length; n=4). The complemented mutant lines harbour a guard cell-specific promoter that is either expressing full-length *GAD2* or a truncated version of *GAD2* that lacks the autoinhibitory calmodulin domain, resulting in GABA overproduction. Pooled data from two to three experimental series are shown. Error bars indicate \pm SEM.

Higher order *GAD* mutants are CO₂-sensitive

In order to clarify the effect of knocking out additional *GAD* genes in *gad2-1*, we examined the CO₂ response of the quadruple mutant *gad1/2/4/5* with T-DNA insertions

in four different GAD genes (*GAD1*, *GAD2*, *GAD4*, and *GAD5*; Figure 2). Like *gad2-1*, *gad1/2/4/5* has impaired GABA production as confirmed by UPLC analysis in leaf material (Supplementary Figure 1 A). Note that *gad1/2/4/5* harbours the same mutation in the *GAD2* gene as *gad2-1* (GABI_474E05), as it has been generated through crossing of *gad* single mutants, including *gad2-1* from the GABI-Kat seed collection.

Gas exchange measurements were conducted in intact plants in response to different CO₂ concentrations (400 ppm $\hat{=}$ ambient, 100 ppm, and 800 ppm CO₂). Transpiration rates in *gad1/2/4/5* changed in response to alterations in atmospheric CO₂ concentrations, similar to that observed in wild-type plants (Figure 3 A). When wild-type and *gad1/2/4/5* plants were subjected to low (100 ppm) CO₂, they showed increased transpiration rates, whereas they revealed a reduced transpiration under high (800 ppm) CO₂ conditions (reduced by 0.462 ± 0.092 mmol m⁻² s⁻¹ in *gad1/2/4/5* and by 0.384 ± 0.055 mmol m⁻² s⁻¹ in the wild type; Figure 3 B), both contrasting the CO₂ phenotype of *gad2-1* (reduction in transpiration rates by 0.092 ± 0.017 mmol m⁻² s⁻¹; Figure 3 B). Not only were transpiration rates comparable to wild-type levels, but so were the change in transpiration rates per minute in *gad1/2/4/5* (Figure 3 C). The transpiration rates recordings were in line with the stomatal aperture data (Figure 3 D), which clearly demonstrates a significant reduction in *gad1/2/4/5* (31.44 %) and in the wild type (24.93%) in response to 800 ppm CO₂, whilst stomatal apertures were only slightly reduced in *gad2-1* (9.57%). At the same time, the three different genotypes were found to have comparable stomatal densities on their abaxial leaf surfaces (Figure 3 E). All experiments were conducted at least twice with comparable outcomes.

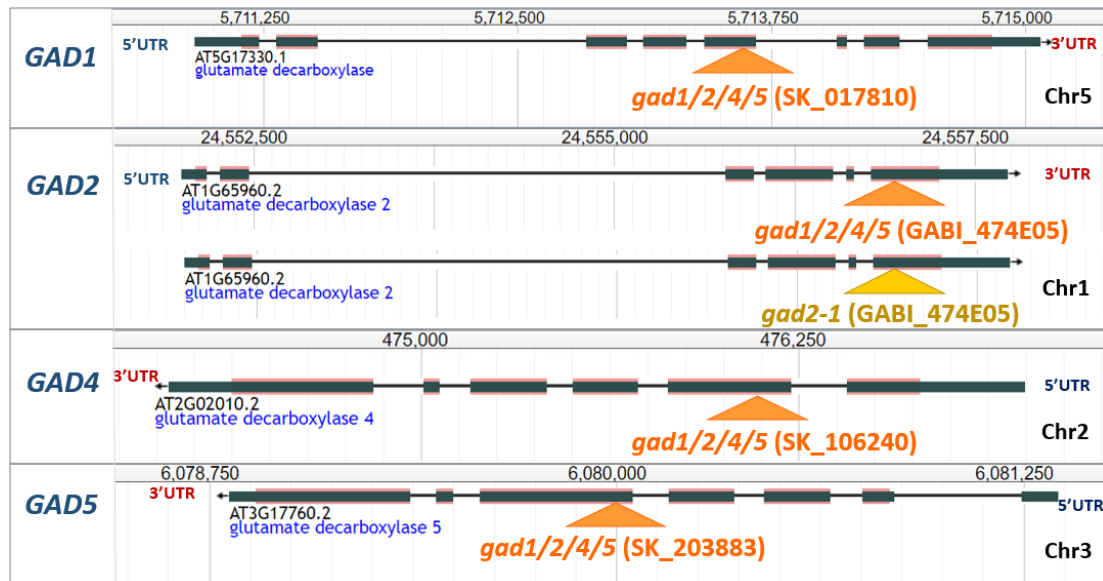
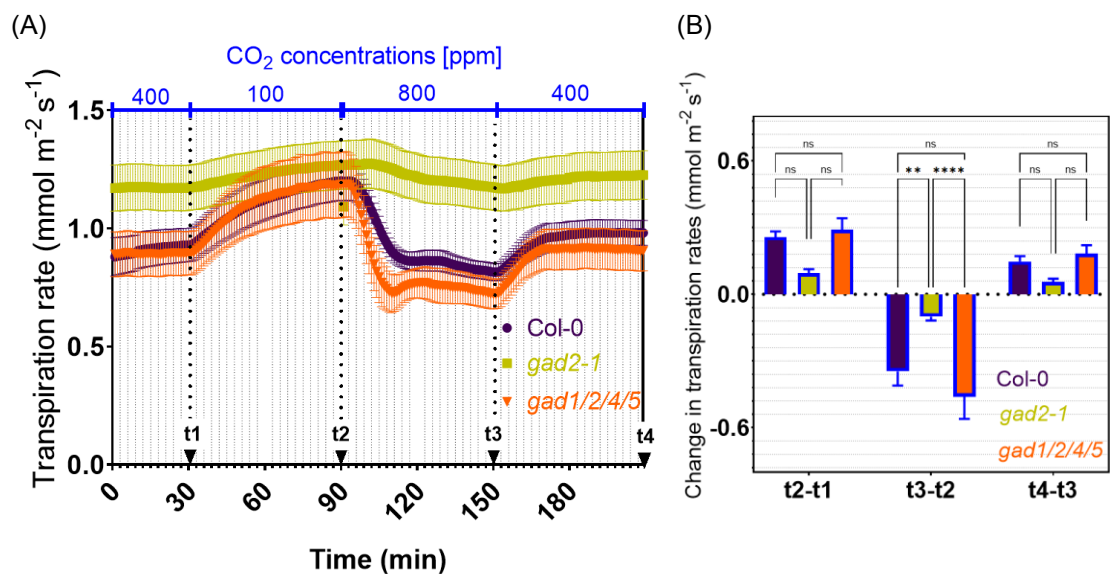


Figure 2: Schematic map of T-DNA insertional sites in the genomes of *gad1/2/4/5* and *gad2-1*.

Overview of T-DNA insertion sites in the genomic regions of *GAD1* (AT5G17330; Chromosome [Chr] 5), *GAD2* (AT1G65960; Chr 1), *GAD4* (AT2G02010; Chr 2), and *GAD5* (AT3G17760; Chr 3) in the quadruple mutant line *gad1/2/4/5*. Like *gad2-1*, *gad1/2/4/5* harbours a GABI_474E05 mutation in the sixth exon of *GAD2*. Gene maps originate from the TAIR10 database.



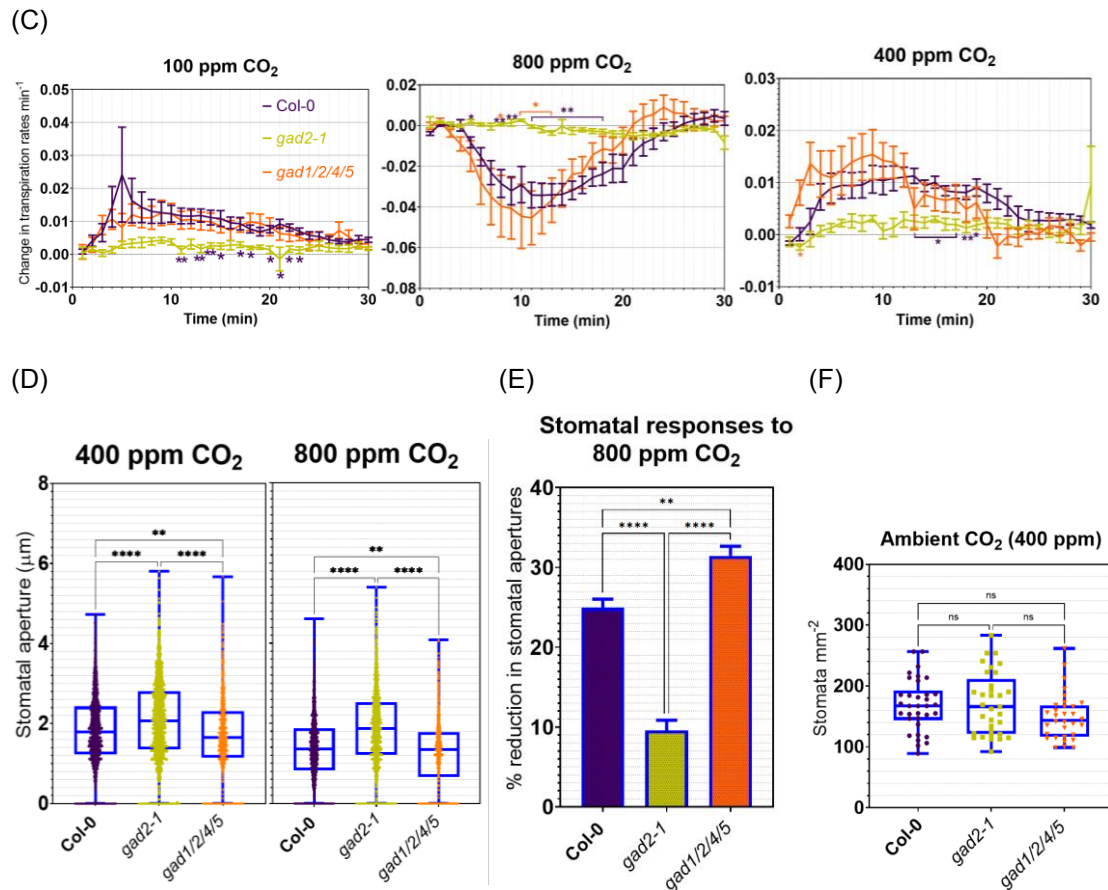


Figure 3: CO₂ responsiveness of *gad1/2/4/5* contrasts with CO₂ insensitivity of *gad2-1*.

(A) Time courses of transpiration rates in response to ambient (400 ppm), reduced (100 ppm), and elevated (800 ppm) CO₂ in intact *A. thaliana* wild-type (*Col-0*; n=10), and GABA-deficient *gad2-1* (n=9) and *gad1/2/4/5* (n=7) plants. On the basis of the data presented in (A), changes in transpiration rates during specific time periods were determined and are illustrated in (B). For calculating these changes, transpiration rates at earlier time points were subtracted from transpiration rates at later points in time. Time points are numbered and denoted by small black arrows in (A). (C) Changes in transpiration rates per minute were calculated using $d\text{Transpiration}/dt$ (min) also on the basis of the time-lapse transpiration rates illustrated in (A). (E) Percentages of stomatal aperture reduction on abaxial leaf surfaces in *Col-0* (n=2217), *gad2-1* (n=1499), and *gad1/2/4/5* (n=1177) in response to 800 ppm CO₂, based on the stomatal aperture data shown in (D). (F) Stomatal densities on abaxial leaf surfaces were determined in *Col-0* (n=34), *gad2-1* (n=33), and *gad1/2/4/5* (n=32). Pooled data from at least two independent experiments is shown. Data was plotted with box and whiskers (D and F): the box illustrates the median, the 25th and 75th percentiles, while the whiskers indicate the minimum and maximum values. Error bars represent \pm SEM. Statistical differences were calculated using multiple Student's t tests (C), two-way (B), or one-way ANOVA (D, E, and F); *P < 0.05, **P < 0.01, ****P < 0.0001.

Allelic mutant lines *gad2-1* and *gad2-2* reveal opposing CO₂ responses

To investigate whether the decreased CO₂ sensitivity in *gad2-1* is indeed linked to the *GAD2* knockout, we evaluated the CO₂ response of another allelic mutant of *GAD2*, known as *gad2-2*. Like *gad2-1*, this mutant line has been generated by a T-DNA insertion in *GAD2*, resulting in defective leaf GABA production as confirmed by UPLC in leaf material (Supplementary Figure 1 B). While *gad2-1* was generated by a T-DNA insertion in exon 6, *gad2-2* contained a T-DNA insertion in the second intron of *GAD2* (Figure 4).

As in *gad2-1*, transpiration rates (Figure 5 A) and stomatal apertures (Figure 5 D) were significantly higher in *gad2-2* than in the wild type at ambient CO₂ (400 ppm). The higher transpiration rates are attributable to larger stomatal apertures in the mutant lines as no differences in stomatal density (on abaxial leaf surfaces) were detected between the wild type and the mutant plants (Figure 5 F).

However, in contrast to *gad2-1*, *gad2-2* revealed a wild-type CO₂ response (Figure 5 A). In response to a concentration shift from 400 to 100 ppm CO₂, transpiration rates in *gad2-2* not only increased more rapidly but also reached a significantly higher level than in *gad2-1*. The maximum change in transpiration rates was 0.429 ± 0.030 mmol m⁻² s⁻¹ in *gad2-2* compared to 0.055 ± 0.023 mmol m⁻² s⁻¹ in *gad2-1* and 0.427 ± 0.029 mmol m⁻² s⁻¹ in the wild type (Figure 5 B). In response to the transition from 100 to 800 ppm CO₂, transpiration rates in *gad2-2* and the wild type dropped to a similar extent. Transpiration rates decreased by 1.067 ± 0.068 mmol m⁻² s⁻¹ in *gad2-2* and by 0.967 ± 0.078 mmol m⁻² s⁻¹ in the wild type, whereas in *gad2-1*, they dropped only by 0.058 ± 0.014 mmol m⁻² s⁻¹ (Figure 5 B). All transpiration rates were consistent with the stomatal widths in the lines (Figure 5 D), which revealed a large reduction in stomatal apertures in *gad2-2* (36.09 %) and the wild type (24.93 %) in response to 800 ppm, whilst only a minor reduction in apertures was detectable in *gad2-1* (9.57 %; Figure 5 E).

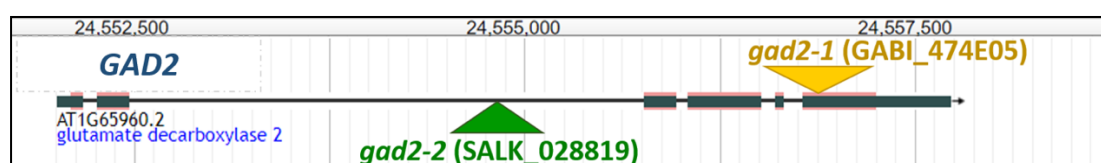


Figure 4: Schematic map of T-DNA insertional sites in the genome of *gad2* mutants.

Localisation of T-DNA insertion sites in the genomic regions of *GAD2* (AT1G65960) on chromosome 1 of the allelic mutant lines *gad2-1* and *gad2-2*. Gene maps originate from the TAIR10 database.

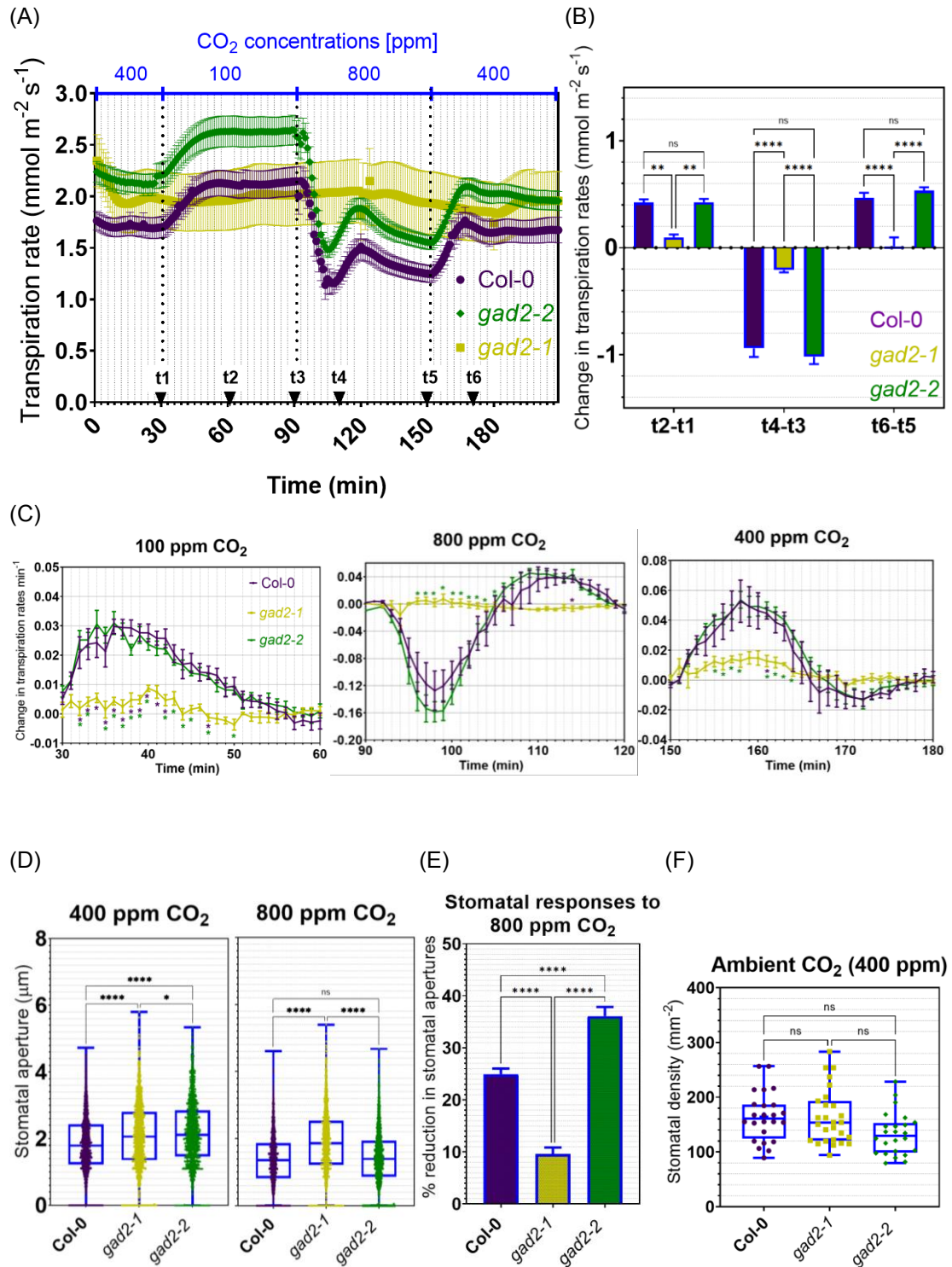


Figure 5: Allelic GAD2 loss-of-function mutants reveal contrary stomatal CO₂ responses.

(A) Time courses of transpiration rates in response to ambient (400 ppm), elevated (800 ppm), and reduced (100 ppm) CO₂ in intact *A. thaliana* wild-type (Col-0; n=7), and GABA-deficient *gad2-1* (n=6) and *gad2-2* (n=8) plants. On the basis of the data presented in (A), changes in transpiration rates during specific time periods were determined and are illustrated in (B). For calculating these changes, transpiration rates at earlier time points were subtracted from transpiration rates at later points in time. Time points are numbered and denoted by small black arrows in (A). (C) Changes in transpiration rates per minute were calculated using $d\text{Transpiration}/dt$ (min), also on the basis of the time-lapse transpiration rates illustrated in (A). (E) Percentages of stomatal aperture reduction on abaxial leaf surfaces in Col-0 (n=2217), *gad2-1* (n=1499), and *gad2-2* (n=842) in response to 800 ppm CO₂, based on the stomatal aperture data shown in (D). (F) Stomatal densities on abaxial leaf surfaces were determined in Col-0 (n=34), *gad2-1* (n=33), and *gad2-2* (n=24). Data was plotted with box and whiskers (D and F): the box illustrates the median, and the 25th and 75th percentiles, while the whiskers indicate the minimum and maximum values. Error bars represent \pm SEM. Statistical differences were calculated using multiple Student's t tests (C), two-way (B), or one-way ANOVA (D, E, and F); *P < 0.05, **P < 0.01, ****P < 0.0001.

Genomic and transcriptomic analyses reveal additional genetic differences in ‘GABA mutants’

The mutant lines *gad2-1* and *gad2-2* had been expected to carry a single T-DNA at two different positions of the same gene (*GAD2*; AT1G65960). Nonetheless, they were found to display contrasting CO₂ responses. Moreover, the presence of additional T-DNA insertions within the GAD genes correlated with the renewed CO₂ sensitivity in *gad1/2/4/5*, despite the *gad2-1* background.

To decipher the genetic cause, comprehensive genomic and transcriptomic studies were conducted in the different GABA-deficient mutant lines (and the GABA-accumulating line *pop2-8*). Whole genome sequencing was performed in the wild type (Col-0) and the mutant lines *gad2-1*, *gad2-2*, *gad1/2/4/5*, and *pop2-8*. For the identification of T-DNA insertion sites in the genome of these lines, discordant reads pairs were extracted, where one mate aligned to the TAIR10 reference genome, and the other mate aligned to the respective T-DNA transformation vector sequence (pROK2 or pAC16). With this approach, we were able to confirm all T-DNA insertional sites. Simultaneously, this approach also uncovered additional mutations in three out of the four mutant lines.

Specifically, the resulting data identified an expected T-DNA insertion in the sixth exon of *GAD2* in *gad2-1* and one in the second intron of *GAD2* in *gad2-2* (Figure 6 A). At the same time, genomic profiling of the *gad2-1* genome also unveiled a non-specific deletion of 4,750 bp in the *MPK12* (AT2G46070) region (18,945,445 bp to 18,950,195 bp) on chromosome 2 of this mutant line (Figure 7 A). This deletion does not only comprise full-length *MPK12* but also full-length *BYPASS2* (*BPS2*; AT2G46080), which is adjacent to *MPK12*. In all the lines tested, *gad2-1* was the only one in which these two genes had been removed. The transgenic mutant line *gad2-2* contained only the target-site mutation.

As expected, the quadruple mutant *gad1/2/4/5* was found to harbour T-DNA insertions in the *GAD1* (AT5G17330), *GAD2* (AT1G65960), *GAD4* (AT2G02010), and *GAD5* (AT3G17760) region (Figure 6 A-D). Note that in the *GAD5* region only one flanking end of the T-DNA insertion was recovered and sequenced. The sequencing data also confirmed that the T-DNA insertion in *GAD2* in the quadruple mutant equals the *GAD2* mutation in the *gad2-1* genome (Figure 6 A). However, the data also points to another, unspecific mutation in the *Phosphofruktokinase 1* (*PFK1*; AT4G29220) region in *gad1/2/4/5* (Figure 7 B). That said, it needs to be taken into account that only one flanking end of the T-DNA insertion was recovered and sequenced. An unspecific mutation was also detected in the genome of the GABA-overproducing mutant line *pop2-8* in addition to the expected mutation in the GABA-T gene (*POP2/GABA-T*; AT3G22200; Supplementary Figure 4). All these specified mutations were absent in the background genome of wild-type ecotype Columbia 0 (Col-0).

As the *Arabidopsis* ecotype Cape Verde Islands (Cvi-0) also displays reduced CO₂ responsiveness and more opened stomata than Col-0 due to a mutation in *MPK12*, the *gad2-1* genome was examined for a potential Cvi contamination by mapping the unmapped reads to the Cvi genome (including T-DNA vector sequences). Apparently, no accidental Cvi contamination was found in the *gad2-1* genome, although some reads could still map (with many SNPs and Indels) to the Cvi genome (Supplementary Figure 5). However, this was also the case for all the other lines (including Col-0), which did not reveal the Cvi phenotype.

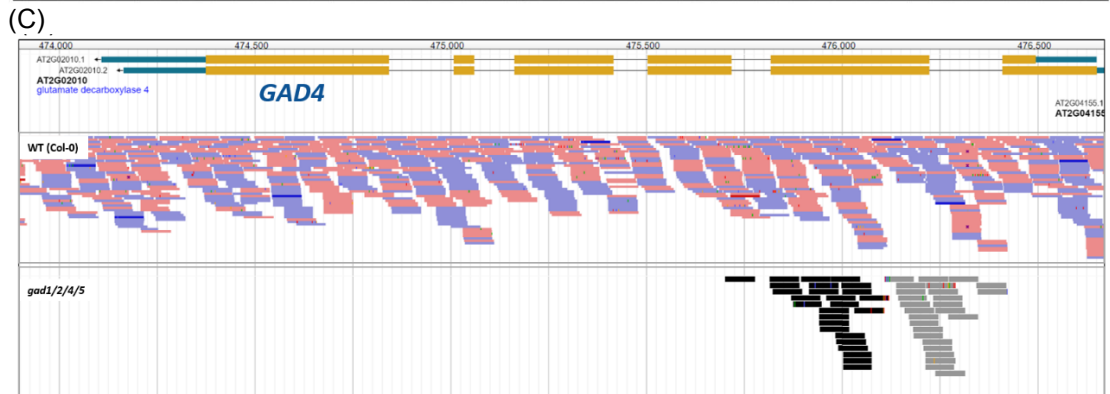
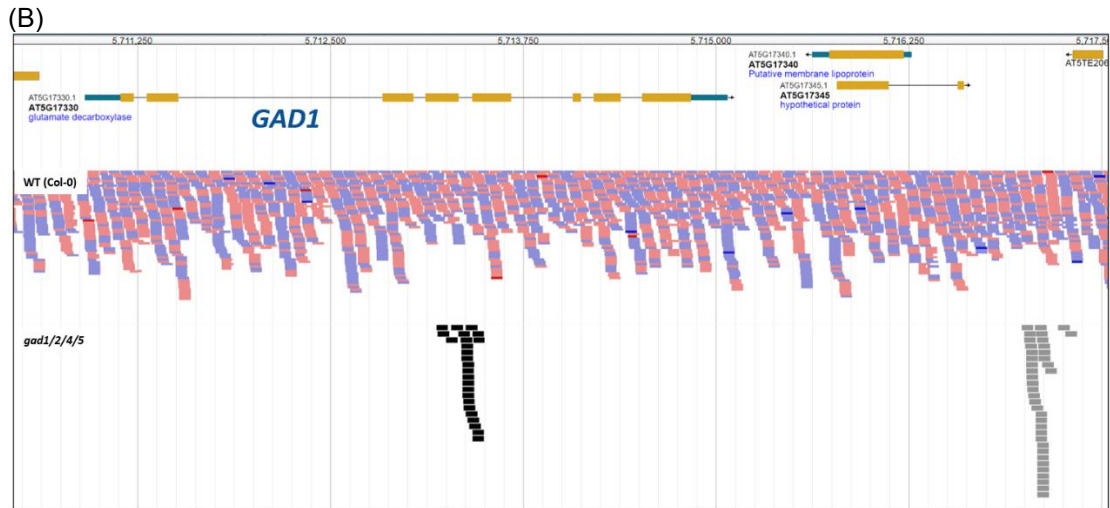
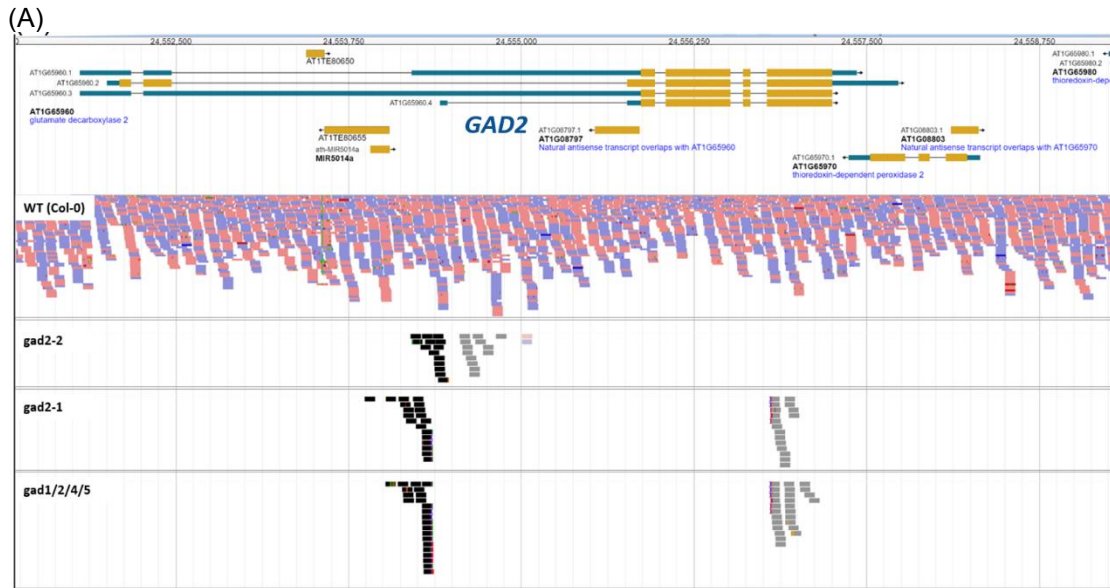


Figure 6: Confirmed T-DNA insertional sites in the genomes of Col-0 and GABA-deficient mutants.

Genome browser view of T-DNA insertion sites in the genomes of the wild type (Col-0), *gad2-1*, *gad2-2*, and *gad1/2/4/5*, as revealed by whole genome sequencing (Illumina). (A) A single T-DNA insertion was detected in the *GAD2* (AT1G65960) region of the *gad2-1*, *gad2-2*, and *gad1/2/4/5* mutant lines. Read mappings show discordant reads (black and grey rectangles) where one mate aligns to chromosome 1 (24,553,868 bp to 24,556,939 bp) of the TAIR10 reference genome and the other mate aligns to the pAC161 vector (*gad2-1* and *gad1/2/4/5*). A smaller insertion was detected at this locus for *gad2-2* where one mate aligns to chromosome 1 (24,554,200 bp to 24,554,817 bp) of the TAIR10 reference genome and the other mate aligns to the pROK2 vector. (B-D) Single T-DNA insertions were found in the (B) *GAD1* (AT5G17330), (C) *GAD4* (AT2G02010), and (D) *GAD5* (AT3G17760) region of *gad1/2/4/5*. Read mappings show discordant reads where one mate aligns to chromosome 5 (B; 5,713,365 bp to 5,715,075 bp), chromosome 2 (C; 475,702 bp to 476,347 bp), and chromosome 3 (D; 6,063,163 bp to 6,080,410 bp) of the TAIR10 reference genome and the other mate aligns to the pROK2 vector. Regarding the *GAD5* mutation, only one flanking end of the T-DNA insertion was recovered and sequenced. No T-DNA insertions were detected in the wild-type genome.

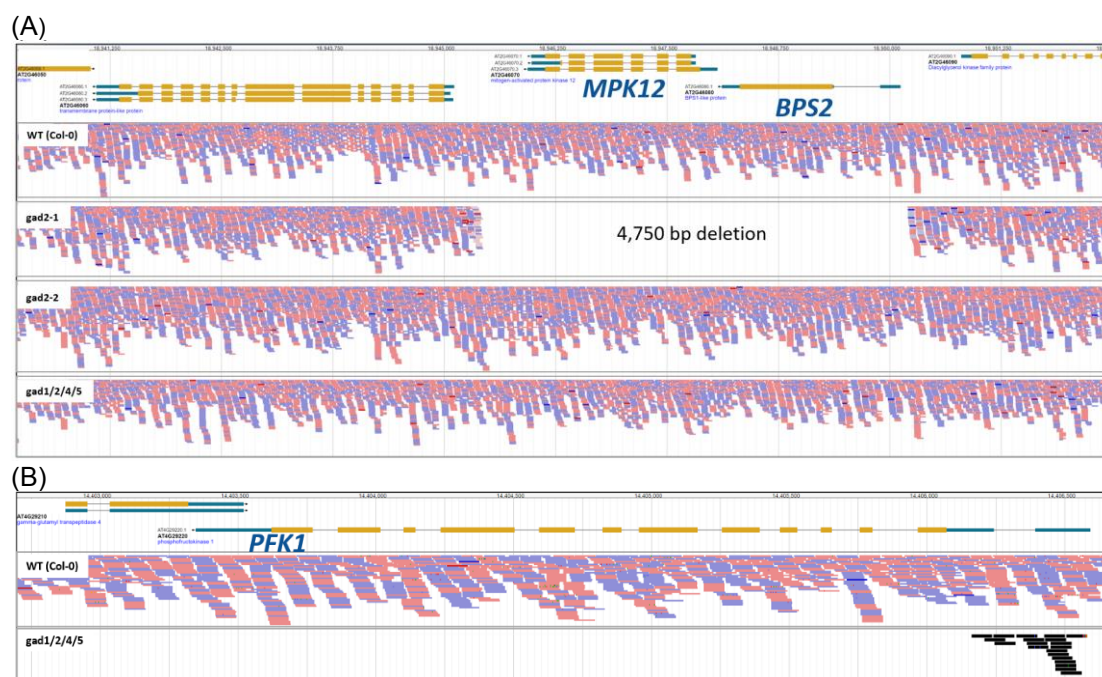


Figure 7: Additional mutations in GABA-deficient mutants as revealed by whole genome sequencing.

Genome browser view of (possible) additional mutations in the genomes of *gad2-1* and *gad1/2/4/5* as revealed by whole genome sequencing (Illumina). (A) A non-T-DNA insertion deletion was detected in the *MPK12* (AT2G46070) region (from 18,945,445 bp to 18,950,195 bp) on chromosome 2 of the transgenic line *gad2-1*. This deletion was absent in the wild type

(Col-0), *gad2-2*, and *gad1/2/4/5* and included another gene (*BPS2*; AT2G46080), adjacent to *MPK12*. (B) A possible additional T-DNA insertion was found in the *Phosphofructokinase 1* (*PFK1*; AT4G29220) region of *gad1/2/4/5* where only one flanking end of the T-DNA insertion was recovered and sequenced. Black rectangles indicate the region where one mate of the read pairs aligns to chromosome 4 (14,406,163 bp to 14,406,506 bp) of the TAIR10 reference genome and the other mate aligns to the pROK2 vector. The flanking sequence overlaps with the 5' UTR #1 and #2 of *PFK1*. No insertion was present in *PFK1* in the wild-type genome.

To complement these studies, we compared gene expression levels between wild-type (Col-0), *gad2-1*, and *gad1/2/4/5* plants using RNA-seq and microarray analysis. The RNA-seq experiment was performed in rosette leaves of the wild type and the two allelic mutant lines *gad2-1* and *gad2-2*. Differential expression analysis was conducted using Deseq2 (Love *et al.*, 2014), where lowly expressed genes (total count number less than 10) were filtered out and genes with $p \text{ adj.} < 0.05$ were considered as differential expressed genes using the Wald-test. A principal component analysis (PCA) separated the three different lines in accordance with their transcription profiles (Supplementary Figure 6). Three samples were removed from the analysis because they did not cluster appropriately in the PCA analysis.

Both *gad2-1* and *gad2-2* possess many genes that were differentially expressed relative to the wild type (Supplementary Figure 7). Pairwise comparison of differentially expressed genes (DEG) numbers identified 1536 DEGs between the wild type and *gad2-1* (643 up and 893 down), and 892 DEGs between the wild type and *gad2-2* (263 up and 629 down). These genes are mostly enriched for functions related to hypoxia and oxygen responses (Supplementary Figure 8).

Numerous genes were also differentially expressed between *gad2-1* and *gad2-2*. Apparently, *gad2-1* has more DEGs than *gad2-2* (in relation to the wild type; $FDR < 0.05$; Supplementary Figure 7 A). However, only three genes were conversely expressed between the two mutants (Supplementary Figure 7 B, C). The allele-specific differentially expressed genes were mainly functionally enriched for glucosinolate/glycoside metabolism (Supplementary Figure 8).

Next, we had a closer look at some specific genes. The corresponding RNA-seq results are presented as \log_2 (transcripts per million [TPM] + 1) after normalisation for gene length and sequencing depth in Figure 8. As expected, we found that the magnitude of

GAD2 expression was significantly lower in both *gad2-1* and *gad2-2* in comparison to the wild type. However, we also discovered that *GAD2* was less expressed in *gad2-2* than in *gad2-1*. Furthermore, the data revealed that the adjacent gene to *GAD2*, known as *Thioredoxin-dependent peroxidase 2* (*TPX2*; AT1G65970; Supplementary Figure 9), was strongly upregulated in *gad2-1* in relation to the wild type and *gad2-2*, while no considerable difference was detected for *TPX1* (AT1G65980; neighbour gene of *TPX2*) expression. On the other hand, *MPK12* and *BPS2* expression was not detectable in *gad2-1*, but present within *gad2-2*.

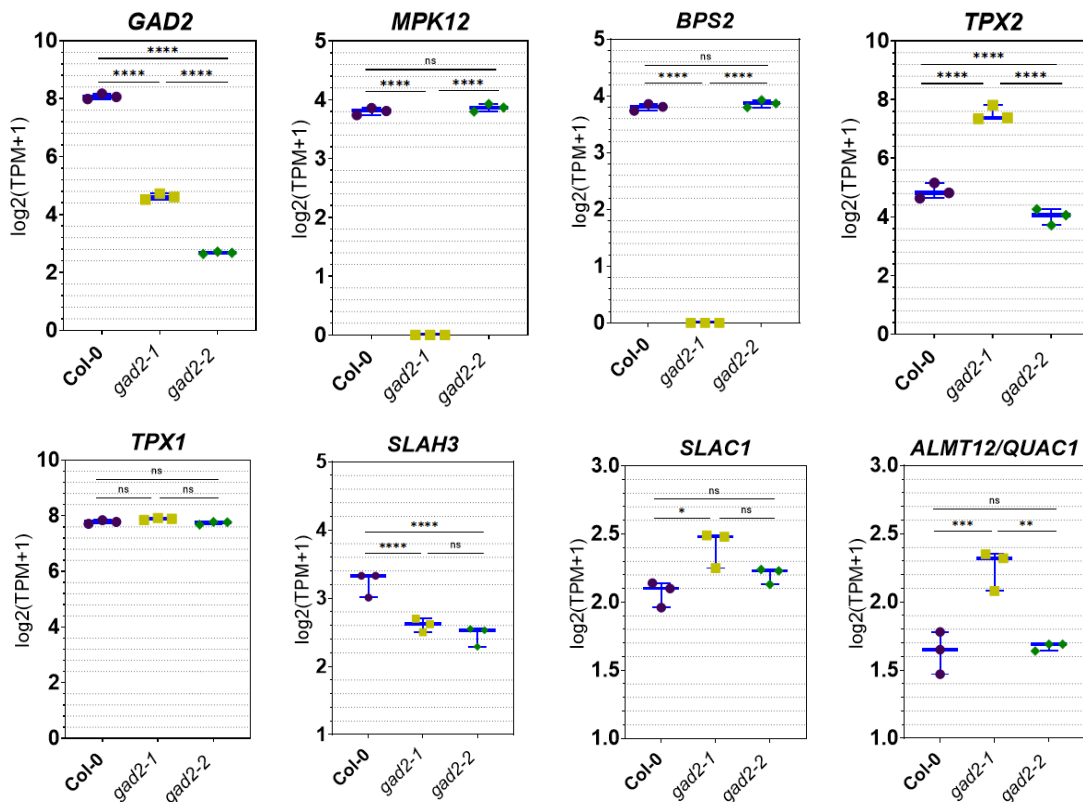
These findings are consistent with the gene expression data from a microarray study in leaf material of Col-0, *gad2-1*, and *gad1/2/4/5*. The resulting data, presented as fold changes in Table 1, revealed the downregulation of *GAD2* expression and concurrent upregulation of *TPX2* expression in *gad2-1* and *gad1/2/4/5*. Moreover, a significant downregulation of *MPK12* and *BPS2* was detected in *gad2-1* in comparison to the wild type and *gad1/2/4/5*.

We investigated whether the mutations in *GAD2*, *MPK12*, and *BPS2* affected the expression levels of other genes that encode key elements of stomatal regulation (Figure 8). On the one hand, similar expression patterns were detected for *GAD2* and *SLAH3* in *gad2-1* and *gad2-2*. However, the microarray experiment did not show any differences regarding *SLAH3* expression in *gad2-1* and *gad1/2/4/5*. On the other hand, *ALMT12/QUAC1* and *SLAC1* were found to be only misexpressed in *gad2-1* but not in *gad2-2*. In contrast to *ALMT12/QUAC1*, which is required for stomatal closure, stomatal opening-related *ALMT9* was not found to be differentially expressed.

We additionally examined the gene expression levels of (further) genes that are involved in CO₂ signalling processes, such as *HT1*, *CA1*, *CA4*, *MPK4*, *GHR1*, *PYL4*, and *PYL5*. Note that the role of *PYL4* and *PYL5* in CO₂-mediated stomatal responses is still controversial (Dittrich *et al.*, 2019; Zhang *et al.*, 2020a). Among all (potential) CO₂ signalling-related genes examined in this study, *PYL4* and *PYL5* were the only genes that were differentially expressed according to $p \text{ adj.} < 0.05$ (Wald-test). *HT1* might appear to be upregulated in *gad2-1*, but it should be noted that the corresponding p -value did not meet the pre-specified level of statistical significance ($p \text{ adj.} < 0.05$).

We further investigated whether other mutant lines from the GABI-Kat collection are also lacking *MPK12*. For this purpose, we compared the CO₂ responses of *almt6-1* from the GABI-Kat and *almt6-2* from the INRA-Versailles collection, which we had available. Simultaneously, we examined both lines for the presence of *MPK12* by genotyping. Both analyses confirmed that neither the GABI-Kat mutant line nor the Versailles mutant line carried the specified *MPK12* deletion (Supplementary Figure 10).

Accordingly, the CO₂ response of both *almt6* mutants was comparable to the wild-type phenotype. In a separate experiment we investigated if another *almt* mutant line, namely a transgenic line lacking functional ALMT9 (*almt9-1*), is impaired in its stomatal CO₂ response and found that this was not the case either (Supplementary Figure 11).



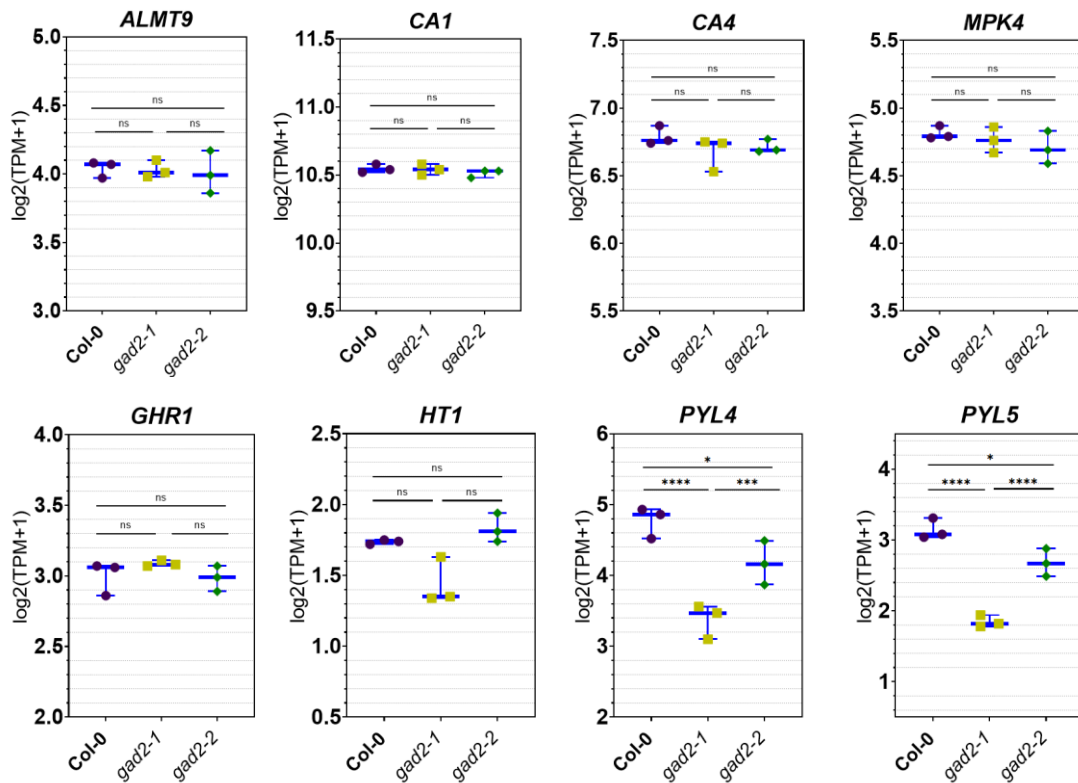


Figure 8: List of genes related to CO₂ regulation in GABA-deficient mutant lines by RNA-seq analysis.

Average log₂(transcripts per million [TPM]+1) values of differentially expressed genes (*GAD2*, *MPK12*, *BPS2*, *TPX2*, *SLAH3*, *ALMT12/QUAC1*, *PYL4*, and *PYL5*) and non-differentially expressed genes which are, *inter alia*, involved in stomatal closure responses; including genes that are related to high CO₂ signalling in guard cells (*ALMT9*, *CA1*, *CA4*, *MPK4*, *GHR1*, and *HT1*) in leaves of the wild type (Col-0), *gad2-1*, and *gad2-2*, based on an RNA-seq analysis. Genes with p adj. < 0.05 were considered as differential expressed genes using Wald-test; p adj. was calculated using the Benjamini-Hochberg method. Individual data points were plotted with the median and minimum and maximum values; ****P < 0.0001, ***P < 0.001, **P < 0.01, and *P < 0.05.

Table 1: Microarray analysis in GABA-deficient mutant lines.

Fold changes (fc) of differentially expressed genes in the wild type (Col-0), *gad2-1*, and *gad1/2/4/5*, based on a microarray experiment. Coloured shading indicates if genes are up-regulated (green) or downregulated (red). *GAD2* (AT1G65960) is downregulated in *gad2-1* and *gad1/2/4/5* compared to the wild type, while *MPK12* (AT2G46070) and its next-door gene *BPS2* (AT2G46080) were significantly lower in *gad2-1* in comparison to the wild type and *gad1/2/4/5*. Gene expression of a neighbour gene of *GAD2*, known as *TPX2* (AT1G65970), was highly upregulated in *gad2-1* and *gad1/2/4/5*. No significant differences in *PFK1* (AT4G29220) expression levels were identified. Only fold-changes with adjusted p-values ≤ 0.05 are shown.

| | fc wt/ <i>gad2-1</i> | fc wt/ <i>gad1245</i> | fc <i>gad2-1</i> / <i>gad1245</i> |
|------------------------|----------------------|-----------------------|-----------------------------------|
| AT1G65960 GAD2 | 15.08 | 11.91 | |
| pValue | 8.6805E-11 | 1.54454E-09 | |
| AT2G46070 MPK12 | 21.1 | | -20 |
| pValue | 2.20746E-17 | | 3.11481E-17 |
| AT2G46080 BPS2 | 189.98 | | -183.7 |
| pValue | 6.32731E-12 | | 7.1887E-12 |
| AT1G65970 TPX2 | -15.19 | -22.71 | |
| pValue | 5.3474E-08 | 5.23735E-09 | |

CO₂ sensitivity in *gad2-1* is restored by guard cell-specific *MPK12* complementation

To ascertain whether CO₂ responsiveness can be recovered in *gad2-1* by driving *MPK12* expression in its guard cells, we transformed *gad2-1* with full-length *MPK12* fused to the guard cell-promoter *GCI*. The transformation success was confirmed via RT-PCR amplification of *MPK12* in corresponding plants (*gad2-1/GCI::MPK12*; Supplementary Figure 12).

Clearly, *gad2-1/GCI::MPK12* revealed an increased CO₂ sensitivity compared to *gad2-1*, as it adjusted transpiration rates in accordance to altered CO₂ concentrations (Figure 9). It responded to both low (100 ppm) and high (800 ppm) CO₂. Not only the speed but also the degree of change in transpiration rates were significantly higher in *gad2-1/GCI::MPK12* than in *gad2-1* (Figure 9).

However, the CO₂ response of *gad2-1/GCI::MPK12* was not as extensive as that of *gad2-2* (Supplementary Figure 13). Particularly, high CO₂-dependent closure was higher in *gad2-2* compared to the *MPK12* complementation line. This was true for the speed as well as the extent of change in transpiration rates. Overall, transpiration rates in both lines were much greater than in the wild type (Figure 10).

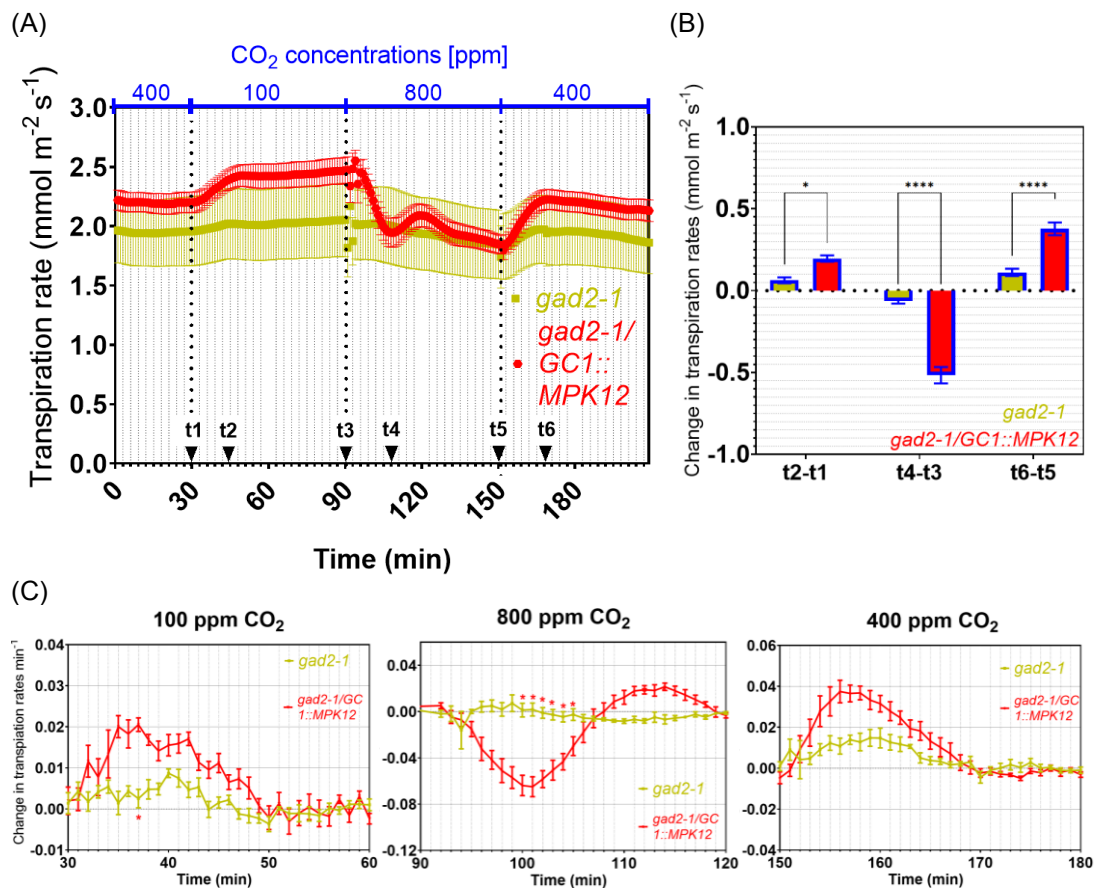


Figure 9: CO₂ responsiveness was recovered by MPK12 complementation in guard cells of *gad2-1*.

(A) Time courses of transpiration rates in response to ambient (400 ppm), reduced (100 ppm), and elevated (800 ppm) CO₂ in intact *A. thaliana* *gad2-1* (n=6) and *gad2-1/GC1::MPK12* (n=6) plants. On the basis of the data presented in (A), changes in transpiration rates during specific time periods were determined and are illustrated in (B). For calculating these changes, transpiration rates at earlier time points were subtracted from transpiration rates at later points in time. Time points are numbered and denoted by small black arrows in (A). (C) Changes in transpiration rates per minute were calculated using $d\text{Transpiration}/dt$ (min) and are also based on the time-lapse transpiration rates illustrated in (A). Pooled data from four different experiments is shown. Error bars in all diagrams represent \pm SEM. Statistical differences were calculated using two-way ANOVA (B) or multiple Student's t tests (C); *P < 0.05, ****P < 0.0001.

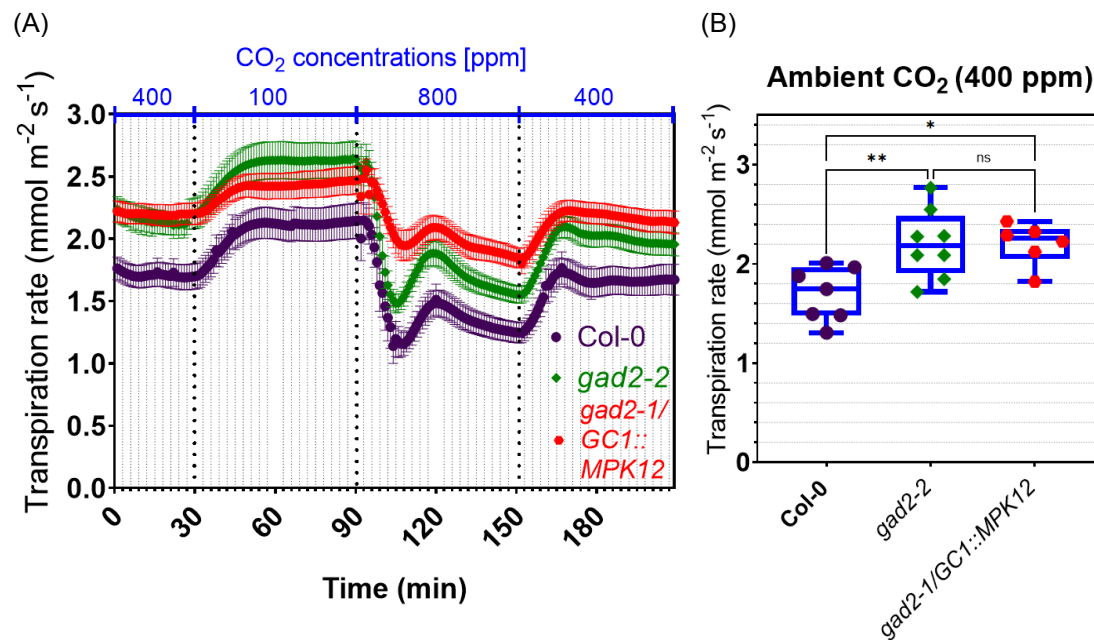


Figure 10. Transpiration rates are increased in both *gad2-2* and *gad2-1/GC1::MPK12*.

(A) Time courses of transpiration rates in response to ambient (400 ppm), elevated (800 ppm), and reduced (100 ppm) CO₂ in intact four- to five-week-old *A. thaliana* wild-type (Col-0; n=7), *gad2-1/GC1::MPK12* (n=6), and *gad2-2* (n=8) plants. Error bars represent \pm SEM. (B) Transpiration rates at ambient CO₂ based on the data presented in (A). Data points originate from the last minute of initial recording at 400 ppm CO₂ (29th minute). Data was plotted with box and whiskers: the box illustrates the median, and the 25th and 75th percentiles, while the whiskers indicate the minimum and maximum values. Statistical differences were calculated using one-way ANOVA; *P < 0.05, **P < 0.01.

Collectively, the downregulation of *MPK12* in *gad2-1* relative to the wild type, *gad2-2*, and *gad1/2/4/5* was detected by both microarray and RNA-seq analysis and correspond to *MPK12* deletion within the genome of *gad2-1*, as identified by whole-genome sequencing. Overall, all CO₂-dependent stomatal phenotypes match the genomic and transcriptomic data presented in this study.

Discussion

GABA has been previously demonstrated to act as a signal in guard cells for the regulation of transpiration. However, the GABA signalling pathway is largely unexplored. Therefore, we explored a possible connection between GABA and CO₂

signalling using different GABA-deficient *gad* mutants for physiological and genetic studies. We analysed the mutant lines *gad2-1* (from the GABI-Kat mutant collection) and *gad2-2* (SALK mutant line), which harbour T-DNA insertions at two different sites in *GAD2*, resulting in GABA depletion. In particular, we note that *gad2-1* has been used for stomatal assays in other stomata-related projects (Scholz *et al.*, 2015; Mekonnen *et al.*, 2016; Deng *et al.*, 2020; Xu *et al.*, 2021a).

As the aim was to clarify if GABA plays a role in CO₂-dependent stomatal responses, we examined *gad2-1* and *gad2-2* for CO₂ sensitivity by monitoring their transpiration rates in response to alternating CO₂ concentrations (high and low CO₂). Under standard CO₂ conditions (ambient \cong 400 ppm CO₂), the data indicated a significant increase in transpiration rates and stomatal pores in both mutant lines, which matches the observations of a previous report (Xu *et al.*, 2021a). It was proposed that this is due to direct or indirect deregulation of the vacuolar anion channel ALMT9, and as a consequence stomata are more open and these plants have a drastically reduced WUE (Xu *et al.*, 2021a).

However, exposure to drastically increased or decreased (800 ppm or 100 ppm) CO₂ concentrations unveiled significant differences in the stomatal phenotype between both allelic mutant lines. In wild-type plants, transpiration rates decreased in response to elevated CO₂ (800 ppm), whereas they increased under low CO₂ (100 ppm) conditions. This is a common mechanism of plants and serves to increase their WUE (Lawson and Blatt, 2014). By contrast, transpiration rates in *gad2-1* varied only slightly in accordance with changing CO₂ concentrations, which suggests a reduced CO₂ sensitivity in *gad2-1*. Neither the transformation of *gad2-1* with a full-length nor with a *GAD2* overexpression construct within *gad2-1* plants could restore CO₂ sensitivity in this mutant line.

Surprisingly, however, *gad2-2* revealed a wild-type CO₂ response as its transpiration rates changed to the CO₂ concentration shifts at the same speed and to the comparable degree as transpiration rates in the wild type, thereby contrasting the CO₂ phenotype of *gad2-1*. The adverse stomatal behaviours of *gad2-1* and *gad2-2* were backed up by stomatal aperture measurements which revealed impaired stomatal closure to 800 ppm CO₂ in *gad2-1* in contrast to *gad2-2*.

Due to the opposing phenotypes of *gad2-1* and *gad2-2*, we suspected at least one additional mutation in one of the mutant lines. To uncover additional unwanted mutations, we conducted a comprehensive transcriptomic and genomic analysis. Notably, the genetic studies revealed clear genotype-phenotype correlations in these lines. As expected, the microarray and RNA-seq analysis detected the downregulation of *GAD2* in both *gad2-1* and *gad2-2*. Thereby, *GAD2* expression was found to be even lower in *gad2-2* than *gad2-1*, probably due to partial (non-functional) *GAD2* transcripts present in the *gad2-1* mutant line (Mekonnen, 2012). Intriguingly, both RNA-seq and microarray analysis revealed the downregulation of *MPK12* in *gad2-1* compared to the wild-type, *gad2-2*, and *gad1/2/4/5* lines used in this study. In accordance with these findings, guard cell-specific *MPK12* complementation rescued that decreased CO₂-insensitive phenotype of *gad2-1*. The stomatal CO₂ responses of the *MPK12* complementation line were slightly weaker than in the case of *gad2-2*, likely linked to *MPK12* expression not being mediated by its native promoter and only being present in the guard cells of *gad2-1/GC1::MPK12*.

Whole genome sequencing provided an explanation for the specific *MPK12* downregulation in *gad2-1*, compared to the other genotypes. Apparently, *MPK12* and its neighbour gene *BPS2* are completely removed from the *gad2-1* genome (4,750 bp in total). According to the TAIR database, *BPS2* encodes a protein linked to BPS1, which was found to be involved in the formation of a root-synthesised mobile signal that induces a growth arrest in young Arabidopsis leaves (Van Norman *et al.*, 2011). It seems that BPS2 function is not linked to stomatal movement, in contrast to *MPK12*. Silencing of *MPK12* is associated with impaired stomatal closure and altered CO₂ responsiveness as shown by the loss-of-function mutant *mpk12-3* in the present and another, independent study (Jakobson *et al.*, 2016). This occurs because *MPK12* suppresses the activity of a negative regulator of high CO₂ signalling, known as HT1 (Hörak *et al.*, 2016; Töldsepp *et al.*, 2018). When *MPK12* is inactive or absent as in *gad2-1* or *mpk12-3*, HT1 constitutively inhibits high CO₂-induced stomatal closure, leading to enlarged stomatal apertures (Hörak *et al.*, 2016; Jakobson *et al.*, 2016; Figure 11).

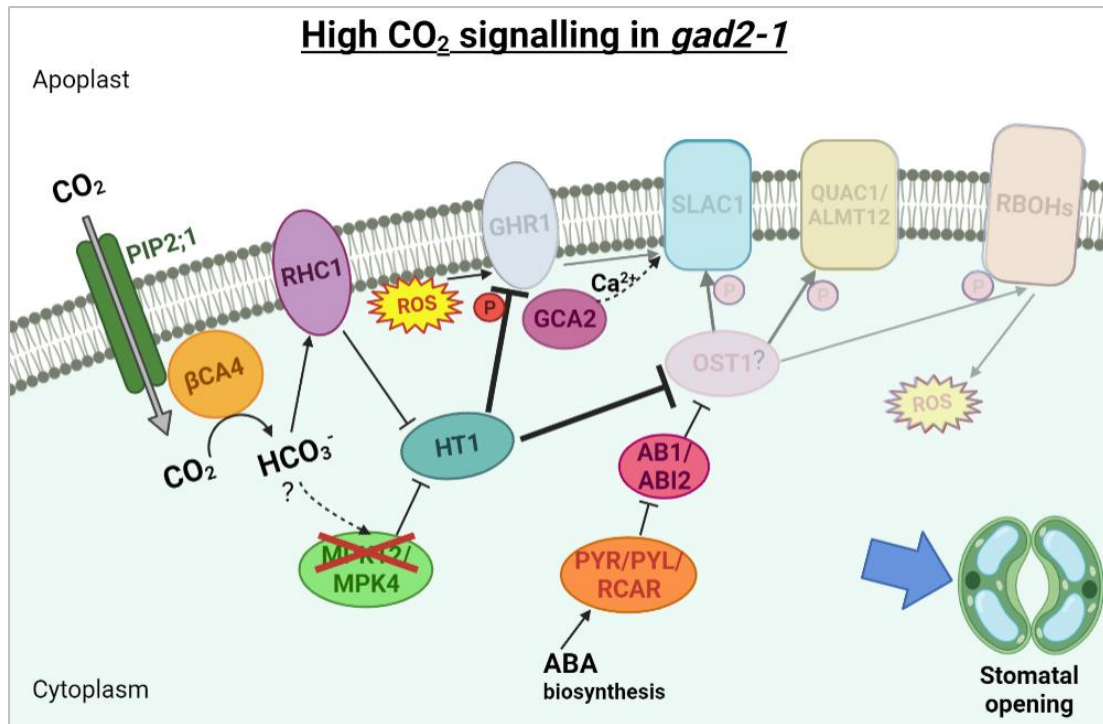


Figure 11: A schematic illustration of impaired CO₂ signalling in *gad2-1*.

Elevated CO₂ concentrations activate carbonic anhydrases, such as βCA1 and βCA4, which catalyse the conversion of CO₂ and H₂O to HCO₃⁻ and H⁺. This reaction leads to the activation of RHC1 and MPK4 but not MPK12, due to deleted *MPK12* in the *gad2-1* genome. As a result of absent MPK12, HT1 is not fully suppressed and is constitutively inhibiting the high CO₂ signalling pathway in guard cells, which includes the activation of the anion channels SLAC1 and QUAC1/ALMT12, and is thereby abolishing stomatal closure. The consequence is a ‘more open stomata’ phenotype and increased CO₂ insensitivity. Own work on the basis of Ma and Bai (2021), including information from Hōrak *et al.* (2016), Jakobson *et al.* (2016), Zhang *et al.* (2018), and Dubeaux *et al.* (2021). Image was created in BioRender.

The link between CO₂ insensitivity and the *MPK12* mutation was originally identified in an *Arabidopsis* accession that originates from the Cape Verde Islands, known as Cvi-0 (Jakobson *et al.*, 2016). This accession appears to be endemic to these islands and it is not known whether its *MPK12* mutation resulted from natural selection or genetic drift (Des Marais *et al.*, 2014). Its geographic conditions, isolation, and a fairly constant Vapour-pressure deficit (VPD) as well as moderate temperatures on the Cape Verde Islands have permitted the continuous existence of the accession (Des Marais *et al.*, 2014). We examined the genome of *gad2-1* for a potential Cvi-0 contamination but this was not detected. Furthermore, Jakobson *et al.* (2016) detected a sequence deletion

of a comparable base pair size (4,772 bp) in two of their GABI-Kat lines. Both *MPK12* and *BPS2* had also been eliminated, leading to enlarged stomata and reduced CO₂ responsiveness. By contrast, corresponding allelic mutant lines from different mutant collections (SALK and SAIL lines) did not reveal this specific deletion, neither did they display any stomatal abnormalities (Jakobson *et al.*, 2016). It is conceivable that these GABI-Kat lines, including *gad2-1*, have been generated in a Col-0 background plants that already contained this specific gene deletion.

Random DNA removal does not seem rare as the genome of angiosperms has been found to be very plastic (Devos *et al.*, 2002; Ma and Bennetzen, 2004; Vitte and Bennetzen, 2006; Bennetzen and Wang, 2018). Illegitimate recombination is estimated to be the most common cause for gene loss in Arabidopsis (probably to a greater extent than unequal homologous recombination), and could be a possible explanation for the gene loss in *gad2-1* and the other GABI-Kat mutant lines (Ehrlich *et al.*, 1993; Devos *et al.*, 2002). Of note, the specified deletion appears not to be universal to all mutant lines from the GABI-Kat catalogue. In our study, a GABI-Kat line (*almt6-1*) and a transgenic line from the INRA-Versailles mutant collection (*almt6-2*) were examined for CO₂-sensitive stomatal responses and *MPK12* expression. The data unveiled that both lines express *MPK12* and are capable of adjusting stomatal apertures sizes to changing CO₂.

Surprisingly, the quadruple mutant *gad1/2/4/5* was found to reveal a robust CO₂ response in contrast to *gad2-1*, although it had been produced by crossing *gad2-1* (also referred to as *gad2-1/mpk12/bps2*) with other *gad* lines. However, our genetic study has uncovered that only *gad2-1* lacks *MPK12* and *BPS2*, whereas *gad1/2/4/5* has gained both genes. A plausible explanation for this genetic difference is that the gene deletion was lost in the quadruple mutant during the crossing processes.

Also, the question as to why the quadruple mutant does not reveal enhanced stomatal opening at standard conditions like *gad2-1* and *gad2-2* remains unanswered. It can be excluded that the *MPK12* deletion is the only cause as it was detectable in *gad2-1* but not in *gad2-2*. It has also become obvious that GABA deficiency is not always linked to the incomplete stomatal closure phenotype. The restoration of wild-type stomatal apertures in *gad1/2/4/5* is likely due to the knockout of additional GAD genes (all confirmed by whole genome sequencing) or might be based on an additional, unspecific

mutation, which has only been found in the quadruple mutant. This mutation affects the gene *Phosphofruktokinase 1 (PFK1)*, which encodes one out of seven Arabidopsis PFK isoforms (Yoshida and Hisabori, 2021). It is, however, unclear whether it is a true loss-of-function mutation because only one flanking end of the T-DNA insertion was recovered and sequenced. This was also the case for the T-DNA insertion in *GAD5* in *gad1/2/4/5*, which, in contrast to T-DNA insertion in *PFK1*, was an intended mutation. Furthermore, according to our microarray experiment, *PFK1* expression was unaltered in *gad2-1* and *gad1/2/4/5*. However, the results from the microarray analysis are potentially not exact as they do not fully match the outcome of our RNA-seq analysis (showing no difference in gene expression, whilst RNA sequencing detected significant changes in expression levels for the same genes). Certainly, assessing *PFK1* expression levels via RT-qPCR would provide some clarity. Phosphofruktokinases are known to catalyse the ATP-consuming conversion of fructose-6-phosphate to fructose-1,6-bisphosphate during plant glycolysis, which precedes the Krebs cycle (O'Leary and Plaxton, 2016). Upon disruption of this metabolic step, an increase in fructose-6-phosphate concentrations would be expected. Thus, the question arises if increased fructose-6-phosphate levels cause or contribute to the wild type-like phenotype of *gad1/2/4/5*. Numerous reports suggest a strong connection between increased sugar concentrations in guard cells and enhanced stomatal movement (Daloso *et al.*, 2015; Kelly *et al.*, 2013). However, the exact role of putative sugar accumulation in stomatal responses of *gad1/2/4/5* still needs to be elucidated.

The genetic analysis detected another striking difference in gene expression levels between the different lines. Interestingly, the RNA-seq analysis revealed the upregulation of *TPX2* in *gad2-1* and *gad1/2/4/5*. *TPX2* has been reported to be involved in antioxidant metabolism (Dietz *et al.*, 2006). Although it seems to be expressed in guard cells (The Arabidopsis Information Resource [TAIR], www.arabidopsis.org/servlets/TairObject?id=27102&type=locus, on www.arabidopsis.org, December 31, 2021), a central function for *TPX2* in guard cells has not been documented. We exclude the possibility that the *TPX2* upregulation is linked to the *MPK12* or *BPS2* deletion in *gad2-1* because we could not find a correlation between the downregulation of *MPK12* and upregulated *TPX2* in all the genotypes (e.i. no downregulation of *MPK12* but high *TPX2* expression in *gad1/2/4/5*). We rather speculate that the high expression of *TPX2* is due to its location next to *GAD2* on

chromosome 1. It is not uncommon that a T-DNA insertion in one gene affects the expression of an adjacent gene, which can, for instance, occur through accidental interference with a cis-regulatory element that controls the expression of the neighbour gene (Tamura *et al.*, 2016).

Both complementation of *gad2-1* by MPK12 and the CO₂-sensitive phenotypes of *gad2-2* and *gad1/2/4/5*, which exhibit wild type-like CO₂ responsiveness, demonstrate that GABA is not required for stomatal responses to high or low CO₂. The enhanced stomatal opening response of *gad2-2* to low CO₂ conditions seems to be independent of ALMT9, since measurements in *almt9-1* revealed a wild type-like CO₂ response, indicating that the lack of ALMT9 does not affect CO₂ sensitivity. The same is true for ALMT6, which, according to our data, is not involved in low CO₂ responses of guard cells. Interestingly, Delloro *et al.* (2021) discovered large increased concentrations of GABA in Arabidopsis plants that had been subjected to low CO₂ conditions for four hours. Thus, GABA might play certain roles under these conditions. However, it appears that these do not include GABA regulation of low CO₂-mediated stomatal movements.

Lastly, we investigated whether the mutations in *MPK12* and *GAD2* indirectly influenced the expression levels of other important, stomata-related genes. For this purpose, we compared the expression levels of genes that encode major CO₂ signalling components between the wild type and the two GABA-deficient mutant lines *gad2-1* (equivalent to *gad2/mpk12/bps2*) and *gad2-2*. The data revealed no significant differences in the gene expression levels of *HT1*, *CA1*, *CA4*, *GHR1*, and *MPK4*. All these components are known as CO₂ signalling elements only and have not been linked to other guard cell signalling pathways. The finding that *MPK4* is not differentially expressed in *gad2-1* is in line with a previous report. As stated by Töldsepp *et al.* (2018), MPK4 and MPK12 act in concert in regulating CO₂ responses of guard cells and only silencing of both *MPK4* and *MPK12* leads to complete abolishment of CO₂ responsiveness. This might explain while the guard cells of *gad2-1* and *mpk12-3* are still partially responding to varying CO₂ concentrations.

ALMT12/QUAC1, *SLAH3*, *SLAC1*, *PYL4*, and *PYL5* have been discovered to be differentially expressed between the wild type and both or one of the two GABA-deficient mutant lines *gad2-1* and *gad2-2*. *ALMT12/QUAC1* and *SLAC1* are anion

channels that are activated in response to both signals, ABA and high CO₂ (Meyer *et al.*, 2010; Jalakas *et al.*, 2021). It is surprising that *ALMT12/QUAC1* was found to be upregulated in *gad2-1* although it is known to be a stomatal closure-related channel. Potentially, the upregulation of *ALMT12/QUAC1* might counteract constitutively active ALMT9 in the *gad2-1* mutant, which, however, does not seem to be sufficient. In contrast to ALMT12/QUAC1 and SLAC1, which regulate both CO₂- and ABA-induced stomatal closure, the anion channel SLAH3 has only been identified as an ABA signalling component (Geiger *et al.*, 2011). The role of the ABA receptor PYL4 and PYL5 is divisive. A recent report dismissed previous findings which had attributed a role for PYL4 and PYL5 in high CO₂ responses (Dittrich *et al.*, 2019; Zhang *et al.*, 2020a).

Taken together, the expression of genes that exclusively relate to CO₂ signalling was not found to be differentially expressed between the different genotypes. Only genes that are also relevant for other signalling cascades, like the ABA signalling pathway, appear to be differentially expressed between the different lines. Thereby, the question arises if the differences in transcript abundance are based on differences in the detected expression levels of *TPX2*, *MPK12*, and/or *GAD2*. Hence, we compared the expression patterns of corresponding genes across the three genotypes (wild type, *gad2-1*, and *gad2-2*). *SLAH3* expression could possibly be dependent on *GAD2* as both, *SLAH3* and *GAD2*, were found to be downregulated in *gad2-1* and *gad2-2*. On the other hand, the upregulation of *SLAC1* and *ALMT12/QUAC1* might correlate with *MPK12* downregulation in *gad2-1*. These gene expression levels are merely clues which require follow up experiments for verification. This is especially relevant, as these levels were not confirmed by the microarray analysis in *gad2-1* and *gad1/2/4/5*.

In summary, we could clearly rule out that GABA-deficiency results in decreased CO₂ sensitivity by attributing the reduced CO₂ responsiveness in *gad2-1* to a second, unintentional mutation in *MPK12*. This is proof that guard cell responses to alterations in atmospheric CO₂ neither involve GABA regulation nor ALMT6 or ALMT9 channels. Therefore, the question arises which other anion channels are required for low CO₂ induced opening, which should be investigated in future research. Our research has also shown the value once again that it is crucial to examine multiple

independent allelic mutant lines and to combine physiological data with genetic analyses in order to avoid misinterpretations of physiological data.

Supplementary Tables and Figures

Supplementary Table 1: Primer used in this study.

| Primer name | Primer sequence (5' → 3') | Purpose | |
|-------------------|------------------------------------|--|--|
| GAD2N(2)-FW | AAGGAGAAGAAGATGGAGAAGGA | Quantitative real-time PCR analysis in <i>gad2-1</i> | |
| GAD2N(2)-RV | CCACACAAAGGCAACACACT | | |
| Actin2-FW | TGAGCAAAGAAATCACAGCACT | | |
| Actin2-RV | CCTGGACCTGCCTCATCATAC | | |
| EF1- α -FW | GACAGGCGTTCTGGTAAGGAG | | |
| EF1- α -RV | GCGGAAAGAGTTTTGATGTTCA | | |
| GAD1-LP | ATGACTTGACTTGAACCTGCG | Genotyping of <i>gad1/2/4/5</i> | |
| GAD1_RP | GGAGCCAATGTTCAAGTAACG | | |
| GAD2_LP | ACGTGATGGATCCAGACAAAG | | |
| GAD2_RP | TCTTCATTTCCACACAAAGGC | | |
| GAD4b_LP | CAATAAAAAGATGACGGTCCGG | | |
| GAD4b_RP | TTGAACCGGAAATTGAGTCAC | | |
| GAD5-seq1_F | TGGATGGAACCTGAGTGTGA | | |
| GAD5-seq3_R | CCATCCTGTCTCTGCGTTTT | | |
| MPK12_CDS_FW | ATGTCTGGAGAATCAAGCTCTG | | Gene cloning (generation of <i>GC1::MPK12</i> construct) |
| MPK12_CDS_RV | TCAGTGGTCAGGATTGAATTTG | | |
| pGC1_FW | ATGTTGCAACAGAGAGGATG | <i>MPK12</i> deletion genotyping in <i>almt6</i> lines | |
| pGC1_RV | GATTCTCCAGACATATTTCTTGAGTAGTGATTTT | | |
| MPK12_RP | ATCTCTGCCATTGTAGGTGAAAC | | |
| MPK12_LP | GTTGTTTTCGCCGTGAAAGG | | |
| MPK12_RP | ATCTCTGCCATTGTAGGTGAAAC | Reverse transcriptional PCR in <i>almt9-1</i> | |
| MPK12_seqF1 | TGAGTTAATGGACACTGATCTTCA | | |
| MPK12_rt_F | TGAGTTAATGGACACTGATCTTCA | | |
| MPK12_rt_R | TCAGTGGTCAGGATTGAATTTG | | |
| GAD2_rt_F | ACGTGATGGATCCAGACAAAG | | |
| GAD2_rt-R | TACATTTTCCGCGATCCCT | | |
| Actin2_rt_F | CAAAGGCCAACAGAGAGAAGA | | |
| Actin2_rt_R | CTGTACTTCTTTCAGGTGGTG | | |

Supplementary Table 2: Chemical components of the Germination Solution for hydroponic growth.

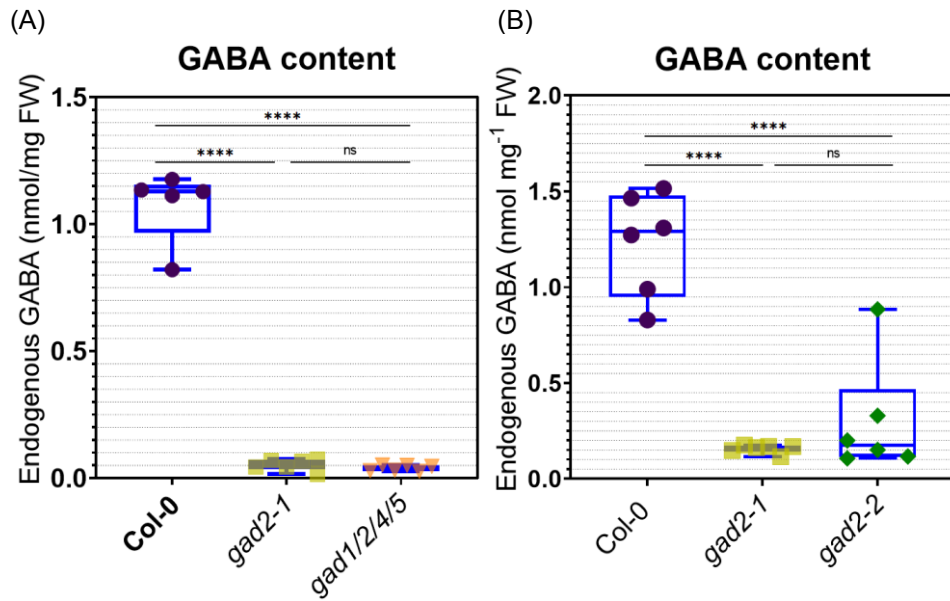
| Macronutrients | Molecular weight | Stock conc. [M] | Vol of stock [mL] for 10 L | Final conc. [mM] |
|--|------------------|-----------------|----------------------------|------------------|
| CaCl ₂ | 1 M solution | 1.0 | 7.5 | 0.75 |
| KCl | 74.55 | 1.0 | 10.0 | 1.0 |
| Ca(NO ₃) ₂ 4·H ₂ O | 236.1 | 0.4 | 6.25 | 0.25 |
| MgSO ₄ 7·H ₂ O | 246.5 | 0.4 | 25.0 | 1.0 |
| KH ₂ PO ₄ | 136.1 | 0.1 | 20.0 | 0.2 |

| Micronutrients | Molecular weight | Stock conc. [mM] | Vol of stock [mL] for 10 L | Final conc. [μM] |
|-------------------------------------|-------------------------|-------------------------|-----------------------------------|-------------------------|
| NaFe(III) EDTA | 367.1 | 50.0 | 1.0 | 50.0 |
| H ₃ BO ₃ | 61.8 | 50.0 | 1.0 | 50.0 |
| MnCl ₂ 4H ₂ O | 197.9 | 5.0 | 1.0 | 5.0 |
| ZnSO ₄ 7H ₂ O | 287.5 | 10 | 1.0 | 10 |
| CuSO ₄ 5H ₂ O | 249.7 | 0.5 | 1.0 | 0.5 |
| Na ₂ MoO ₃ | 242 | 0. | 1.0 | 0.1 |

Supplementary Table 3: Chemical components of the Basal Nutrient Solution for hydroponic growth.

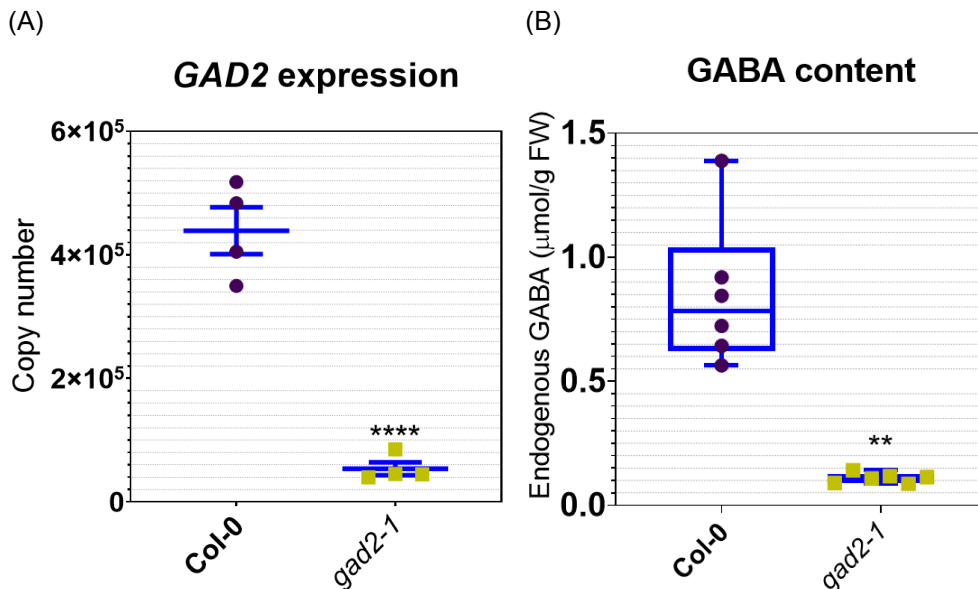
| Macronutrients | Molecular weight | Stock conc. [M] | Vol of stock [mL] for 10 L | Final conc. [mM] |
|---|-------------------------|------------------------|-----------------------------------|-------------------------|
| NH ₄ NO ₃ | 80 | 1 | 20 | 2 |
| NaCl | 58.44 | 1 | 15 | 1.5 |
| MgSO ₄ 7H ₂ O | 246.5 | 0.4 | 50 | 2 |
| KNO ₃ | 101.11 | 1 | 30 | 3 |
| KH ₂ PO ₄ | 136.1 | 0.1 | 60 | 0.6 |
| KCl | 74.55 | 1 | 20 | 2 |
| CaCl ₂ | 1 M solution | 1 | 1 | 0.1 |
| Ca(NO ₃) ₂ 4H ₂ O | 236.1 | 0.4 | 50 | 2 |

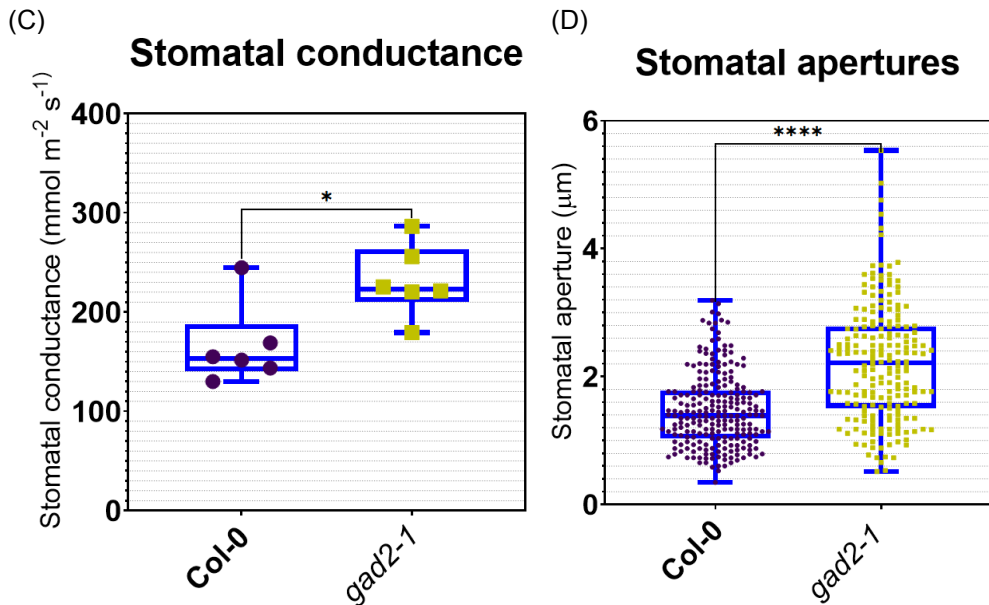
| Micronutrients | Molecular weight | Stock conc. [mM] | Vol of stock [mL] for 10 L | Final conc. [μM] |
|--------------------------------------|-------------------------|-------------------------|-----------------------------------|-------------------------|
| NaFe(III) EDTA | 367.1 | 50 | 10 | 50 |
| H ₃ BO ₃ | 61.8 | 50 | 10 | 50 |
| MnCl ₂ 4·H ₂ O | 197.9 | 5 | 10 | 5 |
| ZnSO ₄ 7·H ₂ O | 287.5 | 10 | 10 | 10 |
| CuSO ₄ 5·H ₂ O | 249.7 | 0.5 | 10 | 0.5 |
| Na ₂ MoO ₃ | 242 | 0.1 | 10 | 0.1 |



Supplementary Figure 1: Endogenous GABA content in leaves of gad(s) mutants.

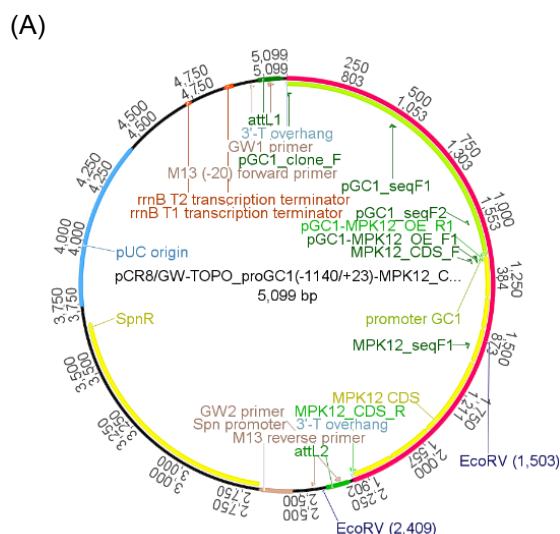
Endogenous GABA concentrations in rosette leaves of *A. thaliana* wild-type (Col-0), *gad2-1*, (A) *gad1/2/4/5*, and (B) *gad2-2* plants, as determined by UPLC (n=6). The data presented in (A) and (B) was generated in two separate experiments and is therefore shown as different diagrams. Data was plotted with box and whiskers: the box illustrates the median, and the 25th and 75th percentiles, while the whiskers indicate the minimum and maximum values. Statistical differences were calculated using one-way ANOVA (A, B); ****P < 0.0001.



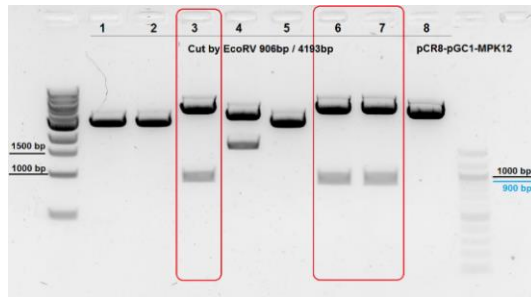


Supplementary Figure 2: GAD2 knockout in GABA-deficient *gad2-1* mutant is associated with increased stomatal conductance.

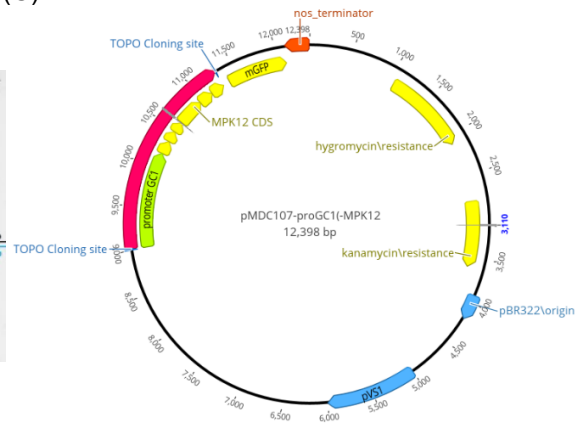
(A) *GAD2* expression in leaves of the wild type (Col-0) and the loss-of-function mutant *gad2-1* as revealed by quantitative real-time PCR analysis (n=4). C_t (threshold cycle) values were converted to copy numbers of native *GAD2* (AT1G65960). (B) GABA concentrations in rosette leaves of wild-type (Col-0) and *gad2-1* plants as determined by UPLC (n=6). (C) Stomatal conductance measurements were performed in both lines using AP4 porometer technology (n=6). (D) Stomatal apertures were determined on the abaxial leaf sides of three leaves per plant (n=3) using epidermal strip assay; Col-0 (n=235 stomata) and *gad2-1* (n= 196 stomata). Data is presented as single values, plotted with (B-D) or without (A) box and whiskers: the box illustrates the median, and the 25th and 75th percentiles, while the whiskers indicate the minimum and maximum values; Error bars indicate \pm SEM (A). Statistical differences were calculated using two-sided Student's t tests (A-D); *P < 0.05, **P < 0.01, ****P < 0.0001.



(B)

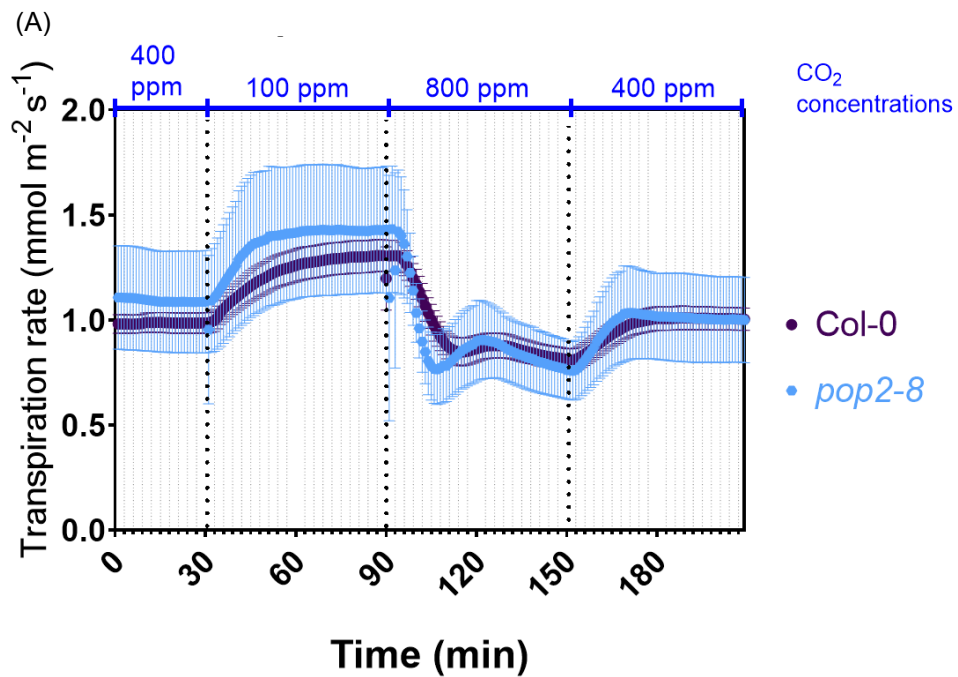


(C)



Supplementary Figure 3: Generating GC1::MPK12 construct for *gad2-1* transformation.

(A) *MPK12* was fused to the guard cell-specific promoter *GC1* through an overlap PCR and was inserted into a pCR8 TOPO cloning vector. (B) Gel image of *EcoRV* digestion product *pCR8-pGC1-MPK12* as verification of cloning success. (C) Construct illustrated in (A) was cloned into destination vector *pMDC107* to generate *pMDC107-pGC1::MPK12* for *A. tumefaciens*-mediated transformation of *gad2-1* plants.



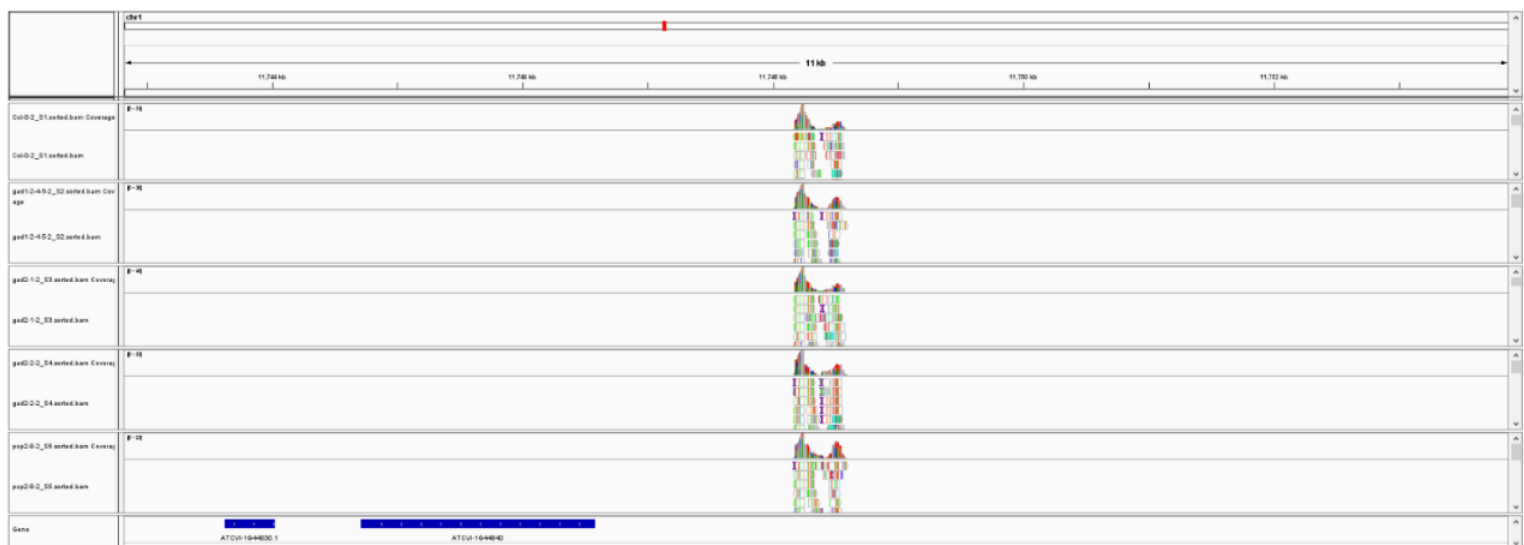


Supplementary Figure 4: Time-resolved patterns of transpiration rates in response to different [CO₂] and T-DNA insertion verification in *pop2-8*.

(A) Time courses of transpiration rates in response to ambient (400 ppm), elevated (800 ppm), and reduced (100 ppm) CO₂ in intact *A. thaliana* wild-type (Col-0; n=10) and GABA-overproducing *pop2-8* (n=3) plants. Error bars represent \pm SEM. (B, C) Whole genome sequencing (Illumina) was used for the identification of the expected T-DNA insertion site in the *pop2-8* genome. (B) Single T-DNA insertion overlaps with pyridoxal phosphate (PLP)-dependent transferases superfamily protein (AT3G22200; *GABA-T*; *POP2*) in the *pop2-8* mutant line. Dark grey arrows indicate region where one mate of the read pairs aligned to chromosome 3 (6,063,163 bp to 6,080,410 bp) of the TAIR10 reference genome and the other mate aligned to the pROK2 vector. No insertion was present in the *POP2* region in the wild type (Col-0). (C) Possible additional T-DNA insertion in the *pop2-8* mutant line. Read mappings show discordant reads where one mate aligned to chromosome 1 (21,044,214 bp to 21,048,002 bp) of the TAIR10 reference genome and the other mate aligned to the pROK2 vector. This insertion completely overlaps with AT1G56225 (hypothetical protein). It also partially overlaps with genes AT1G56220 (dormancy/auxin associated family protein) and AT1G56230 (endolase). This insertion was absent in the wild type.

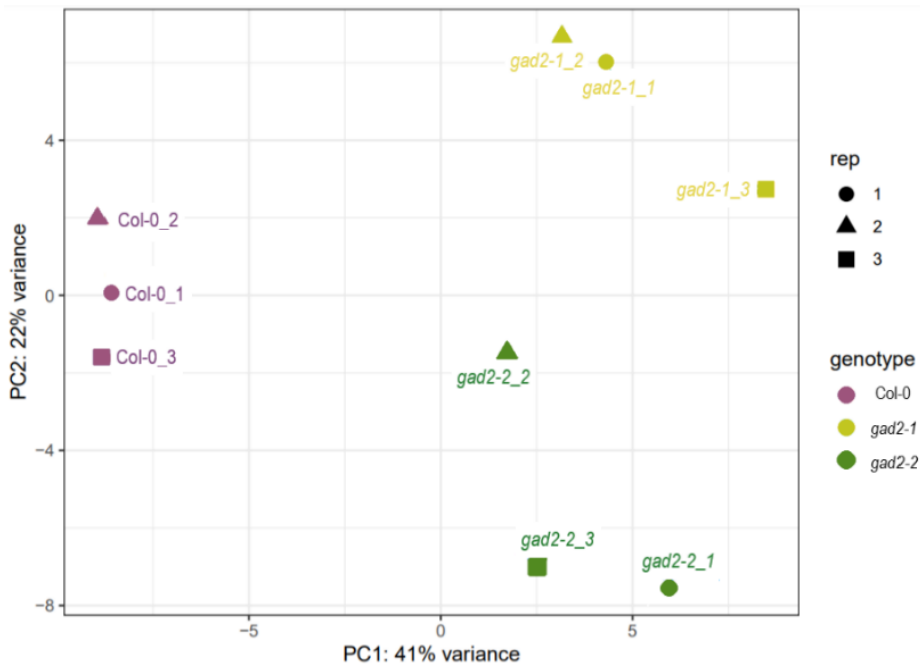
Supplementary Table 4: Overview of T-DNA insertion sites in the genomes of Col-0 and 'GABA mutants'.

| gad1-2-4-5 | Chromosome of insertion | Mapping region start | Mapping region end | Insertion start | Insertion end | Insertion size (bp) | Feature overlap | Vector name | Vector size (bp) | SALK/GABI line | Notes |
|---------------------|-------------------------|----------------------|--------------------|-----------------|---------------|---------------------|--|-------------|------------------|----------------|--|
| gad1-2-4-5-gad1-all | 1 | 5,713,190 | 5,717,266 | 5,713,365 | 5,717,085 | 3,720 | insertion partially overlaps with gene GAD1 in region 5,713,365 to 5,715,075 bp insertion completely overlaps with gene AT5G17340 in region 5,715,624 to 5,716,268 bp insertion completely overlaps with gene AT5G17345 in region 5,715,784 to 5,716,607 bp | pROK2 | 4,307 | SALK_017810 | |
| gad2-1-all | 1 | 24,553,868 | 24,556,939 | 24,554,299 | 24,556,923 | 2,624 | insertion partially overlaps with 5' UTR #5 of gene GAD2 in region 24,554,354 to 24,555,867 bp insertion completely overlaps with 5' UTR #6 of gene GAD2 in region 24,554,413 to 24,555,465 bp insertion completely overlaps 5' UTR #7 of gene GAD2 in region 24,555,769 to 24,555,867 bp insertion partially overlaps with mRNA AT1G6590.4 of GAD2 in region 24,554,354 to 24,555,730 bp insertion completely overlaps with AT1G08797 in region 24,555,535 to 24,555,858 bp | pAC161 | 5,799 | GABI_474_E05 | |
| gad1-2-4-5-gad4-all | 2 | 475,702 | 476,347 | 476,058 | 476,215 | 157 | insertion in mRNA AT2G02010.2 of GAD4 in region 476,058 to 476,215 bp | pROK2 | 4,307 | SALK_106240 | |
| gad1-2-4-5-gad5-all | 3 | 6,063,163 | 6,080,410 | ? | 6,080,026 | ? | flanking sequence overlaps with GAD5 and AT3G17 | pROK2 | 4,307 | SALK_203883 | only one flanking end of the T-DNA insertion was recovered and sequenced |
| gad1-2-4-5-pfk1-all | 4 | 14,406,163 | 14,406,506 | 14,496,561 | ? | ? | flanking sequence overlaps with 5' UTR 1 and 2 of gene AT4G29220 | pROK2 | 4,307 | | possible additional insertion; only one flanking end of the T-DNA |
| gad2-1 | | | | | | | | | | | |
| gad2-1-all | 1 | | | | | | insertion partially overlaps with 5' UTR #5 of gene GAD2 in region 24,554,354 to 24,555,867 bp insertion completely overlaps with 5' UTR #6 of gene GAD2 in region 24,554,413 to 24,555,465 bp insertion completely overlaps 5' UTR #7 of gene GAD2 in region 24,555,769 to 24,555,867 bp insertion partially overlaps with mRNA AT1G6590.4 of GAD2 in region 24,554,354 to 24,555,730 bp insertion completely overlaps with AT1G08797 in region 24,555,535 to 24,555,858 bp | | | | |
| gad2-2 | | 24,553,868 | 24,556,939 | 24,554,299 | 24,556,923 | 2,624 | | pAC161 | 5,799 | GABI_474_E05 | |
| gad2-2-all | 1 | 24,554,200 | 24,554,817 | 24,554,437 | 24,554,700 | 263 | insertion in 5' UTR #5 and #6 of GAD2 in region 24,5 | pROK2 | 4,307 | SALK_028819 | |
| pop2-8 | | | | | | | | | | | |
| pop2-8-1-all | 1 | 21,044,214 | 21,048,002 | 21,044,442 | 21,047,930 | 3,488 | insertion partially overlaps with gene AT1G56220 in the region 21,044,502 to 21,044,998 bp insertion completely overlaps with gene AT1G56225 in region 21,044,756 to 21,045,708 bp insertion partially overlaps with gene AT1G56230 in region 21,045,993 to 21,047,892 bp | pROK2 | 4,307 | SALK_007661 | possible additional insertion |
| pop2-8-2-all | 3 | 7,835,950 | 7,836,241 | ? | 7,836,025 | ? | flanking sequence overlaps with gene AT3G22200 in region 7,836,025 bp | | | | only one flanking end of the T-DNA insertion was recovered and sequenced |



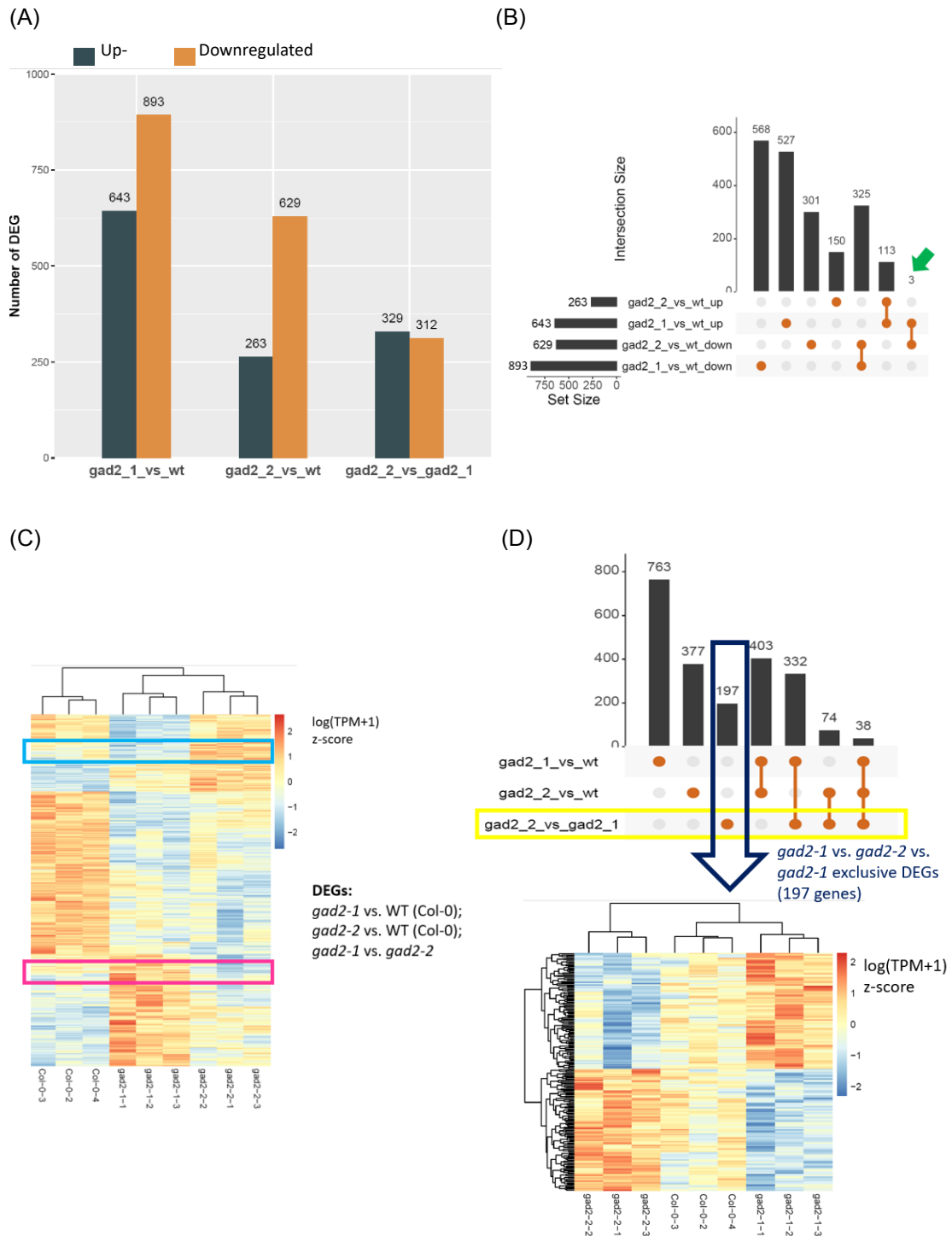
Supplementary Figure 5: Examining mutant genomes for Cvi contamination.

For the identification of a potential Cvi (Arabidopsis accession Cape Verde Island) contamination in the *gad2-1* genome, unmapped reads (in the genome sequencing data of Col-0, *gad2-1*, *gad2-2*, *gad1/2/4/5*, and *pop2-8*) were mapped to the Cvi genome [sequenced by BGI Tech Solutions (Hong Kong) using Illumina technology; Jakobson *et al.* (2016)]. Some reads still map (with many SNPs and Indels) to the Cvi genome, which is the case for all lines analysed (including Col-0).



Supplementary Figure 6: PCA analysis of RNA-seq data.

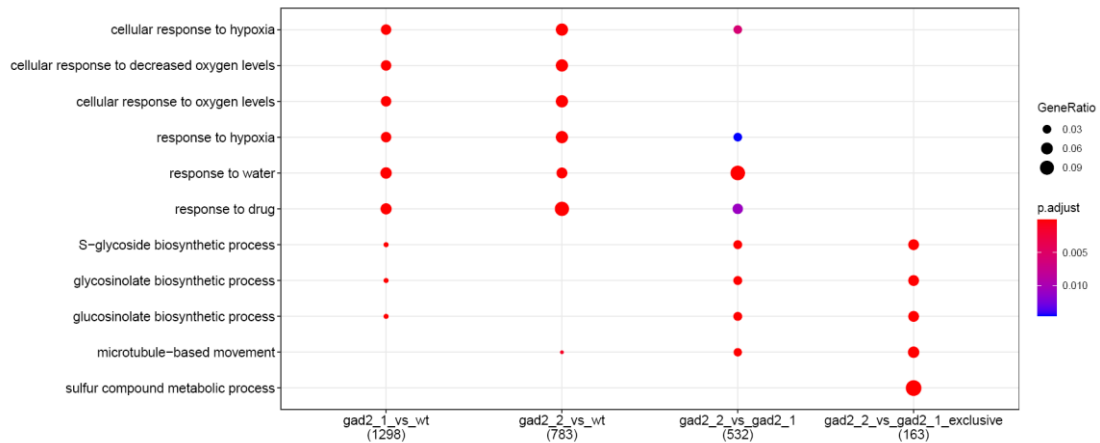
Principal Component Analysis (PCA) was conducted on RNA-seq data using the DESeq2 R package and the 500 highest variable genes. The PCA plot was created using the ggplot2 package in R plot. The two mutants *gad2-1* and *gad2-2* separated from Col-0 in the first principal component (PC1; x-axis), which accounts for 41% variance. In principal component 2 (PC2; y-axis), which represents 22% variance, the two mutants clustered separately from each other.



Supplementary Figure 7: DEG analysis of RNA-seq data.

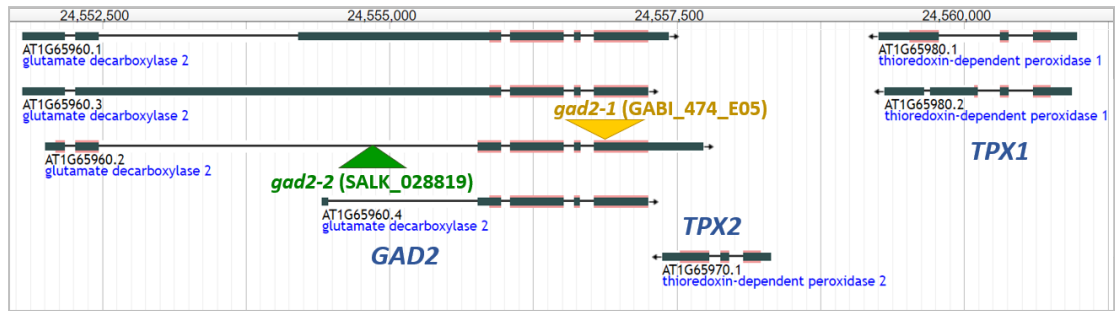
(A) Differentially expressed gene (DEG) distribution between the wild type (Col-0) and the two allelic mutant lines *gad2-1* and *gad2-2* on the basis of RNA-seq data (n=3), showing that *gad2-1* has more DEGs than *gad2-2* in relation to the wild type (FDR < 0.05). (B) Comparison of DEGs between the *gad2* mutants revealed that only three genes were significantly upregulated in *gad2-1*, while downregulated in *gad2-2* (indicated by green arrow). (C) Hierarchical clustering analysis of DEG data presented in the form of a heatmap (light blue frame: downregulated in *gad2-1*, while upregulated in *gad2-2*; pink frame: downregulated in

gad2-2 while upregulated in *gad2-1*). (D) Hierarchy clustering of *gad2-2* vs. *gad2-1* exclusive DEGs (comparison between *gad2-1* and *gad2-2* only, 197 genes, dark blue arrow; by contrast: *gad2-1* vs. *gad2-2* includes DEGs that are also present in the wild type, yellow frame, 641 genes). (C, D) Expression values have been z-score-normalised. Comparison between the genotypes was based on the colour: red shading indicates an increased gene expression, while blue shading represents a decrease in gene expression.



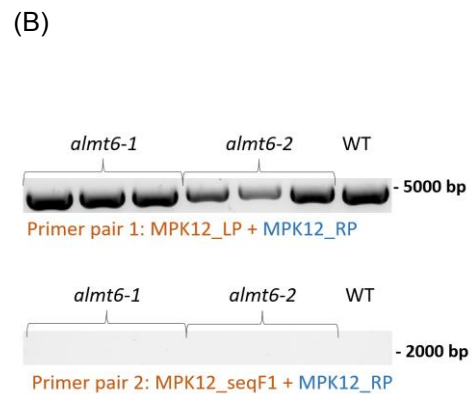
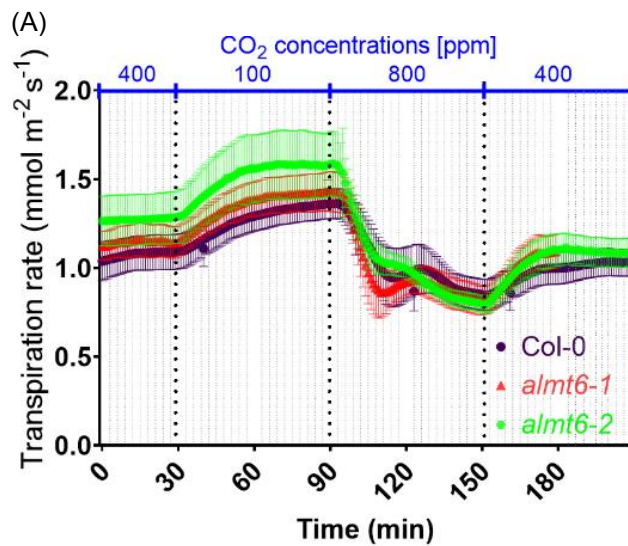
Supplementary Figure 8: Comparison of functional enrichment results from RNA-seq data.

Comparison is based on Gene ontology (GO) enrichment analysis in the wild type (Col-0), *gad2-1*, and *gad2-2*. Experiment was performed using clusterProfiler. Shown are the nodes (GO terms) of differentially expressed genes (DEGs) between *gad2-1* vs. wild type (WT; 1298), *gad2-2* vs. WT (783), *gad2-2* vs. *gad2-1* (532), and *gad2-2* vs. *gad2-1*_exclusive (comparison only between *gad2-1* and *gad2-2*; 163). Size of circular node correlates with the gene ratio (gene number associated with the GO term/total number of genes in the tested list). Node colour represents the level of statistical significance; colour gradient ranges from blue ($\hat{=}$ higher p-value) to red ($\hat{=}$ lower p-value). Genes that are differentially expressed between the wild type and the *gad2* transgenic lines are enriched for functions related to hypoxia and oxygen responses. Genes that are differentially expressed between *gad2-1* and *gad2-2* are functionally enriched for glucosinolate/glycoside metabolism.



Supplementary Figure 9: Gene models illustrating expected T-DNA insertion sites in *gad2* mutants.

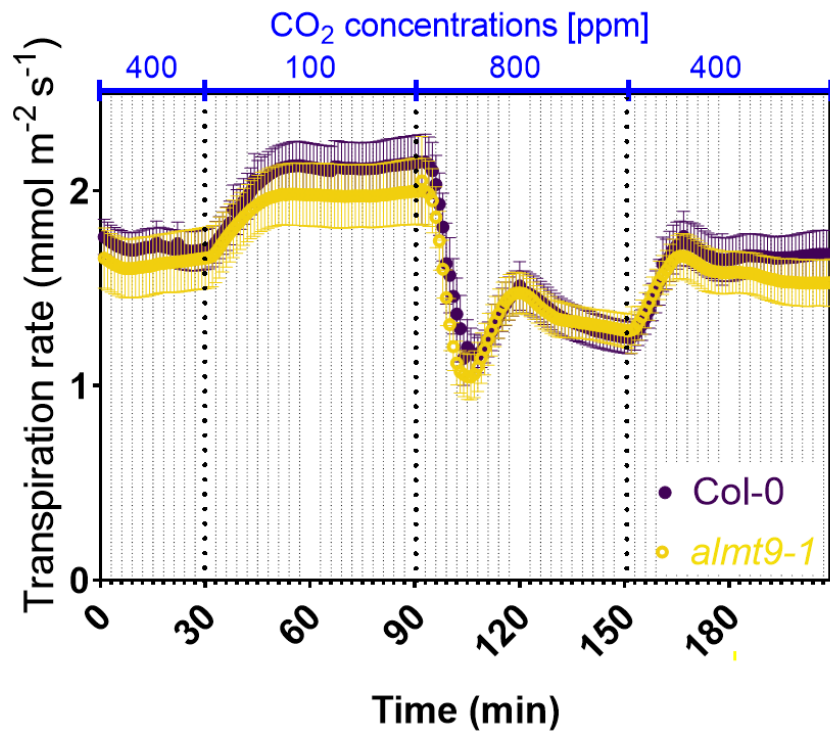
Localisation of T-DNA insertion sites in the genomic region of *GAD2* (AT1G65960) on chromosome 1 of the allelic mutant lines *gad2-1* and *gad2-2* and illustration of downstream neighbour genes of *GAD2*, known as *TPX2* (AT1G65970) and *TPX1* (AT1G65980). Gene maps originate from the TAIR10 database.





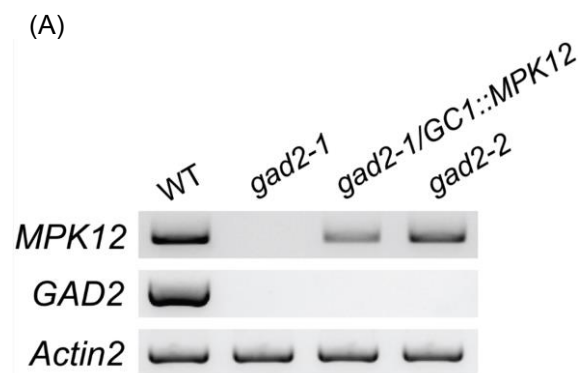
Supplementary Figure 10: Time-resolved patterns of transpiration rates in response to different [CO₂] in *alm6* mutant lines.

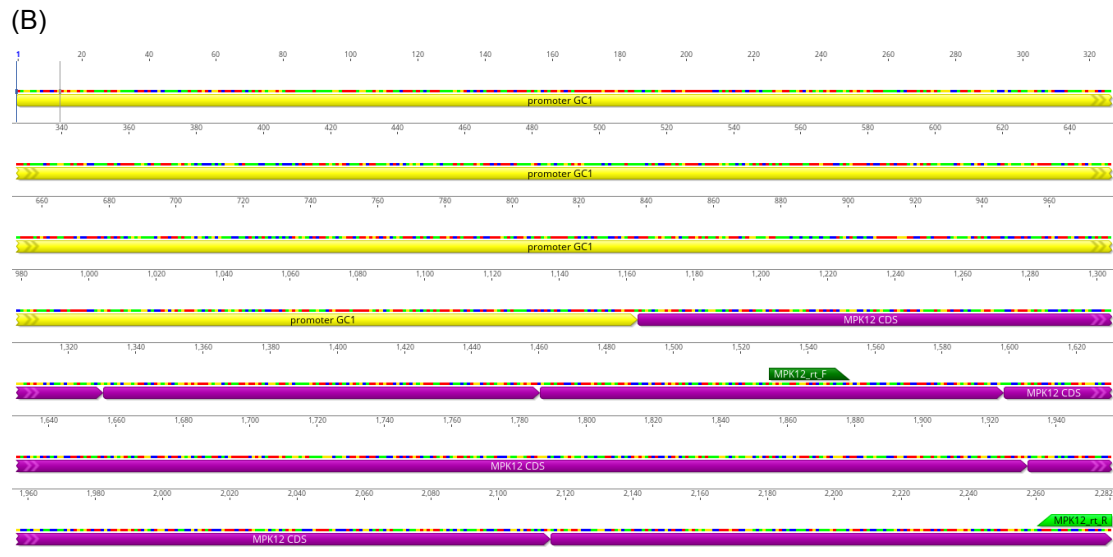
(A) Time courses of transpiration rates in response to ambient (400 ppm), elevated (800 ppm), and reduced (100 ppm) CO₂ in intact 4 ½- to 5 ½-week-old *A. thaliana* wild-type (WT; Col-0; n=10) and *alm6* T-DNA insertion lines (n=3) plants. The mutant line *alm6-1* originates from the GABI-Kat collection, while *alm6-2* was selected from the INRA-Versailles mutant catalogue. Error bars represent ± SEM. (B) *MPK12* deletion genotyping: all *alm6* plants from (A) were examined for the presence of *MPK12*. Primer pair 1 shows if *MPK12* is present, while primer pair 2 is designed to reveal the presence of both *MPK12* and the deletion, thereby revealing if plants are homozygous of *MPK12*. (C) Sequence view indicates the localisation of primer pair 1 (Forward primer 'MPK12_LP' [dark green arrow] and Reverse primer 'MPK12_RP' [light green arrow]) on chromosome 2, thereby framing the undeleted *MPK12-BPS2* region in Col-0 and the *alm6* lines. The 4,750 bp deletion that spans across the *MPK12-BPS2* region in *gad2-1* is shown in grey. Sequence visualisation and primer aligning were performed in Geneious version 2021.0.3.



Supplementary Figure 11: Time-resolved patterns of transpiration rates in response to different [CO₂] in *almt9-1*.

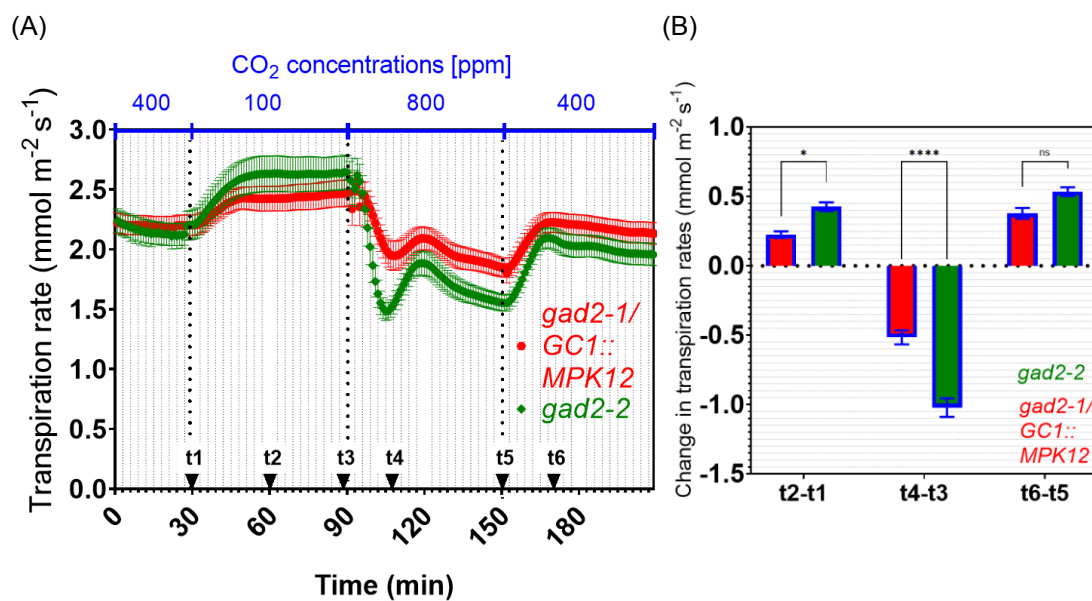
Time courses of transpiration rates in response to ambient (400 ppm), elevated (800 ppm), and reduced (100 ppm) CO₂ in intact 4 ½- to 5 ½-week-old *A. thaliana* wild-type (Col-0; n=7) and *almt9-1* (n=4) plants. Error bars represent ± SEM

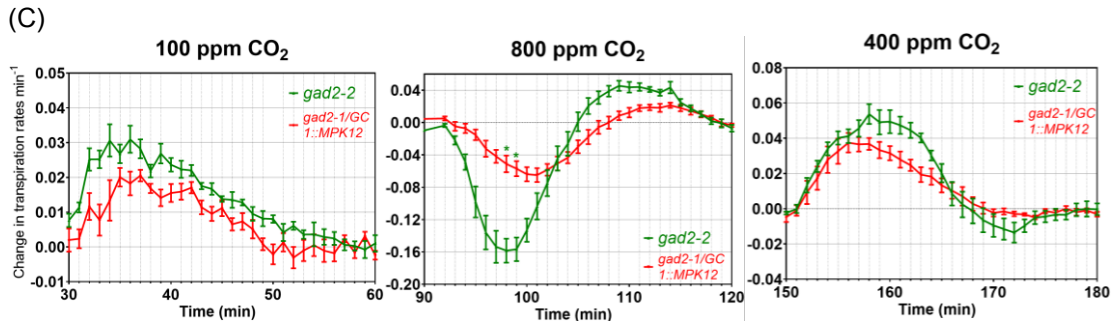




Supplementary Figure 12: Verification of MPK12 expression in *gad2-1/GC1::MPK12*.

(A) RT-PCR products of *MPK12* and *GAD2*, amplified from cDNA of *A. thaliana* wild-type, *gad2-1*, *gad2-2*, and *gad2-1/GC1::MPK12* leaves. The housekeeping gene *Actin2* was additionally amplified as a positive control. (B) Sequence view shows the localisation of a primer pair specific to *MPK12* (Forward primer 'MPK12_rt_F' [dark green arrow] and Reverse primer 'MPK12_rt_R' [light green arrow]), which was utilised to verify the presence of *MPK12* (purple) in *gad2-1/GC1::MPK12*. For driving *MPK12* into the guard cells of *gad2-1*, the guard cell promoter *GC1* had been used, shown here in yellow. Sequence visualisation and primer aligning were performed in Geneious version 2021.0.3.





Supplementary Figure 13: CO₂ responsiveness is higher in *gad2-2* than in *gad2-1/GC1::MPK12*.

(A) Time courses of transpiration rates in response to ambient (400 ppm), reduced (100 ppm), and elevated (800 ppm) CO₂ in intact *A. thaliana gad2-2* (n=8) and *gad2-1/GC1::MPK12* (n=6) plants. On the basis of the data presented in (A), changes in transpiration rates during specific time periods were determined and are illustrated in (B). For calculating these changes, transpiration rates at earlier time points were subtracted from transpiration rates at later points in time. Time points are numbered and denoted by small black arrows in (A). (C) Changes in transpiration rates per minute were calculated using $d\text{Transpiration}/dt$ (min) and are also based on the time-lapse transpiration rates illustrated in (A). Pooled data from four different experiments is shown. Error bars in all diagrams represent \pm SEM. Statistical differences were calculated using two-way ANOVA (B) or multiple Student's *t* tests (C); **P* < 0.05, *****P* < 0.0001.

Acknowledgements

We kindly thank our collaborators Mathew Lewsey, Bhavna Hurgobin, Changyu Yi, and Asha Haslem at the Department of Animal, Plant and Soil Science (La Trobe University) for performing whole genome sequencing and RNA-seq with subsequent data processing.

We gratefully thank Rainer Hedrich and his research group, including Johannes Herrmann, and Peter Ache at the Department for Molecular Plant Physiology and Biophysics - Botany I, Tobias Müller at the Department of Bioinformatics, and Marcus Dittrich at Biocenter, Department of Bioinformatics and Research Center for Infectious Diseases (ZINF) at Julius Maximilians University Würzburg (Germany) for providing preliminary CO₂ response curves, for the microarray analysis with subsequent data assessment, and for the fruitful discussions on the data presented here.

We thank Everard Edwards and Annette Betts from CSIRO Agriculture & Food (Waite Campus, Adelaide) for the kind provision of LI-6400XT Portable Photosynthesis System.

We thank Larissa Chirkova from ARC Industrial Transformation Research Hub for Wheat in a Hot and Dry Climate (University of Adelaide) for the performance of Ultra-Performance Liquid Chromatography.

We appreciate the help of Rosalie Kenyon at ACRF Cancer Genomics Facility (SA Pathology and University of South Australia) for conducting the RNA Labchip assay.

We thank Kylie Neumann and Sandy Khor, Department of Plant Science (University of Adelaide) for the provision of Invitrogen Qubit fluorometer.

We thank Na Sai for the assistance with transcriptomic analysis as well as with stomatal aperture measurements through provision of the stomata auto-measuring system StomaAI. We are also grateful for the great support from Xueying Feng in terms of sample preparation for microarray analysis, plant genotyping and for general useful

advice around various different kinds of assays. Both researchers are from the ARC Centre of Excellence in Plant Energy Biology (University of Adelaide).

This work was funded by ARC Discovery grant DP170104384. Mamoru Okamoto provided support as an independent advisor. A. P. was supported by the GOstralia!/University of Adelaide PhD Scholarship and a School of Agriculture, Food and Wine Short Term Scholarship.

Chapter 3: GABA deficiency does not alter photosynthetic CO₂ assimilation in Arabidopsis

Adriane Piechatzek^{1,2}, Andrew Scafaro³, Andres Garcia³, Owen Atkin³, Changyu Yi⁴, Mathew Lewsey⁴, Rainer Hedrich⁵, Bo Xu^{1,2,*} & Matthew Gilliam^{1,2,*}

¹ Plant Transport and Signalling Lab, ARC Centre of Excellence in Plant Energy Biology, Waite Research Institute, Glen Osmond, SA 5064, Australia

² School of Agriculture, Food and Wine, Waite Research Precinct, University of Adelaide, Glen Osmond, SA 5064, Australia

³ Division of Plant Sciences, The Australian National University (ANU), Canberra ACT 0200, Australia

⁴ Department of Animal, Plant and Soil Science, La Trobe University, Melbourne Victoria 3086, Australia

⁵ Institute for Molecular Plant Physiology and Biophysics, University of Würzburg, Würzburg 97078, Germany

* Correspondence should be addressed to:

Dr Bo Xu
Email: b.xu@adelaide.edu.au;

Professor Matthew Gilliam
Email: matthew.gilliam@adelaide.edu.au
Phone: +61 8 8313 8145

Key words: Elevated CO₂, carbohydrate metabolism, cell walls, GABA, photosynthesis, plant growth

Statement of Authorship

| | |
|---------------------|---|
| Title of Paper | GABA deficiency does not alter photosynthetic CO ₂ assimilation in Arabidopsis |
| Publication Status | <input type="checkbox"/> Published <input type="checkbox"/> Accepted for Publication <input type="checkbox"/> Submitted for Publication <input checked="" type="checkbox"/> Unpublished and Unsubmitted work written in manuscript style |
| Publication Details | Piechatzek, A., Xu, B., Yi, C., Lewsey, M., Scafaro, A., Garcia, A., Atkin, O., Hedrich, R., Gilliam, M. (2022). GABA deficiency does not alter photosynthetic CO ₂ assimilation in Arabidopsis. |

Principal Author

| | | |
|--------------------------------------|--|-----------------|
| Name of Principal Author (Candidate) | Adriane Piechatzek | |
| Contribution to the Paper | Designed and conducted the experiments, analysed most of the data, interpreted it, and wrote the manuscript. | |
| Overall percentage (%) | 75 | |
| Certification: | This paper reports on original research I conducted during the period of my Higher Degree by Research candidature and is not subject to any obligations or contractual agreements with a third party that would constrain its inclusion in this thesis. I am the primary author of this paper. | |
| Signature | | Date 13/01/2022 |

Co-Author Contributions

By signing the Statement of Authorship, each author certifies that:

- i. the candidate's stated contribution to the publication is accurate (as detailed above);
- ii. permission is granted for the candidate to include the publication in the thesis; and
- iii. the sum of all co-author contributions is equal to 100% less the candidate's stated contribution.

| | | | |
|---------------------------|---|------|------------|
| Name of Co-Author | Bo Xu | | |
| Contribution to the Paper | Supervised and designed experiments, interpreted data, and edited the manuscript. | | |
| Signature | | Date | 14/01/2022 |

| | | | |
|---------------------------|----------------------------------|------|---------|
| Name of Co-Author | Mathew Lewsey | | |
| Contribution to the Paper | Supervised the RNA-seq analysis. | | |
| Signature | | Date | 19/1/22 |

| | | | |
|---------------------------|--|------|------------|
| Name of Co-Author | Changyu Yi | | |
| Contribution to the Paper | Conducted the analysis of the RNA-seq data | | |
| Signature | | Date | 19/01/2022 |

| | | | |
|---------------------------|---|------|------------|
| Name of Co-Author | Andrew Scafaro | | |
| Contribution to the Paper | Assisted with A/C, curve analysis and data processing | | |
| Signature | | Date | 17/01/2022 |

| | | | |
|-------------------|---------------|--|--|
| Name of Co-Author | Andres Garcia | | |
|-------------------|---------------|--|--|

| | | | |
|---------------------------|--|------|------------|
| Contribution to the Paper | Performed respiration measurements using Q2 scanning technology. | | |
| Signature | | Date | 17-01-2022 |

| | | | |
|---------------------------|---|------|---------|
| Name of Co-Author | Owen Aktin | | |
| Contribution to the Paper | Supervised Q2 scanning and A/C _i curve analysis. | | |
| Signature | | Date | 17/1/22 |

| | | | |
|---------------------------|--------------------------------|------|------------|
| Name of Co-Author | Rainer Hedrich | | |
| Contribution to the Paper | Contributed to project design. | | |
| Signature | | Date | 19.01.2022 |

| | | | |
|---------------------------|---|------|------------|
| Name of Co-Author | Matthew Gilliam | | |
| Contribution to the Paper | Supervised and designed the project, interpreted data, and edited the manuscript. | | |
| Signature | | Date | 20/01/2022 |

Abstract

The fixation of carbon dioxide (CO₂) from the atmosphere is an integral process underpinning photosynthetic carbon and energy gain of plants. Intriguingly, CO₂ is known to be released into the cytosol as a side-product of GABA synthesis, which occurs during a bypass reaction of the mitochondrial-based Krebs cycle. However, a putative connection between GABA production and CO₂ uptake for photosynthesis from the atmosphere has not been investigated. Here, we show that GABA deficiency caused by the knockout of *Glutamate decarboxylase (GAD)* does not result in altered photosynthetic CO₂ assimilation. Gas exchange measurements in the GABA-depleted transgenic lines *gad2-1* and *gad1/2/4/5* did not reveal any changes in net CO₂ uptake. At the same time, respiratory rates were also found to be unaltered in the mutant lines, as shown by respiration measurements using Q2 scanning technology. Further confirmation for GABA not being directly involved in photosynthetic activities was provided by the determination of V_{cmax} (maximal rate of Rubisco carboxylase activity) and J_{max} (maximal rate of photosynthetic electron transport) on the basis of A_N/C_i (Net assimilation per internal CO₂ concentration) measurements, revealing comparable results between the wild type (WT) and the *gad(s)* mutants. These findings are consistent with the outcome of leaf biomass analyses in wild-type and mutant plants grown in response to long-term exposure to elevated CO₂ concentrations, demonstrating that GABA deficiency is not linked to promoted plant growth. We also investigated how elimination of GADs as key enzymes of the GABA shunt pathway affects the carbon assimilate composition and detected drastically elevated xylose concentrations in leaf material of the GABA-deficient mutant lines. In addition to the finding of numerous differentially expressed genes that are functionally enriched for functions in cell wall remodelling, the data indicates a link between GABA disruption and sugar salvage during wall recycling processes, thereby affirming that the elevation in monosaccharide content in the *gad(s)* mutants is independent of photosynthetic activities.

Introduction

CO₂ is the key building block for the carbon skeletons of which plants are comprised. Plants absorb CO₂ from the atmosphere and use it to produce carbohydrates during photosynthesis. The amount of photosynthetically assimilated CO₂ is generally reflected in the accumulation of plant biomass (Chao *et al.*, 2019). In that respect, it has been shown by previous studies that elevating atmospheric CO₂ concentrations up to a specific point principally triggers the promotion of C3 plant growth. For instance, 'Free Air CO₂ Enrichment' (FACE) experiments, which involve the exposure of a range of different plant species to increased CO₂ concentrations (475-600 ppm) in an open field (Taub, 2010), revealed an increase in light-saturated leaf photosynthetic rates by 31% as well as an increase in shoot and leaf dry mass by 20%; averaged from the data of six independent FACE experiments with 29 different C3 species (Ainsworth and Long, 2005). However, photosynthetic efficiency does not continuously increase in correlation with growing atmospheric CO₂ concentrations. At higher CO₂ concentrations, photosynthesis is constrained by an insufficient supply of inorganic phosphate for the regeneration of ATP as well as by a limited regeneration rate of ribulose biphosphate (RuBP), which serves as substrate for the CO₂-fixing enzyme Ribulose-1,5-bisphosphate carboxylase-oxygenase (Rubisco) (Sharkey *et al.*, 2007; Walker *et al.*, 2013). On the other hand, photosynthesis is also restricted at a low CO₂ partial pressure due to limitations imposed by Rubisco (Sharkey *et al.*, 2007). How C3 photosynthesis is affected by certain perturbations is best described by a model by Farquhar *et al.* (1980). With its help, photosynthetic parameters like the maximum rate of Rubisco carboxylase activity (V_{cmax}) as well as the maximum rate of electron transport (J_{max}) can be easily estimated. The calculation is based on measurements of net CO₂ assimilation (A_{N}) rates in relation to variations in leaf internal CO₂ concentrations (C_i) (Scafaro *et al.*, 2017). Generally, C_i is known to fluctuate in accordance with diurnal photosynthetic CO₂ assimilation rates. As CO₂ assimilation increases concomitant with the increasing irradiation in the morning, C_i is reduced, which raises the demand for CO₂ and thereby induces stomatal opening (Matthews *et al.*, 2017). Conversely, when C_i is high and the plant's need for CO₂ uptake low, stomatal closure is promoted (Matthews *et al.*, 2017).

Sugar metabolism is another factor that is regulated in compliance with photosynthetic activities of the plant and follows a diurnal cycle. Specifically, at the beginning of the day, the sugar that was gained by photosynthesis in the form of 3-phosphoglycerate (3-PGA) is converted to sucrose in the cytosol and turned into starch inside the chloroplasts later in the day (Dennis and Blakeley, 2000). The generated carbohydrates are utilised, *inter alia*, for the formation of cell wall components, which begins with the reversible conversion of sucrose to UDP-glucose by sucrose synthase (Carpita and McCann, 2000; Chibbar *et al.*, 2004). Alternatively, the sugar generated during photosynthesis is utilised by the plant for yielding energy in the form of ATP through cellular respiration (O'Leary and Plaxton, 2016). For this purpose, the energy stored in glucose molecules is released in the form of ATP over three interconnected pathways. One of them is named the 'Krebs cycle' (or alternatively, 'TCA cycle'), in which the reduced forms of the electron carriers Nicotinamide adenine dinucleotide phosphate (NADP) and Flavin adenine dinucleotide (FAD) are being generated for subsequent ATP production by the electron transport chain (Møller *et al.*, 2015).

A special attribute of cellular respiration in plants is its flexible nature due to a couple of bypass reactions, including the so-called GABA shunt pathway (O'Leary and Plaxton, 2020). Stress situations in particular trigger the activation of this reaction, which bypasses the Krebs cycle and leads to the synthesis of GABA via Glutamate decarboxylases (GADs) in the cytosol (Bown and Shelp, 2020). The substrate for GAD enzymes is glutamate, which is a product of the Krebs cycle intermediate 2-oxoglutarate. During the reaction, CO₂ is released into the cytosol. Interestingly, GABA accumulation seems to follow a diurnal rhythm, having its peak at the end of the dark period and is then dropping back in the first hours of the new light period (Espinoza *et al.*, 2010). At this point, it should be noted that GABA production can also occur independently of GAD activity, namely through an enzymatic reaction that involves the amino acid proline or through polyamine catabolism (Michaeli and Fromm, 2015; Podlešáková *et al.*, 2019). Out of the five GAD enzymes present in Arabidopsis, GAD2 is the main GABA synthesis enzyme in leaves and is localised to all plant tissues, while GAD1 activity is essential for GABA production in roots (Scholz *et al.*, 2015). *GAD5*, however, is mostly expressed in male gametes (Podlešáková *et al.*, 2019). Under unstimulated conditions, *GAD3* and *GAD4* expression is minor in leaves and roots (Scholz *et al.*, 2015), whereas *GAD4* is significantly upregulated in response to extreme

external conditions like salt stress, cold, drought, and hypoxia (Renault *et al.*, 2010). Mutations in *GAD1* and *GAD2* have a great impact on GABA production as demonstrated by previous studies. Work by Mekonnen *et al.* (2016) revealed a significant reduction in GABA content in shoot material of the double mutant *gad1/2*. The gene knockouts were furthermore associated with an altered composition of Krebs cycle intermediates and amino acids as well as with a 2-fold increase in shoot glucose content (Mekonnen *et al.*, 2016).

It is known that glucose and fructose are generated as small products during photosynthesis or are derived from starch degradation (Siddiqui *et al.*, 2020). The higher glucose concentrations in the *gad1/2* double mutant could potentially be an indication of enhanced photosynthetic capacity. Also, we note that CO₂ is released into the cytosol as a side-product of GABA synthesis and wonder if this could potentially influence photosynthetic CO₂ assimilation. As mentioned earlier, it is established that elevating atmospheric CO₂ concentrations up to a specific point results in higher C_i, which promotes photosynthetic CO₂ assimilation and stimulates plant growth (Ziska *et al.*, 2009). Carbon is also cleaved off in the form of CO₂ during the Krebs cycle which, however, takes place in the mitochondria of cells and not in the cytosol (Møller *et al.*, 2015). It should also be noted that both GABA synthesis as well as carbon assimilation appear to be circadian regulated. Hence, the question arises if GABA-dependent CO₂ release has an effect on photosynthetic CO₂ assimilation.

Significantly, here we show that GABA deficiency does not result in decreased photosynthetic rates and rosette leaf biomass accumulation. At the same time, our data reveals massively elevated xylose concentrations in leaf tissue as well as major alterations in the expression of cell wall- and carbohydrate metabolism-related genes. Together, we conclude that the increased concentrations of monosaccharides like glucose or xylose in the *gad* loss-of-function lines are not the result of modified photosynthetic rates but could potentially arise from altered cell wall remodelling processes.

Material and Methods

Plant materials and growth conditions

In all experiments, the following *Arabidopsis thaliana* accessions were used: Wild-type ecotype Columbia (Col-0) and mutant lines generated in the Col-0 background. The two allelic mutant lines *gad2-1* (GABI_474E05) and *gad2-2* (SALK_028819) were obtained from the Arabidopsis Biological Resource Centre (ABRC). While *gad2-2* is a confirmed single mutant line, *gad2-1* additionally contains a deletion of full-length *MPK12* (AT2G46070) and *BPS2* (AT2G46080) (Chapter 2). The transgenic mutant line *gad1/2/4/5* was generated by crossing *gad1-1* (SALK_017810), *gad4* (SALK_106240), *gad5* (SALK_203883), and *gad2-1* (GABI_474E05), and was obtained from Shuqun Zhang (Deng *et al.* 2020). All primers used for the genotyping PCR are listed in the [Supplementary Table 1](#).

Unless noted, all plants were raised in hydroponics for five to six weeks following Conn *et al.* (2013): All seeds were stratified for two days in the dark at 4°C and then transferred to short-day growth conditions [10 hrs light ($\sim 100 \mu\text{mol photons m}^{-2} \text{s}^{-1}$)/ 14 hrs dark, average temperature of 22°C, and 56% relative humidity]. In the first three to four weeks, plants grew within the lids of customised black microcentrifuge tubes, with a hole, that had been filled with 0.7% agar and fitted on a 24 well floating microtube rack. The small hydroponic container that contained the rack was filled with a modified Hoagland solution, named Germination Solution (GS), which was replaced every week (nutrient composition is listed in the [Supplementary Table 2](#)). The small hydroponic container was covered with cling wrap, which was perforated after two weeks of growth and completely removed three days before the plant transfer to hydroponic tanks. For a smooth transition from GS to higher concentrated Basal Nutrient Solution (BNS; nutrient composition is listed in the [Supplementary Table](#)), after two weeks of growth, GS was exchanged by 1/3 with BNS on three subsequent days. After 3 ½ weeks of growth, seedlings with the same estimated leaf area were transplanted to individual 50 mL falcon tubes (with bottoms removed) inside aerated hydroponic tanks filled with BNS. For all experiments, different genotypes grew side by side under the same growth conditions and were analysed within a time-period of 10 days.

For soil growth, Arabidopsis seeds were surface-sterilised in 75% ethanol and ~4% Sodium hypochlorite. In a next step, they were sown on half-strength Murashige and Skoog ($\frac{1}{2}$ MS) medium (pH 5.6) supplemented with 0.8 % phytigel (w/v) and 1% sucrose (w/v). After stratification at 4°C for two days, the seeds were transferred to short-day growth conditions (10 hrs light [$\sim 100 \mu\text{mol photons m}^{-2} \text{s}^{-1}$]/14 hrs dark, 22°C, 56% relative humidity). All seedlings were raised in $\frac{1}{2}$ MS medium for 10 days before they were transferred to soil (mixture of coco peat and horticultural sand). Overall, plants were raised up to five to six weeks.

GABA measurements

A non-volatile profiling analysis of whole rosette leaf extracts was conducted using Gas chromatography-mass spectrometry (GC-MS) online derivatisation in collaboration with Metabolomics Australia (The Australian Wine Research Institute, Adelaide). In brief, rosette leaves of six-week-old plants were snap-frozen and ground to fine powder in liquid nitrogen. About 50-100 mg of the frozen leaf tissue was weighed and 500 μL water/methanol/chloroform (1:2:2) was added to each sample. The extracts were centrifuged, and the upper fraction was transferred to a clean 1.5 mL reaction tube. Extraction of the pellet was repeated with 300 μL water/methanol (1:2). The top layer fractions were combined (300 μL) and dried down, resuspended in methanol, transferred to 250 μL glass inserts, dried down and then analysed using a GC-MS-based approach. GC-MS analysis was performed on an Agilent 7890 gas chromatograph equipped with Gerstel MPS2 multipurpose sampler and coupled to an Agilent 5975C VL mass selective detector. Instrument control was performed with Agilent G1701A Revision E.02.01 ChemStation software. The gas chromatograph was fitted with an Agilent CP9013 column (30 m x 0.25 mm x 0.25 μm). Helium (Ultra High Purity) in constant flow mode at approximately 0.9 mL/min with retention time locking applied (locked to δ -mannitol at 21.45 min). The oven temperature was started at 35 °C, held at this temperature for two minutes then increased to 10 °C/min to 315 °C and held at this temperature for 16 minutes. The total run time was 46 minutes. Mass spectral data was acquired from nine minutes to 46 minutes. The mass spectrometer quadrupole was set to 150 °C and the source was set at 230 °C. The analysis was run in SCAN mode with a solvent delay of 8.90 min. For sample derivatisation, 22 μL of methoxyamine hydrochloride in pyridine (20 mg/mL) was injected into the sample vial and the vial

was incubated at 37 °C with agitation for two hours. 22 µL of BSTFA + 1% TMCS was injected into the vial and incubated at 37 °C with agitation for 60 minutes. The sample was allowed to settle at room temperature for 60 minutes before injection.

In a different approach, leaf GABA concentrations were determined using Ultra performance liquid chromatography (UPLC). Briefly, rosette leaves were snap-frozen and homogenised in liquid nitrogen using mortar and pestle. For UPLC analysis, about 50 mg of ground tissue were used. The UPLC analysis was conducted at the Australian Centre for Plant Functional Genomics (University of Adelaide) in accordance with a method described by Xu *et al.* (2021a).

Gas exchange measurements

For time-resolved infrared gas analysis in whole rosettes, four-and-a-half to five-and-a-half-week-old plants were transferred to 50 mL falcon centrifuge tubes filled with BNS solution (Conn *et al.*, 2013). The falcon tubes were placed in a LI-6400XT Portable photosynthesis system (LI-COR Biosciences) fitted with a 6400-17 Whole Plant Arabidopsis Chamber. Prior to the gas exchange measurements, plants were adapted to a light intensity of 350 µmol photons m⁻² s⁻¹ for one hour (30W LED Panel, Arlec) to maximise gas exchange rates. Transpiration and net CO₂ uptake rates of the plants inside the chamber were recorded in response to a variety of CO₂ concentrations (100 ppm, 800 ppm, and 400 ppm CO₂) under the following chamber conditions: 350 µmol photons m⁻² s⁻¹ light intensity with a portion of 10% blue light, 50-60% relative humidity, an average temperature of ~22°C, and an airflow rate of 350 mmol s⁻¹). Measurements were logged every minute and IRGAs were matched at the start of the measurements and then every five minutes. The duration of measurements at each CO₂ step was one hour. For data visualisation, the first 30 min of recording (at 400 ppm CO₂) were omitted. During the last hour of the experiment, gas exchange was recorded in the dark. Following the gas exchange measurements, leaf rosette surfaces of each analysed plant were captured using a Nikon D5100 camera and were measured using the 'Threshold Color' tool in ImageJ. All recorded transpiration rates were normalised to leaf rosette areas.

A_N/C_i curve analysis

Gas exchange measurements for A_N/C_i curve analysis were conducted in fully expanded single leaves of six- to seven-week-old, soil-grown Col-0, *gad2-1*, and *gad1/2/4/5* plants using a LI-6400XT Portable photosynthesis system (LI-COR Biosciences) equipped with a 2 x 3 cm Clear Chamber Bottom cuvette. Net assimilation (A_N) and intercellular CO_2 concentrations (C_i) were recorded in response to step changes in CO_2 concentrations (400, 50, 100, 150, 250, 400, 600, 800, 1000, 1400, and 1800 ppm). The light intensity was set to $600 \mu\text{mol photons m}^{-2} \text{s}^{-1}$, the flow rate was kept at $500 \mu\text{mol s}^{-1}$, and the block temperature was adjusted to 25°C . The measurements were logged five times at each concentration and the average of all five measurements was used for generating A_N/C_i curves, where A_N and C_i concentrations were plotted against each other. The resulting A_N/C_i data was used to estimate V_{cmax} (maximum rate of Rubisco carboxylase activity) and J_{max} (maximum rate of photosynthetic electron transport). The calculation of V_{cmax} followed a Michaelis Menten equation by Farquhar *et al.* (1980), which describes a Rubisco-limited A_N response to CO_2 (Sharkey *et al.*, 2007), where K_c is the Michaelis constant of Rubisco for CO_2 , C_c the CO_2 partial pressure at the carboxylation site (in the chloroplast), O the partial pressure of oxygen at the carboxylation site, K_o the inhibition constant (Michaelis constant), Γ^* the photorespiratory compensation point, and R_d day respiration (mitochondrial).

$$A = V_{\text{cmax}} \left[\frac{C_c - \Gamma^*}{C_c + K_c (1 + O/K_o)} \right] - R_d$$

J_{max} was determined following another equation by Farquhar *et al.* (1980), which describes a RuBP-limited A_N response to CO_2 , where C_c is the CO_2 partial pressure at the carboxylation site, Γ^* the photorespiratory compensation point, and R_d day respiration (mitochondrial).

$$A = J \frac{C_c - \Gamma^*}{4C_c + 8\Gamma^*} - R_d$$

All data was normalised to the dry leaf mass per area (LMA) of respective single leaves. For the leaf area measurements, leaf surfaces were captured using a Nikon D5100 camera and afterwards measured using the 'Threshold Color' tool in ImageJ.

Respiration measurements

Single leaves of eight-week-old hydroponic plants were dissected, weighed, and placed in specialised tubes with fluorescent caps. In particular, during the last weeks of growth, it was ensured that rosette leaves from different plants were not overlapping to allow exposure to comparable light intensities ($120 - 150 \mu\text{mol m}^{-2} \text{s}^{-1}$; arrangement of plants in hydroponic tanks with large gaps in between). Per genotype, four leaves of 12, 14, or 16 plants (different for each plant batch) were measured. Dark respiration (R_{dark}) was determined at room temperature using Q2 scanning technology (Astec-Global), which is described elsewhere (Scafaro *et al.*, 2017). All tubes were sealed airtight and were placed in 48 well plates, with four tubes functioning as standards for calibration. Among these, two contained 100% N_2 (to calibrate for 0% O_2), while the other two contained 100% O_2 (to calibrate for 100% O_2). Plates were scanned in a serpentine order with a frequency of two minutes. The O_2 absorption was determined on the basis of O_2 percentages that had been calculated in relation to the calibration readings. Mole fraction of oxygen was determined using the ideal gas law (Scafaro *et al.*, 2017). All O_2 consumption rates were normalised either to leaf fresh or to dry weight. The dry weight of the rosette leaves was determined after drying in an oven at 65°C for three days. Leaf areas were captured using a Nikon D5100 camera and were measured using the ‘Threshold Color’ tool in ImageJ.

Biomass and stomatal density analysis in high CO_2 -treated plants

Plants were raised on $\frac{1}{2}$ MS agar plates for the first 12 days and were then transferred to soil. For six weeks, control and high CO_2 treated plants were successively grown in a CMP6050 Conviron cabinet under identical conditions (55% relative humidity, 10 hrs light [100 to $110 \mu\text{mol photons m}^{-2} \text{s}^{-1}$ light intensity]/14 hrs dark, and a chamber temperature of $\sim 22^\circ\text{C}$), except for the atmospheric CO_2 concentration. For long-term exposure to high CO_2 , plants were grown at CO_2 concentrations above ambient CO_2 (~ 750 ppm), while all control plants were raised at ambient CO_2 (~ 450 ppm).

For biomass analysis, excised rosette leaves were weighed and captured using a Nikon D5100 camera. Afterwards, leaf areas were measured using the ‘Threshold Color’ tool in ImageJ.

For stomatal density determination, epidermal peels were produced from single leaves. Thereby, single leaves were cut off from rosettes and glued with their adaxial side to the adhesive surface of a piece of masking tape. Sticky tape was attached to the abaxial side of the leaf and the abaxial epidermal layer was peeled off along with the sticky tape. Epidermal peels were kept in MilliQ water until all plants had been processed.

Stomata were imaged using a 10x objective lens on an Axiophot Pol Photomicroscope (Carl Zeiss) and were counted using the multi-point tool in ImageJ. For each experiment, seven to eight biological plant replicates and three leaves per plant replicate were used.

RNA sequencing

Total RNA was extracted from whole rosette leaves of five-week-old plants using four biological replicates per genotype. (*Col-0*, *gad2-1*, and *gad2-2*). The rosette leaves were snap-frozen and ground to fine powder in liquid N₂. Next, the ground material was transferred to 1 mL TRIzol reagent (TRIzol RNA Isolation Reagents, Invitrogen) inside a 2-mL reaction tube. After having added 200 µL acidic chloroform, the mixture was centrifuged at maximum speed for 15 min at 4°C. The supernatant was transferred to tubes that contained 500 µL 100% Isopropanol and the mixture was incubated for 10 min at 4°C. After centrifugation at 11 400 rpm at 4°C, the isolated RNA was washed in 1 mL 75% EtOH and air-dried. Subsequently, the dried RNA pellet was resuspended in 20 µL nuclease-free H₂O. For removal of gDNA contamination, the RNA eluate was treated with DNase using a TURBO DNA-free kit (Ambion) in accordance with the manufacturer's instructions.

The RNA integrity was evaluated using gel electrophoresis as well as spectrophotometry (ND-1000; NanoDrop Technologies), whilst the RNA quantity was determined fluorometrically (Invitrogen Qubit[®] fluorometer). RNA integrity and concentration were also determined using an RNA 6000 Labchip on an Agilent 2100 BioAnalyzer (Version C.01.069) at ACRF Cancer Genomics Facility (SA Pathology and University of South Australia).

RNA sequencing was performed at Animal Plant and Soil Sciences (La Trobe University, Australia). In brief, RNA-seq libraries were constructed using the TruSeq Stranded mRNA Library Prep Kit in accordance with the manufacturer's instructions (Illumina) and sequenced on a NextSeq500 system (Illumina) as 75 bp single-end reads with at least 30 million reads per sample. Reads quality were examined using FastQC (<http://www.bioinformatics.babraham.ac.uk/projects/fastqc>) and low-quality reads and adapters were trimmed using Trim Galore (<https://github.com/FelixKrueger/TrimGalore>). To obtain transcript abundances as transcripts per million (TPM) and estimated counts, trimmed reads were mapped to the Arabidopsis reference transcriptome (Araport 11) using Salmon (Cheng *et al.*, 2017; Patro *et al.*, 2017). Gene-level TPM and count estimates were obtained using tximport (Soneson *et al.*, 2016). Genes with total counts more than 10 in all samples were retained for differential gene expression analysis using DESeq2 and genes with a false discovery rate < 0.05 were considered as differentially expressed genes (Love *et al.*, 2014). Gene ontology enrichment analysis was performed using clusterProfiler (Yu *et al.*, 2012). A Principal component analysis (PCA) was calculated using the DESeq2 R package and the 500 highest variable genes and plotted using the ggplot2 package in R.

Microarray analysis

RNA isolation from rosette leaves was performed as described in the previous subsection (RNA sequencing). RNA integrity and concentration were determined using an RNA 6000 Labchip on an Agilent 2100 BioAnalyzer (Version C.01.069) at ACRF Cancer Genomics Facility (SA Pathology and University of South Australia). Only samples with an RNA Integrity Number (RIN) ≥ 8 were selected for the microarray analysis. Microarray hybridisation and data processing were conducted by our collaborators at Julius-von-Sachs-Institute for Biosciences (Department of Molecular Plant Physiology and Biophysics - Botany I, University of Wuerzburg), following a method described by Dittrich *et al.* (2019).

Statistical analysis

Unless noted, GraphPad Prism (Version 9.0.0 for Windows) was used for statistical analysis of the data presented in this study. In a first step, it was determined whether

the data followed a Gaussian distribution using a D'Agostino & Pearson test. Depending on the data type, one-way ANOVA, two-way ANOVA, unpaired t-tests, or multiple unpaired t-tests were performed. Under the assumption of a Gaussian distribution, one-way Tukey's multiple comparisons test or unpaired t-tests were applied on the data for mean comparisons between different genotypes. If the data was not normally distributed, a one-way ANOVA Dunnet's multiple comparison test was performed. If the data set was based on two variables instead of one, the data was compared using a two-way Tukey's multiple comparison test. All data are presented as mean \pm SEM.

Results

Knocking out GABA synthesis does not result in higher CO₂ uptake

The observation that CO₂ is released as a by-product of GABA synthesis into the cytosol led us to the question if GABA deficiency influences CO₂ assimilation. To approach this question, we examined net CO₂ uptake rates in GABA-deficient mutant lines via infrared gas analysis. The perfect test subjects for this approach were the loss-of function mutant lines *gad2-1*, *gad2-2*, and *gad1/2/4/5*, which have greatly reduced GABA in leaves due to ablation of *Glutamate decarboxylase* (*GAD*) genes (Supplementary Figure 1).

However, no differences in net CO₂ uptake rates were detectable between the wild type and the quadruple mutant (Figure 1). This was revealed by two large-scale experiments that were based on a large number of replicates (between 29 and 41; Figure 1) and were conducted in four-week-old or six-week-old plants as well as by experimental approaches with a smaller number of replicates (between 4 and 13) in five-to-six-week-old plants. Also, using an elevated light intensity (600 instead of 350 $\mu\text{mol photons m}^{-2} \text{ s}^{-1}$) and analysing single instead of rosette leaves did not make a difference (Supplementary Figure 2). Simultaneously, O₂ consumption rates (dark respiration) as well as V_{cmax} (maximum rate of Rubisco carboxylase activity) and J_{max} (maximum rate of photosynthetic electron transport), which were estimated via an $A_{\text{N}}/C_{\text{i}}$ curve analysis, were comparable between the wild type and *gad1/2/4/5* (Figure 2). The GABA-depleted lines *gad2-1* and *gad2-2* had not been included in the large-scale experiments, but additional gas exchange measurements did not reveal any alterations in net CO₂ flux in these lines either (Supplementary Figure 3).

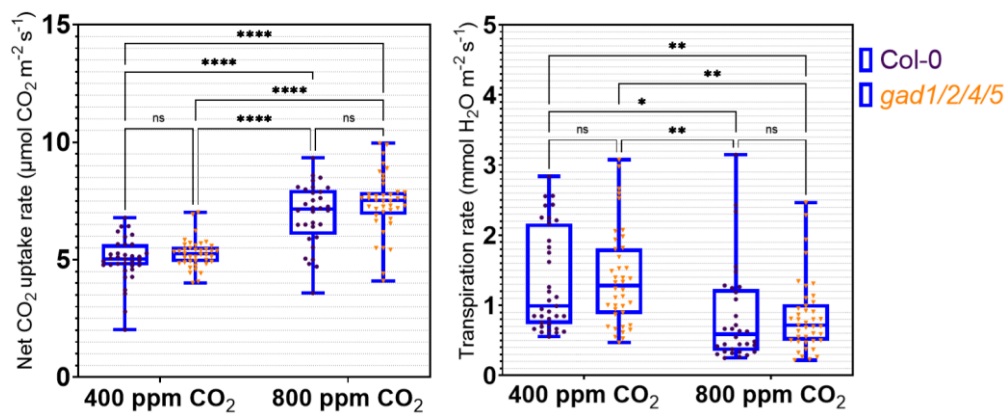
All in all, as net CO₂ uptake rates, V_{cmax} , J_{max} , and respiration rates were unaltered in the GABA-depleted mutant lines, it appears that GABA deficiency is not associated with a decreased photosynthetic capacity.

Not only net CO₂ flux, but also transpiration rates were determined in the different genotypes using the infrared gas analyser (Figure 1 A, B). Similarly, no differences were detected between the wild type and *gad1/2/4/5*. Thus, also the instantaneous water use efficiency (WUE), which was determined through division of net CO₂ uptake rates by transpiration rates, was found to be unaltered in the *gad1/2/4/5* (Figure 1 C).

What is more, the data revealed differences in CO₂ responsiveness in connection with plant age. Younger plants (four-week-old, Figure 1 A) exhibited a significant reduction in transpiration rates in response to elevated (800 ppm) CO₂ conditions, which was absent in older plants (6-week-old; Figure 1 B). Consequently, a clearly enhanced WUE was observed in young plants in response to 800 ppm, regardless of their genotype.

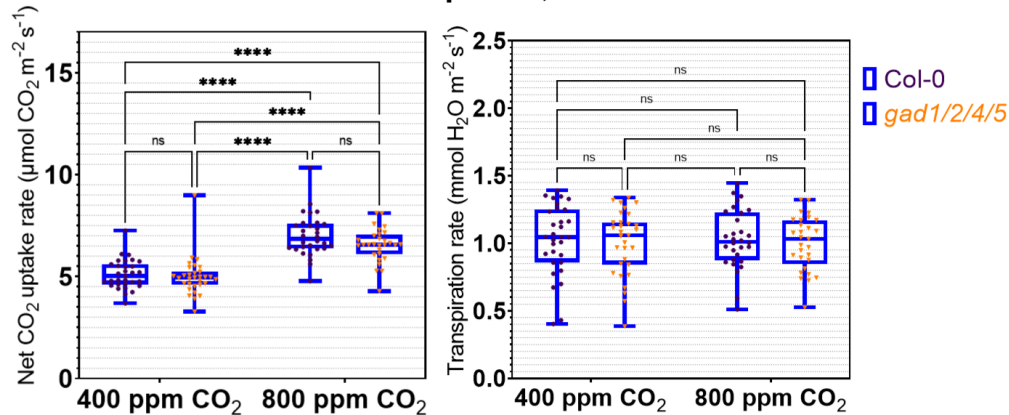
(A)

IRGA in 4-week-old plants, rosette leaves



(B)

IRGA in 6-week-old plants, rosette leaves



(C)

Instantaneous WUE, rosette leaves

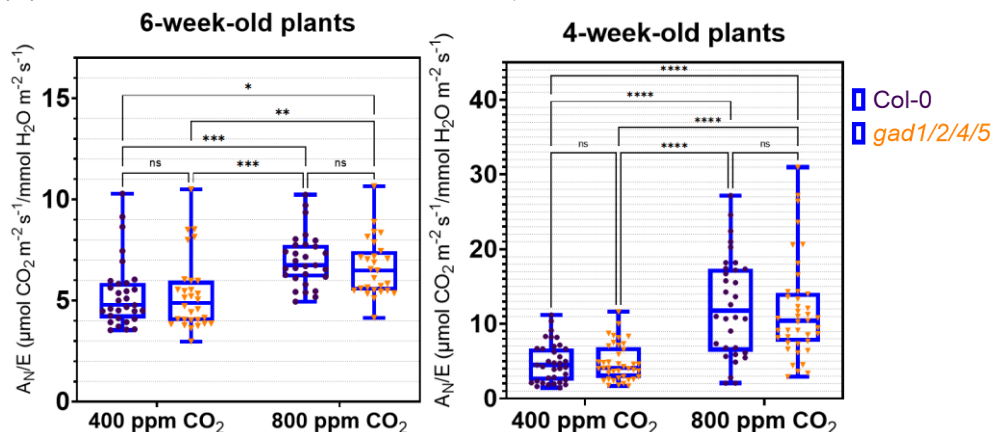


Figure 1: Net CO₂ consumption rates are not altered in GABA-deficient mutant lines.

Outcome of Infrared gas (IRGA) analysis in rosette leaves of intact hydroponic *A. thaliana* wild-type (Col-0) and *gad1/2/4/5* plants at ambient CO₂ (400 ppm) and elevated CO₂ (800 ppm). The analysis was performed as a large-scale experiment with a large number of replicates using a LI-6400XT Portable Photosynthesis System at a light intensity of 350 μmol photons m⁻² s⁻¹. (A) Net CO₂ uptake rates and transpiration (E) rates in four-week-old Col-0 (n=35) and *gad1/2/4/5* (n=40) plants at 400 ppm CO₂ as well as in four-week-old Col-0 (n=32) and *gad1/2/4/5* (n=41) plants at 800 ppm CO₂. (B) Illustration shows net CO₂ consumption rates in six-week-old Col-0 (n=31) and *gad1/2/4/5* (n=31) at 400 ppm CO₂ as well as Col-0 (n=30) and *gad1/2/4/5* (n=29) plants at the same age in response to 800 ppm CO₂. (C) Instantaneous WUE (A_N/E) in four-week-old and six-week-old wild-type and *gad1/2/4/5* plants as estimated on the basis of the data presented in (A) and (B). Data was plotted with box and whiskers: the box illustrates the median, and the 25th and 75th percentiles, while the whiskers indicate the minimum and maximum values. Statistical differences were calculated using two-way ANOVA (A-C); *P < 0.05, **P < 0.01, ***P < 0.001, ****P < 0.0001.

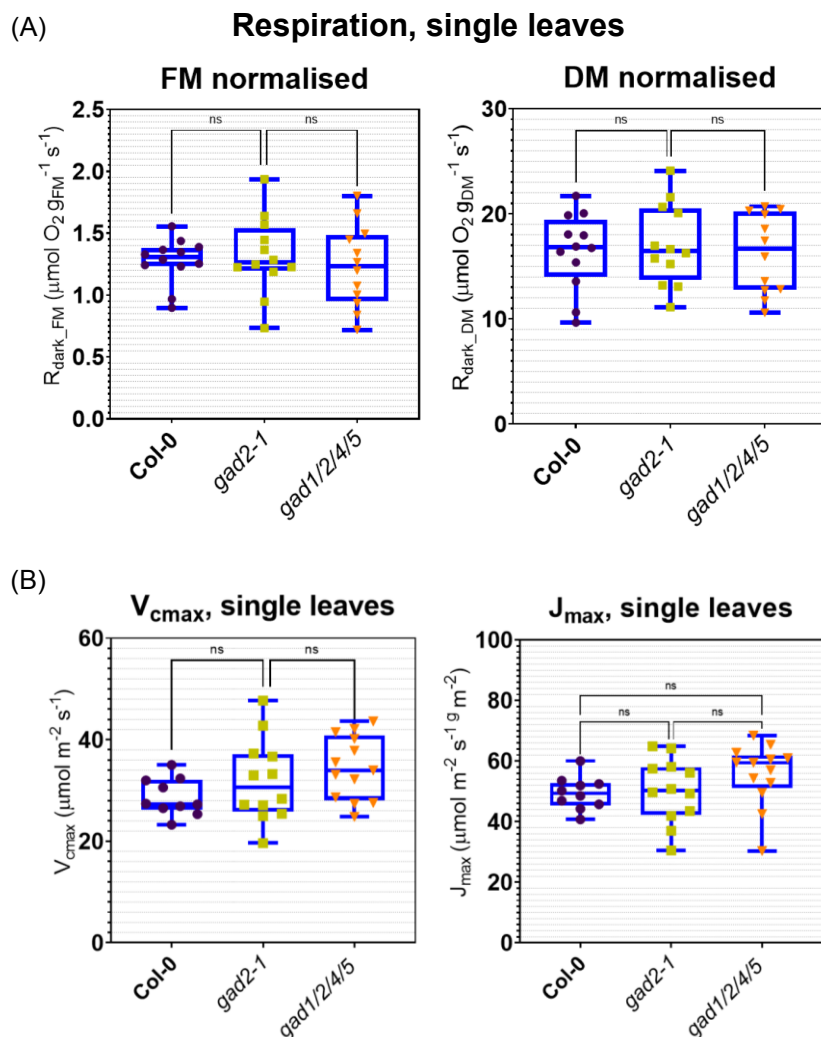


Figure 2: CO₂ assimilation is not altered in GABA-deficient mutant lines.

(A) Outcome of dark Respiration (R_{dark}) measurements in *A. thaliana* wild-type (Col-0), *gad2-1*, and *gad1/2/4/5* plants, based on leaf fresh mass (FM)- or dry mass (DM)-normalised oxygen consumption rates (n=12), which were determined using a Q2 scanner. (B) J_{max} (maximum rate of photosynthetic electron transport) and V_{cmax} (maximum rate of Rubisco carboxylase activity) were estimated on the basis of $A_{\text{N}}/C_{\text{i}}$ (Net assimilation/leaf internal CO₂ concentration) data. A_{N} and C_{i} values had been determined in response to a series of different CO₂ concentrations (50, 100, 150, 250, 400, 600, 800, 1000, 1400, and 1800 ppm) in single leaves of Col-0 (n=10), *gad2-1* (n=12), and *gad1/2/4/5* (n=13) using a LI-6400XT Portable Photosynthesis System and were plotted against each other at every CO₂ set point. Data was plotted with box and whiskers: the box illustrates the median, and the 25th and 75th percentiles, while the whiskers indicate the minimum and maximum values. Statistical differences were calculated using one-way ANOVA.

GABA deficiency does not lead to a decrease in plant biomass

Principally, biomass accumulation is coupled to a plant's photosynthetic performance (Ainsworth and Rogers, 2007; Kebeish *et al.*, 2007). If C₃ plants are subjected to high CO₂, photosynthetic rates and biomass production are generally increased up until an inflection point (Ainsworth and Rogers, 2007; Sandquist, 2015). We therefore examined whether the absence of photosynthetic impairment in *gad1/2/4/5* was also reflected in an unaltered biomass. For this purpose, a time-lapse growth experiment was conducted in wild-type (Col-0) and GABA-deficient *gad1/2/4/5* plants. All plants were raised up to six weeks in a growth chamber with a CO₂ concentration of either ambient (~450 ppm) or elevated (~750 ppm) CO₂.

No differences in rosette leaf area, fresh mass, or leaf mass per area (LMA) were detected between the wild type and the quadruple mutant, neither at ambient nor at elevated CO₂ concentrations (Figure 3). In both genotypes, elevated CO₂ promoted plant growth in comparison to ambient CO₂. Leaf weights had doubled, while leaf areas had increased 4-fold upon high CO₂ treatment. At the same time, the LMA, which is known to positively correlate with photosynthetic rates on an area basis (Letts *et al.*, 2012), remained unchanged.

Elevated CO₂ does not only lead to higher biomass but was also discovered to cause a reduction in stomatal density (Woodward and Kelly, 1995). Therefore, we additionally investigated whether long-term CO₂ exposure resulted in an altered stomatal density in

gad1/2/4/5. As expected, stomatal numbers were significantly decreased in high CO₂-treated plants compared to the control plants. However, no differences in stomatal densities were detected between the wild type and *gad1/2/4/5*.

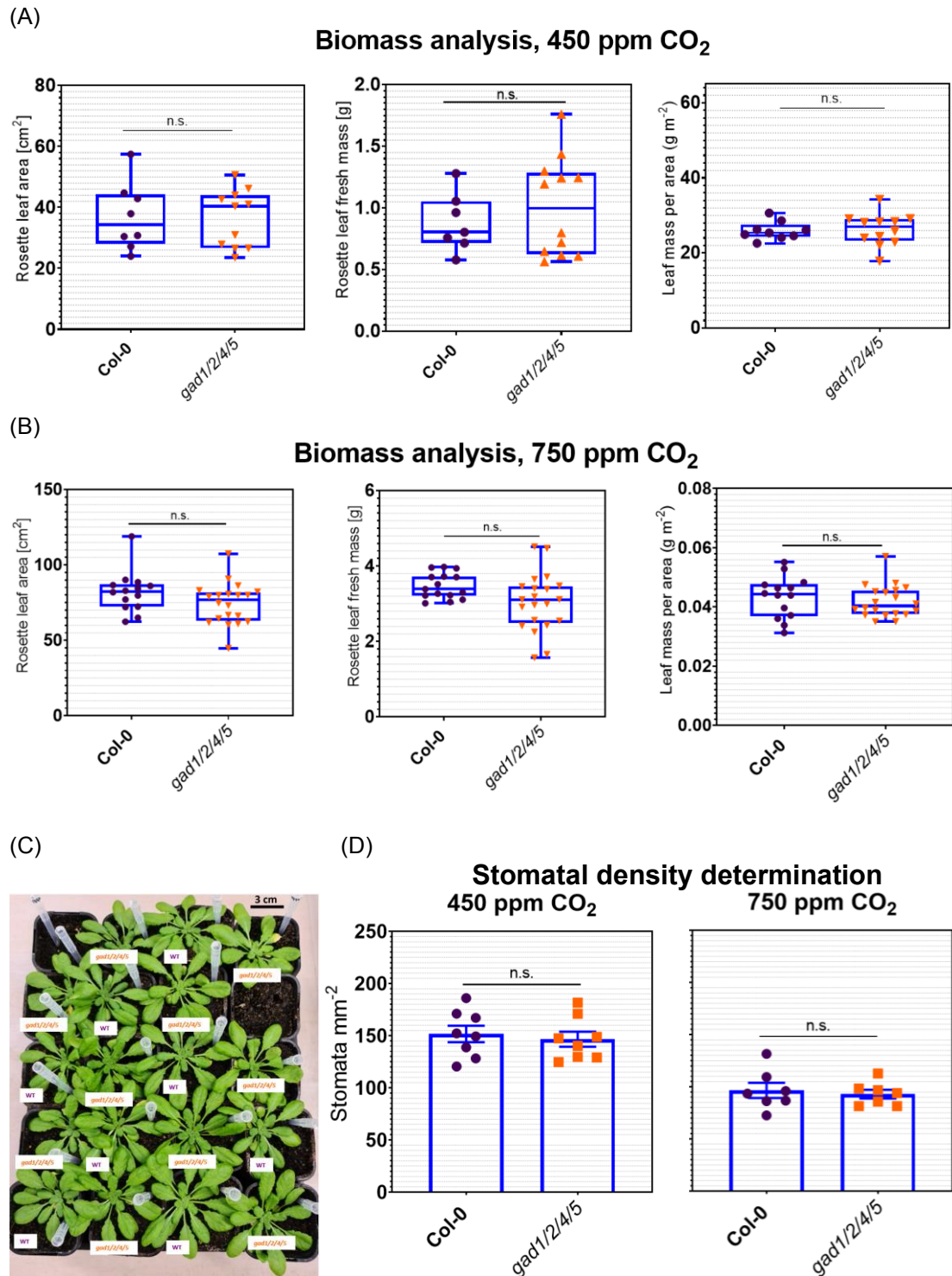


Figure 3: Biomass and stomatal density are unchanged in GABA-deficient mutant line.

Rosette leaf areas, rosette leaf fresh mass, and leaf mass per area (LMA) ratios of six-week-old *A. thaliana* wild-type (Col-0) and *gad1/2/4/5* plants raised (A) at ambient CO₂ (~450 ppm;

n=7-11) or (B) at elevated CO₂ (~750 ppm; n=14-20). (C) Representative image of wild-type (WT) and *gad1/2/4/5* plants arranged in alternating order within the growth chamber. (D) Stomatal density determination on abaxial leaf surfaces of three leaves per plant at ambient (n=8) and high (n=7) CO₂ conditions. All experiments were conducted three times. Data was plotted with bars (D) or box and whiskers (A, B): the box illustrates the median, and the 25th and 75th percentiles, while the whiskers indicate the minimum and maximum values. Error bars represent ± SEM (D). Statistical analysis was conducted using a two-sided Student's t-test (A, B, D).

The GABA-deficient mutant lines *gad2-1* and *gad2-2* had been excluded from the large-scale biomass analysis for simplification of experimental procedures. However, the biomass of *gad2-1* and *gad2-2* plants was quantified in other experiments (Figure 4 and Supplementary Figure 4). Rosette leaf fresh masses, dry masses, and areas were all slightly decreased in the *gad2-1* mutant line in comparison to the wild type, *gad2-2*, and the *gad* quadruple mutant. At the same time, LMA values were comparable between all three genotypes. Regarding the root biomass, we did not find any variations in root dry masses between the different genotypes either (Supplementary Figure 4). Collectively, no enhanced biomass production was detected in the GABA-deficient mutant lines.

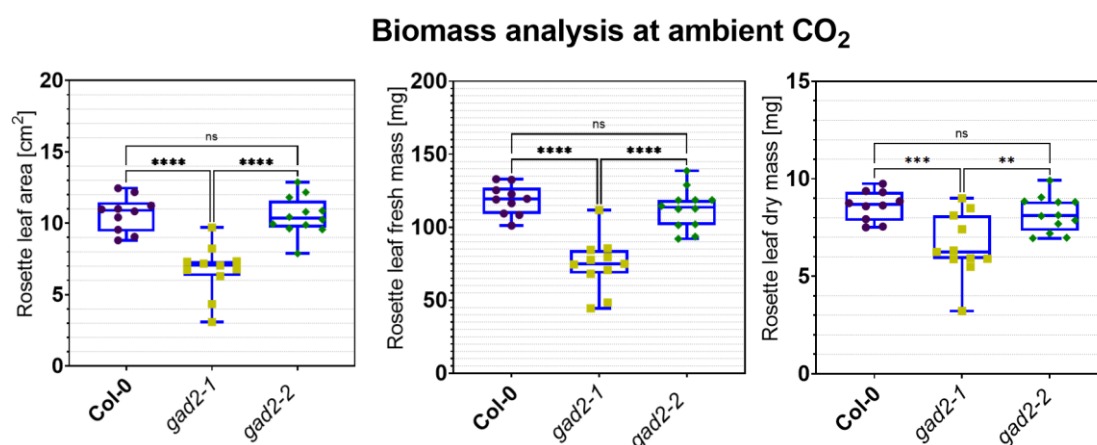


Figure 4: Leaf biomass is reduced in *gad2-1* in contrast to *gad2-2*.

Rosette leaf areas, fresh mass, and dry mass of four-week-old *A. thaliana* wild-type (Col-0; n=1), *gad2-1* (n=11) and *gad2-2* (n=12) plants raised in soil at ambient CO₂. Data was plotted with box and whiskers: the box illustrates the median, and the 25th and 75th percentiles, while the whiskers indicate the minimum and maximum values. Statistical analysis was conducted using one-way ANOVA; **P < 0.01, ***P < 0.001, ****P < 0.0001.

GABA deficiency is associated with increased monosaccharide concentrations

A previous study revealed major alterations in the carbon metabolite profile of the GABA-depleted double mutant *gad1/2*. To ascertain the effect of GABA deficiency on the metabolite composition in the mutant lines in our project, we conducted a non-targeted GC-MS analysis in root and rosette leaf tissue of the wild type Col-0 and the GABA-deficient mutant lines *gad2-1*, *gad2-2*, and *gad1/2/4/5*.

Highly increased monosaccharide concentrations were detected in leaf material of the GABA-deficient mutant lines. To be more exact, concentrations of the monosaccharide xylose were found to be increased 22- to 28-fold in the GABA-deficient mutant lines in relation to the wild type (Figure 5). Preliminary GC-MS results indicated a significant increase in concentrations of the monosaccharides D-(-)-Fructose and D-Glucose in *gad1/2/4/5* in comparison the wild type (Supplementary Figure 5). Sucrose concentrations were found to be unaltered in the GABA-deficient mutant lines. The GC-MS experiment also unveiled significantly increased 2-oxoglutarate concentrations in the quadruple *gad* mutant (Supplementary Figure 5). Only metabolites with a Library Match Factor equal or higher to 50% were considered for further data processing as the compound identification is unreliable at lower scores. The metabolites of interest were confirmed via standard retention time.

In terms of root tissue, no considerable differences in carbon metabolite composition were detected between the wild type and the *gad* mutant lines. The only striking difference involved the plant metabolite ascorbic acid, which was significantly increased in concentrations in the GABA-deficient mutant line *gad2-2* in comparison to all the other lines, including *gad2-1*. Unfortunately, a large variation in wild-type data points prevented a discrimination between the wild type and the transgenic plants. For instance, the wild-type data points of malic acid concentrations were separated into two groups, one being at the level of the mutant lines, while the other one was significantly increased (Supplementary Figure 5). The variation in the mutant data was much smaller. However, no distinct differences in metabolite composition were detectable between the transgenic lines either.

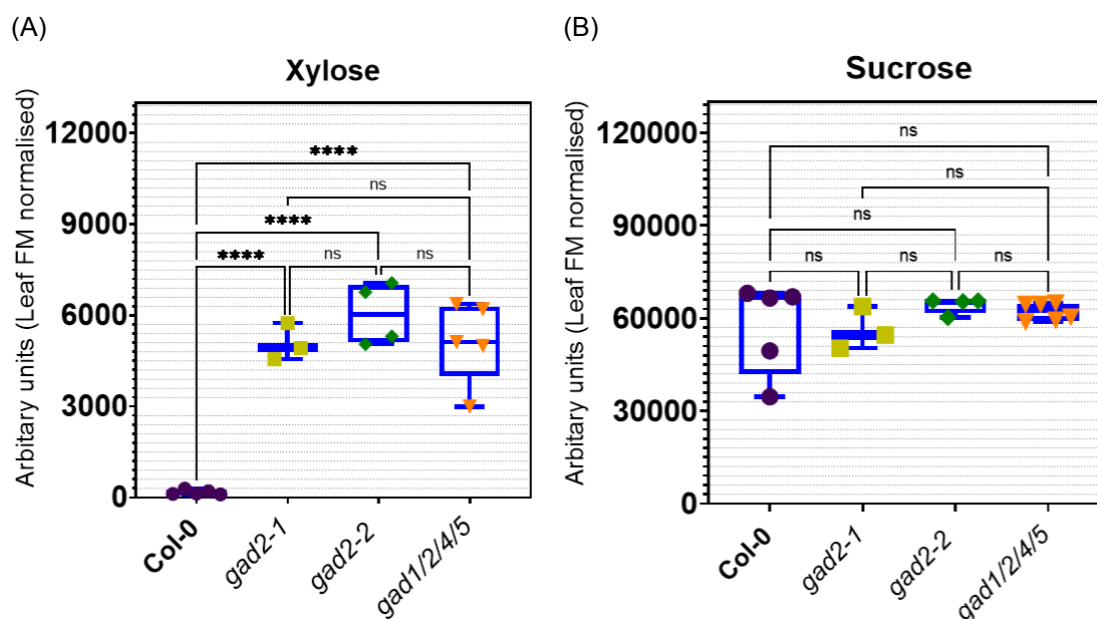


Figure 5: GC-MS analysis in leaves of GABA-deficient mutant lines.

Outcome of a non-targeted gas chromatography–mass spectrometry (GC-MS) experiment in rosette leaves of *A. thaliana* wild-type (Col-0; n=5), *gad2-1* (n=3), *gad2-2* (n=4), and *gad1/2/4/5* (n=5-6) plants. (A) Significantly increased xylose concentrations were detected in the *gad* lines, while (B) sucrose concentrations were unaltered in these lines. Data was plotted with box and whiskers: the box illustrates the median, and the 25th and 75th percentiles, while the whiskers indicate the minimum and maximum values. Statistical differences were calculated using one-way ANOVA; ****P < 0.0001.

The monosaccharide xylose is known as a main component of many cell wall polysaccharides (Ebert *et al.*, 2015). Therefore, we examined our RNA sequencing data for changes in the expression of genes that are involved in carbohydrate and cell wall metabolic processes. Indeed, the data indicates a correlation between *GAD2* knockout and genes that are functionally enriched for ‘carbohydrate metabolism’ as revealed by Gene Ontology (GO) enrichment analysis in both *gad2-1* and *gad2-2* (Figure 6). In fact, the corresponding functional module was identified as the largest GO category in both mutant lines. In *gad2-1*, genes from this cluster are, *inter alia*, functionally enriched in cellular carbohydrate and cell wall macromolecule metabolism, including hemicellulose and cellular polysaccharide metabolic/catabolic processes. Differentially expressed genes (DEGs) from the corresponding gene set in *gad2-2* were functionally enriched in the metabolism/catabolism of carbohydrates, including starch and other polysaccharides. The GO enrichment analysis also revealed the upregulation of genes

that are associated with photosynthetic and respiratory processes in *gad2-2*, as reflected in another, smaller gene cluster. However, this gene cluster was found to be absent in *gad2-1*.

In a following step, a closer look was taken at the cell wall-/carbohydrate-related DEGs. Thereby, several genes were identified that were differentially expressed in *gad2-1* and *gad2-2* in relation to the wild type (Table 1). In many cases, the differences in gene expression were extremely significant (****P < 0.0001; Supplementary Figure 7). It is striking that members from the *Xyloglucan endotransglucosylase/hydrolase protein (XTH)* gene family made up the highest number of DEGs in the GO category 'carbohydrate metabolism' in both *gad2-1* and *gad2-2*. The highest DEG number in total was determined for genes encoding members of the Glycosyltransferase GT1 family (Supplementary Table 4) which are, however, not involved in cell wall metabolic processes (Zhang *et al.*, 2020b). Other DEGs that were functionally enriched for cell wall remodelling were genes encoding, *inter alia*, β -glucosidases (*BGLUs*), β -D-xylosidases (*BXLs*), and expansins (*EXPs*). In terms of cell wall synthesis-related genes, DEGs encoding Cellulose synthesis-like (CSL) and Trichome Birefringence-like (TBL) proteins were detected in the mutant lines, among others. DEGs related to sugar transport were also found in both mutant lines, which involved both sucrose and glucose transport. A low number of DEGs were discovered to be functionally enriched in starch/sucrose metabolism, including genes encoding β -amylases (*BAMs*), and sucrose/starch synthases (*SUS/SS*).

Altogether, *gad2-1* owns many more DEGs in the GO category 'carbohydrate metabolism' than *gad2-2* does, and there is an overlap in genes that are differentially expressed in *gad2-2* and *gad2-1* in the specified category. Another striking aspect is that considerably more of these genes are downregulated (50 in *gad2-1*; 20 in *gad2-2*) than upregulated (23 in *gad2-1*; 9 in *gad2-2*).

The GABA-deficient mutant line *gad1/2/4/5* had not been included in the RNA-seq analysis. Less information was provided by the microarray experiment regarding the expression levels of genes in general. However, the microarray data indicated that genes encoding TBL and EXP proteins were differentially expressed in *gad1/2/4/5* as well (Supplementary Table 5).

expressed genes using Wald-test. Presented are total counts and the number of up/down-regulated genes.

| | <i>gad2-1</i> | | | <i>gad2-2</i> | | | Function |
|---|----------------|--------------|----------------|----------------|--------------|----------------|---------------------------|
| | Number of DEGs | Up-regulated | Down-regulated | Number of DEGs | Up-regulated | Down-regulated | |
| Xyloglucan endotransglucosylase/hydrolase (XTH) | 15 | 2↑ | 13↓ | 6 | 1↑ | 5↓ | Cell wall remodelling |
| Arabinogalactan protein (AGP) | 8 | 0↑ | 8↓ | 0 | 0↑ | 0↓ | Cell wall remodelling |
| Beta-glucosidase (BGLU) | 5 | 2↑ | 3↓ | 2 | 1↑ | 1↓ | Cell wall remodelling |
| Beta-D-xylosidase (BXL) | 5 | 2↑ | 3↓ | 1 | 0↑ | 1↓ | Cell wall remodelling |
| Cellulose synthesis-like (CSL) | 5 | 3↑ | 2↓ | 1 | 1↑ | 0↓ | Cell wall synthesis |
| Wall-associated receptor kinase-like (WAKL) | 4 | 0↑ | 4↓ | 3 | 0↑ | 3↓ | Cell wall remodelling |
| Sugar transporter ERD6-like (SUGTL) | 4 | 1↑ | 3↓ | 2 | 0↑ | 2↓ | Sugar transport |
| Expansin (EXP) | 4 | 4↑ | 0↓ | 1 | 1↑ | 0↓ | Cell wall remodelling |
| Polygalacturonase | 4 | 2↑ | 2↓ | 1 | 0↑ | 1↓ | Cell wall remodelling |
| Beta-amylase (BAM) | 3 | 2↑ | 1↓ | 2 | 1↑ | 1↓ | Starch/Sucrose metabolism |
| Protein trichome birefringence-like (TBL) | 3 | 0↑ | 3↓ | 2 | 0↑ | 2↓ | Cell wall synthesis |
| Pectinesterase inhibitor (PMEI) | 3 | 1↑ | 2↓ | 0 | 0↑ | 0↓ | Cell wall remodelling |
| Pectin acetyltransferase (PAE) | 2 | 0↑ | 2↓ | 2 | 1↑ | 1↓ | Cell wall remodelling |
| Bidirectional sugar transporter (SWEET) | 2 | 1↑ | 1↓ | 2 | 1↑ | 1↓ | Sugar transport |
| Sucrose transporter (SUC) | 2 | 1↑ | 1↓ | 1 | 0↑ | 1↓ | Sugar transport |
| Pectin lyase-like superfamily protein | 2 | 1↑ | 1↓ | 0 | 0↑ | 0↓ | Cell wall remodelling |
| Beta-galactosidase (BGAL) | 2 | 0↑ | 2↓ | 1 | 1↑ | 0↓ | Cell wall remodelling |
| Starch synthase (SS) | 1 | 1↑ | 0↓ | 1 | 1↑ | 0↓ | Starch/Sucrose metabolism |
| Glucuronoxylan glucuronosyltransferase (IRX) | 1 | 0↑ | 1↓ | 1 | 0↑ | 1↓ | Cell wall synthesis |
| Pectin methylesterase (QUA) | 1 | 1↑ | 0↓ | 0 | 0↑ | 0↓ | Cell wall remodelling |
| Beta-galactosyltransferase (GALT) | 1 | 1↑ | 0↓ | 0 | 0↑ | 0↓ | Cell wall synthesis |
| Sucrose synthase (SUS) | 0 | 0↑ | 0↓ | 1 | 0↑ | 1↓ | Starch/Sucrose metabolism |
| | 77 | 25↑ | 52↓ | 30 | 9↑ | 21↓ | In total |
| | 55 | 15↑ | 40↓ | 17 | 5↑ | 12↓ | Cell wall remodelling |
| | 10 | 4↑ | 6↓ | 4 | 1↑ | 3↓ | Cell wall synthesis |
| | 8 | 3↑ | 5↓ | 5 | 1↑ | 4↓ | Sugar transport |
| | 4 | 3↑ | 1↓ | 4 | 2↑ | 2↓ | Starch/Sucrose metabolism |

Discussion

The primary objective of this work was to investigate the impact of manipulated GABA synthesis on CO₂ assimilation and carbon metabolism in Arabidopsis. It is known that GABA synthesis is associated with the release of CO₂ molecules into the cytosol. Decarboxylation reactions also occur during the Krebs cycle but there they happen within the mitochondrion and not in the cytosol (O'Leary and Plaxton, 2016). Moreover, it is established that elevating CO₂ concentrations above ambient CO₂ generally promotes photosynthetic CO₂ assimilation (Ehleringer and Sandquist, 2015).

Our findings that net CO₂ uptake rates, respiration rates as well as the maximum rates of Rubisco carboxylase activity and photosynthetic electron transport were unaltered in the GABA-deficient mutants *gad2-1* and *gad1/2/4/5* strongly suggest that there is no direct link between GABA synthesis and CO₂ assimilation in Arabidopsis. Significantly, the observation that photosynthetic rates were unchanged in the GABA-deficient mutant lines is supported by biomass measurements. The GABA-deficient mutants did not exhibit an altered growth phenotype, neither at ambient nor at elevated

CO₂. Only the GABA-depleted mutant line *gad2-1* revealed diminished leaf growth. This finding was in agreement with the observation of reduced rosette leaf expansion in a *gad1/2* double mutant as seen in a previous study (Mekonnen *et al.*, 2016), but not by Xu *et al.* (2021a). Research has shown that GABA is involved in root, hypocotyl, and pollen tube growth (Renault *et al.*, 2011; Yu *et al.*, 2014). According to Renault *et al.* (2011), GABA supplement causes aberrant root growth and hypocotyl elongation, thereby documenting a role for GABA in plant growth processes. However, there was no mention about its role in leaf biomass. Furthermore, the GABA-deficient mutant lines *gad1/2/4/5* and *gad2-2* revealed wild-type leaf growth. Therefore, it is unlikely that GABA deficiency caused the reduction in leaf biomass in *gad2-1* and *gad1/2*.

Research has also revealed that both *gad2-1* and *gad2-2* display significantly enlarged stomatal apertures (Chapter 2; Xu *et al.* 2021a). Therefore, growth defects of *gad2-1* might be due to another factor, which is presumably linked to the additional mutations in its genome (eliminated *MPK12*, *BPS2*; Chapter 2). To our knowledge, no information is available regarding the leaf biomass of *mpk12* loss-of-function mutants. Töldsepp *et al.* (2018) only reported that the *mpk12* mutant and the wild-type Col-0 ‘visually’ resemble each other; but it seems that *mpk12* leaf biomass has not been quantified. On the other hand, it has been observed that the transgenic line *mpk4*, which lacks a mitogen kinase that operates in concert with MPK12, exhibits an obvious growth-arrest phenotype (Hörak *et al.*, 2016; Töldsepp *et al.*, 2018). Notably, *gad2-1* was used for generating the *gad1/2* double mutant described above (Mekonnen *et al.*, 2016), and we assume that the double mutant owns the same additional mutations as *gad2-1*. Another study failed to detect differences in shoot fresh and shoot dry weight in the very same transgenic line (*gad1/2*) as used by Mekonnen *et al.* (2016) (Wu *et al.*, 2021). Conversely, in response to hypoxia stress, they found *gad1/2* fresh mass to be drastically reduced in comparison to the wild type (Wu *et al.*, 2021). The differences in leaf phenotypes between the different studies might be based on differences in growth conditions. Conceivably, plants might have been slightly stressed in some situations, which did not impact the wild type and the other mutant lines but had a severe effect on the development of *gad2-1* and *gad1/2* plants due to their additional mutations.

Notably, GO enrichment analysis of the RNA-seq data identified a relatively small cluster of genes that are enriched in functions related to photosynthesis, cellular respiration, and electron transport in *gad2-2*. What is more, Li *et al.* (2017) observed

improved chlorophyll synthesis in GABA-treated plants upon drought exposure in comparison with control plants. Chlorophyll, which is involved in the light reactions of photosynthesis, has been related to the photosynthetic capacity of plants (Croft *et al.*, 2017). However, no difference in chlorophyll content was detected between the GABA-treated and the control plants under standard conditions (Li *et al.*, 2017). In addition, the RNA-seq data in the present study did not give any indication of changes in chlorophyll synthesis-related gene expression in both *gad2-1* and *gad2-2*. The differentially expressed genes (DEGs) that formed photosynthesis- and cellular respiration-related gene cluster mostly encoded proteins associated with electron transport such as NADH/NAD(P)H dehydrogenase, ATP synthase, and Photosystem I and II units. It seems that this gene category does not include genes enriched for functions related to the Calvin Benson cycle, which involves the reduction of atmospheric CO₂ to carbohydrates (Buchanan and Wolosiuk, 2015). Besides, the specified gene cluster was only identified in *gad2-2* and not in *gad2-1*.

It was demonstrated by a previous study that eliminating GABA synthesis perturbs plant carbon metabolism (Mekonnen *et al.*, 2016). According to corresponding metabolite profiles, interrupting the GABA shunt pathway by *GAD* knockout resulted in massive changes in the leaf concentrations of different Krebs cycle intermediates. Knocking out *GAD1* and *GAD2* led to a decline in the concentrations of fumarate, oxalacetate, malate, and citrate, accompanied by an increase in glutamate and succinate concentrations (Mekonnen *et al.*, 2016). Unfortunately, it was difficult to draw conclusions from our GC-MS data due to a great variability that primarily affected wild-type replicates. To be specific, the wild-type replicates were split into two groups; in many cases, with an enormous discrepancy between them. This was, *inter alia*, true for malate. One of the two groups was on the same level as the malate concentrations in the GABA-deficient (*gad2-1*, *gad2-2*, and *gad1/2/4/5*) plants, while the other one was 27-fold increased. As mentioned above, Mekonnen *et al.* (2016) also detected massively increased malate concentrations in shoot material of wild-type plants compared to *gad1/2*. According to the authors, the alterations in concentrations of Krebs cycle intermediates is presumably based on the blockage of the GABA shunt, resulting in a shift in the metabolite pool towards the Krebs cycle (Mekonnen *et al.*, 2016). In one respect, our metabolomics data provided new insights. Metabolic profiling in the GABA-deficient mutants uncovered drastically increased xylose

concentrations. The monosaccharide xylose is an essential component of two hemicellulose types that are essential parts of the plant cell wall (Ebert *et al.*, 2015). GABA depletion appears to cause elevations in the concentration of other monosaccharides as well. A preliminary GC-MS analysis in rosettes of *gad1/2/4/5* revealed higher glucose and fructose concentrations in relation to the wild type, which could not be replicated in a second experiment due to the increased variability in wild-type data points. However, also Mekonnen *et al.* (2016) recognised a doubling of glucose content in the GABA-depleted *gad1/2* transgenic line. At the same time, sucrose and starch concentrations were found to be unaltered in this line (Mekonnen *et al.*, 2016). Similarly, both GC-MS analyses in our project failed to identify alterations in sucrose accumulation in *gad2-1*, *gad2-2*, and *gad1/2/4/5*. Having said this, one gene encoding a sucrose synthase (SUS) was found to be upregulated in *gad2-2* relative to the wild type. However, this was not the case for *gad2-1* and involved only SUS3, which is apparently not linked to changes in starch and sugar accumulation (Barratt *et al.*, 2009). It is established that glucose and fructose accumulate in the plant either due to sucrose degradation or as minor products of photosynthesis (Siddiqui *et al.*, 2020). As sucrose as well as photosynthesis rates seem to be unaltered by GABA deficiency, we assume that the additional amount of monosaccharides detected in the mutant lines originates from a different source.

Regarding metabolite profiling in root tissue, no major differences were found between the different genotypes, except for significantly elevated ascorbic acid (AsA) concentrations in *gad2-2*. Astonishingly, no increase in AsA concentrations were detected in *gad2-1* and *gad1/2/4/5*. It is not surprising that we have seen so little variation between the wild type and the *gad2* mutant lines regarding other metabolites. We would rather expect altered metabolite concentrations in *gad1/2/4/5*, which is the only genotype with eliminated GAD1 activity. Among the five GAD isoforms, GAD1 has been identified as the key biosynthesis enzyme of GABA in roots (Bouché *et al.*, 2004). The other GAD enzymes, including GAD2, are not contributing much to the overall root GABA content (Mekonnen, 2012).

In compliance with the detection of largely increased xylose concentrations, the GO enrichment analysis identified a large gene cluster associated with cell wall and carbohydrate metabolism in both *gad2-1* and *gad2-2*. A closer look at specific genes revealed an altered transcript abundance of a great number of genes encoding cell wall

remodelling enzymes like XTHs, BXLs, BGLUs, and EXPs. XTHs and EXPs function as important cell wall-loosening enzymes (Carpita and McCann, 2000); XTHs catalyse the cleavage and realignment of xyloglucan chains to allow turgor-driven cell expansion (Campbell and Braam, 1999; Carpita and McCann, 2000). Xyloglucan, as well as xylan, are defined as a types of hemicellulose, which is an important class of cell wall polysaccharides with β 1-4 linkages (Scheller and Ulvskov, 2010). While xyloglucan forms chains out of glucose molecules (glucan) with α -D-xylose molecules arranged as side chains at the O6 position, the latter is composed of xylose backbone molecules (Nishinari *et al.*, 2007). Not only *XTHs* and *EXPs* but also genes encoding BXLs are differentially expressed in the *gad* mutant lines. Whilst XTHs are targeting xyloglucan, BXLs have been found to catalyse the degradation of xylan (Barnes and Anderson, 2018). Both XTHs and BXLs are involved in cell wall recycling. However, while XTHs are required for *in muro* recycling, BXLs are cleaving off single sugars from polysaccharides during a process named ‘metabolic recycling’, which involves the internalisation and salvage of the cleavage products for the formation of new wall polysaccharides (Barnes and Anderson, 2018). At this point, it is tempting to speculate that there could be a connection between the changes in transcript abundance of cell wall remodelling genes and the detection of free xylose molecules.

Genes that are linked to the *de novo* synthesis of cell wall components as well as to starch/sucrose metabolism were also found to be differentially expressed. However, the number of these DEGs was low in relation to the quantity of genes associated with cell wall remodelling processes. The highest number of DEGs was counted for genes encoding UDP-glycosyltransferases (UGTs). UGTs catalyse the transfer of sugar residues to a large variety of acceptor molecules and are, *inter alia*, involved in cell wall formation (Hansen *et al.*, 2012; Ross *et al.*, 2001). However, all the UGTs with significant changes in gene expression levels were found to transfer single sugars to secondary metabolites, nucleic acid, and proteins that are not linked to cell wall metabolism (Zhang *et al.*, 2020b).

A link between manipulated GABA concentrations and altered expression levels of cell wall-related genes was found in two previous studies (Renault *et al.*, 2011; Roberts, 2007). Of note, gene expression levels were examined in GABA-enriched plants (*pop2* and GABA-treated wild-type plants) and not in GABA-depleted mutant lines as in the present study. Interestingly, some genes that encode proteins from the same protein

families were found to be affected in the GABA hyperaccumulating *pop2* mutant line – expansins, AGPs, and BGL1 (Renault *et al.*, 2011). However, the three expansin-encoding genes *EXPA1*, *EXPA10*, and *EXPA15* were downregulated in the GABA overproducing mutant line, while they were upregulated (*EXPA10* and *EXPA15*) or non-differentially expressed (*EXPA1*) in the GABA-depleted mutant lines in our investigation. The expression of *BGL1* and two *AGP* genes (*AGP22* and *AGP30*) was unaltered in the GABA-deficient lines in our study, whilst their expression was significantly decreased in the *pop2* mutant line (Renault *et al.*, 2011). According to the authors, cell wall-loosening malfunction was the cause for the cell elongation defects they detected in vegetative and reproductive tissue of *pop2* (Renault *et al.*, 2011).

To sum up, our data suggests that disruption of GABA synthesis does not increase photosynthetic CO₂ assimilation and biomass accumulation in Arabidopsis but may affect cell wall-remodelling processes, which warrants future investigations.

Supplementary Tables and Figures

Supplementary Table 1: Primer used in this study.

| Primer name | Primer sequence (5' → 3') | Purpose |
|-------------|---------------------------|--------------------|
| GAD1-LP | ATGACTTGACTTGAACCTGCG | Genotyping primers |
| GAD1_RP | GGAGCCAATGTTCAAGTAACG | |
| GAD2_LP | ACGTGATGGATCCAGACAAAG | |
| GAD2_RP | TCTTCATTTCCACACAAAGGC | |
| GAD4b_LP | CAATAAAAAGATGACGGTCGG | |
| GAD4b_RP | TTGAACCGGAAATTGAGTCAC | |
| GAD5-seq1_F | TGGATGGAACCTGAGTGTGA | |
| GAD5-seq3_R | CCATCCTGTCTCTGCGTTTT | |

Supplementary Table 2: Chemical components of the Germination Solution for hydroponic growth.

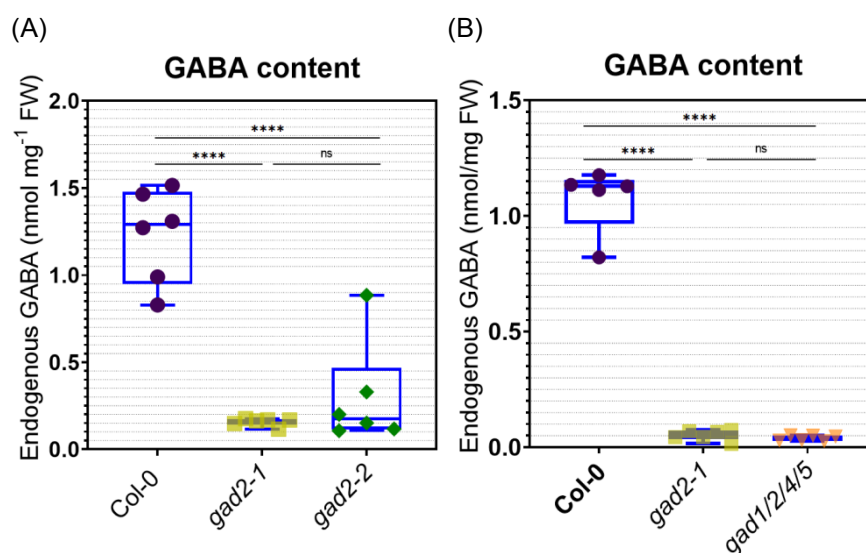
| Macronutrients | Molecular weight | Stock conc. [M] | Vol of stock [mL] for 10 L | Final conc. [mM] |
|--|------------------|-----------------|-------------------------------|------------------|
| CaCl ₂ | 1 M solution | 1.0 | 7.5 | 0.75 |
| KCl | 74.55 | 1.0 | 10.0 | 1.0 |
| Ca(NO ₃) ₂ · 4·H ₂ O | 236.1 | 0.4 | 6.25 | 0.25 |
| MgSO ₄ · 7·H ₂ O | 246.5 | 0.4 | 25.0 | 1.0 |
| KH ₂ PO ₄ | 136.1 | 0.1 | 20.0 | 0.2 |

| Micronutrients | Molecular weight | Stock conc. [mM] | Vol of stock [mL] for 10 L | Final conc. [μM] |
|---------------------------------------|------------------|------------------|-------------------------------|------------------|
| NaFe(III) EDTA | 367.1 | 50.0 | 1.0 | 50.0 |
| H ₃ BO ₃ | 61.8 | 50.0 | 1.0 | 50.0 |
| MnCl ₂ · 4H ₂ O | 197.9 | 5.0 | 1.0 | 5.0 |
| ZnSO ₄ · 7H ₂ O | 287.5 | 10 | 1.0 | 10 |
| CuSO ₄ · 5H ₂ O | 249.7 | 0.5 | 1.0 | 0.5 |
| Na ₂ MoO ₃ | 242 | 0. | 1.0 | 0.1 |

Supplementary Table 3: Chemical components of the Basal Nutrient Solution for hydroponic growth.

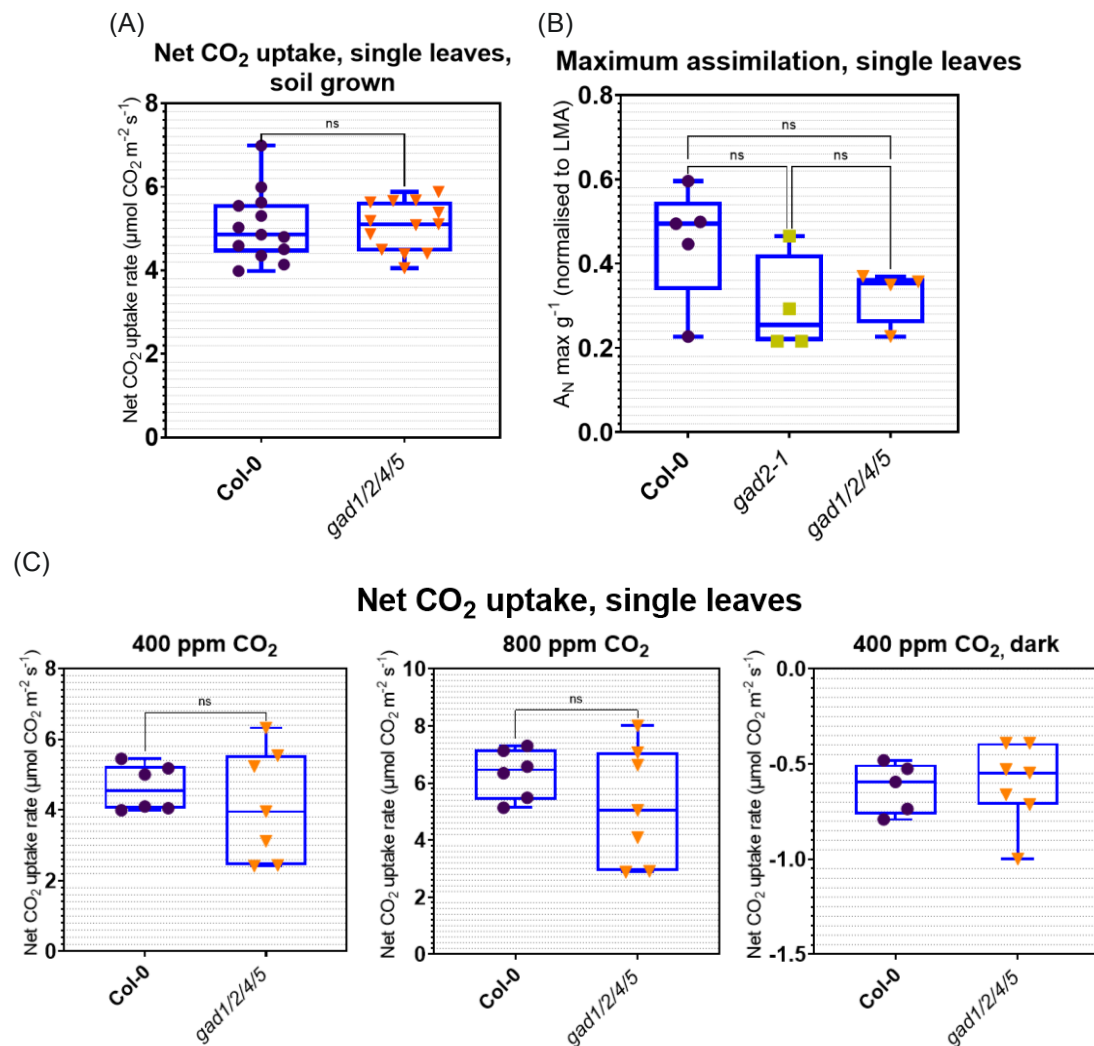
| Macronutrients | Molecular weight | Stock conc. [M] | Vol of stock [mL] for 10 L | Final conc. [mM] |
|---|------------------|-----------------|----------------------------|------------------|
| NH ₄ NO ₃ | 80 | 1 | 20 | 2 |
| NaCl | 58.44 | 1 | 15 | 1.5 |
| MgSO ₄ 7H ₂ O | 246.5 | 0.4 | 50 | 2 |
| KNO ₃ | 101.11 | 1 | 30 | 3 |
| KH ₂ PO ₄ | 136.1 | 0.1 | 60 | 0.6 |
| KCl | 74.55 | 1 | 20 | 2 |
| CaCl ₂ | 1 M solution | 1 | 1 | 0.1 |
| Ca(NO ₃) ₂ 4H ₂ O | 236.1 | 0.4 | 50 | 2 |

| Micronutrients | Molecular weight | Stock conc. [mM] | Vol of stock [mL] for 10 L | Final conc. [μM] |
|--------------------------------------|------------------|------------------|----------------------------|------------------|
| NaFe(III) EDTA | 367.1 | 50 | 10 | 50 |
| H ₃ BO ₃ | 61.8 | 50 | 10 | 50 |
| MnCl ₂ 4·H ₂ O | 197.9 | 5 | 10 | 5 |
| ZnSO ₄ 7·H ₂ O | 287.5 | 10 | 10 | 10 |
| CuSO ₄ 5·H ₂ O | 249.7 | 0.5 | 10 | 0.5 |
| Na ₂ MoO ₃ | 242 | 0.1 | 10 | 0.1 |



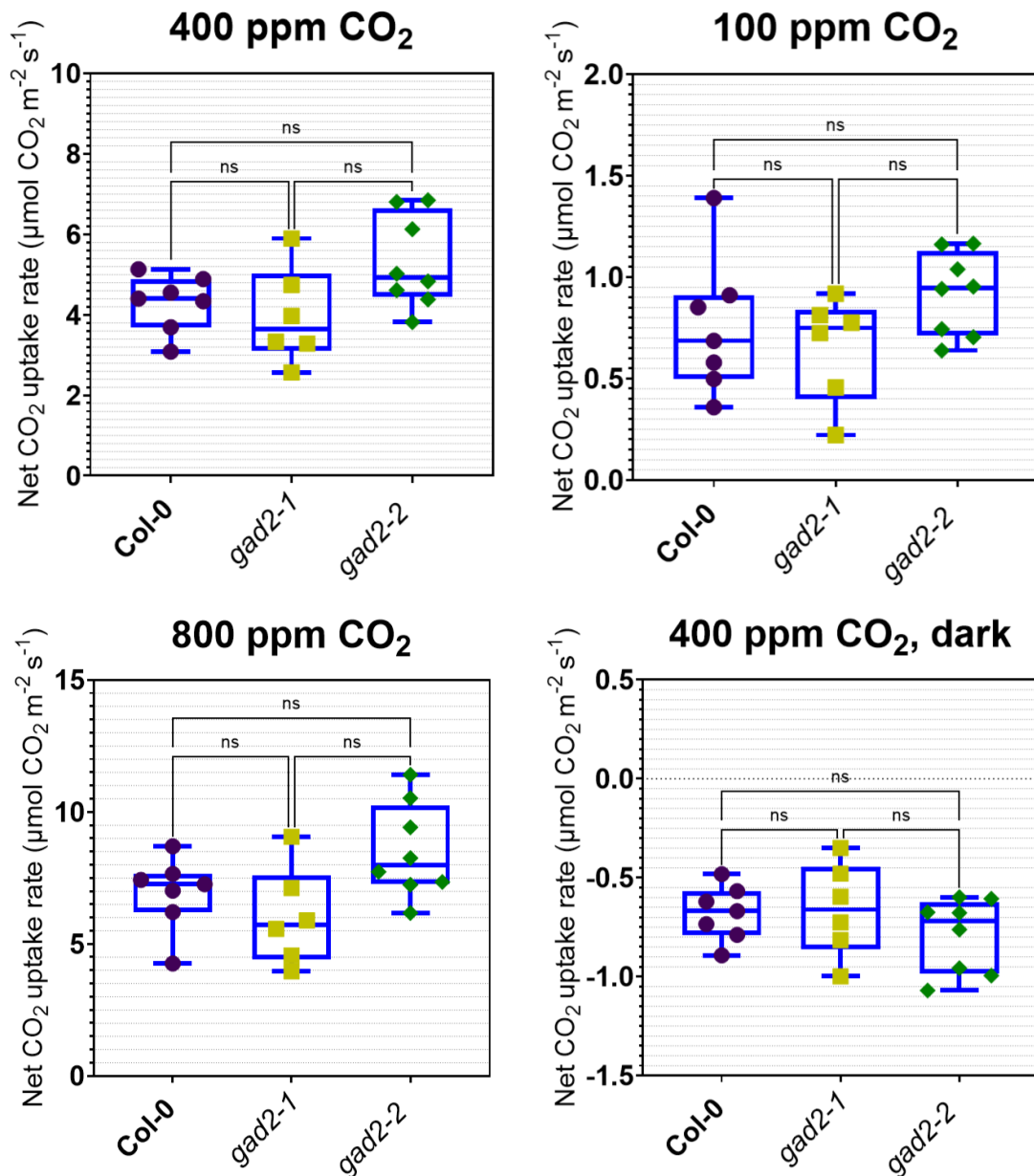
Supplementary Figure 1: Endogenous GABA content in leaves of gad(s) mutants.

Endogenous GABA concentrations in rosette leaves of the wild type (Col-0) and the loss-of-function mutant lines *gad2-1*, (A) *gad2-2*, and (B) *gad1/2/4/5* (n=6), as determined by UPLC. Data was plotted with box and whiskers: the box illustrates the median, and the 25th and 75th percentiles, while the whiskers indicate the minimum and maximum values. Statistical differences were calculated using one-way ANOVA; ****P < 0.0001.



Supplementary Figure 2: CO₂ assimilation rates are not altered in GABA-deficient mutant lines.

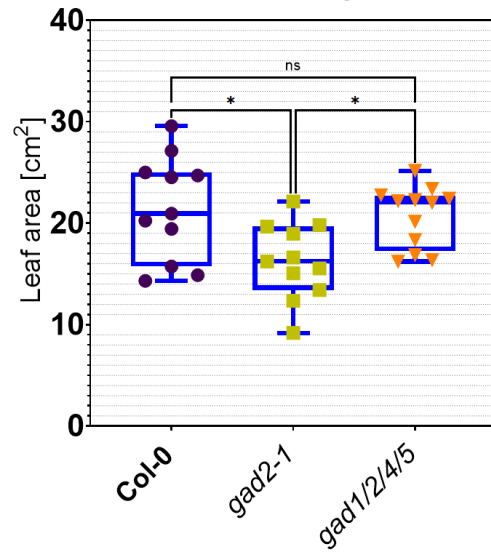
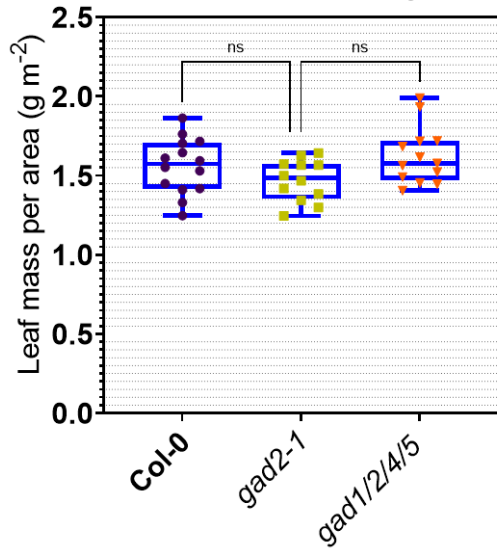
Additional data showing unaltered net CO₂ uptake rates in GABA-deficient *A. thaliana* plants, as determined by Infrared gas analysis using a LI-6400XT Portable Photosynthesis System. (A) Net CO₂ uptake in intact rosette leaves of soil-grown wild-type (Col-0; n=13) and *gad1/2/4/5* (n=12) plants at ambient CO₂ (400 ppm). (B) Maximum CO₂ assimilation rates in intact single leaves of hydroponic wild-type (Col-0; n=5), *gad2-1* (n=3), and *gad1/2/4/5* (n=4) plants as determined by gas exchange measurements at a light intensity of 600 μmol m⁻² s⁻¹ and over a time period of 80 min. Data was normalised to leaf mass per area (g m⁻²). (C) Net CO₂ uptake rates in intact single leaves of hydroponic wild-type (Col-0; n=6) and *gad1/2/4/5* (n=7) plants at ambient (400 ppm) CO₂. Data was plotted with box and whiskers: the box illustrates the median, and the 25th and 75th percentiles, while the whiskers indicate the minimum and maximum values. Statistical differences were calculated either using one-way ANOVA (B) or a two-sided Student's t-test (A, C).



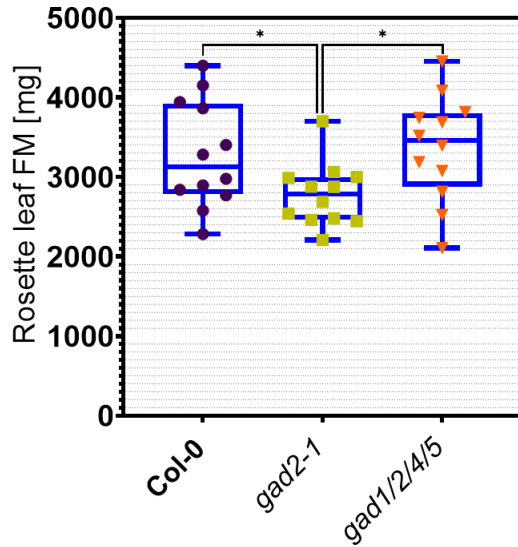
Supplementary Figure 3: Gas exchange measurements in high/low CO₂-treated *gad2* mutant lines.

Outcome of Infrared gas analysis in rosette leaves of intact 4 ½- to 5 ½-week-old hydroponic *A. thaliana* plants after one hour at ambient CO₂ (400 ppm), decreased CO₂ (100 ppm), elevated (800 ppm) CO₂, or in darkness at ambient CO₂ using a LI-6400XT Portable Photosynthesis System. The net CO₂ uptake rates were determined in the wild type (Col-0; n=7), *gad2-1* (n=6), and *gad2-2* (n=8). Data was plotted with box and whiskers: the box illustrates the median, and the 25th and 75th percentiles, while the whiskers indicate the minimum and maximum values. Statistical differences were calculated using one-way ANOVA.

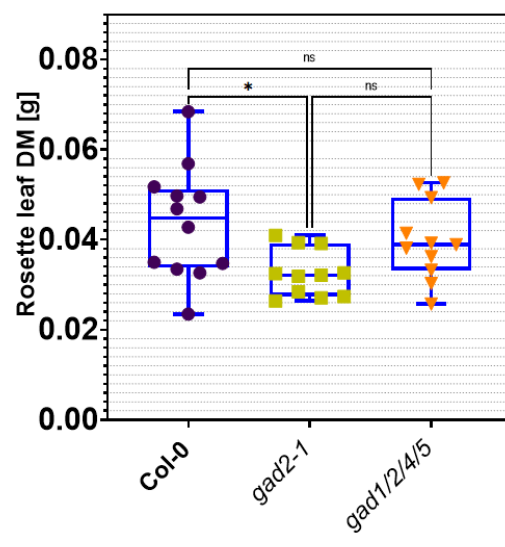
(A) Leaf FM per area, single leaves (B) Leaf area, single leaves



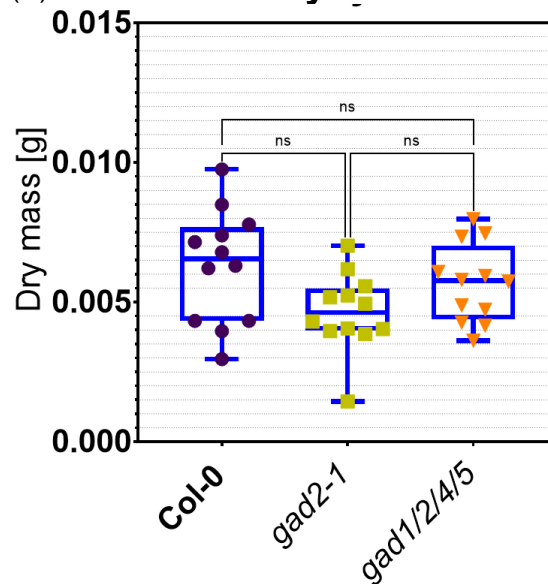
(C) Fresh mass, single leaves



(D) Dry mass, single leaves

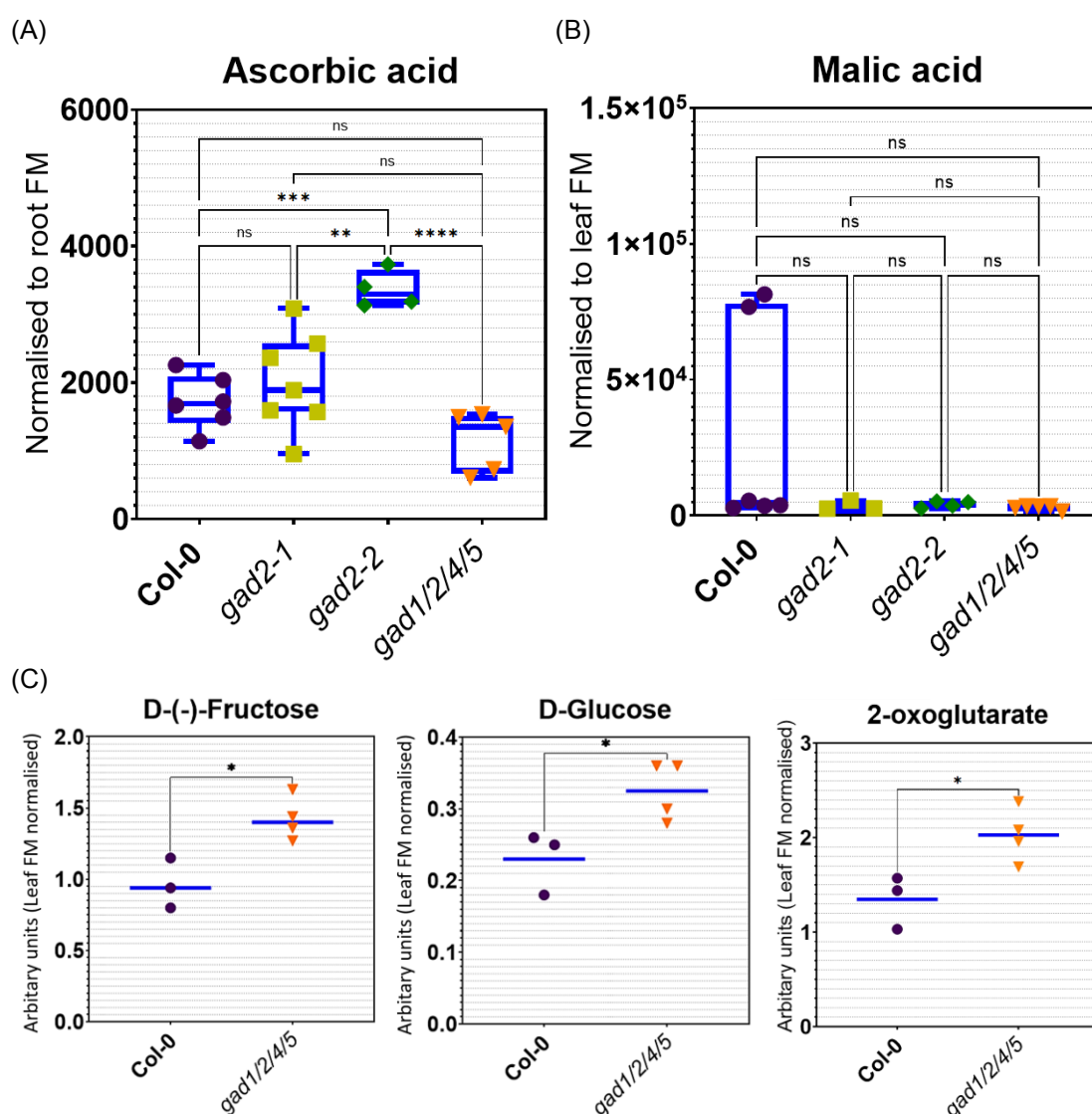


(E) Root dry mass



Supplementary Figure 4: Biomass and stomatal density analysis in plants grown at ambient and elevated CO₂.

Shown are rosette (A) leaf mass per area (LMA), (B) leaf areas, (C) fresh mass, (D) dry mass in *A. thaliana* wild-type (Col-0), *gad2-1*, and *gad1/2/4/5* plants raised at ambient CO₂ (n=11-12). (E) Root dry mass in wild-type, *gad2-1*, and *gad1/2/4/5* plants raised at ambient CO₂ (n=12). Data was plotted with box and whiskers: the box illustrates the median, and the 25th and 75th percentiles, while the whiskers indicate the minimum and maximum values. Statistical differences were calculated using one-way ANOVA; *P < 0.05.

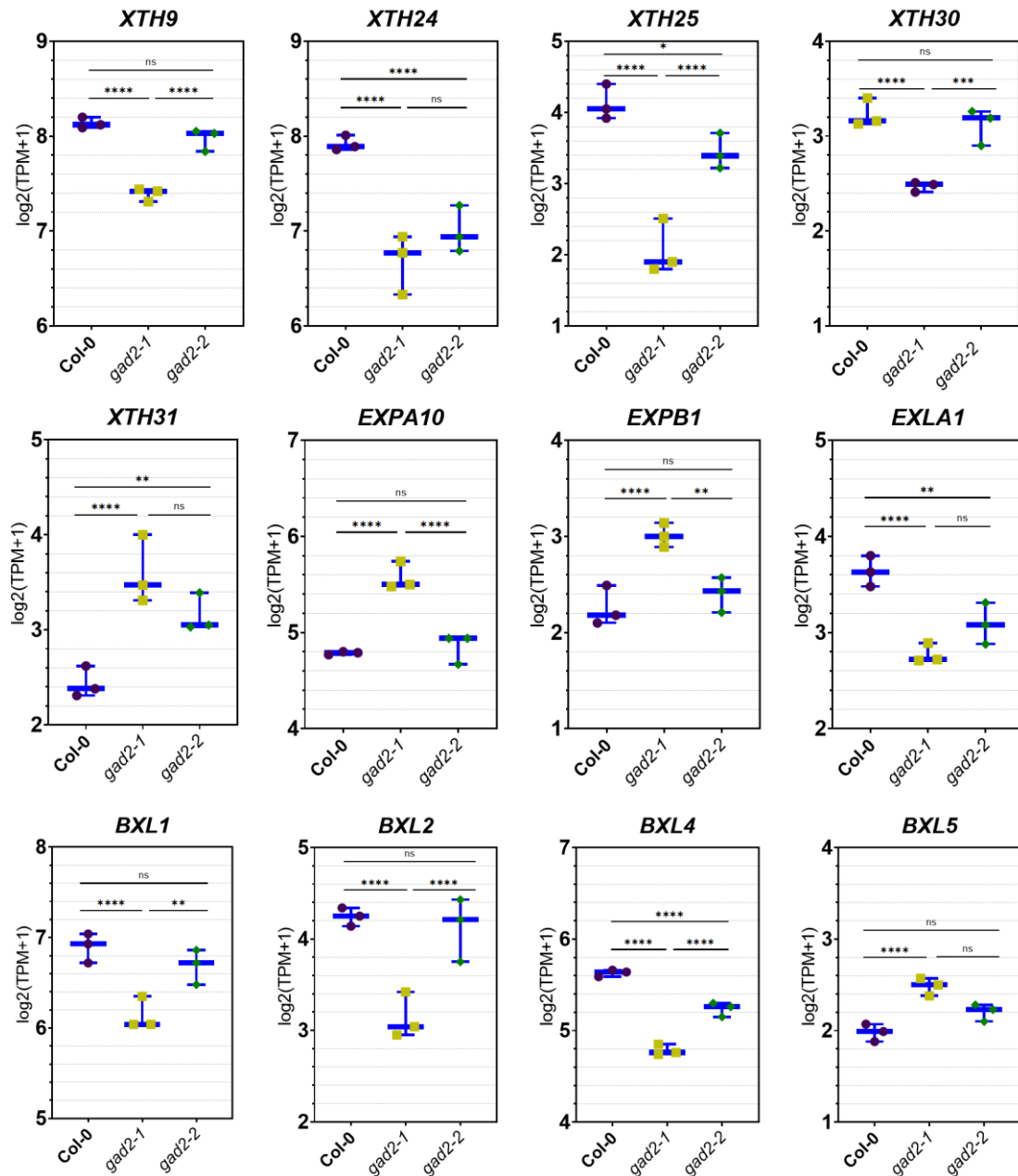


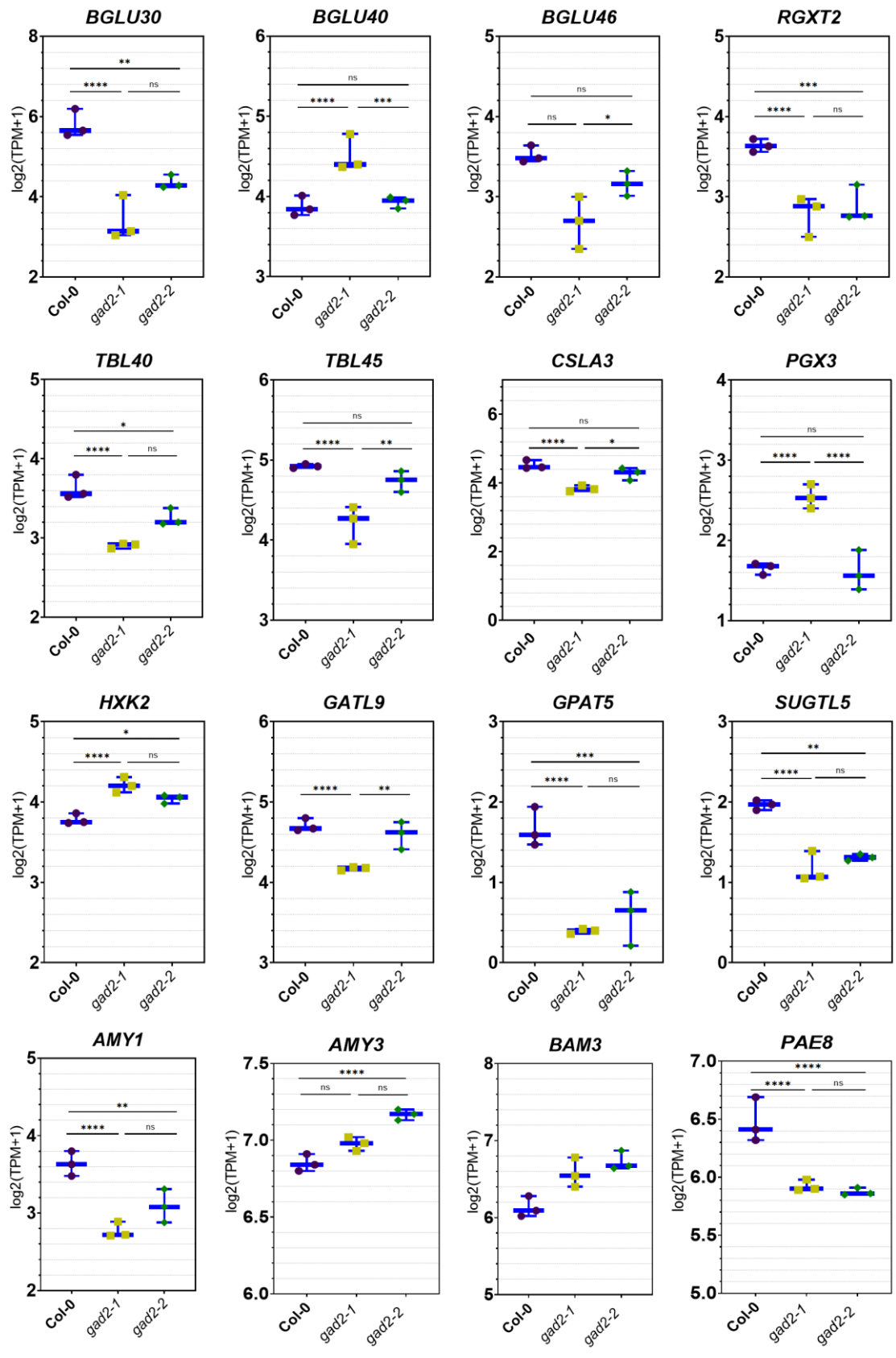
Supplementary Figure 5: GC-MS analysis in GABA-deficient mutant lines.

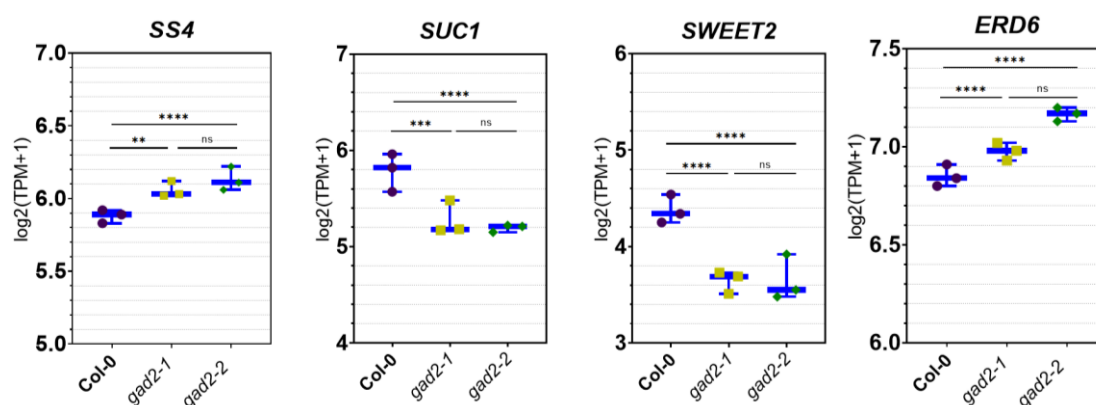
Outcome of a non-targeted Gas chromatography–mass spectrometry (GC-MS) experiment in (A) roots of *A. thaliana* wild-type (WT; Col-0; n=6), *gad2-1* (n=7), *gad2-2* (n=4), and *gad1/2/4/5* (n=5) plants. Significantly increased ascorbic acid concentrations were detected in *gad2-2* in comparison to all the other lines. (B) GC-MS analysis in rosettes of WT (n=6), *gad2-1* (n=3), *gad2-2* (n=4), and *gad1/2/4/5* (n=5) plants revealed massively increased malate concentrations

analysis was performed using Deseq2. Genes with p adj. < 0.05 were considered as differentially expressed genes using Wald-test.

| | <i>gad2-1</i> | | | <i>gad2-2</i> | | | Function |
|--------------------------------|----------------|--------------|----------------|----------------|--------------|----------------|-------------------------------------|
| | Number of DEGs | Up-regulated | Down-regulated | Number of DEGs | Up-regulated | Down-regulated | |
| UDP- Glycosyltransferase (UGT) | 20 | 6 | 14 | 11 | 1 | 10 | Biotic and abiotic stress responses |







Supplementary Figure 7: Extremely significant carbohydrate-related DEGs in *gad* mutants.

Log₂(transcripts per million [TPM]+1) values of differentially expressed genes (DEGs) which are involved in carbohydrate and cell wall metabolic processes in leaves of *A. thaliana* wild-type (Col-0), *gad2-1*, and *gad2-2* plants, as determined by RNA-seq analysis. Listed are only extremely significant DEGs (between the wild type and *gad2-1* and/or *gad2-2*; *p* adj < 0.0001), which were considered as differentially expressed using Wald-test; the adjusted P value was calculated using the Benjamini-Hochberg method. Individual data points were plotted with the median and minimum and maximum values; *****P* < 0.0001, ****P* < 0.001, ***P* < 0.01* *P* < 0.05.

Supplementary Table 5: Microarray analysis in *gad2-1* and *gad1/2/4/5*.

(A) Outcome of a microarray experiment revealing differentially expressed genes in *A. thaliana* *gad2-1* and *gad1/2/4/5* plants (n=6) that are involved in cell wall and carbohydrate metabolism as well as in enzymic glycosyl transfer. Listed are fold changes (fc; *p* adj. < 0.05) that are highlighted in colour; green shading represents upregulated genes and red shading indicates downregulated genes. Expansin A8 (EXP8), Trichome Birefringence-like 15 (TBL15), Trichome Birefringence-like 37 (TBL37), Cytochrome P450 (CYP79B3), and Flavin-monooxygenase glucosinolate S-oxygenase 2 (FMO GS-OX2).

| | fc wt/ <i>gad2-1</i> | fc wt/ <i>gad1245</i> | fc <i>gad2-1</i> / <i>gad1245</i> | |
|--|----------------------|-----------------------|-----------------------------------|---|
| AT2G40610 EXP8 | | -4.211784556 | | Plant-type cell wall loosening |
| pValue | | 4.9E-02 | | |
| AT2G37720 TBL15 | | -2.861026723 | | Carbohydrate metabolism, cell wall biogenesis, xylan acetylation/biosynthesis |
| pValue | | 0.012166239 | | |
| AT2G41640 Glycosyl-transferase family 61 protein | | -2.254147668 | -2.533480033 | Establishment of natural glycosidic linkages |
| pValue | | 0.025121891 | 0.00732806 | |
| AT2G34070 TBL37 | | 1.70177482 | | Plant-type cell wall modification |
| pValue | | 0.043663256 | | |
| AT2G22330 CYP79B3 | | 1.912388016 | | Defense response by callose deposition in cell wall |
| pValue | | 0.041264454 | | |
| AT1G62540 FMO GS-OX2 | | 1.927085102 | | Glucosinolate biosynthetic process |
| pValue | | 0.041264454 | | |

Acknowledgements

We kindly thank our collaborators Mathew Lewsey, Bhavna Hurgobin, Changyu Yi, and Asha Haslem from the Department of Animal, Plant and Soil Science (La Trobe University) for performing whole-genome and RNA sequencing with subsequent data processing on our behalf.

We thank Rainer Hedrich and his research group, including Peter Ache from the Department for Molecular Plant Physiology and Biophysics - Botany I, Tobias Müller from the Department of Bioinformatics, and Marcus Dittrich from the Department of Bioinformatics and Research Center for Infectious Diseases (ZINF) at Julius Maximilians University Würzburg for conducting the microarray analysis and providing subsequent data assessment.

Our gratitude also goes to Owen Atkin and Andrew Scafaro from the Research School of Biology at The Australian National University (ANU) for kind provision of LI-6400XT Portable Photosynthesis Systems. In addition, we are very grateful for Andrew Scafaro's great support with the A_N/C_i curve analyses and the kind provision of two .

We would like to express our gratitude to Owen Atkin also for provision of the Q2 scanner for respiration measurements. Our gratitude also goes to Andres Garcia from the Owen Atkin group for his guidance in handling the Q2 scanner. We also thank Harvey Millar, Brendan O'Leary, and Glenda Oh from the University of Western Australia for their helpful advice on the performance of the respiration measurements.

We thank Everard Edwards and Annette Betts from CSIRO Agriculture & Food (Waite Campus, Adelaide) for the provision of a LI-6400XT Portable Photosynthesis System.

We acknowledge the support of Natoiya Lloyd, Luca Nicolotti, and Georgia Davidson (Metabolomics SA, The Australian Wine Research Institute) for performing Gas Chromatography-Mass Spectrometry analysis and providing subsequent data processing.

We thank Larissa Chirkova from ARC Industrial Transformation Research Hub for Wheat in a Hot and Dry Climate (University of Adelaide) for performing Ultra-Performance Liquid Chromatography on our behalf.

We appreciate the help of Rosalie Kenyon at ACRF Cancer Genomics Facility (SA Pathology and University of South Australia) by conducting the RNA Labchip assay.

We thank Kylie Neumann and Sandy Khor from the Department of Plant Science (University of Adelaide) for the provision of the Invitrogen Qubit fluorometer.

We thank Na Sai for the assistance with transcriptomic analysis. We are also extremely grateful for the support from Xueying Feng in terms microarray analysis, plant genotyping and general useful advice. Both researchers are from the ARC Centre of Excellence in Plant Energy Biology (University of Adelaide).

We are grateful to Jenny Mortimer from the School of Agriculture, Food, and Wine (University of Adelaide) for the valuable advice on interpreting the cell wall data.

This work was funded by ARC Discovery grant DP170104384. Mamoru Okamoto provided support as an independent advisor. A. P. was supported by the GOstralia!/University of Adelaide PhD Scholarship and a School of Agriculture, Food and Wine Short Term Scholarship.

Chapter 4: General discussion and future outlook

4.0 Key findings

Since information on the role of GABA in response to altered atmospheric CO₂ is scarce, this study investigated the effect of modified GABA concentrations on the CO₂ response of guard cells, and subsequently moved on to explore the relationship between GABA deficiency and carbon assimilation in plants. In both cases, the GABA-deficient *GAD* knockout mutant lines (*gad2-1*, *gad2-2*, and *gad1/2/4/5*) were at the centre of the investigations. The quadruple mutant line *gad1/2/4/5* lacks four *GAD* genes, while *gad2-1* and *gad2-2* were thought to be single mutants harbouring a T-DNA insertion only in *GAD2*, the main GABA synthesis enzyme in leaves.

Stomatal activity was monitored in response to either ambient (400 ppm), lowered (100 ppm), or elevated (800 ppm) CO₂ concentrations in time-lapse experiments using infrared gas analysis (Chapter 2). While the wild type exhibited enhanced stomatal opening in response to low CO₂ and promoted stomatal closure in high CO₂ conditions, *gad2-1* barely responded to the change in CO₂ concentrations. This decrease in CO₂ sensitivity was also observed in *gad2-1* mutants that were complemented with either a full-length or an active *GAD2* construct specifically in guard cells. The GABA-deficient mutant *gad1/2/4/5*, however, displayed a wild type-like CO₂ stomatal response. Surprisingly, the mutant line *gad2-2*, which is a different *GAD2* T-DNA insertional allele than *gad2-1*, revealed a clear CO₂-sensitive response.

To unravel the mystery of the adverse CO₂ responses between *gad2-1* and *gad2-2*, gene expression as well as genomic profiles of the mutant lines were created. The sequencing data revealed a deletion of *MPK12* and its neighbour gene *BPS2* in *gad2-1*, which were absent in the wild-type, *gad2-2*, and *gad1/2/4/5* lines. The sequencing data was in line with the outcome of a microarray analysis that uncovered the downregulation of *MPK12* in *gad2-1* in relation to *gad1/2/4/5* and the wild type. All the results from the genetic studies matched unmistakably the CO₂ responses of the different lines. What is more, bringing *MPK12* back to the guard cells of *gad2-1* plants restored CO₂ sensitivity, which leaves no doubt that the elimination of *MPK12* was the cause for the aberrant CO₂ responsiveness in *gad2-1*. The higher stomatal aperture phenotypes of both *gad2-*

1 and *gad2-2* at ambient CO₂ are most likely due to the mutation in the *GAD2* gene and the resulting GABA deficiency.

CO₂ is known to be released into the cytosol as a by-product of GABA synthesis. Therefore, in the second part of my research, gas exchange measurements were performed in the aforementioned GABA-deficient mutant lines to identify differences in CO₂ uptake rates (Chapter 3). However, no significant difference in net CO₂ uptake was detected in *gad1/2/4/5* and *gad2-1* in comparison to the wild type, neither at ambient nor at elevated CO₂. At the same time, respiratory rates in the mutant lines were found to be unaltered, as shown by respiration measurements using Q2 scanning technology. The findings suggest that photosynthetic CO₂ assimilation is the same in wild-type and mutant plants. This assumption has been confirmed by the determination of V_{cmax} (maximal rate of Rubisco carboxylase activity) and J_{max} (maximal rate of photosynthetic electron transport) on the basis of A_N/C_i (Net assimilation per internal CO₂ concentration) measurements, which appeared to be comparable between the wild type and the *gad* mutants. Another piece of evidence for our assumption was provided by leaf biomass analyses in wild-type and mutant plants grown in response to an increased light intensity (150 μmol m⁻² s⁻¹ instead of 100 μmol m⁻² s⁻¹) or elevated CO₂ concentrations (750 ppm CO₂) for several weeks. In both cases, no significant differences could be detected.

In a last step (Chapter 3), it was investigated whether the elimination of GADs as key enzymes of the GABA shunt pathway has a significant impact on the carbon assimilate composition in leaf and root tissue. Interestingly, significantly elevated monosaccharide (in particular the hemicellulose monosaccharide xylose) concentrations were detected in the leaf material of all of GABA-deficient mutant lines. At the same time, Gene ontology (GO) enrichment analysis of the RNA-seq data indicated a correlation between the *GAD2* knockout and alterations in the expression of a large number of genes that are functionally enriched for carbohydrate and cell wall metabolism. In fact, many genes encoding key enzymes in cell wall remodelling processes were found to be differentially expressed in both *gad2-1* and *gad2-2* mutant lines, proposing that monosaccharide molecules might be scavenged from cell wall polymers upon GABA deficiency. However, since the assumption is based on preliminary data, future work is required to confirm this observation. A number of new research lines naturally flow from my findings and these are discussed below.

4.1 Which anion channels other than GABA-regulated ALMT9 are implicated in low CO₂ responses of guard cells?

In previous years, much information has been gathered on the closure-related signalling network in guard cells, particularly, in connection with ABA-induced stomatal closure (Roelfsema *et al.*, 2012). Less information is available regarding high CO₂-triggered stomatal closure and very little is known about the low CO₂ signalling pathway in guard cells (Hayashi *et al.*, 2020; Hiyama *et al.*, 2017). Our research did not unveil novel CO₂ signalling components but provided evidence that clearly excluded GABA involvement in CO₂-mediated stomatal movements (Chapter 2). Simultaneously, this study unveiled some intriguing insights, especially in the context of low CO₂ signalling in guard cells, which will be outlined below together with some suggestions for future research.

To date, it has been established that the high CO₂-dependent signalling pathway begins with the perception of CO₂ via carbonic anhydrases which turn CO₂ and H₂O into H⁺ and HCO₃⁻ (Hu *et al.*, 2010; DiMario *et al.*, 2017). This signalling pathway eventually leads to the activation of the S-type anion channel SLAC1 and the R-type anion channel ALMT12/QUAC1 (Negi *et al.*, 2008; Meyer *et al.*, 2010; Engineer *et al.*, 2016). The activity of both anion channels is indirectly suppressed by HT1, which has been identified as a negative regulator of high CO₂-induced stomatal closure (Hashimoto *et al.*, 2006; Hōrak *et al.*, 2016). On the other hand, HT1 functions as a positive regulator of the low CO₂ signalling pathway, which is activated by reductions in intracellular [CO₂] due to CO₂ consumption during photosynthesis and involves the Raf-like kinases Convergence of Blue light (BL) and CO₂ 1/2 (CBC1 and CBC2; Figure 1) (Hiyama *et al.*, 2017; Matthews *et al.*, 2019). Hiyama *et al.* (2017) discovered that CBC1 and CBC2 are phosphorylated and simultaneously activated by High leaf temperature (HT1), while CBC1 activity is stimulated by the blue-light receptor phototropin 1 (phot1), which together with phot2 undergoes an autophosphorylation in response to blue light exposure (Kinoshita *et al.*, 2001; Christie, 2007; Matthews *et al.*, 2019). Notably, CBC1/CBC2 have been identified as a convergence point between blue light- and red light-induced stomatal opening cascades. Red light has been discovered to switch on the photosynthetic machinery in the chloroplasts, resulting in CO₂ fixation by Rubisco and consequently a drop in the intercellular CO₂ concentration (Roelfsema *et al.*, 2002), which activates the low CO₂ signalling pathway in guard cells through activation of HT1 as mentioned above (Hiyama *et al.*, 2017; Matthews *et al.*, 2019). CBC1 and

CBC2 in turn suppress the activity of S-type anion channels at the plasma membrane (Hiyama *et al.*, 2017). Blue light-activated H⁺-ATPases pump protons out of the cytosol, leading to membrane hyperpolarisation and activation of inward rectifying K⁺ channels (Driesen *et al.*, 2020; Kinoshita *et al.*, 2001; Kinoshita and Shimazaki, 1999). Admittedly, a recent report claims that the H⁺-ATPase is not activated by blue light but is in fact repressed by the blue-light receptors phot1 and phot2 (Hayashi *et al.*, 2020). These contradictory results emphasise the necessity of future investigations to unravel the hitherto under investigated low CO₂ signalling pathway in guard cells.

To counterbalance the positively charged potassium ions, Cl⁻ and Mal²⁻ are transported into the cytosol via the activity of K⁺/H⁺ exchangers NHX1 and NHX2, the Chloride channel c (CLCc), and tonoplast ALMTs [Matthews *et al.* (2019) and all references therein]. These processes reduce the water potential within the guard cell, leading to water uptake, guard cell swelling and, consequently, stomatal opening (Driesen *et al.*, 2020). It is noted in my research that a role for ALMT6 and ALMT9 in the CO₂ response of guard cells has been ruled out (Supplementary Figures 10 and 11, Chapter 2). If ALMT9 was involved in this process, we would expect the low CO₂ opening response of the GABA-deficient mutants to differ from the wild-type CO₂ response, since GABA is known to negatively control ALMT9 to modulate stomatal opening and its concentration significantly enhanced under low CO₂ conditions (Dellero *et al.*, 2021; Xu *et al.*, 2021a). Also, it would be expected that the low CO₂ phenotype of plants that lack functional ALMT9 (*almt9-1*) differs from the wild-type phenotype. This, however, was not the case in our study.

ALMT9 is known as an anion channel that mediates stomatal opening upon light exposure (De Angeli *et al.*, 2013). By stimulating photosynthesis, white light illumination (which includes red light) causes a decline in intercellular CO₂ (Roelfsema *et al.*, 2002), and thereby seemingly results in the activation of ALMT9 (De Angeli *et al.*, 2013); nevertheless the *almt9* mutant has a similar extent of low CO₂-induced 'more opened stomata' with wild-type plants (Supplementary Figure 11, Chapter 2). In such circumstances, ALMT9 activity might not be sufficient for the stomatal opening response and additional, low CO₂-stimulated anion channels might get involved or the open state probability of already operating channels increases.

This raises the question, which other anion channels are participating in guard cell responses to low atmospheric CO₂. It appears that GABA-modulated anion channels are unlikely to be involved here. ALMT9 is so far the only guard cell channel that is assuredly known to be controlled by GABA (Xu *et al.*, 2021a). In which way or if GABA is involved in modifying the activity of the stomatal closure channel ALMT12/QUAC1, which mediates anion efflux across plasma membranes in response to ABA as well as high CO₂ (Meyer *et al.*, 2010), is unclear. The uncertainty is due to the observation that GABA suppressed stomatal opening in epidermal strips and in intact plants, whilst it inhibited stomatal closure only in the former case (Xu *et al.*, 2021a). In terms of CO₂-dependent stomatal movement, the loss-of-function mutant *almt12* reveals impaired stomatal closure, whereas stomatal opening is obviously unaffected (Meyer *et al.*, 2010), which suggests that ALMT12/QUAC1 is an essential component of high CO₂ signalling but not low CO₂ signal transduction.

Besides ALMT9 and ALMT12, we also reject the possibility that ALMT6 is part of the CO₂ signalling network in guard cells. Like ALMT9, ALMT4-6 have been identified as clade II members from the Arabidopsis ALMT family that span across the tonoplast (Meyer *et al.*, 2011; Eisenach *et al.*, 2017; Medeiros *et al.*, 2018). In contrast to ALMT9, ALMT6 activity has been proposed to be functionally redundant in guard cells as stomatal movement was not found to be impaired in mutant lines lacking intact *ALMT6* (Meyer *et al.*, 2011). As in the case of *almt9-1*, we identified a wild type-like CO₂ response in *almt6-1* and *almt6-2*, which supports the assumption that stomatal adjustment to altered CO₂ concentrations occurs independently of ALMT6 as well. Regarding the tonoplast-localised channel ALMT4, it was reported that it has an opposing role to ALMT9. While ALMT9 is known to drive anions into the vacuole during stomatal opening, ALMT4 was found to transport anions in the opposite direction during ABA-induced stomatal closure (De Angeli *et al.*, 2013; Eisenach *et al.*, 2017). According to Eisenach *et al.* (2017), light-mediated stomatal opening is unaffected. However, no information is available about the function of ALMT4 in stomatal responses to altered external CO₂ conditions.

As mentioned above, the other anion channel that was reported to contribute to light-induced stomatal opening besides ALMT9 is CLCc (Jossier *et al.*, 2010; Matthews *et*

al., 2019). However, to our knowledge, the role of CLCc enzymes in low CO₂-triggered stomatal opening has not been investigated so far.

It would be highly intriguing to identify the anion channels that are involved in stomatal responses to low atmospheric CO₂. Using infrared gas analysis, CO₂ sensitivity could be examined, *inter alia*, in transgenic lines that are mutated in *CLCc* in response to low CO₂ concentrations. In complement, epidermal strip assays could be performed, where guard cells of these mutant lines are exposed to low CO₂.

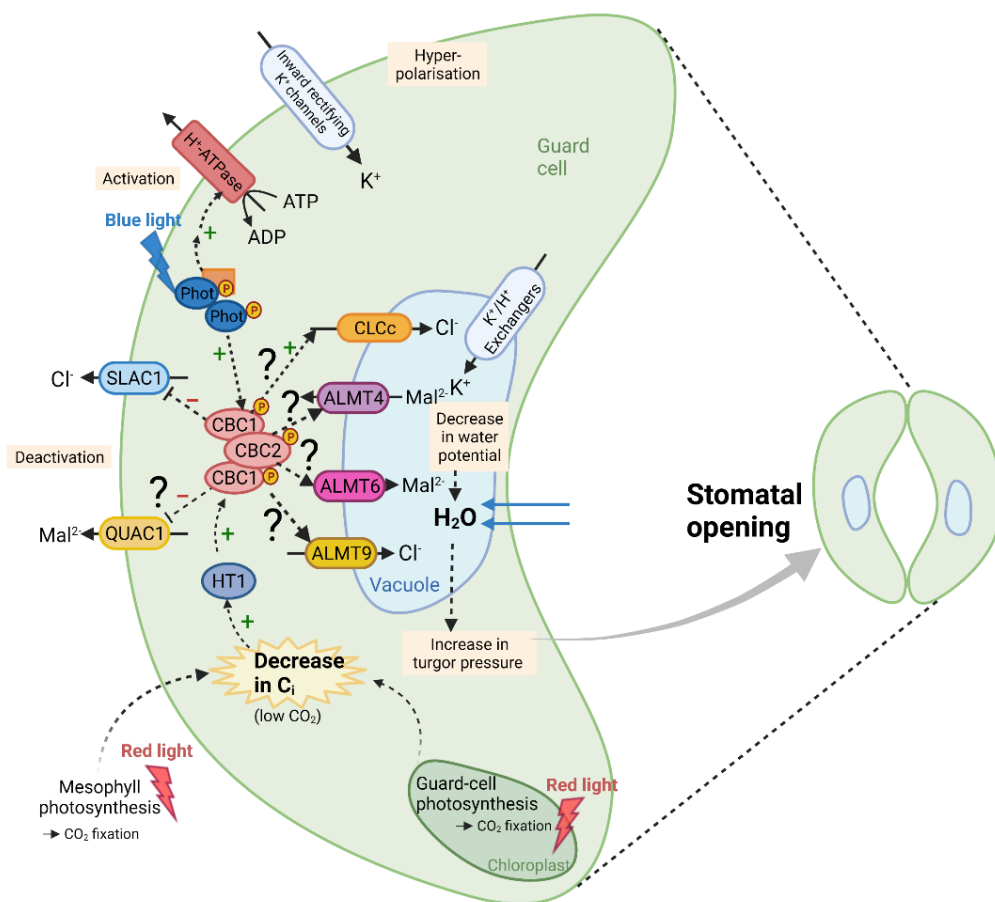


Figure 1: Low CO₂ signalling in guard cells.

Guard cells respond to a decrease in leaf internal CO₂ concentrations (C_i) as a result of photosynthetic CO₂ fixation by activating a signalling pathway that leads to stomatal opening. A reduction in C_i results in the activation of HT1 which in turn phosphorylates and thereby activates CBC1 and CBC2. Both proteins function in concert to inhibit anion channels that mediate anion efflux during stomatal closure responses, such as SLAC1. Evidence that confirms QUAC1/ALMT12 inhibition by CBC1/CBC2 is still lacking. It is also unknown if CBC1 and CBC2 have a stimulating effect on CLCc or any other tonoplast-localised anion channel

that is required for stomatal opening responses. ALMT9 seems to play a role in stomatal opening responses to light, which include decreases in intercellular CO₂. However, according to the data presented in this study, stomatal opening induced by low atmospheric CO₂ concentrations, such as 100 ppm CO₂, appears to be independent of ALMT9. ALMT9 activation by CBC1/CBC2 would possibly only occur during light-induced stomatal opening. Stomatal responses to low atmospheric CO₂ do not seem to require the vacuolar anion channel ALMT6 either, which does not rule out the possibility that it is involved in light responses of guard cells. Whether there is a role for the tonoplast-localised channel ALMT4 during CO₂-dependent stomatal opening is elusive. The CBC1/CBC2 proteins seemingly constitute a cross point of interaction between the low CO₂ and the blue light-dependent signalling pathway in guard cells. CBC1 is activated via phosphorylation by blue light-excited phototropins (phot1 and phot2). Another consequence of the excitation of these blue light receptors is the subsequent activation of plasma membrane-localised H⁺-ATPases, which pump protons out of the guard cells and are thereby hyperpolarising the guard cell membrane. This initiates the activation of inward rectifying K⁺ channels at the plasma membrane and K⁺/H⁺ exchanger at tonoplast membrane of the guard cells. A counterbalance is achieved through imported anions. As a consequence of the resulting decrease in guard cell water potential, water enters the cells, leading to an increase in turgor pressure, guard cell swelling, and stomatal opening. Full arrows point to the direction of ion transport. Dashed arrows indicate the signal direction (might include several steps). 'P' marks phosphorylated proteins. Light yellow shading highlights central physiological activities that take place during stomatal opening. Own work, mainly on the basis of Matthews *et al.* (2020), and in parts based on Hiyama *et al.* (2017), and Driesen *et al.* (2020). Illustration was created in BioRender.

4.2 Which mutation(s) restored the wild-type phenotype in *gad1/2/4/5*?

Surprisingly, adverse phenotypes between the GABA-deficient mutants were unveiled in this study. The quadrupole mutant line *gad1/2/4/5* exhibited wild type-like stomatal apertures and, in this regard, differed considerably from *gad2-1* (and *gad2-2*) (Chapter 2). Similarly, the rosette leaf biomass was found to be wild type-like in *gad1/2/4/5*, while *gad2-1* exhibited a clearly reduced leaf biomass (Chapter 3). As a matter of fact, *gad1/2/4/5* was produced by crossing *gad2-1* with other *gad* mutant lines (Deng *et al.*, 2020) and, consequently, both mutant lines harbour the same T-DNA insertion in *GAD2*. Therefore, the contradictory observations constitute a puzzle and are going to be discussed in further detail below.

All mutant lines used in the present study, except for *gad2-2*, were found to carry mutations that are unrelated to the gene of interest. A detailed overview of all mutations is provided by Table 1. Due to the additional mutations, tracing back a specific phenotypic phenomenon to the responsible mutation is quite challenging. This is the case for the quadruple mutant line *gad1/2/4/5*. In addition to *GAD2*, *gad1/2/4/5* owns mutations in three other *GAD* genes (*GAD1*, *GAD4*, and *GAD5*) as well as possibly an unwanted mutation in *PFK1*, which encodes a kinase that is catalysing an essential step during glycolysis (Perby *et al.*, 2021). Seven *PFK* isoforms have been identified in Arabidopsis, out of which *PFK1* and *PFK7* have been found to be essential for sugar homeostasis during metabolic processes in leaves (Perby *et al.*, 2021). Apparently, mutant plants lacking functional *PFK1* (*pfk1*) do not exhibit an altered rosette leaf biomass, whereas their total PFK activity seems to be significantly decreased (Perby *et al.*, 2021). However, this reduced PFK activity is obviously not associated with an altered glucose, fructose, sucrose, starch, or fructose-2,6-bisphosphate (product of PFK activity) content in rosette leaves (Perby *et al.*, 2021). Therefore, it is not clear whether or in which way the putative loss of PFK1 activity would recover the wild-type phenotype in the quadruple mutant. To completely rule out the possibility of a link between the dissimilar phenotypes of *gad2-1* vs. *gad1/2/4/5* and differences in sugar metabolism, a comprehensive GC-MS analysis should be considered. As there are seemingly also differences in leaf growth between *gad2-1* and *gad2-2*, the transgenic mutant line *gad2-2* should be included in this analysis to determine if different sugar compositions underpin the phenotypic dissimilarities between these two lines as well.

In contrast to *gad1/2/4/5*, *gad2-1* is lacking *MPK12* and *BPS2* due to a deletion mutation. *BPS2* is associated with the production of a mobile compound, known as the *bps* signal, which functions in embryogenesis and vegetative growth (Lee *et al.*, 2012). However, severe growth defects have only been observed in regard to dysfunctional *BPS1*, not *BPS2* alone (Lee *et al.*, 2012). Thus, we assume that the alterations in *gad2-1* leaf biomass are rather due to the deletion of *MPK12*. The *GAD2* knockout can be excluded as a possible cause due to the wild type-like leaf phenotype of the single mutant *gad2-2*. In fact, the elimination of *MPK12* obviously also caused a reduction in CO₂ responsiveness in *gad2-1* and appears to be epistatic to the *GAD2* mutation which is not related to the altered CO₂ phenotype. It is conceivable that the deletion of *MPK12* is also epistatic to other mutations/gene deregulations in *gad2-1*. The present study

revealed that *TPX2*, which is associated with ROS detoxification (Dietz *et al.*, 2006) and which is located adjacent to *GAD2* on chromosome 2, was highly upregulated in *gad2-1* and *gad1/2/4/5* but not in *gad2-2* (Chapter 2). If *TPX2* was indeed required for stomatal responses it might be subordinated by *MPK12* in *gad2-1* guard cells as well. Hypothetically, enhanced *TPX2* activity in *gad1/2/4/5* might bring stomatal apertures back to wild-type level, whilst *TPX2* activity is not promoted in *gad2-1* due to the epistatic effect of *MPK12*. To our knowledge, a role for *TPX2* in stomatal movement has not been revealed yet. However, it seems that *TPX2* is expressed in guard cells, proposing a putative role in stomatal function (The Arabidopsis Information Resource [TAIR], www.arabidopsis.org/servlets/TairObject?id=27102&type=locus, on www.arabidopsis.org, November 30, 2021).

It is common knowledge that ROS generation is vital for stomatal closure (Singh *et al.*, 2017). What is more, ROS accumulation is not only critical for ABA-induced stomatal closure but is also mediating high CO₂-induced stomatal movement (Shi *et al.*, 2015). A central part in this process plays the NADPH oxidase Respiratory burst oxidase homolog 1 (RBOH1) which mediates the generation of ROS during high CO₂-stimulated stomatal closure (Kwak *et al.*, 2003; Shi *et al.*, 2015). Conceivably, due to differences in *TPX* activity, ROS accumulation in guard cells might differ between the different mutant lines.

Reactive oxygen species (ROS) are known to have a dual role in plants as they accumulate as both a guard cell signal and a toxic side-product of aerobic metabolic processes (Al-Quraan, 2015; Mittler, 2017). As ROS have toxic effects on plants, it is essential for the plant to keep a fair balance between ROS generation and ROS quenching (Pitzschke *et al.*, 2006). Interestingly, a connection between GABA accumulation and increased ROS decomposition was previously observed (Ramesh *et al.*, 2017; Wu *et al.*, 2021; Xu *et al.*, 2021b). It was suggested that GABA is required for mitigating the harmful effect of ROS on proteins, lipids, DNA, and RNA, also referred to as 'oxidative stress' (Al-Quraan, 2015; Mittler, 2017). According to Wu *et al.* (2021), GABA reduces oxidative stress by controlling the expression of genes that are associated with ROS (H₂O₂) production as well as by governing the activity of Guard cell outwardly-rectifying potassium (GORK) channels. Interestingly, the GABA-overproducing mutant *pop2-5* was found to accumulate significantly less H₂O₂ than the control plants (Wu *et al.*, 2021). It was proposed that this result was, *inter alia*,

based on an increased activity of ascorbate peroxidases (APXs) (Kalhor *et al.*, 2018; Wu *et al.*, 2021). Increased APX activity results in H₂O₂ reduction and concomitant ascorbic acid (AsA) oxidation, thereby controlling the cytosolic H₂O₂ concentration and minimising oxidative stress (Smirnoff, 2000).

Remarkably, in the present study, AsA concentrations were significantly elevated in the roots of the *gad2-2* mutant line compared to all the other lines, including *gad2-1* (Chapter 3). As the rise in concentration was only true for *gad2-2* and not for the other GABA-deficient lines, it seems that disrupted GABA production is not linked to AsA accumulation in roots. However, one hypothesis is that the differences in AsA content could be due to augmented presence of TPX2 protein in the roots of *gad2-1* and *gad1/2/4/5*. Research revealed that TPX2 functions in an alternative H₂O₂ detoxification cycle to APX (Figure 2) (Dietz *et al.*, 2006; Sosa *et al.*, 2011). It is conceivable that ROS production is altered in the GABA-depleted *gad* lines, impelling *gad2-2* to increase AsA production, while TPX2 enzymes are increasingly active in *gad2-1* and *gad1/2/4/5*. This theory is supported by the discovery of an ‘electron transport’ gene cluster in *gad2-2* that was absent in *gad2-1* (Chapter 3). In previous studies, connections have been found between AsA accumulation and the photosynthetic as well as the mitochondrial electron transport chain (Bartoli *et al.*, 2000; Ivanov, 2014). Moreover, the RNA-seq analysis also uncovered the differentially expression of many peroxidase (PX) genes in *gad2-1* and *gad2-2*, including genes encoding ascorbate peroxidases (Table 2). In some cases, the same PX genes were differentially expressed in *gad2-1* and *gad2-2*, while in other cases, different DEGs were found in the two mutant lines. It is intriguing to note that genes encoding APX were only differentially expressed in *gad2-2* but not *gad2-1* (Table 2), which is consistent with the different AsA concentrations detected in the two genotypes. Admittedly, our assumption is based on limited information and, therefore, is only worth to be followed up in case the differences in AsA accumulation between the *gad* mutant lines can be confirmed. In case our speculation proves true, antioxidant enzymatic activity assays would tell if the altered AsA concentration in *gad2-2* is due to altered APX activity (Wu *et al.*, 2021).

Regardless of APX activity being modulated in *gad2-1* or not, our transcriptomic data (Table 2) matches previous observations of GABA being implicated in the regulation

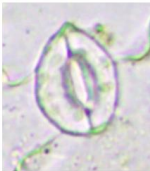

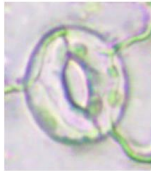

of enzymatic antioxidants (Fu *et al.*, 2017; Mahmud *et al.*, 2017; Ramos-Ruiz *et al.*, 2019; Yang *et al.*, 2008). As mentioned above, it is possible that differences in ROS signalling underpin the different stomatal phenotypes of the *gad* mutants, which could be elucidated through quantification of ROS concentrations in guard cells.

The determination of ROS formation in the guard cells of the different mutant lines could be realised by staining epidermal strips with 2',7'-dichlorodihydrofluorescein diacetate (H2DCF-DA) and 4,5-diaminofluorescein-2 diacetate (DAF-2DA) of epidermal peels with subsequent imaging of guard cell fluorescence (Khokon *et al.*, 2011).

Also, including *gad1/2/4/5* in the RNA-seq analysis would be helpful to ascertain whether genes encoding peroxidases are altered in this mutant line in relation to *gad2-2*.

Table 1: Profiles of GABA-deficient mutant lines.

Overview of mutations and phenotypical traits in wild-type (WT; Col-0), *gad2-1*, *gad2-2*, and *gad1/2/4/5* plants. Besides stomatal phenotypes like opening width and CO₂ responsiveness, differences in rosette leaf biomass are indicated. Not only targeted T-DNA insertion mutations but also additional, unintended mutations as well as misexpressed *TPX2* are listed here. The dark red framing of genes in the last column contains genes whose mutation/deregulation are presumably responsible for the WT-like stomatal phenotype of *gad1/2/4/5*.

| | Wild type (WT) | <i>gad2-1</i> | <i>gad2-2</i> | <i>gad1/2/4/5</i> |
|---------------------------------|---|--|---|---|
| Mutations | N/A | <i>GAD2</i> knockout (leaf GABA prod.) N/A | <i>GAD2</i> knockout (leaf GABA prod.) N/A | <i>GAD2</i> knockout (leaf GABA prod.) <i>GAD1</i> knockout (root GABA prod.) <i>GAD4</i> knockout (stress-activated) <i>GAD5</i> knockout (male gametes) <i>PPK1</i> knockout (putative; unintended) N/A N/A |
| Deregulated genes (not mutated) | N/A | <i>MPK12</i> deletion (unintended) <i>BPS2</i> deletion (unintended) | <i>TPX2</i> upregulation (located adjacent to <i>GAD2</i> ; unintended) | <i>TPX2</i> (upregulation; located adjacent to <i>GAD2</i> ; unintended) |
| GABA production | Intact | Impaired | Impaired | Heavily impaired |
| Average stomatal phenotype |  Standard |  More open stomata |  More open stomata |  WT-like stomata |
| CO ₂ responsiveness | Intact | Decreased | WT-like | WT-like |
| ALMT9 activity | Regulated by GABA | Uncontrolled | Uncontrolled | ? |
| Rosette leaf biomass | Standard | Decreased | WT-like | WT-like |

Another explanation why *gad2-1* and *gad1/2/4/5* differ in their stomatal behaviour might be the knockout of additional GAD genes in *gad1/2/4/5*. GAD activity is not only associated with GABA production *per se* but also influences the intracellular pH, CO₂ concentration, Ca²⁺ signalling, glutamate metabolism, and carbon fluxes into the Krebs cycle (Bouché and Fromm, 2004; Xu *et al.*, 2021b). This shows that GAD enzymes constitute central regulators of stress-induced physiological responses in plants. Conceivably, if several GAD genes are silenced, another regulatory element might ‘step in’ to balance the disturbed biochemical homeostasis. Which regulator could get involved here is elusive?

Bringing back GAD genes to *gad1/2/4/5* via plant transformation might provide some helpful clues in that regard. Additionally, it could be worth investigating if altered glutamate concentrations in the GABA deficient mutant lines influence glutamate receptors (GLRs)-regulated stomatal movement. Interestingly, research has demonstrated that overexpression of the receptor GLR3.1 hampers Ca²⁺-oscillation-mediated stomatal movement in *Arabidopsis* (Cho *et al.*, 2009). In this context, it could be examined whether the mutant lines differ in guard cell Ca²⁺ patterns prior or during events that trigger stomatal movement. This is also relevant as GAD activity is governed by (Ca²⁺)/calmodulin (CaM) and cytosolic pH (Baum *et al.*, 1996; Snedden *et al.*, 1995). Interestingly, it seems that not all GAD isoforms are dependent on Ca²⁺/CaM binding. In fact, *in silico* analysis have revealed that GAD3 and GAD5 are not regulated by Ca²⁺/CaM, which could potentially serve as another explanation for the stomatal differences between *gad2-1* and the *GAD5*-lacking quadruple mutant *gad1/2/4/5* [Shelp and Zarei (2017), Feng, 2021; unpublished]. To complement this, the use of a GABA sensor as developed by Marvin *et al.* (2019) might show if there are differences in GABA distribution and accumulation in guard cells between *gad1/2/4/5* and *gad2-1*. Used in combination with a cytosolic Ca²⁺ and pH sensors (CapHensor) (Li *et al.*, 2021), the GABA reporter could be a powerful tool to ascertain how Ca²⁺ and/or pH fluctuations and GABA production correlate and if there are discrepancies between *gad2-1* and *gad1/2/4/5* in that respect.

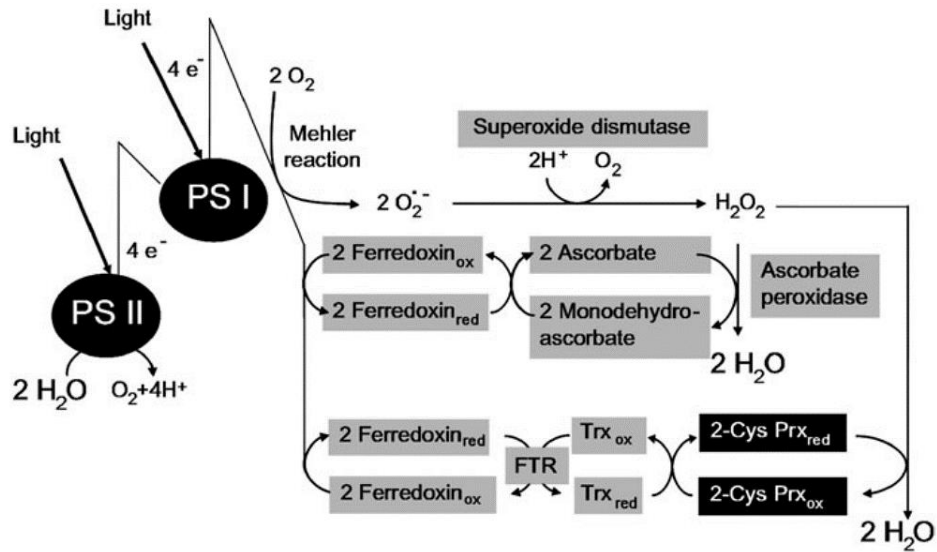


Figure 2: TPX/PRX-based H_2O_2 detoxification cycle.

Scheme illustrates the detoxification cycle of H_2O_2 which is generated during the light reactions of photosynthesis as a result of excessive e^- flux and can occur via two alternative pathways. One is based on the activity of the ascorbate peroxidase, while the other one is mediated via TPX/PRX (Thioredoxin-dependent Peroxidase/Peroxiredoxin), both resulting in the decomposition of H_2O_2 to water. Adapted from Dietz *et al.* (2006).

Table 2: DEGs associated with peroxidase activity.

List of differentially expressed genes (DEGs) that are enriched in functions related to peroxidase activity, as determined by RNA-seq analysis. A distinction was made between genes encoding peroxidases (upper part of table) and genes encoding ascorbate peroxidases (lower part of table). Differential gene expression analysis was performed using Deseq2. Genes with p adj. < 0.05 were considered as differentially expressed genes using Wald-test. Listed are log₂-fold changes, which are highlighted in colour; green shading represents upregulated genes and red shading indicates downregulated genes.

| | | <i>gad2-1</i> vs. WT | | <i>gad2-2</i> vs. WT | | <i>gad2-2</i> vs. <i>gad2-1</i> | |
|-----------|---------------------------------|-----------------------------|--------|-----------------------------|--------|---------------------------------|--------|
| | | log ₂ FoldChange | padj | log ₂ FoldChange | padj | log ₂ FoldChange | padj |
| AT4G33420 | Peroxidase 47 (PER47) | -0.6841 | 0.0004 | -0.6085 | 0.0040 | 0.0756 | 0.9279 |
| AT1G14540 | Peroxidase 4 (PER4) | -0.5042 | 0.0120 | -0.1513 | 0.7811 | 0.3529 | 0.1706 |
| AT1G71695 | Peroxidase 12 (PER12) | 0.1102 | 0.3184 | 0.2462 | 0.0031 | 0.1359 | 0.2684 |
| AT3G49120 | Peroxidase 34 (PER34) | -0.3339 | 0.0762 | -0.3839 | 0.0458 | -0.0499 | 0.9456 |
| AT4G21960 | Peroxidase 42 (PER42) | 0.3169 | 0.0005 | 0.2992 | 0.0020 | -0.0177 | 0.9682 |
| AT4G37530 | Peroxidase 51 (PER51) | -0.4374 | 0.0254 | -0.3968 | 0.0730 | 0.0407 | 0.9607 |
| AT5G39580 | Peroxidase 62 (PER62) | -0.5414 | 0.0057 | 0.0415 | 0.9657 | 0.5829 | 0.0047 |
| AT5G64110 | Peroxidase 70 (PER70) | 0.0288 | 0.9518 | -0.4879 | 0.0059 | -0.5167 | 0.0031 |
| AT4G11290 | Peroxidase 39 (PER39) | 0.5190 | 0.0062 | 0.5787 | 0.0028 | 0.0597 | 0.9442 |
| AT1G77490 | L-ascorbate peroxidase T (APXT) | 0.1175 | 0.3206 | 0.2039 | 0.0409 | 0.0864 | 0.6825 |
| AT4G08390 | L-ascorbate peroxidase S (APXS) | 0.1017 | 0.5726 | -0.3271 | 0.0047 | -0.4287 | 0.0001 |
| AT4G09010 | ascorbate peroxidase 4 (APX4) | 0.0951 | 0.3072 | 0.1663 | 0.0328 | 0.0712 | 0.6580 |

4.3 Which other signalling pathways does GABA signalling interact with?

The present study has explored the possibility of crosslinks between CO₂- and GABA-mediated stomatal regulation, thereby rejecting this hypothesis. However, large parts of the puzzle are still missing, and future research is recommended to further dissect the GABA signalling network in guard cells. There are many indications of interactions between GABA and other guard cell signal transduction pathways, which are outlined below.

Firstly, research has unveiled that GABA influences the production of ABA and *vice versa*. It was discovered that *nc3-2* knockout mutants, which are mutated in the ABA synthesis-related gene *NCED3*, upregulate *GAD4* gene expression upon dehydration (Urano *et al.*, 2009). Based on this knowledge, it can be assumed that ABA negatively controls GABA accumulation in response to water shortage. Furthermore, it was noted that GABA application to epidermal peels attenuates ABA-induced stomatal closure (Xu *et al.*, 2021a). The observed effect was, however, only true upon treatment with 2.5 µM ABA. In response to excessive concentrations of ABA (25 µM), the regulative effect of GABA was overridden and stomata were fully closed. Conversely, application of high ABA concentrations failed to induce complete stomatal closure in GABA-depleted *gad2* mutant line, proposing that plants are less sensitive to high concentrations of ABA upon GABA deficiency (Xu *et al.*, 2021a). Further evidence for a connection between GABA and ABA is provided by a study in poplar roots (*Populus alba* × *Populus glandulosa* cv. '84K'), which showed a correlation between increased GABA shunt activity and altered expression levels of ABA-related genes (Yue *et al.*, 2018).

To conclude, it appears that GABA and ABA signalling pathways function antagonistically in stomatal closure responses to drought. However, it is not known at which point and which additional factors are involved in this interaction. One common target might be the anion channel ALMT12/QUAC1. It was reported that ABA activates the kinase OST1 leading to the stimulation of ALMT12/QUAC1 activity by phosphorylation (Malcheska *et al.*, 2017). GABA, on the other hand, inhibits ALMT12/QUAC1-mediated Cl⁻ transport in COS-7 cells and pollen grain protoplasts where *ALMT12* is expressed (Domingos *et al.*, 2019). Due to inconsistencies between results from different experimental approaches, the connection between GABA

accumulation and ALMT12/QUAC1 activity still requires further clarification in guard cells (Xu *et al.*, 2021a). To further unravel the regulation network, other central ABA signalling components could be envisaged for investigations in the context of putative GABA interaction.

Another phytohormone that is involved in stomatal regulation is ethylene (ET) (Desikan *et al.*, 2006). Evidence suggests that GABA and ET exert reciprocal influence on their biosynthesis. Kathiresan *et al.* (1997) reported that GABA application raises ethylene concentration up to 14-fold in *Helianthus annuus*, probably due to enhanced ACS expression (Lancien and Roberts, 2006). Conversely, experiments based on the exogenous application of the ET inhibitor aminoethoxyvinylglycine (AVG) revealed that a reduction in ET concentration is linked to a decrease in GABA content during heat stress (Jespersen *et al.*, 2015). A role for GABA in ET-mediated stress signalling was not only suggested in terms of heat stress but also with regard to salt stress. Ji *et al.* (2018) found ET accumulation and ET-related gene expression to be significantly altered in poplar (*Populus tomentosa* Carr.) plants upon exogenous GABA application. Conversely, also GABA depletion appears to be associated with altered ET-related gene expression. Transcriptional data in this thesis implies that, in particular, genes encoding ET-responsive transcription factors (ERFs) are differentially expressed in the GABA-deficient mutant lines *gad2-1* and *gad2-2* (Table 3). ERFs have been found to be important regulators of ET-related defence genes (Huang *et al.*, 2015). Notably, one publication discussed a putative link between the induction of ERF genes and ABA accumulation [Müller (2021) and all references therein], impelling the author to conclude that ET could possibly regulate ABA production via ERF proteins (Müller, 2021). Furthermore, it was observed that guard cells of *ERF96*-overexpressing plants were more ABA-sensitive in comparison to control plants, suggesting a positive correlation between the abundance of *ERF96* and ABA-induced stomatal closure (Wang *et al.*, 2015). As links have already been identified between GABA accumulation and ABA-elicited stomatal closure, it is conceivable that GABA regulates the expression of ERF genes and thereby indirectly influences the synthesis of ABA in guard cells.

Significantly, also a connection between ALMTs and ET was identified in a previous study. There, it was demonstrated that ET blocks Al^{3+} -induced malate efflux from

wheat root tips by negatively regulating TaALMT1 (Tian *et al.*, 2014). Likewise, GABA is known to reduce Al³⁺-triggered malate extrusion by suppressing TaALMT1 activity (Ramesh *et al.*, 2015). It is unknown whether ET and GABA negatively regulate TaALMT1 via altering endogenous metabolism of the other?

It would be intriguing to know how exogenous ET affects manipulated GABA content in plants and *vice versa*. To determine the ET sensitivity of mutant plants that are overproducing GABA and ones that are deficient in GABA production, epidermal strip assays could be performed on corresponding plants treated with the ET precursor ACC. This assay could also be conducted the other way round by treating ET signalling/biosynthesis mutants, such as *etr1* or *ein3/ eto1*, with exogenous GABA/muscimol (Tanaka *et al.*, 2005).

Table 3: DEGs associated with ethylene (ET) activity.

List of differentially expressed genes (DEGs) that are enriched in functions related to ET activity, as determined by RNA-seq analysis. Most of the DEGs are genes that encode ET-responsive transcription factors (ERFs). Genes that are differentially expressed in both *gad2-1* and *gad2-2* (framed in dark blue) are related to drought resistance, immunity responses, and flowering regulation (Bethke *et al.*, 2009; Ding *et al.*, 2013; Gras *et al.*, 2017; Zhu *et al.*, 2014). Differential gene expression analysis was performed using Deseq2. Genes with p adj. < 0.05 were considered as differentially expressed genes using Wald-test. Listed are log₂-fold changes which are highlighted in colour: green shading represents upregulated genes, while red shading denotes downregulated genes.

| | | <i>gad2-1</i> vs. WT | | <i>gad2-2</i> vs. WT | | <i>gad2-2</i> vs. <i>gad2-1</i> | |
|-----------|---|-----------------------------|--------------|-----------------------------|--------------|---------------------------------|--------------|
| | | log ₂ FoldChange | padj | log ₂ FoldChange | padj | log ₂ FoldChange | padj |
| AT1G01840 | AP2-like ethylene-responsive transcription factor SNZ | 0.298 | 0.2803308360 | 0.054 | 0.9418166470 | -0.244 | 0.5763355980 |
| AT2G39250 | AP2-like ethylene-responsive transcription factor SNZ | 0.545 | 0.0000000018 | 0.264 | 0.0287053150 | -0.281 | 0.0145201600 |
| AT3G23150 | Ethylene receptor 2 (ETR2) | 0.210 | 0.3299679380 | 0.415 | 0.0158708660 | 0.205 | 0.4910635440 |
| AT4G17500 | Ethylene-responsive transcription factor 1A (ERF1A) | -0.370 | 0.0680748520 | -0.464 | 0.0188918350 | -0.094 | 0.8830715160 |
| AT2G23340 | Ethylene-responsive transcription factor 8 (ERF008) | 0.415 | 0.0119367840 | -0.011 | 0.9877351600 | -0.426 | 0.0159049790 |
| AT3G50260 | Ethylene-responsive transcription factor 11 (ERF011) | -0.276 | 0.2235537730 | -0.479 | 0.0129536490 | -0.203 | 0.5862187600 |
| AT1G77640 | Ethylene-responsive transcription factor 13 (ERF013) | -0.533 | 0.010481629 | -0.448 | 0.074095367 | 0.085 | 0.901346493 |
| AT1G71520 | Ethylene-responsive transcription factor 20 (ERF020) | -0.412 | 0.0382678590 | -0.423 | 0.0447903550 | -0.011 | NA |
| AT1G01250 | Ethylene-responsive transcription factor 23 (ERF023) | 0.713 | 0.0003053210 | -0.060 | 0.9388317290 | -0.773 | 0.0001067800 |
| AT1G36060 | Ethylene-responsive transcription factor 55 (ERF055) | -0.663 | 0.0007995480 | -0.501 | 0.0356983790 | 0.162 | 0.7645644390 |
| AT1G64380 | Ethylene-responsive transcription factor 61 (ERF061) | 0.468 | 0.0353649750 | -0.161 | 0.7237144180 | -0.629 | 0.0026749690 |
| AT1G06160 | Ethylene-responsive transcription factor 94 (ERF094) | -0.556 | 0.0046172550 | -0.240 | 0.4949768070 | 0.316 | 0.2943316960 |
| AT5G61600 | Ethylene-responsive transcription factor 104 (ERF104) | -0.452 | 0.0349822880 | -0.481 | 0.0316634470 | -0.029 | 0.9732965260 |
| AT5G51190 | Ethylene-responsive transcription factor 105 (ERF105) | -0.204 | 0.4785312250 | -0.691 | 0.0001421290 | -0.487 | 0.0190104560 |
| AT5G07580 | Ethylene-responsive transcription factor 106 (ERF106) | -0.594 | 0.0000004150 | -0.002 | 0.9967834630 | 0.592 | 0.0000011000 |
| AT5G61590 | Ethylene-responsive transcription factor 107 (ERF107) | -0.522 | 0.0000066700 | -0.155 | 0.4897841420 | 0.366 | 0.0077648530 |

GABA might also play a role in Jasmonate (JA)-mediated systemic defences against pathogen attacks (Xu *et al.*, 2021b). Although GABA and JA are both known to be implicated in herbivory-induced defence responses (Peña-Cortés *et al.*, 2004; Scholz *et*

al., 2015), research has shown that a manipulated GABA content in plants due to *GAD* or *GABA-T* knockout does not have an effect on the biosynthesis of JA or its activated form jasmonoyl-isoleucine (JA-Ile) when wounded by the insect caterpillar *Spodoptera littoralis* (Scholz *et al.*, 2015). Conversely, another study found that treatment of loquat (*Eriobotrya japonica* L. cv. Jiefangzhong) fruits with methyl jasmonate (MeJA), which has been proposed to be a systemic signal in plants (Cheong and Choi, 2003), clearly promoted GABA production and GAD activity (Cao *et al.*, 2012). On the basis of this knowledge, it is difficult to tell if GABA and JA signalling pathways are intertwined. Therefore, future investigations are required to provide clarification.

As stated by Ramesh *et al.* (2017), crosslinks between GABA signalling and other phytohormones seem to exist only in connection with specific stimuli. There is a growing body of evidence suggesting central roles for GABA, JA, and ET in submergence responses of plants (Allan *et al.*, 2008; Kamal and Komatsu, 2016; Zhang *et al.*, 2016; Kuroha *et al.*, 2018; Chapter 2, [Supplementary Figure 8](#); Chapter 3, [Figure 6](#)). Accordingly, these signalling molecules might ‘crosstalk’ during submergence, which is worth to be examined more closely.

4.4 Under which circumstances does GABA influence photosynthetic carbon assimilation in plants?

Xu *et al.* (2021a) revealed that GABA does not elicit a stomatal change by itself. Upon a stimulus, like water shortage or light-to-dark transitions or *vice versa*, GABA tends to influence stomatal activity. Likewise, it is conceivable that GABA does not alter photosynthetic CO₂ assimilation under standard conditions, but regulates photosynthetic activity only when conditions are unfavourable.

Previous research demonstrated that exogenous GABA can rescue a heat stress-dependent reduction in Rubisco activity in leaves of mungbean (*Vigna radiata* L.) plants (Priya *et al.*, 2019). The authors of this publication also reported about higher sucrose concentrations in leaves and anthers of heat-stressed mungbean plants upon GABA treatment relative to the control plants. Similarly, it was observed that a heat stress-induced growth inhibition as well a reduction in chlorophyll content and net photosynthesis were mitigated by exogenous GABA application in creeping bentgrass

(*Agrostis stolonifera* L.) (Zeng *et al.*, 2021). Exogenous GABA application was also found to alleviate reduced net photosynthetic rates and damages of PSII caused by salinity-alkalinity stress in muskmelon (*Cucumis melo* L., cv. Yipintianxia) seedlings (Xiang *et al.*, 2016).

Altogether, these are interesting findings as the GABA-deficient mutant plants in our study did not show any differences in Rubisco activity determined by A_N/C_i curve analysis or sucrose content as revealed by GC-MS analysis (Chapter 3). However, the analyses were performed in GABA-deficient mutants and did not include the effect of elevated GABA concentrations or stress exposure. Therefore, it would be worth including the GABA-hyperaccumulating *pop2* mutant in the studies and to analyse plants under stressed conditions in comparison to non-stressed conditions. In this regard, exposure of these plants to different kinds of environmental stresses could be considered, including stresses like drought, hypoxia, pathogen attacks, and other environmental cues that have been found to trigger GABA synthesis in plants (Park *et al.*, 2010; Wu *et al.*, 2021; Xu *et al.*, 2021a).

Additionally, it was ascertained in previous research that GABA can have a promotive effect on the biomass and length as well as on net photosynthesis rates of maize seedlings under non-stressed conditions (Li *et al.*, 2016). Our analyses were only conducted in four-, five-, and, six-week-old plants, which did not show any differences in the aforementioned parameters. Hence, we cannot exclude that growth and photosynthetic rates are affected by GABA depletion at an early growth stage in *Arabidopsis*, which, therefore, needs to be elucidated in future works.

4.5 Is cell wall-derived sugar salvage promoted in the GABA-deficient lines?

When generally thinking about walls, a picture of a rigid and static construction comes to mind. By contrast, plant cell walls have been discovered to be dynamic, flexible structures that allow cell expansion and modifications in accordance to physiological requirements (Liepman *et al.*, 2010). It is known that plants are highly flexible and capable to acclimatise to exterior changes through modulation of their metabolism and physiology (O'Leary and Plaxton, 2016). As mentioned above, plants have been

discovered to accumulate the signalling compound GABA in large concentrations in response to various environmental stimuli (Ramesh *et al.*, 2017), which appears to be associated with a higher acclimation capacity (Seifikalhor *et al.*, 2019). Possibly, GABA does not only impact stomatal movement but might also modulate cell walls to allow for an increased acclimation to altered external conditions. This possibility will be discussed in more detail in the following paragraphs.

Intriguingly, Renault *et al.* (2011) unveiled a reduction in the expression of cell wall-related genes in the GABA-overproducing mutant line *pop2-1* after GABA application. Transcriptomic data generated in this study also revealed major alterations in cell wall-related gene expression in the GABA-depleted mutant lines *gad2-1* and *gad2-2* (Chapter 3). By comparison, if the same gene was differentially expressed in the GABA-over accumulating mutant [in the study by Renault *et al.* (2011)] and the GABA-deficient mutant (in our study), the gene expression change was in the opposite direction. Furthermore, the expression data by Renault *et al.* (2011) did not include genes that encoded other essential cell wall remodelling proteins such as xyloglucan endotransglycosylases/hydrolases (XTHs) or β -D-xylosidases (BXLs). In that regard, it should be added that a Fourier-transform infrared spectroscopy (FT-IR) analysis failed to detect any modifications in the cell wall composition in the GABA-treated plants (Renault *et al.*, 2011). Whether the cell wall composition is altered in GABA-deficient plants is not known.

Another intriguing piece of information from the publication by Renault *et al.* (2011) is the mention that additional glucose application resulted in the upregulation of many GABA-dependent down-regulated genes. The relationship between GABA and glucose is not well-established yet but appears to be an interesting question to be followed up.

We speculate that the accumulated monosaccharides in the GABA-depleted lines (Chapter 3) could derive from the cell wall. Free xylose molecules are generally the result of hemicellulose cleavage, while hemicellulose formation utilises UDP-xylose during *de novo* pathways, which derives from photosynthesis products (Figure 3) (Geserick and Tenhaken, 2013; Rennie and Scheller, 2014). Besides, the GABA shunt and the xylose metabolic pathway are not directly linked (Figure 3). Why should cell wall-derived sugar salvage be promoted in the GABA-depleted lines? Our theory is that the elevated concentrations of free monosaccharides might be due to altered carbon

metabolism (i.e. increased starvation), resulting in enhanced salvage from the cell wall (J. Mortimer, personal communication). Hence, more soluble xylose is present, which is then fed into central metabolism and might be the cause for altered cell walls (J. Mortimer, personal communication).

We are aware that our data does not give any direct proof that GABA deficiency modifies cell wall recycling processes. Our results merely provide a platform for more in-depth research. Future investigations might include an Alcohol insoluble residue (AIR)-based analysis of cell wall components (Fangel *et al.*, 2021). On the basis of this approach, different kinds of polysaccharides can be detected in combination with additional techniques like high-performance anion exchange chromatography-with pulsed amperometric detection (HPAEC-PAD) and Micro Array Polymer Profiling (MAPP) (Fangel *et al.*, 2021). The outcome might give us an idea of differences in the abundance of certain cell wall polysaccharides like xylan or xyloglucan and could provide an explanation for the massively increased proportion of free xylose in the GABA-deficient mutants. To complement this, enzyme assays as thoroughly described by Maris *et al.* (2009) and Minic *et al.* (2004), might reveal if differences in xylose and glucose content are indeed based on alterations in XTH and BXL activity. In parallel to these assays, microscopic analysis of leaf cross sections could be performed in the GABA-deficient mutants to ascertain whether the altered expression pattern of cell wall-related genes manifests into abnormal cell structures. Additionally, repeating the GC-MS analysis with a more robust replicate number would surely provide additional, valuable information about the metabolite composition in the different *gad(s)* mutant lines.

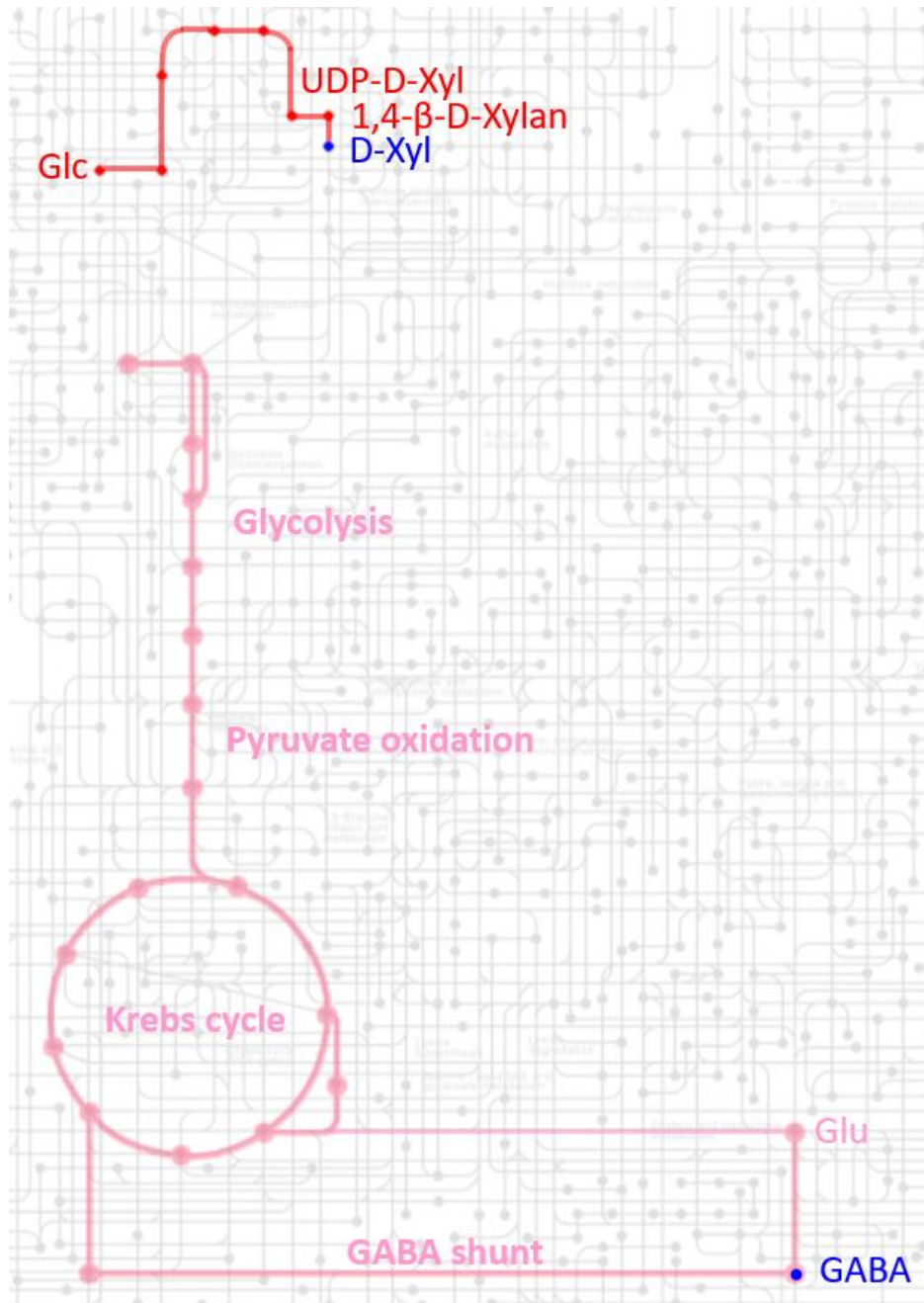


Figure 3: Mapping the GABA shunt and the xylose metabolic pathway.

This map was taken from the Kyoto Encyclopedia of Genes and Genomes (KEGG) database and the metabolic pathways highlighted in colour were mapped using the 'KEGG Color tool'. The pathway of xylose metabolism was identified using the KEGG map 'Amino sugar and nucleotide sugar metabolism' (map00520; Kanehisa, 2021). Glycolysis, Krebs (TCA) cycle, and GABA shunt were identified in the reference pathways (metabolic pathways) through selection of predetermined pathway modules (M00002: 'Glycolysis, core module involving three-carbon compounds', M00307: 'Pyruvate oxidation', M00009: 'Citrate cycle', M00027: 'GABA shunt'. Glc, Glucose; Xyl, Xylose; Glu, Glutamate.

4.6 Concluding remarks

This study provided data-driven evidence for there being no link between GABA production and guard cell responses to alterations in atmospheric CO₂. Likewise, CO₂ assimilation and biomass production were found to occur independently of GABA. The lack of an expected effect of GABA on CO₂ responses of guard cells and photosynthesis in this thesis was informative because with this finding a putative research gap has been fully investigated and allows future research to focus on other aspects of GABA signalling and GABA metabolism.

While conducting this research, it became apparent that off-target mutations in the genome of plants can lead to misleading interpretations of phenotypic findings. In other words, the present study sheds light on random, non-intended mutations in the genomes of some GABA-deficient/-overproducing T-DNA insertion mutant lines. In doing so, the research community shall be informed about these mutations to avoid erroneous interpretation of results in future works.

Within the scope of this research, other interesting research gaps were identified, which are related to the involvement of anion channels in low CO₂ signalling in guard cells as well as to sugar salvage upon GABA deficiency. Future studies are also required to further evaluate the role of GABA in guard cell signalling and to dissect the GABA signalling network. Since GABA has been reported to be involved in plant responses to a large range of different environmental factors, there are likely to be other signal transduction pathways that share the same elements with GABA signalling and whose discovery can aid in the understanding of GABA's role in plant responses to changing environmental conditions.

Appendix I: Preliminary results revealing accelerated guard cell responses to CO₂ in *gad2-2*

Material and Methods

Plant material and growth conditions

In the following experiments, the following *Arabidopsis thaliana* lines were used: Wild-type ecotype Columbia (Col-0) and a mutant line generated in the Col-0 background. The T-DNA insertion line *gad2-2* (SALK_028819) was obtained from the Arabidopsis Biological Resource Centre (ABRC).

All plants were raised in hydroponics for four and a half to five and a half weeks following Conn *et al.* (2013): the seeds were stratified for two days at 4°C in the dark and then transferred to short-day growth conditions [10 hrs light (~100 $\mu\text{mol photons m}^{-2} \text{ s}^{-1}$)/14 hrs dark, average temperature of 22°C, and 56% relative humidity]. In the first three to four weeks, plants grew within the lids of customised black microcentrifuge tubes, with a hole, that had been filled with 0.7% agar and fitted on a 24 well floating microtube rack. The small hydroponic container that contained the rack was filled with a modified Hoagland solution, named Germination Solution (GS), which was replaced every week. The small hydroponic container was covered with cling wrap, which was perforated after two weeks of growth and completely removed three days before the plant transfer to hydroponic tanks. For a smooth transition from GS to higher concentrated Basal Nutrient Solution (BNS) after two weeks of growth, GS was exchanged by 1/3 with BNS on three subsequent days. After three and a half weeks of growth, seedlings with the same estimated leaf area were transplanted to individual 50 mL falcon tubes (with bottoms removed) inside aerated hydroponic tanks filled with BNS. For all experiments, the different genotypes grew side by side under the same growth conditions and were analysed within a time-period of 10 days.

Gas exchange measurements

For time-resolved infrared gas analysis in whole rosettes, four-and-a-half to five-and-a-half-week-old plants were transferred to 50 mL falcon centrifuge tubes filled with BNS solution (Conn *et al.*, 2013). The falcon tubes were placed in a LI-6400XT

Portable photosynthesis system (LI-COR Biosciences) fitted with a 6400-17 Whole Plant Arabidopsis Chamber. Prior to the gas exchange measurements, to maximise gas exchange rates, plants were adapted to light with a light intensity of 350 $\mu\text{mol photons m}^{-2} \text{ s}^{-1}$ for one hour (30W LED Panel, Arlec). Transpiration rates of the plants inside the chamber were recorded in response to a variety of CO₂ concentrations (100 ppm, 800 ppm, and 400 ppm CO₂) under the following chamber conditions: 350 $\mu\text{mol photons m}^{-2} \text{ s}^{-1}$ light intensity with a portion of 10% blue light, 50-60% relative humidity, an average temperature of $\sim 22^{\circ}\text{C}$, and an airflow rate of 350 mmol s^{-1} . Measurements were logged every minute and IRGAs were matched at the start of the measurements and then every five minutes. The duration of measurements at each CO₂ step was one hour. For data visualisation, the first 30 min of recording (at 400 ppm CO₂) were omitted. During the last hour of the experiment, gas exchange was recorded in the dark. Following the gas exchange measurements, leaf rosette surfaces of each analysed plant were captured using a Nikon D5100 camera and were measured using the ‘Threshold Color’ tool in ImageJ. All recorded transpiration rates were normalised to leaf rosette areas. Changes in transpiration rates per minute were calculated using the formula $d\text{Transpiration}/dt$ (min).

For the statistical analysis of the data presented here, GraphPad Prism (Version 9.0.0 for Windows) was used.

Results and Discussion

Within the scope of Objective 1 (Chapter 2), gas exchange measurements were conducted, *inter alia*, in intact Arabidopsis wild-type (Col-0) plants and the loss-of-function mutant line *gad2-2*. In the case of both wild-type and *gad2-2* plants, a clear CO₂-sensitive phenotype was observed. However, a discrepancy in terms of the response magnitude, differences were detected between an initial and a later gas exchange experiment. Preliminary results (Experiment 1; Figure A1.1 A) suggested an accelerated stomatal response to both low and high CO₂ in the single mutant line *gad2-2* in relation to the wild type (Experiment 1; Figure A1.1 E). Also, the degree of high

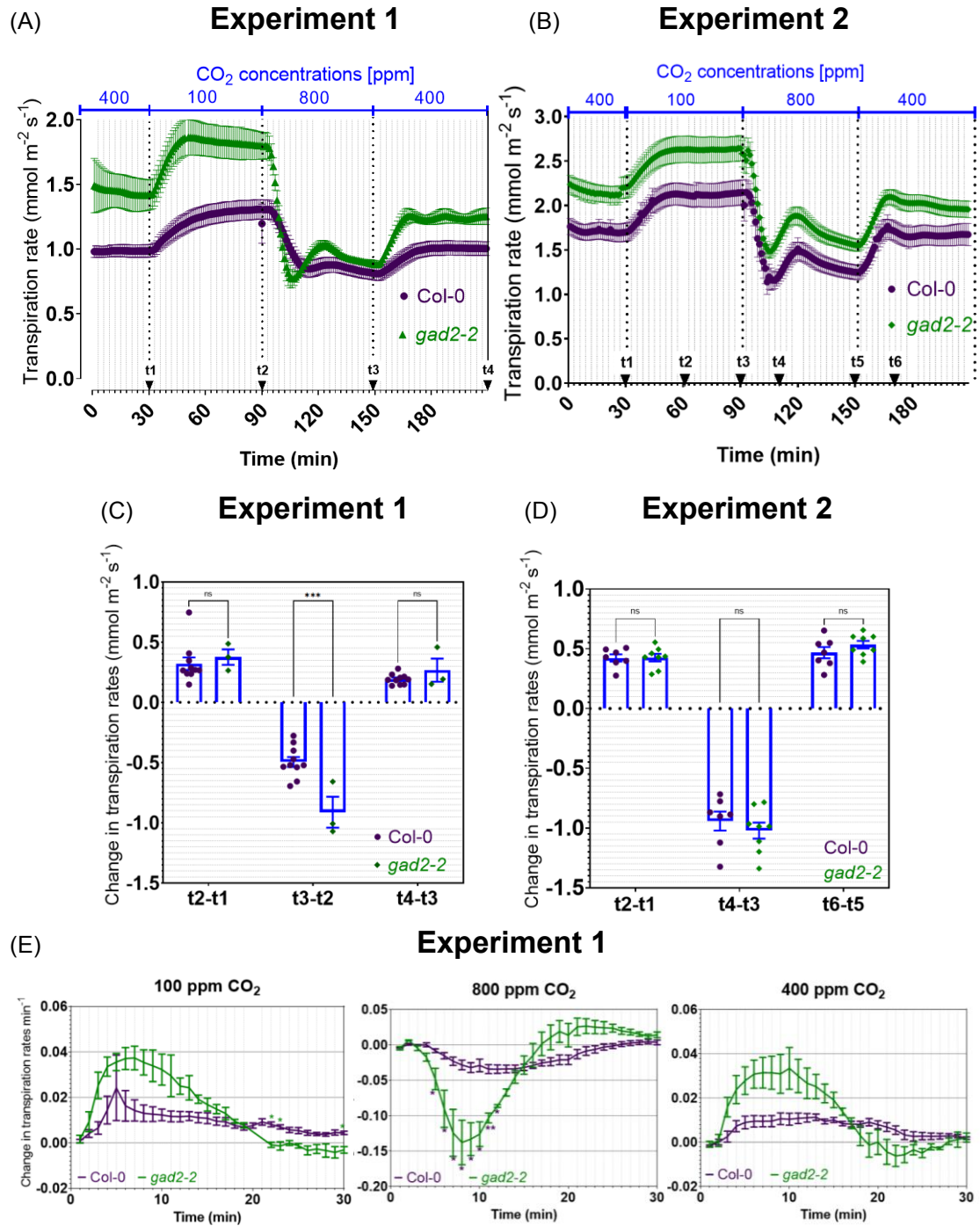
CO₂-induced stomatal closure appeared to be significantly larger in *gad2-2* compared to the wild type (Experiment 1; Figure A1.1 C).

Having said this, when repeating this experiment at a later point in time, no difference in CO₂ responsiveness was found between the wild type and *gad2-2* (Experiment 2; Figure A1.1 B), neither in terms of the degree nor the speed of stomatal opening/closure (Experiment 2; Figure A1.1 D and Figure A1 F). In fact, when comparing the results of Experiment 1 and 2, it became apparent that, in the case of the latter, transpiration rates were in total much higher relative to the former one. This was true for the wild type and for *gad2-2* (Figure A1.2 A). Further comparisons between Experiment 1 and 2 revealed that the change in stomatal apertures was the same for *gad2-2*, whereas significant differences were detectable in that respect in the wild type between both experiments (Figure A1.2 B).

We suspect that the discrepancies in wild-type transpiration rates between Experiment 1 and 2 are due to the rise in baseline stomatal apertures at ambient CO₂ in Experiment 2. In other words, stomatal apertures that were already more open than in Experiment 1 were exposed to low CO₂, which seemingly led to an accelerated CO₂ response. Why low CO₂-dependent stomatal opening is higher and more rapid at a raised aperture baseline is unclear.

The result of Experiment 2 appears to be more reliable as it includes more replicates for *gad2-2* and, besides, all tested plants were of the same plant batch, while in Experiment 1, all three *gad2-2* plants in addition to one wild-type plant originated from one plant batch while the data of the other wild-type plants derived from previous gas exchange experiments. The observed phenotypical differences occurred between the two experiments despite the effort to keep all conditions identical. The only difference was that in Experiment 2, which was conducted 2 years after Experiment 1, a different kind of desiccant had been used (Orange Silica beads in Experiment 1 vs. Drierite in Experiment 2), which seemed to have caused a difference in the overall relative humidity inside the Arabidopsis whole plant chamber of the Infrared gas analyser. Obviously, an increased aperture baseline due to a higher relative humidity results in an increase in CO₂ responsiveness, as in the case of *gad2-2*. Accordingly, it can be assumed that no difference was detected between the CO₂ response curves in *gad2-2* between both experiments because *gad2-2* transpiration rates are generally increased, due to its *GAD2* mutation (Xu *et al.*, 2021a). Clearly, transpiration rates in *gad2-2* were

already relatively high in the first experiment and increased upon an elevation in atmospheric CO₂ concentrations.



(F)

Experiment 2

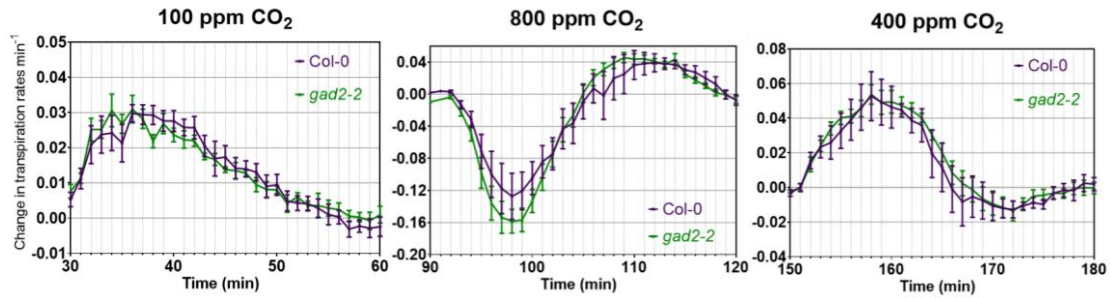
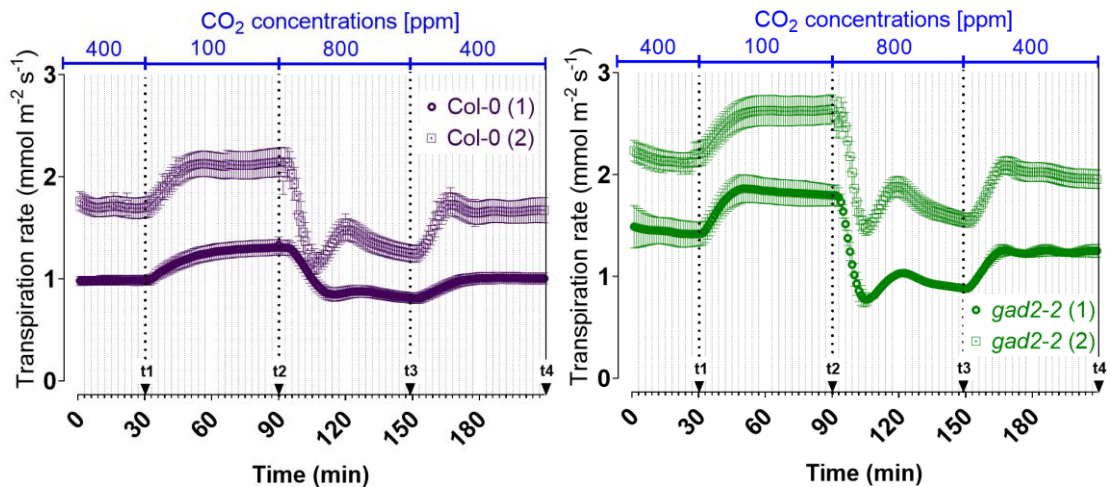


Figure A1.1: Comparing stomatal CO₂ responses of plants from two different experiments.

Data from an initial gas exchange experiment (Experiment 1) and from a later analysis (Experiment 2) is presented here, showing (A, B) time courses of transpiration rates in response to ambient (400 ppm), low (100 ppm), and elevated (800 ppm) CO₂ concentrations in intact *A thaliana* wild-type (Col-0; n=7) and GABA-deficient *gad2-2* (n=8) plants. On the basis of the data presented in (A) and (B), changes in transpiration rates during specific time periods were determined and are illustrated in (C) and (D). For calculating these changes, transpiration rates at earlier time points were subtracted from transpiration rates at later points in time. Time points are numbered and denoted by small black arrows in (A) and (B). (E, F) Changes in transpiration rates per minute were calculated using $d\text{Transpiration}/dt$ (min) and are also based on the time-lapse transpiration rates illustrated in (A) and (B). Pooled data from four experimental series is shown. Error bars indicate \pm SEM. Statistical differences were calculated using two-way ANOVA (C, D) or multiple Student's t test (E, F); *P < 0.05, **P < 0.01, ***P < 0.001.

(A)

Experiment 1 vs. Experiment 2



(B)

Experiment 1 vs. Experiment 2

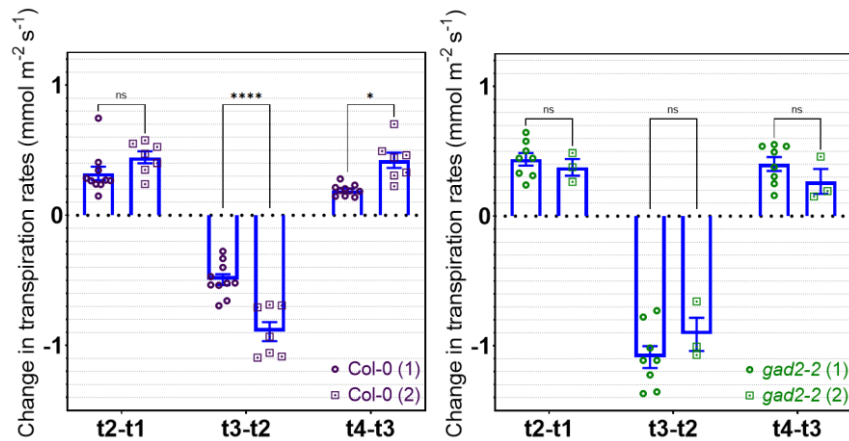


Figure A1.2: Direct comparisons between Experiment 1 and 2.

Data from an initial gas exchange experiment (Experiment 1) and a later analysis (Experiment 2) is directly compared here, showing (A) time courses of transpiration rates in response to ambient (400 ppm), low (100 ppm), and elevated (800 ppm) CO₂ concentrations in intact *A. thaliana* wild-type (Col-0; n=7) and GABA-deficient *gad2-2* (n=8) plants. On the basis of the data presented in (A), changes in transpiration rates during specific time periods were determined and are illustrated in (B). For calculating these changes, transpiration rates at earlier time points were subtracted from transpiration rates at later points in time. Time points are numbered and denoted by small black arrows in (A). Plants from Experiment 1 are named 'Col-0 (1)' and '*gad2-2* (1)', while plants from Experiment 2, are specified as 'Col-0 (2)' and '*gad2-2* (2)'. Pooled data from four experimental series is shown. Error bars indicate ± SEM. Statistical differences were calculated using two-way ANOVA (B); *P < 0.05, ****P < 0.0001.

Appendix II: Preliminary results showing increased photosynthetic rates in *gad1/2/4/5*

Material and Methods

Plant material and growth conditions

In the following experiments, the following *Arabidopsis thaliana* accessions were used: Wild-type ecotype Columbia (Col-0) and the T-DNA insertion line *gad2-1* (GABI_474E05) which was obtained from the Arabidopsis Biological Resource Centre (ABRC). The transgenic mutant line *gad1/2/4/5* was generated by crossing *gad1-1* (SALK_017810), *gad4* (SALK_106240), *gad5* (SALK_203883), and *gad2-1* (GABI_474E05), and was obtained from Shuqun Zhang (Deng *et al.* 2020).

All plants were raised in hydroponics for four and a half to five and a half weeks following Conn *et al.* (2013): The seeds were stratified for two days at 4°C in the dark and then transferred to short-day growth conditions [10 hrs light (~100 $\mu\text{mol photons m}^{-2} \text{ s}^{-1}$)/14 hrs dark, average temperature of 22°C, and 56% relative humidity]. In the first three to four weeks, plants grew within the lids of customised black microcentrifuge tubes, with a hole, that had been filled with 0.7% agar and fitted on a 24 well floating microtube rack. The small hydroponic container that contained the rack was filled with a modified Hoagland solution, named Germination Solution (GS), which was replaced every week. The small hydroponic container was covered with cling wrap, which was perforated after two weeks of growth and completely removed three days before the plant transfer to hydroponic tanks. For a smooth transition from GS to higher concentrated Basal Nutrient Solution (BNS) after two weeks of growth, GS was exchanged by 1/3 with BNS on three subsequent days. After three and a half weeks of growth, seedlings with the same estimated leaf area were transplanted to individual 50 mL falcon tubes (with bottoms removed) inside aerated hydroponic tanks filled with BNS. For all experiments, the different genotypes grew side by side under the same growth conditions and were analysed within a time-period of 10 days.

Gas exchange measurements

For time-resolved infrared gas analysis in whole rosettes, four-and-a-half to five-and-a-half-week-old plants were transferred to 50 mL falcon centrifuge tubes filled with BNS solution (Conn *et al.*, 2013). The falcon tubes were placed in a LI-6400XT Portable photosynthesis system (LI-COR Biosciences) fitted with a 6400-17 Whole Plant Arabidopsis Chamber. Prior to the gas exchange measurements, plants were adapted to light with a light intensity of $350 \mu\text{mol photons m}^{-2} \text{s}^{-1}$ for one hour (30W LED Panel, Arlec). Net CO_2 uptake rates of the plants inside the chamber were recorded in response to a variety of CO_2 concentrations (100 ppm, 800 ppm, and 400 ppm CO_2) under the following chamber conditions: $350 \mu\text{mol photons m}^{-2} \text{s}^{-1}$ light intensity with a portion of 10% blue light, 50-60% relative humidity, an average temperature of $\sim 22^\circ\text{C}$, and an airflow rate of 350 mmol s^{-1}). Measurements were logged every minute and IRGAs were matched at the start of the measurements and then every five minutes. The duration of measurements at each CO_2 step was one hour. For data visualisation, the first 30 min of recording (at 400 ppm CO_2) were omitted. During the last hour of the experiment, gas exchange was recorded in the dark. Following the gas exchange measurements, leaf rosette surfaces of each analysed plant were captured using a Nikon D5100 camera and were measured using the 'Threshold Color' tool in ImageJ.

For the statistical analysis of the data presented in this study, GraphPad Prism (Version 9.0.0 for Windows) was used.

A_N/C_i curve analysis

Gas exchange measurements for A_N/C_i curve analysis were conducted in fully expanded single leaves of six-to-seven-week-old, soil-grown Col-0, *gad2-1*, and *gad1/2/4/5* plants using a LI-6400XT Portable photosynthesis system (LI-COR Biosciences) equipped with a 2 x 3 cm Clear Chamber Bottom cuvette. Net assimilation (A_N) and intercellular CO_2 concentrations (C_i) were recorded in response to step changes in CO_2 concentrations (400, 50, 100, 150, 250, 400, 600, 800, 1000, 1400, and 1800 ppm). The light intensity was set to $600 \mu\text{mol photons m}^{-2} \text{s}^{-1}$, the flow rate was kept at $500 \mu\text{mol s}^{-1}$, and the block temperature was adjusted to 25°C . The measurements were logged five times at each concentration and the average of all five measurements was used for generating A_N/C_i curves, where A_N and C_i concentrations were plotted against each

other. The resulting A_N/C_i data was used to estimate V_{cmax} (maximum rate of Rubisco carboxylase activity) and J_{max} (maximum rate of photosynthetic electron transport). The calculation of V_{cmax} followed a Michaelis Menten equation by Farquhar *et al.* (1980), which describes a Rubisco-limited A_N response to CO_2 (Sharkey *et al.*, 2007), where K_c is the Michaelis constant of Rubisco for CO_2 , C_c the CO_2 partial pressure at the carboxylation site (in the chloroplast), O the partial pressure of oxygen at the carboxylation site, K_o the inhibition constant (Michaelis constant), Γ^* the photorespiratory compensation point, and R_d day respiration (mitochondrial).

$$A = V_{cmax} \left[\frac{C_c - \Gamma^*}{C_c + K_c(1 + O/K_o)} \right] - R_d$$

J_{max} was determined following another equation by Farquhar *et al.* (1980), which describes a RuBP-limited A_N response to CO_2 , where C_c is the CO_2 partial pressure at the carboxylation site, Γ^* the photorespiratory compensation point, and R_d day respiration (mitochondrial).

$$A = J \frac{C_c - \Gamma^*}{4C_c + 8\Gamma^*} - R_d$$

All data was normalised to the dry leaf mass per area (LMA) of respective single leaves. For the leaf area measurements, leaf surfaces were captured using a Nikon D5100 camera and afterwards measured using the ‘Threshold Color’ tool in ImageJ.

For the statistical analysis of the data presented here, GraphPad Prism (Version 9.0.0 for Windows) was used.

Results and Discussion

Intriguingly, preliminary results from our study showed an increase in photosynthetic activity in the GABA-deficient mutant *gad1/2/4/5* compared to the wild type – but this could not be replicated in subsequent experiments (Chapter 3). Initially, net CO_2 assimilation that had been recorded in response to different CO_2 concentrations

(ambient [\approx 400 ppm], low [\approx 100 ppm], and high [\approx 800 ppm] CO₂) using infrared gas analyser was found to be significantly higher in *gad1/2/4/5* under high CO₂ conditions (Figure A2.1). Dark respiration was additionally monitored in three independent experiments using a Q2 scanning system in single leaf tissue (Chapter 3). In addition, net CO₂ uptake rates were also recorded in the dark (at ambient CO₂) using infrared gas analyser (Figure A2.1). Both approaches suggested unaltered respiration rates, which, in combination with the detected increase in net CO₂ uptake rates, pointed to an enhanced photosynthetic capacity in *gad1/2/4/5*. This initial observation was supported by the outcome of an initial A_N/C_i curve analysis. For generating the A_N/C_i curve, net assimilation rates and leaf internal CO₂ concentrations had been recorded in response to 10 different CO₂ concentrations between 400 and 1800 ppm CO₂ and had been plotted against each other (Figure A2.3). The A_N/C_i data was used for estimating the maximum rate of rubisco carboxylase activity (V_{cmax}) as well as the maximum rate of photosynthetic electron transport (J_{max} ; Figure A2.3). Both J_{max} and V_{cmax} appeared to be enhanced in *gad1/2/4/5* in our preliminary data set. However, when using a more robust number of replicates (between 29 and 41) for the net CO₂ flux measurements, no differences in net CO₂ uptake rates were detectable between the wild type and the quadruple mutant (Chapter 3). This large-scale experiment was performed twice, using either four-week-old or six-week-old plants (Chapter 3). Moreover, also the previously observed elevation in V_{cmax} and J_{max} in *gad1/2/4/5* (Figure A2.3) could not be replicated with a larger number of replicates. Infrared gas analysis in *gad1/2/4/5* was conducted three more times using slightly modified approaches (Chapter 3). Single-leaf as well as whole-plant measurements were performed under highly elevated or standard light conditions (Chapter 3). In all six independent experiments (including the two large-scale experiments and the A_N/C_i curve analysis) no higher CO₂ uptake rates were observed in *gad1/2/4/5* (Chapter 3).

Net CO₂ uptake, rosette leaves

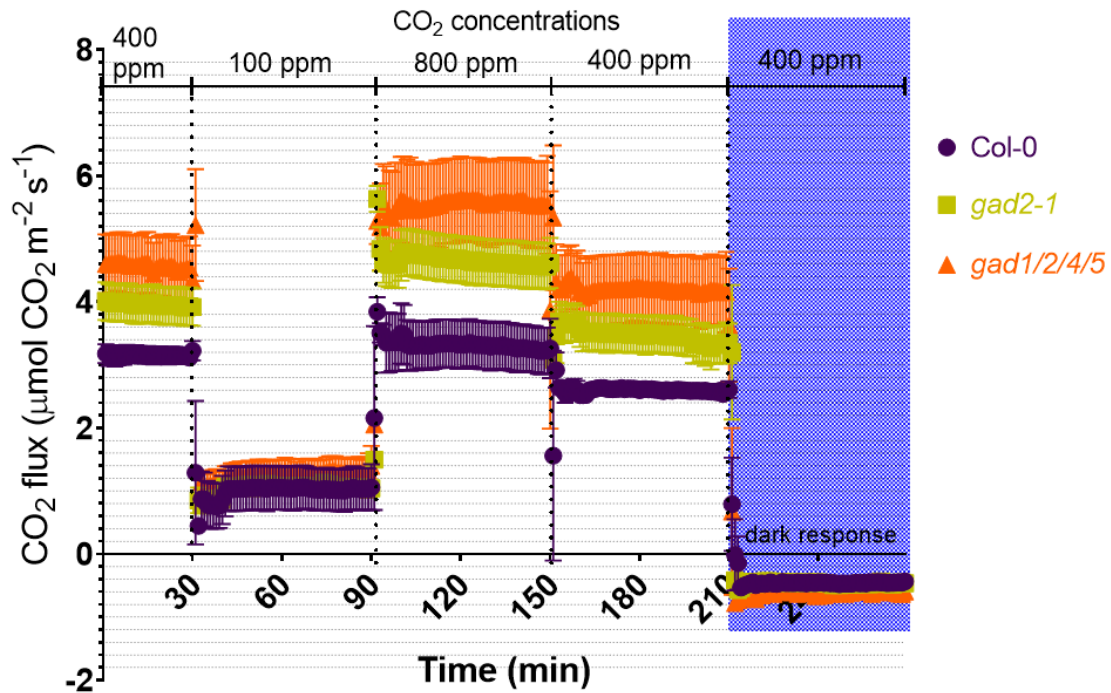
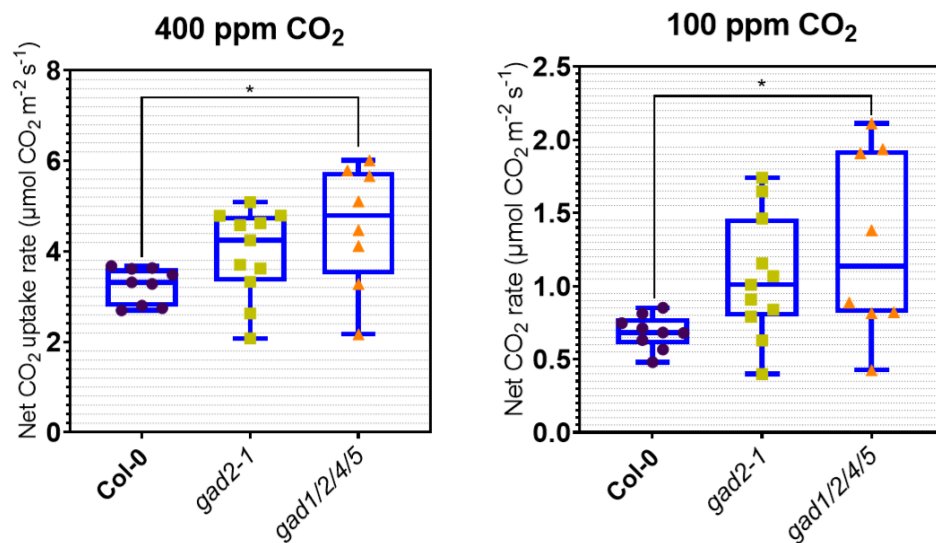


Figure A2.1: Net CO₂ uptake rates in response to different CO₂ concentrations.

Preliminary outcome of Infrared gas analysis in rosette leaves of intact four-and-a-half-week-old hydroponic *A. thaliana* plants at ambient CO₂ (400 ppm), decreased CO₂ (100 ppm), elevated (800 ppm) CO₂, and in darkness at ambient CO₂ using LI-6400XT Portable Photosynthesis System. CO₂ uptake rates in response to each CO₂ concentration was determined in the wild type (Col-0; n=9), *gad2-1* (n=11), and *gad1/2/4/5* (n=8). Error bars indicate ± SEM.

(A)

Net CO₂ uptake, rosette leaves



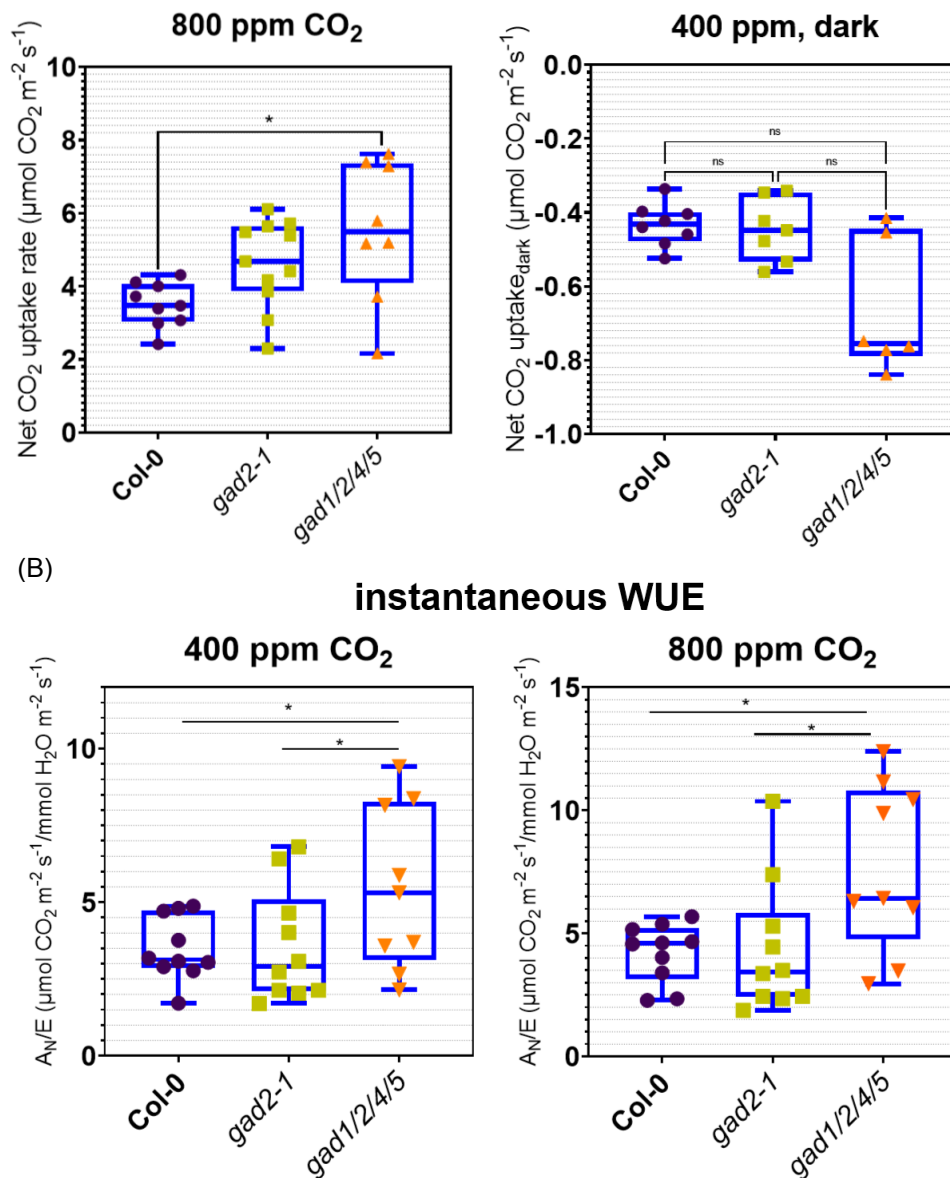


Figure A2.2: Gas exchange measurements in high/low CO₂-treated GABA-deficient mutant lines.

Preliminary outcome of Infrared gas analysis in rosette leaves of intact four-and-a-half-week-old hydroponic *A. thaliana* plants at ambient CO₂ (400 ppm), decreased CO₂ (100 ppm), elevated (800 ppm) CO₂, and in darkness at ambient CO₂ using LI-6400XT Portable Photosynthesis System, based on the same data as in Figure A2.1. Data points derived from the last five minutes of recording at each CO₂ concentration. (A) CO₂ uptake rates in response to each CO₂ concentration was determined in the wild type (Col-0; n=9), *gad2-1* (n=11), and *gad1/2/4/5* (n=8). (B) Instantaneous WUE was calculated using the data presented in (A). Data was plotted with box and whiskers: the box illustrates the median, and the 25th and 75th percentiles, while the whiskers indicate the minimum and maximum values. Statistical differences were calculated using one-way ANOVA; *P < 0.05.

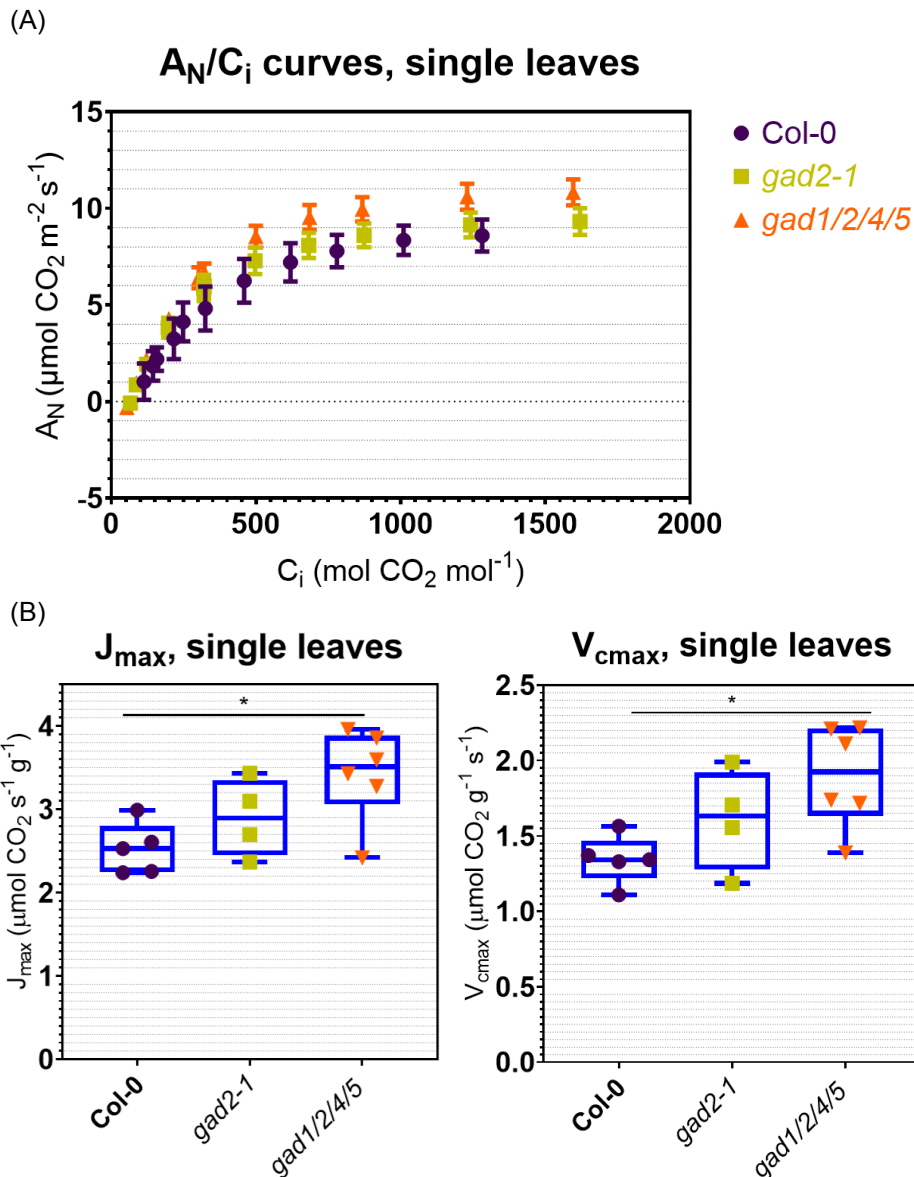


Figure A2.3: A_N/C_i curve analysis in GABA-deficient mutants.

(A, B) Outcome of Infrared gas analysis in intact single leaves of hydroponic plants using a LI-6400XT Portable Photosynthesis System. (A) Changes in net Assimilation (A_N) and leaf internal CO_2 concentrations (C_i) were determined in *A. thaliana* wild-type (Col-0; $n=5$), *gad2-1* ($n=4$), and *gad1/2/4/5* ($n=6$) plants in response to 10 different CO_2 concentrations (50, 100, 150, 250, 400, 600, 800, 1000, 1400, and 1800 ppm) and were plotted against each other at every CO_2 set point. (B) On the basis of the resulting A_N/C_i data, J_{max} (maximum rate of photosynthetic electron transport) and V_{cmax} (maximum rate of Rubisco carboxylase activity) were estimated. Data was plotted with box and whiskers: the box illustrates the median, and the 25th and 75th percentiles, while the whiskers indicate the minimum and maximum values. Error bars represent \pm SEM. Statistical differences were calculated using one-way ANOVA; * $P < 0.05$.

In fact, a large variability was detected in the net CO₂ uptake data of the quadruple mutant in the first two experiments (net CO₂ flux and A_N/C_i curve analysis), which was reflected in a significantly higher Coefficient of variation (standard deviation/mean value; Figure A2.4) (Pélabon *et al.*, 2020). Conversely, in the large-scale experiments with an enlarged number of replicates, no differences in variability were found between the wild type and *gad1/2/4/5*. All quadruple mutant plants were homozygous and a mixing up of genotypes could be excluded by genotyping (Figure A2.5). Our findings that net CO₂ uptake rates, respiration rates as well as the maximum rate of Rubisco carboxylase activity and photosynthetic electron transport were unaltered in the GABA-deficient mutants *gad2-1* and *gad1/2/4/5* strongly suggest that there is no direct link between GABA synthesis and CO₂ assimilation in Arabidopsis.

The arrangement of plants of the same genotype in close proximity to one another in hydroponic tanks in combination with non-uniform lighting might have resulted in irradiation differences between the genotypes in our initial experiments. It is well established that the light intensity is greatly defining a plant's photosynthetic capacity (Vemmos *et al.*, 2013). Later experimental designs involved the periodical repositioning of single hydroponic plants to allow for an even irradiation. In addition, a higher number of replicates was used for subsequent experiments.

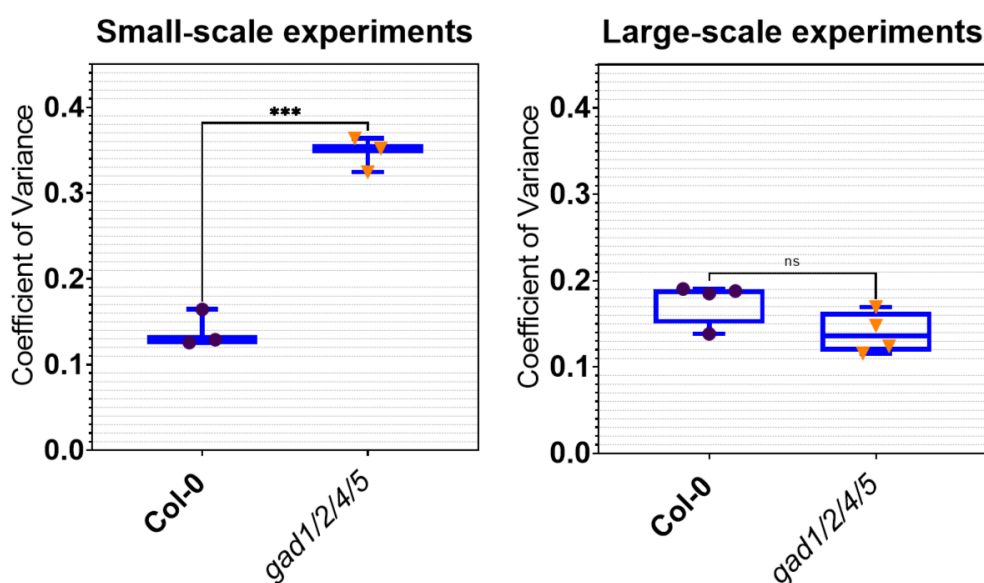


Figure A2.4: Coefficient of variation determined in gas exchange experiments.

Data shows the Coefficient of variation which was determined for wild-type (Col-0) and *gad1/2/4/5* data points from three independent small-scale (Chapter 3, Supplementary Figure

2 C; Figures A2.2 A and A2.3 B) and four large-scale experiments with an increased number of replicates (Chapter 3, Figures 1 A, B and 2 B; Supplementary Figure 2 A) using the calculation standard deviation/mean. Data was plotted with box and whiskers: the box illustrates the median, and the 25th and 75th percentiles, while the whiskers indicate the minimum and maximum values. Statistical differences were using two-sided Student's t-test; ***P < 0.001.

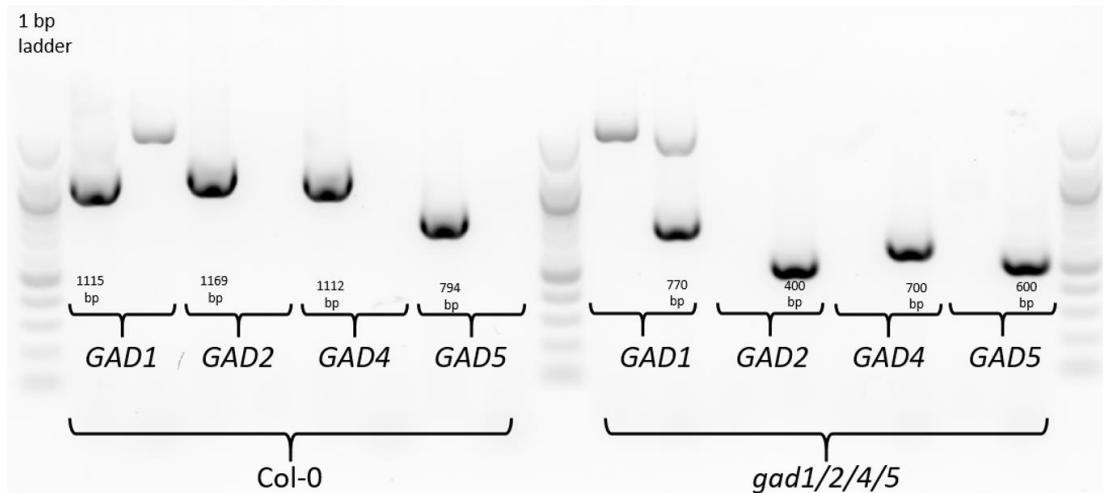


Figure A2.5: Gel image showing *gad1/2/4/5* genotyping result.

Outcome of genotyping PCR which was conducted in leaves of *A. thaliana* wild-type (Col-0) and *gad1/2/4/5* plants using eight different primer sets. Four of them had been designed to pick up *GAD1*, *GAD2*, *GAD4*, and *GAD5* in the wild type, while the other four primer pairs were used for amplification of the respective T-DNA insertion in each gene.

Bibliography

- Ainsworth, E.A., Davey, P.A., Bernacchi, C.J., Dermody, O.C., Heaton, E.A., Moore, D.J., Morgan, P.B., Naidu, S.L., Yoo Ra, H.-s., Zhu, X.-g., et al. (2002).** A meta-analysis of elevated [CO₂] effects on soybean (*Glycine max*) physiology, growth and yield. *Global Change Biology* 8, 695-709.
- Ainsworth, E.A., and Long, S.P. (2005).** What have we learned from 15 years of free-air CO₂ enrichment (FACE)? A meta-analytic review of the responses of photosynthesis, canopy properties and plant production to rising CO₂. *New Phytologist* 165, 351-372.
- Ainsworth, E.A., and Rogers, A. (2007).** The response of photosynthesis and stomatal conductance to rising [CO₂]: mechanisms and environmental interactions. *Plant, Cell & Environment* 30, 258-270.
- Al-Quraan, N.A. (2015).** GABA shunt deficiencies and accumulation of reactive oxygen species under UV treatments: insight from *Arabidopsis thaliana* calmodulin mutants. *Acta Physiologiae Plantarum* 37.
- Allan, W.L., Simpson, J.P., Clark, S.M., and Shelp, B.J. (2008).** γ -Hydroxybutyrate accumulation in *Arabidopsis* and tobacco plants is a general response to abiotic stress: putative regulation by redox balance and glyoxylate reductase isoforms. *Journal of Experimental Botany* 59, 2555-2564.
- Allen, G.J., Chu, S.P., Harrington, C.L., Schumacher, K., Hoffman, T., Tang, Y.Y., Grill, E., and Schroeder, J.I. (2001).** A defined range of guard cell calcium oscillation parameters encodes stomatal movements. *Nature* 411, 1053-1057.
- Andrews, S. (2010).** FastQC: a quality control tool for high throughput sequence data. (Babraham Institute, Babraham Bioinformatics).
- Balfagón, D., Gómez-Cadenas, A., Rambla, J.L., Granell, A., Ollas, C.d., Mittler, R., and Zandalinas, S.I. (2021).** GABA plays a key role in plant acclimation to a combination of high light and heat stress. *bioRxiv*, 2021.2002.2013.431103.
- Barnes, W.J., and Anderson, C.T. (2018).** Release, recycle, rebuild: cell-wall remodeling, autodegradation, and sugar salvage for new wall biosynthesis during plant development. *Molecular Plant* 11, 31-46.

- Barratt, D.H.P., Derbyshire, P., Findlay, K., Pike, M., Wellner, N., Lunn, J., Feil, R., Simpson, C., Maule, A.J., and Smith, A.M. (2009).** Normal growth of *Arabidopsis* requires cytosolic invertase but not sucrose synthase. *Proceedings of the National Academy of Sciences* *106*, 13124-13129.
- Bartoli, C.G., Pastori, G.M., and Foyer, C.H. (2000).** Ascorbate biosynthesis in mitochondria is linked to the electron transport chain between complexes III and IV. *Plant Physiology* *123*, 335-344.
- Batushansky, A., Kirma, M., Grillich, N., Toubiana, D., Pham, P.A., Balbo, I., Fromm, H., Galili, G., Fernie, A.R., and Fait, A. (2014).** Combined transcriptomics and metabolomics of *Arabidopsis thaliana* seedlings exposed to exogenous GABA suggest its role in plants is predominantly metabolic. *Molecular Plant* *7*, 1065-1068.
- Baum, G., LevYadun, S., Fridmann, Y., Arazi, T., Katsnelson, H., Zik, M., and Fromm, H. (1996).** Calmodulin binding to glutamate decarboxylase is required for regulation of glutamate and GABA metabolism and normal development in plants. *The Embo Journal* *15*, 2988-2996.
- Beale, S.I., Gough, S.P., and Granick, S. (1975).** Biosynthesis of delta-aminolevulinic acid from the intact carbon skeleton of glutamic acid in greening barley. *Proceedings of the National Academy of Sciences* *72*, 2719-2723.
- Bennetzen, J.L., and Wang, X. (2018).** Relationships between gene structure and genome instability in flowering plants. *Molecular Plant* *11*, 407-413.
- Bethke, G., Unthan, T., Uhrig, J.F., Pöschl, Y., Gust, A.A., Scheel, D., and Lee, J. (2009).** Flg22 regulates the release of an ethylene response factor substrate from MAP kinase 6 in *Arabidopsis thaliana* via ethylene signaling. *Proceedings of the National Academy of Sciences* *106*, 8067-8072.
- Blumwald, E., and Mittler, R. (2015).** Abiotic stress. In *Plant Physiology and Development*, A.D. Sinauer, ed. (Sunderland, Massachusetts: Sinauer Associates, Inc), pp. 732-761.
- Bouché, N., Fait, A., Zik, M., and Fromm, H. (2004).** The root-specific glutamate decarboxylase (GAD1) is essential for sustaining GABA levels in *Arabidopsis*. *Plant Molecular Biology* *55*, 315-325.
- Bouche, N., and Fromm, H. (2004).** GABA in plants: just a metabolite? *Trends in Plant Science* *9*, 110-115.

- Bown, A.W., and Shelp, B.J. (2016).** Plant GABA: not just a metabolite. *Trends in Plant Science* *21*, 811-813.
- Bown, A.W., and Shelp, B.J. (2020).** Does the GABA shunt regulate cytosolic GABA? *Trends in Plant Science* *25*, 422-424.
- Buchanan, B.B., and Wolosiuk, R.A. (2015).** Photosynthesis: The carbon reactions. In *Plant Physiology and Development*, L. Taiz, E. Zeiger, I.M. Møller, and A. Murphy, eds. (Sunderland: Sinauer Associates Incorporated), pp. 203-244.
- Buels, R., Yao, E., Diesh, C.M., Hayes, R.D., Munoz-Torres, M., Helt, G., Goodstein, D.M., Elsik, C.G., Lewis, S.E., Stein, L., and Holmes I.H. (2016).** JBrowse: a dynamic web platform for genome visualization and analysis. *Genome Biology* *17*, 66.
- Bunce, J.A. (2004).** Carbon dioxide effects on stomatal responses to the environment and water use by crops under field conditions. *Oecologia* *140*, 1-10.
- Caird, M.A., Richards, J.H., and Donovan, L.A. (2007).** Nighttime stomatal conductance and transpiration in C3 and C4 plants. *Plant Physiology* *143*, 4.
- Campbell, P., and Braam, J. (1999).** Xyloglucan endotransglycosylases: diversity of genes, enzymes and potential wall-modifying functions. *Trends in Plant Science* *4*, 361-366.
- Cao, S., Cai, Y., Yang, Z., and Zheng, Y. (2012).** MeJA induces chilling tolerance in loquat fruit by regulating proline and γ -aminobutyric acid contents. *Food Chemistry* *133*, 1466-1470.
- Carpita, N., and McCann, M. (2000).** The cell wall. In *Biochemistry & Molecular Biology of plants*, B. Buchanan, W. Gruissem, and R.L. Jones, eds. (Rockville: American Society of Plant Physiologists), pp. 52-108.
- Chao, Z., Liu, N., Zhang, P., Ying, T., and Song, K. (2019).** Estimation methods developing with remote sensing information for energy crop biomass: a comparative review. *Biomass and Bioenergy* *122*, 414-425.
- Cheng, C.-Y., Krishnakumar, V., Chan, A.P., Thibaud-Nissen, F., Schobel, S., and Town, C.D. (2017).** Araport11: a complete reannotation of the *Arabidopsis thaliana* reference genome. *The Plant Journal* *89*, 789-804.

- Cheong, J.-J., and Choi, Y.D. (2003).** Methyl jasmonate as a vital substance in plants. *Trends in Genetics* 19, 409-413.
- Chibbar, R.N., Ganeshan, S., Båga, M., and Khandelwal, R.L. (2004).** Carbohydrate metabolism. In *Encyclopedia of Grain Science*, C. Wrigley, ed. (Oxford: Elsevier), pp. 168-179.
- Cho, D., Kim, S.A., Murata, Y., Lee, S., Jae, S.-K., Nam, H.G., and Kwak, J.M. (2009).** De-regulated expression of the plant glutamate receptor homolog AtGLR3.1 impairs long-term Ca²⁺-programmed stomatal closure. *The Plant Journal* 58, 437-449.
- Christie, J.M. (2007).** Phototropin blue-light receptors. *Annual Review of Plant Biology* 58, 21-45.
- Conn, S.J., Hocking, B., Dayod, M., Xu, B., Athman, A., Henderson, S., Aukett, L., Conn, V., Shearer, M.K., Fuentes, S., et al. (2013).** Protocol: optimising hydroponic growth systems for nutritional and physiological analysis of *Arabidopsis thaliana* and other plants. *Plant Methods* 9, 11.
- Cotelle, V., and Leonhardt, N. (2019).** Chapter Four - ABA signaling in guard cells. In *Advances in Botanical Research*, M. Seo, and A. Marion-Poll, eds. (Academic Press), pp. 115-170.
- Croft, H., Chen, J.M., Luo, X., Bartlett, P., Chen, B., and Staebler, R.M. (2017).** Leaf chlorophyll content as a proxy for leaf photosynthetic capacity. *Global Change Biology* 23, 3513-3524.
- Daloso, D.M., Antunes, W.C., Pinheiro, D.P., Waquim, J.P., Araújo, W.L., Loureiro, M.E., Fernie, A.R., and Williams, T.C. (2015).** Tobacco guard cells fix CO₂ by both Rubisco and PEPcase while sucrose acts as a substrate during light-induced stomatal opening. *Plant, Cell & Environment* 38, 2353-2371.
- Daszkowska-Golec, A., and Szarejko, I. (2013).** Open or close the gate - stomata action under the control of phytohormones in drought stress conditions. *Frontiers in Plant Science* 4, 16.
- De Angeli, A., Zhang, J.B., Meyer, S., and Martinoia, E. (2013).** AtALMT9 is a malate-activated vacuolar chloride channel required for stomatal opening in *Arabidopsis*. *Nature Communications* 4, 10.

- Dellero, Y., Mauve, C., Jossier, M., and Hodges, M. (2021).** The impact of photorespiratory glycolate oxidase activity on *Arabidopsis thaliana* leaf soluble amino acid pool sizes during acclimation to low atmospheric CO₂ concentrations. *Metabolites* *11*, 501.
- Deng, X., Xu, X., Liu, Y., Zhang, Y., Yang, L., Zhang, S., and Xu, J. (2020).** Induction of γ -aminobutyric acid plays a positive role to *Arabidopsis* resistance against *Pseudomonas syringae*. *Journal of Integrative Plant Biology* *62*.
- Dennis, D.T., and Blakeley, S.D. (2000).** Carbohydrate metabolism. In *Biochemistry & Molecular Biology of plants*, B. Buchanan, W. Gruissem, and R.L. Jones, eds. (Rockville: American Society of Plant Physiologists), pp. 631-675.
- Des Marais, D.L., Auchincloss, L.C., Sukamtoh, E., McKay, J.K., Logan, T., Richards, J.H., and Juenger, T.E. (2014).** Variation in MPK12 affects water use efficiency in *Arabidopsis* and reveals a pleiotropic link between guard cell size and ABA response. *Proceedings of the National Academy of Sciences* *111*, 2836-2841.
- Desikan, R., Last, K., Harrett-Williams, R., Tagliavia, C., Harter, K., Hooley, R., Hancock, J.T., and Neill, S.J. (2006).** Ethylene-induced stomatal closure in *Arabidopsis* occurs via AtrbohF-mediated hydrogen peroxide synthesis. *Plant Journal* *47*, 907-916.
- Devos, K.M., Brown, J.K., and Bennetzen, J.L. (2002).** Genome size reduction through illegitimate recombination counteracts genome expansion in *Arabidopsis*. *Genome Res* *12*, 1075-1079.
- Dietz, K.-J., Jacob, S., Oelze, M.-L., Laxa, M., Tognetti, V., de Miranda, S.M.N., Baier, M., and Finkemeier, I. (2006).** The function of peroxiredoxins in plant organelle redox metabolism. *Journal of Experimental Botany* *57*, 1697-1709.
- DiMario, R.J., Clayton, H., Mukherjee, A., Ludwig, M., and Moroney, J.V. (2017).** Plant carbonic anhydrases: structures, locations, evolution, and physiological roles. *Molecular Plant* *10*, 30-46.
- Ding, Y., Liu, N., Virlouvet, L., Riethoven, J.-J., Fromm, M., and Avramova, Z. (2013).** Four distinct types of dehydration stress memory genes in *Arabidopsis thaliana*. *BMC Plant Biology* *13*, 229.
- Dittrich, M., Mueller, H.M., Bauer, H., Peirats-Llobet, M., Rodriguez, P.L., Geilfus, C.M., Carpentier, S.C., Al Rasheid, K.A.S., Kollist, H., Merilo, E.,**

- et al.* (2019). The role of Arabidopsis ABA receptors from the PYR/PYL/RCAR family in stomatal acclimation and closure signal integration. *Nature Plants* 5, 1002-1011.
- Domingos, P., Dias, P.N., Tavares, B., Portes, M.T., Wudick, M.M., Konrad, K.R., Gilliam, M., Bicho, A., and Feijó, J.A. (2019).** Molecular and electrophysiological characterization of anion transport in *Arabidopsis thaliana* pollen reveals regulatory roles for pH, Ca²⁺ and GABA. *New Phytologist* 223, 1353-1371.
- Domínguez, E., Heredia-Guerrero, J.A., and Heredia, A. (2017).** The plant cuticle: old challenges, new perspectives. *Journal of Experimental Botany* 68, 5251-5255.
- Driesen, E., Van den Ende, W., De Proft, M., and Saeys, W. (2020).** Influence of environmental factors light, CO₂, temperature, and relative humidity on stomatal opening and development: A review. *Agronomy* 10, 1975.
- Du, L., Yang, T., Puthanveetil, S.V., and Poovaiah, B.W. (2011).** Decoding of calcium signal through calmodulin: calmodulin-binding proteins in plants. In *Coding and Decoding of Calcium Signals in Plants*, S. Luan, ed. (Berlin, Heidelberg: Springer Berlin Heidelberg), pp. 177-233.
- Dubeaux, G., Hsu, P.-K., Ceciliato, P. H. O., Swink, K., Rappel, W.-J., and Schroeder, J.I. (2021).** Deep dive into CO₂-dependent molecular mechanisms driving stomatal responses in plants. *Plant Physiology* 187, 2032-2042.
- Ebert, B., Rautengarten, C., Guo, X., Xiong, G., Stonebloom, S., Smith-Moritz, A.M., Herter, T., Chan, L.J.G., Adams, P.D., Petzold, C.J., et al. (2015).** Identification and characterization of a golgi-localized UDP-xylose transporter family from Arabidopsis. *The Plant Cell* 27, 1218-1227.
- Edwards, K., Johnstone, C., and Thompson, C. (1991).** A simple and rapid method for the preparation of plant genomic DNA for PCR analysis. *Nucleic Acids Research* 19, 1349-1349.
- Ehleringer, J., and Sandquist, D.R. (2015).** Photosynthesis: Physiological and ecological considerations. In *Plant Physiology and Development*, A.D. Sinauer, ed. (Sunderland, Massachusetts: Sinauer Associates, Inc), pp. 245-268.
- Ehrlich, S.D., Bierne, H., d'Alençon, E., Vilette, D., Petranovic, M., Noirot, P., and Michel, B. (1993).** Mechanisms of illegitimate recombination. *Gene* 135, 161-166.

- Eisenach, C., Baetz, U., Huck, N.V., Zhang, J.B., De Angeli, A., Beckers, G.J.M., and Martinoia, E. (2017).** ABA-induced stomatal closure involves ALMT4, a phosphorylation-dependent vacuolar anion channel of Arabidopsis. *The Plant Cell* *29*, 2552-2569.
- Engineer, C.B., Hashimoto-Sugimoto, M., Negi, J., Israelsson-Nordstrom, M., Azoulay-Shemer, T., Rappel, W.J., Iba, K., and Schroeder, J.I. (2016).** CO₂ sensing and CO₂ regulation of stomatal conductance: advances and open questions. *Trends in Plant Science* *21*, 16-30.
- Espinoza, C., Degenkolbe, T., Caldana, C., Zuther, E., Leisse, A., Willmitzer, L., Hinch, D.K., and Hannah, M.A. (2010).** Interaction with diurnal and circadian regulation results in dynamic metabolic and transcriptional changes during cold acclimation in Arabidopsis. *PLoS One* *5*, 19.
- Ewels, P., Magnusson, M., Lundin, S., and Källér, M. (2016).** MultiQC: summarize analysis results for multiple tools and samples in a single report. *Bioinformatics* *32*, 3047-3048.
- Fait, A., Fromm, H., Walter, D., Galili, G., and Fernie, A.R. (2008).** Highway or byway: the metabolic role of the GABA shunt in plants. *Trends in Plant Science* *13*, 14-19.
- Falkowski, P., Scholes, R.J., Boyle, E., Canadell, J., Canfield, D., Elser, J., Gruber, N., Hibbard, K., Höglberg, P., Linder, S., *et al.* (2000).** The global carbon cycle: a test of our knowledge of earth as a system. *Science* *290*, 291-296.
- Fangel, J.U., Jones, C.Y., Ulvskov, P., Harholt, J., and Willats, W.G.T. (2021).** Analytical implications of different methods for preparing plant cell wall material. *Carbohydrate Polymers* *261*, 117866.
- Farquhar, G.D., von Caemmerer, S., and Berry, J.A. (1980).** A biochemical model of photosynthetic CO₂ assimilation in leaves of C₃ species. *Planta* *149*, 78-90.
- Fromm, H. (2020).** GABA signaling in plants: targeting the missing pieces of the puzzle. *Journal of experimental botany* *71*, 6238-6245.
- Fu, D., Sun, Y., Yu, C., Zheng, X., Yu, T., and Lu, H. (2017).** Comparison of the effects of three types of aminobutyric acids on the control of *Penicillium expansum* infection in pear fruit. *Journal of the Science of Food and Agriculture* *97*, 1497-1501.

- Geiger, D., Maierhofer, T., Al-Rasheid, K.A.S., Scherzer, S., Mumm, P., Liese, A., Ache, P., Wellmann, C., Marten, I., Grill, E., et al. (2011).** Stomatal closure by fast abscisic acid signaling is mediated by the guard cell anion channel SLAH3 and the receptor RCAR1. *Science Signaling* 4, 12.
- Geiger, D., Scherzer, S., Mumm, P., Marten, I., Ache, P., Matschi, S., Liese, A., Wellmann, C., Al-Rasheid, K.A.S., Grill, E., et al. (2010).** Guard cell anion channel SLAC1 is regulated by CDPK protein kinases with distinct Ca²⁺ affinities. *Proceedings of the National Academy of Sciences* 107, 8023-8028.
- Geiger, D.R., and Servaites, J.C. (1994).** Diurnal regulation of photosynthetic carbon metabolism in C3 plants. *Annual Review of Plant Physiology and Plant Molecular Biology* 45, 235-256.
- Geserick, C., and Tenhaken, R. (2013).** UDP-sugar pyrophosphorylase is essential for arabinose and xylose recycling, and is required during vegetative and reproductive growth in Arabidopsis. *The Plant Journal* 74, 239-247.
- Gilliham, M., and Tyerman, S.D. (2016).** Linking metabolism to membrane signaling: the GABA-malate connection. *Trends in Plant Science* 21, 295-301.
- Glazebrook, J., and Weigel, D. (2002).** Transformation of Agrobacterium using the freeze-thaw method. In *How to Transform Arabidopsis* (Cold Spring Harbor, NY, USA: Cold Spring Harbor Laboratory Press).
- Gras, D.E., Vidal, E.A., Undurraga, S.F., Riveras, E., Moreno, S., Dominguez-Figueroa, J., Alabadi, D., Blázquez, M.A., Medina, J., and Gutiérrez, R.A. (2017).** SMZ/SNZ and gibberellin signaling are required for nitrate-elicited delay of flowering time in *Arabidopsis thaliana*. *Journal of Experimental Botany* 69, 619-631.
- Gunasekera, D., Kim, Y., Tulloh, C., and Ford, M. (2007).** Climate change - impacts on Australian agriculture. *Australian Commodities*, pp. 657-676.
- Hansen, S., Harholt, J., Oikawa, A., and Scheller, H. (2012).** Plant glycosyltransferases beyond CAZy: a perspective on DUF families. *Frontiers in Plant Science* 3.
- Hashimoto, M., Negi, J., Young, J., Israelsson, M., Schroeder, J.I., and Iba, K. (2006).** Arabidopsis HT1 kinase controls stomatal movements in response to CO₂. *Nature Cell Biology* 8, 391-U352.

- Hauser, F., Li, Z.X., Waadt, R., and Schroeder, J.I. (2017).** SnapShot: abscisic acid signaling. *Cell* *171*, 1708.
- Hayashi, M., Sugimoto, H., Takahashi, H., Seki, M., Shinozaki, K., Sawasaki, T., Kinoshita, T., and Inoue, S.-i. (2020).** Raf-like kinases CBC1 and CBC2 negatively regulate stomatal opening by negatively regulating plasma membrane H⁺-ATPase phosphorylation in Arabidopsis. *Photochemical & Photobiological Sciences* *19*, 88-98.
- Healey, A., Furtado, A., Cooper, T., and Henry, R.J. (2014).** Protocol: a simple method for extracting next-generation sequencing quality genomic DNA from recalcitrant plant species. *Plant Methods* *10*, 21.
- Hiyama, A., Takemiya, A., Munemasa, S., Okuma, E., Sugiyama, N., Tada, Y., Murata, Y., and Shimazaki, K.-i. (2017).** Blue light and CO₂ signals converge to regulate light-induced stomatal opening. *Nature Communications* *8*.
- Holbrook, N.M. (2015).** Water balance of plants. In *Plant Physiology and Development*, L. Taiz, E. Zeiger, I.M. Møller, and A. Murphy, eds. (Sinauer), pp. 99-118.
- Hörak, H., Sierla, M., Töldsepp, K., Wang, C., Wang, Y.-S., Nuhkat, M., Valk, E., Pechter, P., Merilo, E., Salojärvi, J., *et al.* (2016).** A dominant mutation in the HT1 kinase uncovers roles of MAP kinases and GHR1 in CO₂-induced stomatal closure. *The Plant cell* *28*, 2493-2509.
- Horrer, D., Flütsch, S., Pazmino, D., Matthews, J.S., Thalmann, M., Nigro, A., Leonhardt, N., Lawson, T., and Santelia, D. (2016).** Blue light induces a distinct starch degradation pathway in guard cells for stomatal opening. *Current biology : CB* *26*, 362-370.
- Hosotani, S., Yamauchi, S., Kobayashi, H., Fuji, S., Koya, S., Shimazaki, K.-i., and Takemiya, A. (2021).** A BLUS1 kinase signal and a decrease in intercellular CO₂ concentration are necessary for stomatal opening in response to blue light. *The Plant Cell* *33*, 1813-1827.
- Hosy, E., Vavasseur, A., Mouline, K., Dreyer, I., Gaymard, F., Porée, F., Boucherez, J., Lebaudy, A., Bouchez, D., Véry, A.A., *et al.* (2003).** The Arabidopsis outward K⁺ channel GORK is involved in regulation of stomatal movements and plant transpiration. *Proceedings of the National Academy of Sciences of the United States of America* *100*, 5549-5554.

- Hsu, P.-K., Takahashi, Y., Munemasa, S., Merilo, E., Laanemets, K., Waadt, R., Pater, D., Kollist, H., and Schroeder, J.I. (2018).** Abscisic acid-independent stomatal CO₂ signal transduction pathway and convergence of CO₂ and ABA signaling downstream of OST1 kinase. *Proceedings of the National Academy of Sciences* *115*, E9971.
- Hsu, P.K., Dubeaux, G., Takahashi, Y., and Schroeder, J.I. (2021).** Signaling mechanisms in abscisic acid-mediated stomatal closure. *The Plant Journal* *105*, 307-321.
- Hu, H.H., Boisson-Dernier, A., Israelsson-Nordstrom, M., Bohmer, M., Xue, S.W., Ries, A., Godoski, J., Kuhn, J.M., and Schroeder, J.I. (2010).** Carbonic anhydrases are upstream regulators of CO₂-controlled stomatal movements in guard cells. *Nature Cell Biology* *12*, 87-U234.
- Hua, D., Wang, C., He, J., Liao, H., Duan, Y., Zhu, Z., Guo, Y., Chen, Z., and Gong, Z. (2012).** A plasma membrane receptor kinase, GHR1, mediates abscisic acid- and hydrogen peroxide-regulated stomatal movement in *Arabidopsis*. *The Plant cell* *24*, 2546-2561.
- Huang, P.-Y., Catinot, J., and Zimmerli, L. (2015).** Ethylene response factors in *Arabidopsis* immunity. *Journal of Experimental Botany* *67*, 1231-1241.
- Hubbard, K.E., Siegel, R.S., Valerio, G., Brandt, B., and Schroeder, J.I. (2012).** Abscisic acid and CO₂ signalling via calcium sensitivity priming in guard cells, new CDPK mutant phenotypes and a method for improved resolution of stomatal stimulus-response analyses. *Annals of Botany* *109*, 5-17.
- Imes, D., Mumm, P., Böhm, J., Al-Rasheid, K.A., Marten, I., Geiger, D., and Hedrich, R. (2013).** Open stomata 1 (OST1) kinase controls R-type anion channel QUAC1 in *Arabidopsis* guard cells. *The Plant Journal* *74*, 372-382.
- Israelsson, M., Siegel, R.S., Young, J., Hashimoto, M., Iba, K., and Schroeder, J.I. (2006).** Guard cell ABA and CO₂ signaling network updates and Ca²⁺ sensor priming hypothesis. *Current Opinion in Plant Biology* *9*, 654-663.
- Ivanov, B.N. (2014).** Role of ascorbic acid in photosynthesis. *Biochemistry (Moscow)* *79*, 282-289.
- Jakobson, L., Vaahtera, L., Töldsepp, K., Nuhkat, M., Wang, C., Wang, Y.-S., Hõrak, H., Valk, E., Pechter, P., Sindarovska, Y., *et al.* (2016).** Natural

variation in *Arabidopsis* Cvi-0 accession reveals an important role of MPK12 in guard cell CO₂ signaling. *PLoS Biology* 14, e2000322.

Jalakas, P., Nuhkat, M., Vahisalu, T., Merilo, E., Brosché, M., and Kollist, H. (2021). Combined action of guard cell plasma membrane rapid- and slow-type anion channels in stomatal regulation. *Plant Physiology* 187, 2126-2133.

Jensen, R. (2004). Activation of Rubisco controls CO₂ assimilation in light: a perspective on its discovery. *Photosynthesis Research* 82, 187-193.

Ji, J., Yue, J., Xie, T., Chen, W., Du, C., Chang, E., Chen, L., Jiang, Z., and Shi, S. (2018). Roles of γ -aminobutyric acid on salinity-responsive genes at transcriptomic level in poplar: involving in abscisic acid and ethylene-signalling pathways. *Planta* 248, 675-690.

Jossier, M., Kroniewicz, L., Dalmas, F., Le Thiec, D., Ephritikhine, G., Thomine, S., Barbier-Brygoo, H., Vavasseur, A., Filleur, S., and Leonhardt, N. (2010). The *Arabidopsis* vacuolar anion transporter, AtCLC_c, is involved in the regulation of stomatal movements and contributes to salt tolerance. *The Plant Journal* 64, 563-576.

Kalhor, M.S., Aliniaiefard, S., Seif, M., Asayesh, E.J., Bernard, F., Hassani, B., and Li, T. (2018). Enhanced salt tolerance and photosynthetic performance: Implication of γ -amino butyric acid application in salt-exposed lettuce (*Lactuca sativa* L.) plants. *Plant Physiology and Biochemistry* 130, 157-172.

Kamal, A.H.M., and Komatsu, S. (2016). Jasmonic acid induced protein response to biophoton emissions and flooding stress in soybean. *Journal of Proteomics* 133, 33-47.

Kathiresan, A., Tung, P., Chinnappa, C.C., and Reid, D.M. (1997). γ -Aminobutyric acid stimulates ethylene biosynthesis in sunflower. *Plant Physiology* 115, 129-135.

Kebeish, R., Niessen, M., Thiruveedhi, K., Bari, R., Hirsch, H.-J., Rosenkranz, R., Stähler, N., Schönfeld, B., Kreuzaler, F., and Peterhänsel, C. (2007). Chloroplastic photorespiratory bypass increases photosynthesis and biomass production in *Arabidopsis thaliana*. *Nature Biotechnology* 25, 593-599.

Kelly, G., Moshelion, M., David-Schwartz, R., Halperin, O., Wallach, R., Attia, Z., Belausov, E., and Granot, D. (2013). Hexokinase mediates stomatal closure. *The Plant Journal* 75, 977-988.

- Khokon, M.A.R., Okuma, E., Hossain, M.A., Munemasa, S., Uraji, M., Nakamura, Y., Mori, I.C., and Murata, Y. (2011).** Involvement of extracellular oxidative burst in salicylic acid-induced stomatal closure in *Arabidopsis*. *Plant, Cell & Environment* *34*, 434-443.
- Kim, T.H., Bohmer, M., Hu, H.H., Nishimura, N., and Schroeder, J.I. (2010).** Guard cell signal transduction network: advances in understanding abscisic acid, CO₂, and Ca²⁺ signaling. In *Annual Review of Plant Biology*, Vol 61, S. Merchant, W.R. Briggs, and D. Ort, eds. (Palo Alto: Annual Reviews), pp. 561-591.
- Kimball, B.A., Mauney, J.R., Nakayama, F.S., and Idso, S.B. (1993).** Effects of increasing atmospheric CO₂ on vegetation. *Vegetatio* *104*, 65-75.
- Kinoshita, T., and Shimazaki, K.-i. (1999).** Blue light activates the plasma membrane H⁺-ATPase by phosphorylation of the C-terminus in stomatal guard cells. *The EMBO Journal* *18*, 5548-5558.
- Kinoshita, T., Doi, M., Suetsugu, N., Kagawa, T., Wada, M., and Shimazaki, K.-i. (2001).** phot1 and phot2 mediate blue light regulation of stomatal opening. *Nature* *414*, 656-660.
- Kinoshita, T., Nishimura, M., and Shimazaki, K. (1995).** Cytosolic concentration of Ca²⁺ regulates the plasma membrane H⁺-ATPase in guard cells of fava bean. *The Plant Cell* *7*, 1333.
- Kollist, H., Nuhkat, M., and Roelfsema, M.R.G. (2014).** Closing gaps: linking elements that control stomatal movement. *New Phytologist* *203*, 44-62.
- Kuroha, T., Nagai, K., Gamuyao, R., Wang, D.R., Furuta, T., Nakamori, M., Kitaoka, T., Adachi, K., Minami, A., Mori, Y., et al. (2018).** Ethylene-gibberellin signaling underlies adaptation of rice to periodic flooding. *Science* *361*, 181-186.
- Kwak, J.M., Mori, I.C., Pei, Z.M., Leonhardt, N., Torres, M.A., Dangel, J.L., Bloom, R.E., Bodde, S., Jones, J.D.G., and Schroeder, J.I. (2003).** NADPH oxidase *AtrbohD* and *AtrbohF* genes function in ROS-dependent ABA signaling in *Arabidopsis*. *The Embo Journal* *22*, 2623-2633.
- Lancien, M., and Roberts, M.R. (2006).** Regulation of *Arabidopsis thaliana* 14-3-3 gene expression by gamma-aminobutyric acid. *Plant Cell and Environment* *29*, 1430-1436.

- Langmead, B., and Salzberg, S.L. (2012).** Fast gapped-read alignment with Bowtie 2. *Nature Methods* *9*, 357-359.
- Lavergne, A., Graven, H., De Kauwe, M.G., Keenan, T.F., Medlyn, B.E., and Prentice, I.C. (2019).** Observed and modelled historical trends in the water-use efficiency of plants and ecosystems. *Global Change Biology* *25*, 2242-2257.
- Lawson, T., and Blatt, M.R. (2014).** Stomatal size, speed, and responsiveness impact on photosynthesis and water use efficiency. *Plant Physiology* *164*, 1556-1570.
- Lawson, T., Simkin, A.J., Kelly, G., and Granot, D. (2014).** Mesophyll photosynthesis and guard cell metabolism impacts on stomatal behaviour. *New Phytologist* *203*, 1064-1081.
- Leakey, A.D.B., Ferguson, J.N., Pignon, C.P., Wu, A., Jin, Z., Hammer, G.L., and Lobell, D.B. (2019).** Water use efficiency as a constraint and target for improving the resilience and productivity of C3 and C4 crops. *Annual Review of Plant Biology* *70*, 781-808.
- Lee, D.-K., Van Norman, J.M., Murphy, C., Adhikari, E., Reed, J.W., and Sieburth, L.E. (2012).** In the absence of BYPASS1-related gene function, the bps signal disrupts embryogenesis by an auxin-independent mechanism. *Development* *139*, 805-815.
- Letts, M., Rodríguez-Calcerrada, J., Rolo, V., and Rambal, S. (2012).** Long-term physiological and morphological acclimation by the evergreen shrub *Buxus sempervirens* L. to understory and canopy gap light intensities. *Trees* *26*, 479-491.
- Li, K., Prada, J., Damineli, D.S.C., Liese, A., Romeis, T., Dandekar, T., Feijó, J.A., Hedrich, R., and Konrad, K.R. (2021).** An optimized genetically encoded dual reporter for simultaneous ratio imaging of Ca²⁺ and H⁺ reveals new insights into ion signaling in plants. *New Phytologist* *230*, 2292-2310.
- Li, L., Li, C., and Howe, G.A. (2001).** Genetic analysis of wound signaling in tomato. Evidence for a dual role of jasmonic acid in defense and female fertility. *Plant Physiology* *127*, 1414-1417.
- Li, S., Li, X., Wei, Z., and Liu, F. (2020).** ABA-mediated modulation of elevated CO₂ on stomatal response to drought. *Current Opinion in Plant Biology* *56*, 174-180.

- Li, W., Liu, J., Ashraf, U., Li, G., Li, Y., Lu, W., Gao, L., Han, F., and Hu, J. (2016).** Exogenous γ -aminobutyric acid (GABA) application improved early growth, net photosynthesis, and associated physio-biochemical events in maize. *Frontiers in Plant Science* 7.
- Li, Z., Yu, J.J., Peng, Y., and Huang, B.R. (2017).** Metabolic pathways regulated by abscisic acid, salicylic acid and γ -aminobutyric acid in association with improved drought tolerance in creeping bentgrass (*Agrostis stolonifera*). *Physiologia Plantarum* 159, 42-58.
- Liepman, A.H., Wightman, R., Geshi, N., Turner, S.R., and Scheller, H.V. (2010).** Arabidopsis – a powerful model system for plant cell wall research. *The Plant Journal* 61, 1107-1121.
- Lima, M.d.F., Eloy, N.B., Siqueira, J.A.B.d., Inzé, D., Hemerly, A.S., and Ferreira, P.C.G. (2017).** Molecular mechanisms of biomass increase in plants. *Biotechnology Research and Innovation* 1, 14-25.
- Linder, B., and Raschke, K. (1992).** A slow anion channel in guard cells, activating at large hyperpolarization, may be principal for stomatal closing. *FEBS Lett* 313, 27-30.
- Love, M.I., Huber, W., and Anders, S. (2014).** Moderated estimation of fold change and dispersion for RNA-seq data with DESeq2. *Genome Biology* 15, 550.
- Ma, J., and Bennetzen, J.L. (2004).** Rapid recent growth and divergence of rice nuclear genomes. *Proceedings of the National Academy of Sciences of the United States of America* 101, 12404-12410.
- Ma, X., and Bai, L. (2021).** Elevated CO₂ and reactive oxygen species in stomatal closure. *Plants* 10, 410.
- Mahmud, J.A.L., Hasanuzzaman, M., Nahar, K., Rahman, A., Hossain, M.S., and Fujita, M. (2017).** γ -Aminobutyric acid (GABA) confers chromium stress tolerance in *Brassica juncea* L. by modulating the antioxidant defense and glyoxalase systems. *Ecotoxicology* 26, 675-690.
- Malcheska, F., Ahmad, A., Batool, S., Muller, H.M., Ludwig-Mueller, J., Kreuzwieser, J., Randewig, D., Hansch, R., Mendel, R.R., Hell, R., et al. (2017).** Drought-enhanced xylem sap sulfate closes stomata by affecting ALMT12 and guard cell ABA synthesis. *Plant Physiology* 174, 798-814.

- Maris, A., Suslov, D., Fry, S.C., Verbelen, J.-P., and Vissenberg, K. (2009).** Enzymic characterization of two recombinant xyloglucan endotransglucosylase/hydrolase (XTH) proteins of *Arabidopsis* and their effect on root growth and cell wall extension. *Journal of Experimental Botany* *60*, 3959-3972.
- Marvin, J.S., Shimoda, Y., Magloire, V., Leite, M., Kawashima, T., Jensen, T.P., Kolb, I., Knott, E.L., Novak, O., Podgorski, K., et al. (2019).** A genetically encoded fluorescent sensor for *in vivo* imaging of GABA. *Nature Methods* *16*, 763-770.
- Matrosova, A., Bogireddi, H., Mateo-Peñas, A., Hashimoto-Sugimoto, M., Iba, K., Schroeder, J.I., and Israelsson-Nordström, M. (2015).** The HT1 protein kinase is essential for red light-induced stomatal opening and genetically interacts with OST1 in red light and CO₂-induced stomatal movement responses. *New Phytologist* *208*, 1126-1137.
- Matthews, J.S.A., Violet-Chabrand, S., and Lawson, T. (2019).** Role of blue and red light in stomatal dynamic behaviour. *Journal of Experimental Botany* *71*, 2253-2269.
- Matthews, J.S.A., Violet-Chabrand, S.R.M., and Lawson, T. (2017).** Diurnal variation in gas exchange: the balance between carbon fixation and water loss. *Plant Physiology* *174*, 614.
- Medeiros, D.B., Fernie, A.R., and Araújo, W.L. (2018).** Discriminating the function(s) of guard cell ALMT channels. *Trends in Plant Science* *23*, 649-651.
- Mekonnen, D.W. (2012).** Phenotypic and chemotypic characterization of GABA-shunt mutants in *Arabidopsis thaliana*. In *Faculty of Mathematics and Natural Sciences (University of Cologne)*, p. 143.
- Mekonnen, D.W., Flügge, U.I., and Ludewig, F. (2016).** Gamma-aminobutyric acid depletion affects stomata closure and drought tolerance of *Arabidopsis thaliana*. *Plant Science* *245*, 25-34.
- Meyer, A., Eskandari, S., Grallath, S., and Rentsch, D. (2006).** AtGAT1, a high affinity transporter for γ -aminobutyric acid in *Arabidopsis thaliana*. *Journal of Biological Chemistry* *281*, 7197-7204.
- Meyer, S., Mumm, P., Imes, D., Endler, A., Weder, B., Al-Rasheid, K.A.S., Geiger, D., Marten, I., Martinoia, E., and Hedrich, R. (2010).** AtALMT12 represents

an R-type anion channel required for stomatal movement in Arabidopsis guard cells. *Plant Journal* 63, 1054-1062.

Meyer, S., Scholz-Starke, J., De Angeli, A., Kovermann, P., Burla, B., Gambale, F., and Martinoia, E. (2011). Malate transport by the vacuolar AtALMT6 channel in guard cells is subject to multiple regulation. *Plant Journal* 67, 247-257.

Michaeli, S., and Fromm, H. (2015). Closing the loop on the GABA shunt in plants: Are GABA metabolism and signaling entwined? *Frontiers in Plant Science* 6, 419.

Minic, Z., Rihouey, C., Do, C.T., Lerouge, P., and Jouanin, L. (2004). Purification and characterization of enzymes exhibiting β -d-xylosidase activities in stem tissues of Arabidopsis. *Plant Physiology* 135, 867-878.

Mittler, R. (2006). Abiotic stress, the field environment and stress combination. *Trends in Plant Science* 11, 15-19.

Mittler, R. (2017). ROS are good. *Trends in Plant Science* 22, 11-19.

Møller, I.M., Browse, J., and Rasmusson, A.G. (2015). Respiration and lipid metabolism. In *Plant Physiology and Development*, L. Taiz, E. Zeiger, I.M. Møller, and A. Murphy, eds. (Sinauer), pp. 317-352.

Morison, J.I.L. (1987). Concentration and stomatal response to CO₂. In *Stomatal Function*, E. Zeiger, G.D. Farquhar, and I.R. Cowan, eds. (Stanford, California: Stanford University Press), pp. 229-252.

Müller, M. (2021). Foes or friends: ABA and ethylene interaction under abiotic stress. *Plants* 10, 448.

Munemasa, S., Hauser, F., Park, J., Waadt, R., Brandt, B., and Schroeder, J.I. (2015). Mechanisms of abscisic acid-mediated control of stomatal aperture. *Current Opinion in Plant Biology* 28, 154-162.

Mustilli, A.-C., Merlot, S., Vavasseur, A., Fenzi, F., and Giraudat, J. (2002). Arabidopsis OST1 protein kinase mediates the regulation of stomatal aperture by abscisic acid and acts upstream of reactive oxygen species production. *Plant Cell* 14, 3089-3099.

- Narsai, R., Gouil, Q., Secco, D., Srivastava, A., Karpievitch, Y.V., Liew, L.C., Lister, R., Lewsey, M.G., and Whelan, J. (2017).** Extensive transcriptomic and epigenomic remodelling occurs during *Arabidopsis thaliana* germination. *Genome Biology* 18, 172.
- Negi, J., Matsuda, O., Nagasawa, T., Oba, Y., Takahashi, H., Kawai-Yamada, M., Uchimiya, H., Hashimoto, M., and Iba, K. (2008).** CO₂ regulator SLAC1 and its homologues are essential for anion homeostasis in plant cells. *Nature* 452, 483-486.
- Nishinari, K., Takemasa, M., Zhang, H., and Takahashi, R. (2007).** Storage plant polysaccharides: xyloglucans, galactomannans, glucomannans. In *Comprehensive Glycoscience*, H. Kamerling, ed. (Oxford: Elsevier), pp. 613-652.
- Norby, R.J., and Zak, D.R. (2011).** Ecological lessons from free-air CO₂ enrichment (FACE) experiments. In *Annual Review of Ecology, Evolution, and Systematics*, Vol 42, D.J. Futuyma, H.B. Shaffer, and D. Simberloff, eds. (Palo Alto: Annual Reviews), pp. 181-203.
- O'Leary, B. and Plaxton, W.C. (2016).** Plant respiration. eLS, 1-11.
- O'Leary, B., and Plaxton, W.C. (2020).** Multifaceted functions of post-translational enzyme modifications in the control of plant glycolysis. *Current Opinion in Plant Biology* 55, 28-37.
- Ohama, N., Sato, H., Shinozaki, K., and Yamaguchi-Shinozaki, K. (2017).** Transcriptional regulatory network of plant heat stress response. *Trends in Plant Science* 22, 53-65.
- Park, D.H., Mirabella, R., Bronstein, P.A., Preston, G.M., Haring, M.A., Lim, C.K., Collmer, A., and Schuurink, R.C. (2010).** Mutations in γ -aminobutyric acid (GABA) transaminase genes in plants or *Pseudomonas syringae* reduce bacterial virulence. *The Plant Journal* 64, 318-330.
- Patro, R., Duggal, G., Love, M.I., Irizarry, R.A., and Kingsford, C. (2017).** Salmon provides fast and bias-aware quantification of transcript expression. *Nature Methods* 14, 417-419.
- Pei, Z.M., Murata, Y., Benning, G., Thomine, S., Klusener, B., Allen, G.J., Grill, E., and Schroeder, J.I. (2000).** Calcium channels activated by hydrogen peroxide mediate abscisic acid signalling in guard cells. *Nature* 406, 731-734.

- Pélabon, C., Hilde, C.H., Einum, S., and Gamelon, M. (2020).** On the use of the coefficient of variation to quantify and compare trait variation. *Evolution Letters* 4, 180-188.
- Pelvan, A., Bor, M., Yolcu, S., Özdemir, F., and Türkan, I. (2021).** Day and night fluctuations in GABA biosynthesis contribute to drought responses in *Nicotiana tabacum* L. *Plant Signaling & Behavior* 16, 1899672.
- Peña-Cortés, H., Barrios, P., Dorta, F., Polanco, V., Sánchez, C., Sánchez, E., and Ramírez, I. (2004).** Involvement of jasmonic acid and derivatives in plant response to pathogen and insects and in fruit ripening. *Journal of Plant Growth Regulation* 23, 246-260.
- Perby, L.K., Richter, S., Weber, K., Hieber, A.J., Hess, N., Crocoll, C., Mogensen, H.K., Pribil, M., Burow, M., Nielsen, T.H., et al. (2021).** Cytosolic phosphofructokinases are important for sugar homeostasis in leaves of *Arabidopsis thaliana*. *Annals of Botany*.
- Pitzschke, A., Forzani, C., and Hirt, H. (2006).** Reactive oxygen species signaling in Plants. *Antioxidants & Redox Signaling* 8, 1757-1764.
- Podlešáková, K., Ugena, L., Spíchal, L., Doležal, K., and De Diego, N. (2019).** Phytohormones and polyamines regulate plant stress responses by altering GABA pathway. *New Biotechnology* 48, 53-65.
- Priya, M., Sharma, L., Kaur, R., Bindumadhava, H., Nair, R.M., Siddique, K.H.M., and Nayyar, H. (2019).** GABA (γ -aminobutyric acid), as a thermo-protectant, to improve the reproductive function of heat-stressed mungbean plants. *Scientific Reports* 9, 7788.
- Ramesh, S.A., Kamran, M., Sullivan, W., Chirkova, L., Okamoto, M., Degryse, F., McLaughlin, M., Gilliam, M., and Tyerman, S.D. (2018).** Aluminum-activated malate transporters can facilitate GABA transport. *Plant Cell* 30, 1147-1164.
- Ramesh, S.A., Tyerman, S.D., Gilliam, M., and Xu, B. (2017).** Gamma-aminobutyric acid (GABA) signalling in plants. *Cellular and Molecular Life Sciences* 74, 1577-1603.
- Ramesh, S.A., Tyerman, S.D., Xu, B., Bose, J., Kaur, S., Conn, V., Domingos, P., Ullah, S., Wege, S., Shabala, S., et al. (2015).** GABA signalling modulates

plant growth by directly regulating the activity of plant-specific anion transporters. *Nature Communications* 6, 9.

Ramos-Ruiz, R., Martinez, F., and Knauf-Beiter, G. (2019). The effects of GABA in plants. *Cogent Food & Agriculture* 5, 1670553.

Raghavendra, A.S. and Y. Murata (2017). Editorial: signal transduction in stomatal guard cells. *Frontiers in Plant Science* 8, 114.

Raschke, K. (1975). Simultaneous requirement of carbon dioxide and abscisic acid for stomatal closing in *Xanthium strumarium* L. *Planta* 125, 243-259.

Renault, H., El Amrani, A., Palanivelu, R., Updegraff, E.P., Yu, A., Renou, J.-P., Preuss, D., Bouchereau, A., and Deleu, C. (2011). GABA accumulation causes cell elongation defects and a decrease in expression of genes encoding secreted and cell wall-related proteins in *Arabidopsis thaliana*. *Plant Cell Physiology* 52, 894-908.

Renault, H., Roussel, V., El Amrani, A., Arzel, M., Renault, D., Bouchereau, A., and Deleu, C. (2010). The *Arabidopsis pop2-1* mutant reveals the involvement of GABA transaminase in salt stress tolerance. *Bmc Plant Biology* 10, 16.

Rennie, E.A., and Scheller, H.V. (2014). Xylan biosynthesis. *Current Opinion in Biotechnology* 26, 100-107.

Roberts, M.R. (2007). Does GABA act as a signal in plants? Hints from molecular studies. *Plant Signaling & Behavior* 2, 408-409.

Roelfsema, M.R.G., Hanstein, S., Felle, H.H., and Hedrich, R. (2002). CO₂ provides an intermediate link in the red light response of guard cells. *The Plant Journal* 32, 65-75.

Roelfsema, M.R.G., and Hedrich, R. (2005). In the light of stomatal opening: new insights into 'the Watergate'. *New Phytologist* 167, 665-691.

Roelfsema, M.R.G., Hedrich, R., and Geiger, D. (2012). Anion channels: master switches of stress responses. *Trends in Plant Science* 17, 221-229.

Ross, J., Li, Y., Lim, E.-K., and Bowles, D.J. (2001). Higher plant glycosyltransferases. *Genome Biology* 2, reviews3004.3001.

- Sai, N., Bockman, J.P., Chen, H., Watson-Haigh, N., Xu, B., Feng, X., Piechatzek, A., Shen, C., and Gilliam, M. (2022).** SAI: fast and automated quantification of stomatal parameters on microscope images. *BioRxiv* doi: <https://doi.org/10.1101/2022.02.07.479482>. [Preprint].
- Saito, S., and Uozumi, N. (2019).** Guard cell membrane anion transport systems and their regulatory components: an elaborate mechanism controlling stress-induced stomatal closure. *Plants* *8*, 9.
- Sandquist, D.R. (2015).** Photosynthesis: physiological and ecological considerations. In *Plant physiology and development*, A.D. Sinauer, ed. (Sunderland, Massachusetts, U.S.A.: Sinauer Associates, Inc), pp. 245-268.
- Sasaki, T., Mori, I.C., Furuichi, T., Munemasa, S., Toyooka, K., Matsuoka, K., Murata, Y., and Yamamoto, Y. (2010).** Closing plant stomata requires a homolog of an aluminum-activated malate transporter. *Plant and Cell Physiology* *51*, 354-365.
- Scafaro, A.P., Xiang, S., Long, B.M., Bahar, N.H.A., Weerasinghe, L.K., Creek, D., Evans, J.R., Reich, P.B., and Atkin, O.K. (2017).** Strong thermal acclimation of photosynthesis in tropical and temperate wet-forest tree species: the importance of altered Rubisco content. *Global Change Biology* *23*, 2783-2800.
- Scheller, H.V., and Ulvskov, P. (2010).** Hemicelluloses. *Annual Review of Plant Biology* *61*, 263-289.
- Scholz, S.S., Reichelt, M., Mekonnen, D.W., Ludewig, F., and Mithofer, A. (2015).** Insect herbivory-elicited GABA accumulation in plants is a wound-induced, direct, systemic, and jasmonate-independent defense response. *Frontiers in Plant Science* *6*, 1128.
- Seifikalhor, M., Aliniaiefard, S., Hassani, B., Niknam, V., and Lastochkina, O. (2019).** Diverse role of γ -aminobutyric acid in dynamic plant cell responses. *Plant Cell Reports* *38*, 847-867.
- Sharkey, T.D., Bernacchi, C.J., Farquhar, G.D., and Singaas, E.L. (2007).** Fitting photosynthetic carbon dioxide response curves for C₃ leaves. *Plant, Cell & Environment* *30*, 1035-1040.

- Sharma, T., Dyer, I., Kochian, L., and Piñeros, M. (2016).** The ALMT family of organic acid transporters in plants and their involvement in detoxification and nutrient security. *Frontiers in Plant Science* 7, 1488.
- Shelp, B.J., and Zarei, A. (2017).** Subcellular compartmentation of 4-aminobutyrate (GABA) metabolism in Arabidopsis: an update. *Plant Signaling & Behavior* 12, e1322244.
- Shi, K., Li, X., Zhang, H., Zhang, G., Liu, Y., Zhou, Y., Xia, X., Chen, Z., and Yu, J. (2015).** Guard cell hydrogen peroxide and nitric oxide mediate elevated CO₂-induced stomatal movement in tomato. *New Phytologist* 208, 342-353.
- Siddiqui, H., Sami, F., and Hayat, S. (2020).** Glucose: sweet or bitter effects in plants- a review on current and future perspective. *Carbohydrate Research* 487, 107884.
- Singh, R., Parihar, P., Singh, S., Mishra, R.K., Singh, V.P., and Prasad, S.M. (2017).** Reactive oxygen species signaling and stomatal movement: current updates and future perspectives. *Redox Biology* 11, 213-218.
- Smirnoff, N. (2000).** Ascorbic acid: metabolism and functions of a multi-faceted molecule. *Current Opinion in Plant Biology* 3, 229-235.
- Smith, E.W., Tolbert, N.E., and Ku, H.S. (1976).** Variables affecting the CO₂ compensation point. *Plant Physiology* 58, 143-146.
- Snedden, W.A., Arazi, T., Fromm, H., and Shelp, B.J. (1995).** Calcium/calmodulin activation of soybean glutamate decarboxylase. *Plant Physiology* 108, 543.
- Soneson, C., Love, M.I., and Robinson, M.D. (2016).** Differential analyses for RNA-seq: transcript-level estimates improve gene-level inferences 4, 1521.
- Song, Y., Miao, Y., and Song, C.-P. (2014).** Behind the scenes: the roles of reactive oxygen species in guard cells. *New Phytologist* 201, 1121-1140.
- Sosa, L.G.A., Agostini, E., and Medina, M.I. (2011).** Antioxidant response of tobacco (*Nicotiana tabacum*) hairy roots after phenol treatment. *Plant Physiology and Biochemistry* 49, 1020-1028.
- Stanhill, G. (1986).** Water use efficiency. In *Advances in Agronomy*, N.C. Brady, ed. (Academic Press), pp. 53-85.

- Stinziano, J.R., Adamson, R.K., and Hanson, D.T. (2019).** Using multirate rapid A/C_i curves as a tool to explore new questions in the photosynthetic physiology of plants. *New Phytologist* *222*, 785-792.
- Taiz, L., Murphy, A., Monshausen, G.B., and Peer, W. (2015).** Signals and signal transduction. In *Plant Physiology and Development*, A.D. Sinauer, ed. (Sunderland, Massachusetts: Sinauer Associates, Inc), pp. 408-445.
- Tamura, K., Kawabayashi, T., Shikanai, T., and Hara-Nishimura, I. (2016).** Decreased expression of a gene caused by a T-DNA insertion in an adjacent gene in Arabidopsis. *PLoS One* *11*, e0147911.
- Tanaka, Y., Sano, T., Tamaoki, M., Nakajima, N., Kondo, N., and Hasezawa, S. (2005).** Ethylene inhibits abscisic acid-induced stomatal closure in Arabidopsis. *Plant Physiology* *138*, 2337-2343.
- Taub, D. (2010).** Effects of rising atmospheric concentrations of carbon dioxide on plants. *Nature Education Knowledge* *1*, 21.
- Taub, D.R., Miller, B., and Allen, H. (2008).** Effects of elevated CO₂ on the protein concentration of food crops: a meta-analysis. *Global Change Biology* *14*, 565-575.
- Taub, D.R., and Wang, X. (2008).** Why are nitrogen concentrations in plant tissues lower under elevated CO₂? A critical examination of the hypotheses. *Journal of Integrative Plant Biology* *50*, 1365-1374.
- Terrer, C., Phillips, R.P., Hungate, B.A., Rosende, J., Pett-Ridge, J., Craig, M.E., van Groenigen, K.J., Keenan, T.F., Sulman, B.N., Stocker, B.D., *et al.* (2021).** A trade-off between plant and soil carbon storage under elevated CO₂. *Nature* *591*, 599-603.
- Tian, Q.Y., Zhang, X.X., Ramesh, S., Gilliham, M., Tyerman, S.D., and Zhang, W.H. (2014).** Ethylene negatively regulates aluminium-induced malate efflux from wheat roots and tobacco cells transformed with TaALMT1. *Journal of Experimental Botany* *65*, 2415-2426.
- Tian, W., Hou, C., Ren, Z., Pan, Y., Jia, J., Zhang, H., Bai, F., Zhang, P., Zhu, H., He, Y., *et al.* (2015).** A molecular pathway for CO₂ response in Arabidopsis guard cells. *Nature Communications* *6*, 6057.

- Töldsepp, K., Zhang, J., Takahashi, Y., Sindarovska, Y., Hõrak, H., Ceciliato, P.H.O., Koolmeister, K., Wang, Y.-S., Vaahtera, L., Jakobson, L., et al. (2018).** Mitogen-activated protein kinases MPK4 and MPK12 are key components mediating CO₂-induced stomatal movements. *The Plant Journal* *96*, 1018-1035.
- Tominaga, J., Shimada, H., and Kawamitsu, Y. (2018).** Direct measurement of intercellular CO₂ concentration in a gas-exchange system resolves overestimation using the standard method. *Journal of Experimental Botany* *69*, 1981-1991.
- Ülker, B., Peiter, E., Dixon, D.P., Moffat, C., Capper, R., Bouché, N., Edwards, R., Sanders, D., Knight, H., and Knight, M.R. (2008).** Getting the most out of publicly available T-DNA insertion lines. *The Plant Journal* *56*, 665-677.
- Urano, K., Maruyama, K., Ogata, Y., Morishita, Y., Takeda, M., Sakurai, N., Suzuki, H., Saito, K., Shibata, D., Kobayashi, M., et al. (2009).** Characterization of the ABA-regulated global responses to dehydration in *Arabidopsis* by metabolomics. *The Plant Journal* *57*, 1065-1078.
- Van Norman, J., Murphy, C., and Sieburth, L. (2011).** BYPASS1: Synthesis of the mobile root-derived signal requires active root growth and arrests early leaf development. *BMC plant biology* *11*, 28.
- Vemmos, S.N., Petri, E., and Stournaras, V. (2013).** Seasonal changes in photosynthetic activity and carbohydrate content in leaves and fruit of three fig cultivars (*Ficus carica* L.). *Scientia Horticulturae* *160*, 198-207.
- Vitte, C., and Bennetzen, J.L. (2006).** Analysis of retrotransposon structural diversity uncovers properties and propensities in angiosperm genome evolution. *Proceedings of the National Academy of Sciences* *103*, 17638-17643.
- Von Wettstein, D., Gough, S., and Kannangara, C.G. (1995).** Chlorophyll biosynthesis. *The Plant cell* *7*, 1039-1057.
- Walker, B., Ariza, L.S., Kaines, S., Badger, M.R., and Cousins, A.B. (2013).** Temperature response of in vivo Rubisco kinetics and mesophyll conductance in *Arabidopsis thaliana*: comparisons to *Nicotiana tabacum*. *Plant, Cell & Environment* *36*, 2108-2119.
- Wang, C., Hu, H.H., Qin, X., Zeise, B., Xu, D.Y., Rappel, W.J., Boron, W.F., and Schroeder, J.I. (2016).** Reconstitution of CO₂ regulation of SLAC1 anion

channel and function of CO₂-permeable PIP2;1 aquaporin as carbonic anhydrase4 interactor. *Plant Cell* 28, 568-582.

Wang, X., Liu, S., Tian, H., Wang, S., and Chen, J.-G. (2015). The small ethylene response factor ERF96 is involved in the regulation of the abscisic acid response in *Arabidopsis*. *Frontiers in Plant Science* 6.

Wang, Y., and Frei, M. (2011). Stressed food – The impact of abiotic environmental stresses on crop quality. *Agriculture, Ecosystems & Environment* 141, 271-286.

Wingler, A., Lea, P.J., Quick, W.P., and Leegood, R.C. (2000). Photorespiration: metabolic pathways and their role in stress protection. *Philosophical Transactions of the Royal Society B: Biological Sciences* 355, 1517-1529.

Woodward, F.I., and Kelly, C.K. (1995). The influence of CO₂ concentration on stomatal density. *New Phytologist* 131, 311-327.

Wu, Q., Su, N., Huang, X., Cui, J., Shabala, L., Zhou, M., Yu, M., and Shabala, S. (2021). Hypoxia-induced increase in GABA content is essential for restoration of membrane potential and preventing ROS-induced disturbance to ion homeostasis. *Plant Communications* 2, 100188.

Xiang, L., Hu, L., Xu, W., Zhen, A., Zhang, L., and Hu, X. (2016). Exogenous γ -aminobutyric acid improves the structure and function of Photosystem II in muskmelon seedlings exposed to salinity-alkalinity stress. *PLoS One* 11, e0164847.

Xu, B., Long, Y., Feng, X., Zhu, X., Sai, N., Chirkova, L., Betts, A., Herrmann, J., Edwards, E.J., Okamoto, M., et al. (2021a). GABA signalling modulates stomatal opening to enhance plant water use efficiency and drought resilience. *Nature Communications* 12, 1952.

Xu, B., Sai, N., and Gilliam, M. (2021b). The emerging role of GABA as a transport regulator and physiological signal. *Plant Physiology*.

Yang, Y., Costa, A., Leonhardt, N., Siegel, R.S., and Schroeder, J.I. (2008). Isolation of a strong *Arabidopsis* guard cell promoter and its potential as a research tool. *Plant Methods* 4, 6-6.

Yoshida, K., and Hisabori, T. (2021). Biochemical basis for redox regulation of chloroplast-localized phosphofructokinase from *Arabidopsis thaliana*. *Plant and Cell Physiology* 62, 401-410.

- Young, J.J., Mehta, S., Israelsson, M., Godoski, J., Grill, E., and Schroeder, J.I. (2006).** CO₂ signaling in guard cells: calcium sensitivity response modulation, a Ca²⁺-independent phase, and CO₂ insensitivity of the *gca2* mutant. *Proceedings of the National Academy of Sciences* *103*, 7506.
- Yu, G., Wang, L.-G., Han, Y., and He, Q.-Y. (2012).** clusterProfiler: an R package for comparing biological themes among gene clusters. *OMICS: a Journal of Integrative Biology* *16*, 284-287.
- Yu, G.-H., Zou, J., Feng, J., Peng, X.-B., Wu, J.-Y., Wu, Y.-L., Palanivelu, R., and Sun, M.-X. (2014).** Exogenous γ -aminobutyric acid (GABA) affects pollen tube growth via modulating putative Ca²⁺-permeable membrane channels and is coupled to negative regulation on glutamate decarboxylase. *Journal of Experimental Botany* *65*, 3235-3248.
- Yue, J., Du, C., Ji, J., Xie, T., Chen, W., Chang, E., Chen, L., Jiang, Z., and Shi, S. (2018).** Inhibition of α -ketoglutarate dehydrogenase activity affects adventitious root growth in poplar via changes in GABA shunt. *Planta* *248*, 963-979.
- Žárský, V. (2015).** Signal transduction: GABA receptor found in plants. *Nature Plants* *1*, 15115.
- Zeiger, E. (2015).** Stomatal biology. In *Plant Physiology and Development*, A.D. Sinauer, ed. (Sunderland, Massachusetts: Sinauer Associates, Inc), pp. 269-284.
- Zeng, W., Hassan, M.J., Kang, D., Peng, Y., and Li, Z. (2021).** Photosynthetic maintenance and heat shock protein accumulation relating to γ -aminobutyric acid (GABA)-regulated heat tolerance in creeping bentgrass (*Agrostis stolonifera*). *South African Journal of Botany* *141*, 405-413.
- Zhang, J.B., De-oliveira-Ceciliato, P., Takahashi, Y., Schulze, S., Dubeaux, G., Hauser, F., Azoulay-Shemer, T., Toldsepp, K., Kollist, H., Rappel, W.J., et al. (2018).** Insights into the molecular mechanisms of CO₂-mediated regulation of stomatal movements. *Current Biology* *28*, R1356-R1363.
- Zhang, L., Takahashi, Y., Hsu, P.-K., Kollist, H., Merilo, E., Krysan, P.J., and Schroeder, J.I. (2020a).** FRET kinase sensor development reveals SnRK2/OST1 activation by ABA but not by MeJA and high CO₂ during stomatal closure. *eLife* *9*, e56351.

- Zhang, P., Zhang, Z., Zhang, L., Wang, J., and Wu, C. (2020b).** Glycosyltransferase GT1 family: phylogenetic distribution, substrates coverage, and representative structural features. *Computational and Structural Biotechnology Journal* *18*, 1383-1390.
- Zhang, X., Lin, H.-m., Hu, H., Hu, X., and Hu, L. (2016).** Gamma-aminobutyric acid mediates nicotine biosynthesis in tobacco under flooding stress. *Plant Diversity* *38*, 53-58.
- Zhang, X., Zhang, L., Dong, F.C., Gao, J.F., Galbraith, D.W., and Song, C.P. (2001).** Hydrogen peroxide is involved in abscisic acid-induced stomatal closure in *Vicia faba*. *Plant Physiology* *126*, 1438-1448.
- Zhang, X.R., Henriques, R., Lin, S.S., Niu, Q.W., and Chua, N.H. (2006).** Agrobacterium-mediated transformation of *Arabidopsis thaliana* using the floral dip method. *Nature Protocols* *1*, 641-646.
- Zhu, D., Wu, Z., Cao, G., Li, J., Wei, J., Tsuge, T., Gu, H., Aoyama, T., and Qu, L.-J. (2014).** Translucent Green, an ERF family transcription factor, controls water balance in Arabidopsis by activating the expression of Aquaporin genes. *Molecular Plant* *7*, 601-615.
- Zik, M., Arazi, T., Snedden, W.A., and Fromm, H. (1998).** Two isoforms of glutamate decarboxylase in Arabidopsis are regulated by calcium/calmodulin and differ in organ distribution. *Plant Molecular Biology* *37*, 967-975.
- Ziska, L.H., Epstein, P.R., and Schlesinger, W.H. (2009).** Rising CO₂, climate change, and public health: exploring the links to plant biology. *Environmental Health Perspectives* *117*, 155-158.
- Zvereva, E.L., and Kozlov, M.V. (2006).** Consequences of simultaneous elevation of carbon dioxide and temperature for plant–herbivore interactions: a metaanalysis. *Global Change Biology* *12*, 27-41.